

POLYMER – INORGANIC NANOCOMPOSITES

INFLUENCE OF COLLOIDAL SILICA

MARÍA MONSERRAT DE LA LUZ GARCÍA CURIEL

Promotie-commissie

Voorzitter/Secretari s:	prof. dr. ing. M. Wessling	(UTwente)
Promotor:	prof. dr. ing. D.H.A. Blank	(UTwente)
Assistent-promotor:	dr. W.E. van Zyl	(UTwente)
Referent:	dr. L. Winnubst	(UTwente)
	dr. Ing. M. van Es	(DSM)
Leden	prof. dr. ir. L. Lefferts	(UTwente)
	prof. dr. ing-habil G. Weickert	(UTwente)
	prof. dr. ir. H.E.H. Meijer	(TU Eindhoven)
	prof. dr. ir. D.J. Schipper	(UTwente)
	dr. J.F. Chávez Ríos	(UPrinceton/PEMEX)

The research described in this thesis was funded by the Netherlands Organization for Scientific Research (NWO-PPM) project 700.26.624.

García Curiel, María Monserrat de la Luz
Polymer-Inorganic Nanocomposites
Thesis University of Twente, Enschede-With ref.-With summaries in Dutch,
English and Spanish.
ISBN: 90-365-2013-4

Copyright© M.M.L. García Curiel, Enschede, The Netherlands, 2004
Email: m.m.garciacuriel@utwente.nl

Printed by PrintPartners Ipskamp B.V., Enschede, The Netherlands

Cover design: Lic. Claudia Mayra Ordáz Velázquez. Front-cover: TEM picture made with a JEOL 2010F of a polyamide-silica nanocomposites. Back-cover: The Tower of the drowned village Drienerlo (Wim T. Schippers). Photo acknowledgement: A. Reef/UT-nieuws.

POLYMER – INORGANIC NANOCOMPOSITES

INFLUENCE OF COLLOIDAL SILICA

PROEFSCHRIFT

ter verkrijging van
de graad van doctor aan de Universiteit Twente,
op gezag van de rector magnificus,
prof. dr. F. A. van Vught,
volgens besluit van het College voor Promoties
in het openbaar te verdedigen
op vrijdag 23 januari 2004 om 16.45 uur

door

María Monserrat de la Luz García Curiel

geboren op 27 April 1971

te Mexico-Stad, Mexico

Dit proefschrift is goedgekeurd door de promotor
prof. dr. ing. D.H.A. Blank
en assistent-promotor
dr. W.E. van Zyl

Dedicated to :

The memory of Prof. Dra. Lydia Rodríguez-Hahn†

Dr. Roberto Salcedo, M.enC. Jorge Cárdenas, Dr. Stephen Muhl
I learned a lot from you!

A mi Mamá, Papá, Soco, Chelo y Georgina,
y sobre todo a Tomas,
¡Para tí cariño!

Table of Contents

Summary.....	v
1 General Introduction.....	1
1.1 Overview of the Project.....	2
1.2 Structure of thesis	4
1.3 References	7
2 Hybrid Organic/Inorganic Nanocomposites	9
2.1 Polyamides	10
2.2 Polypropylene	13
2.3 Inorganic Filler Particles	13
2.4 Stabilising suspensions using polymers	16
2.5 Hybrid organic/inorganic composites	16
2.6 Nylon-6-Silica nanocomposites.....	18
2.7 Conclusions.....	19
2.8 References	19
3 Synthesis, Microstructure and Mechanical Testing of Nanocomposites	23
3.1 Introduction.....	24
3.2 Objectives	24
3.3 Experimental	25
3.3.1 Synthesis	25
3.3.2 Characterisation of nanocomposites	26
3.4 Results and Discussion.....	28
3.4.1 Dispersion	28
3.4.2 Solution ¹ H and ¹³ C-NMR of nanocomposites.....	30
3.4.3 Crystallinity and melting of nanocomposites.....	31
3.4.4 Mechanical tests of nanocomposites	38
3.4.5 Morphology	39
3.4.6 Impact Toughness.....	41
3.5 General Discussion	42
3.6 Conclusions.....	44
3.7 References	45
4 Friction and Wear Studies on Nylon-6/Silica Nanocomposites.....	47
4.1 Introduction.....	48
4.2 Experimental	49
4.2.1 Synthesis	49
4.2.2 Characterisation	49
4.2.3 Tribological conditions	50
4.3 Results	51
4.3.1 Sample characteristics	51
4.3.2 Tribological tests.....	52
4.4 Discussion.....	57
4.5 Contact Model and Friction Model.....	60
4.5.1 Single-asperity contact model.....	60
4.5.2 Multi-asperities contact model.....	63
4.5.3 The static contact model	63
4.6 The friction model.....	67

4.6.1	Friction force due to adhesion	68
4.6.2	Friction force due to ploughing	68
4.6.3	The Total friction force.....	69
4.7	Model validation.....	69
4.8	Conclusions	71
4.9	References	72
5	Rheology of Nanocomposites.....	73
5.1	Introduction.....	74
5.2	Experimental	77
5.3	Results and discussion	77
5.4	General discussion.....	88
5.5	Conclusions	89
5.6	References	90
6	Production of Nanocomposites: Processing and Characterization..	91
6.1	Introduction.....	92
6.2	Experimental	93
6.3	Characterization Methods	98
6.4	Results and discussion	99
6.5	Conclusions	105
6.6	References	106
7	Mechanical Models.....	107
7.1	Introduction.....	108
7.2	Mechanical Models.....	110
7.3	Results	112
7.4	Discussion	113
7.5	Conclusions	114
7.6	References	114
8	PP/Silica Nanocomposites in a Slurry Phase Polymerisation Reactor.....	115
8.1	Introduction.....	116
8.2	Experimental Section	117
8.2.1	Materials and Silica Modification	117
8.2.2	Reactor Set-up and Catalyst.....	118
8.2.3	Pre-Polymerisation Reaction and Filler Addition.....	119
8.2.4	Characterization Methods.....	119
8.2.5	Kinetics: Theory	120
8.3	Results and Discussion	121
8.3.1	Synthesis	121
8.3.2	Spectroscopy.....	122
8.3.3	Degree of crystallinity.....	123
8.3.4	Composite morphology	125
8.3.5	Catalyst	126
8.4	Conclusions	128
8.5	References	129
9	Polypropylene/SiO₂ Nanocomposites: Mechanical and Thermal Properties	131
9.1	Introduction.....	132
9.2	Experimental	133
9.3	Results	134
9.4	Conclusions	139
9.5	References	140

10 Conclusions and Recommendations	141
10.1 References	144
Appendix A.....	145
Controlling interparticle forces to create stable suspensions	145
Appendix B.....	149
Quantitative data from TEM analysis.....	149
Appendix C.....	153
Composite models	153
Samenvatting.....	157
Resúmen	159
Curriculum vitae	
Publications	
Acknowledgements	
List of Abbreviations	
List of Symbols	
Index	

Summary

An inorganic-polymer nanocomposite was formed by incorporating nanosize silica filler particles ($\varnothing < 30$ nm) into a nylon-6 matrix. Thin films were made by dissolving nylon-6 in formic acid and mixing the solution with the silica sol, and then casting the mixture. Several films were melted together and subsequently compression moulded. The composites were examined with TEM, which revealed that the silica particles were well dispersed and non-aggregated. The degree of crystallinity increased with low silica loadings (< 7 wt%) but upon further increasing filler wt%, the degree of crystallinity decreased again, and for the thin films, more dramatically compared to the compression moulded samples. Compared to pure nylon-6, the nanocomposite showed an increase in E-modulus as a function of filler percentage, and an increased strain-at-break of > 0.5 .

The friction and wear properties of the aforementioned compression moulded nanocomposites were investigated. A pin on disk tribometer was used running a flat pin of steel against a nylon-silica composite disc. The addition of 2 wt% SiO₂ resulted in a friction reduction (μ) from 0.45 to 0.18, in comparison with neat nylon-6. This low silica loading also led to a reduction in wear rate by a factor of 140. The influence of higher silica loadings was less pronounced. The smooth surface of the disc obtained after the wear test indicated the negligible contribution of the pin to the wear of the nanocomposite.

The rheological properties of the polymer (nanocomposite) melt were studied under small deformation conditions. The results showed that the dynamic viscosity decreased with high filler contents of 18 wt% and 22 wt%, noticeably at strains larger than 1%. An increase of 3 decades in the viscosity could be observed. This increase in viscosity might have been caused by post-condensation (agglomeration) of the silica particles, which is also indicated by the increase of the dynamic modulus. Addition of silica to PA6 thus increased the elasticity and the viscosity when compared to unfilled nylon-6.

PA6-silica composites were also made by using a twin-screw extruder. A silica sol was mixed with the molten polymer inside the extruder. As determined by WAXD, the nanosilica containing PA6 showed higher amounts of γ -phase when compared to nanosilica containing PA6 samples described in literature, made by other synthesis methods, such as *in-situ* polymerisation. TEM pictures showed that the silica particles of the extruded composite were aggregated. Nevertheless, upon addition of 14 wt% silica the E-modulus increased from 2.7 GPa to 3.9 GPa. This increase is larger compared to the one in the literature described (nanosilica containing PA6 composites), indicating that an effective mechanical coupling with the polymer was achieved. The

addition of silica did not decrease the average molecular weight of the polymer matrix.

Conventional (mechanical) theoretical models such as the Mori-Tanaka and Kerner models were used to predict the reinforcing efficiency of spherical particles containing composites. The measured moduli of the different aforementioned nanosilica containing composites were higher than the moduli that were predicted by these models for such spherical particles containing composites.

The influence of the presence of silica on the *in-situ* polymerisation of polypropylene (PP) was studied, utilizing a one-liter Slurry Phase Polymerisation (SPP) reactor containing a MgCl_2 -supported Ziegler-Natta (fourth generation) catalyst. The size of the silica filler ranged from the nano- to micron-size domain. The surface of the silica particles was modified with a silane-coupling agent to prevent catalyst deactivation and to achieve better polymer/filler synergy by increasing the hydrophobicity of the silica particle surface. The effect of the filler on the melting point and on the crystallite size of PP was studied with Differential Scanning Calorimetry (DSC) and Wide-Angle X-ray Diffraction (WAXD) respectively. The addition of reinforcing nanosilica did not cause a decrease in the activity of the catalyst, contrary to the addition of micro-silica, which did lead to a decrease in catalyst activity.

Polypropylene- SiO_2 nanocomposites were synthesized also by using twin-screw extruders. Addition of colloidal silica to the polymer matrix led to a good filler dispersion while the use of powder silica resulted in aggregated silica particles in the polymer matrix (both fillers were in the nano-dimensions range). At a loading of 4.5 wt% colloidal silica a reinforcing and toughening effect of the nanoparticles on the polymer matrix were observed. This amount of 4.5 wt% is lower compared to conventional particulate filled composites. The presence of colloidal particles in the polymer matrix led to an increase of the Young modulus from 1.2 GPa to 1.6 GPa and impact strength from 3.4 KJ/m^2 to 5.7 KJ/m^2 , while the tensile strength remained constant. The use of colloidal silica led to a better mechanical performance compared to powder silica composites, since there was no noticeable improvement of the mechanical properties when powder silica was added to the pure polymer.

1 General Introduction

The beginning of research on nanotechnology and nanoscience can be traced back over 40 years, first described in a lecture entitled, 'There's Plenty of Room at the Bottom' in 1959 by Richard P. Feynman [1]. However, it is during the past decade that nanotechnology went through a variety of disciplines. From chemistry to biology, from materials science to electrical engineering, scientists are creating the tools and developing the expertise to bring nanotechnology out of the research labs and into the market place. Nanostructured composite materials, when using organic polymer and inorganic fillers, represent a merger between traditional organic and inorganic materials, resulting in compositions that are truly hybrid. Nature has created many (composite) materials, such as diatoms, radiolarian [2] and bone [3], from which scientists can learn (Fig. 1). Organic-inorganic composites with nanoscale dimensions are of growing interest because of their unique properties, and numerous potential applications such as enhancement of conductivity [4,5], toughness [6], optical activity [7,8], catalytic activity [9], chemical selectivity [10,11] etc. In these materials, inorganic and organic components are mixed or hybridised at nanometer scale with virtually any composition leading to the formation of hybrid/nanocomposite materials [12-22].

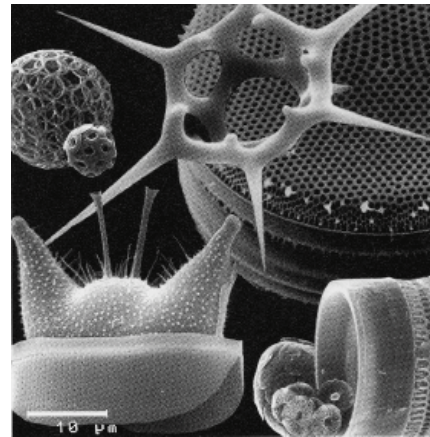


Fig. 1. Diatoms, like radiolaria, represent the incredible control Nature exerts over the assembly of organic-inorganic materials. [Reproduced with permission from ref. 2].

Ceramics are generally known for their hardness and brittleness, along with their resistance to high temperatures and severe physical/chemical environments [23, 24]. In addition, many inorganic materials such as silica glass have excellent optical properties such as transparency [25]. For most applications, the brittleness (lack of impact strength) is the major, sometimes fatal, deficiency of ceramics [23]. On the other hand, organic polymers are usually noted for their low density and high toughness. (i.e., high impact strength). They can

be tailor-made to exhibit excellent elasticity (e.g., synthetic rubber) or optical transparency (e.g., polymethacrylates or Plexiglas™). However, lack of hardness is one of the most significant flaws of polymers in many applications. Associated with the lack of hardness are the problems of low wear and scratch resistance as well as dimensional stability [26]. The developments of conventional composite materials with ceramics as fillers and polymers as matrices are being researched extensively. Important examples of these composite materials are the semi-crystalline polymers mixed with inorganic particles [27]. They consist of an amorphous-crystalline matrix (with a lamella thickness of typical size of 10 to 100 nm) and dispersed nanoparticles.

Nanotechnology can be defined as the design and synthesis of functional materials within nanometer scale in at least one dimension (up to 100 nm) and control and exploitation of (novel) properties and phenomena in physics, chemistry and biology depending on this length scale. The study and exploration of the potential properties of nanocomposites is the motivation of this thesis.

1.1 Overview of the Project

Why Nanotechnology?

‘What are the potential uses of nanotechnology?’ In the limited number of years that nanotechnology has been investigated, a plethora of answers to this question have been presented. It seems that nanotechnology could potentially solve almost any problem; thus, a more interesting question is, ‘what real problems will nanotechnology solve?’ Nanocomposite technology has been described as the next great frontier of material science. For example, polymer resins containing well-dispersed layered silicate nanoclays are emerging as a new class of nanocomposites. The reason is that by employing minimal addition levels of filler (< 10 wt%) nanoclays enhance mechanical, thermal, dimensional and barrier performance properties significantly. It has been said that for every 1 wt% addition, a property increase on the order of 10% (or more) is realized. This loading-to-performance ratio is known as the “nano-effect” [28].

Project motivation

The possibility of forming a nanocomposite through homogeneously dispersed inorganic fillers in a technically interesting polymer has been investigated since the early 1980’s where the advantages of *nano-* over *microstructured* particles in polymer matrices was reported [29]. Thermoplastics such as nylon (a polyamide) and polypropylene (PP) have found widespread applications in diverse areas such as household, automobile and electrical industries. These polymers derive their usefulness and versatility from their inherent toughness, chemical resistance, and good mechanical and electrical properties.

Recently, interest in rigid particle-strengthened thermoplastics has developed. With the growth of nanocomposite materials research, additional unique mechanical and shaping properties can now be realized not previously accessible with traditional composites. For example, in 1998, a nylon/silica nanocomposite was obtained through a novel method, *In-situ* polymerisation, by first suspending agglomerated 100 nm (solid) silica particles in caproamide and then polymerising the mixture at high temperature under an N₂ atmosphere [30]. Surprising was the fact that upon addition of 5 wt% of silica nanoparticles, the mechanical properties such as impact strength, tensile strength and elongation at break of the nanocomposites showed a tendency to increase. For normal polymers it is known that stiffness, impact resistance and hardness never appear in combination in which all have favourable attributes. More recently, in 2001 [31] silica sol and caprolactam were mixed into a reactor achieving a good dispersion of the nanoparticles ~50 nm. The most striking result obtained from that study was the evidence of a filler size effect on the filler dispersion (within the limited particle size studied). The surface treatment of SiO₂ by silane-coupling agent was reported in 2002 [32] improving to some extent the strength and toughness of the nylon-6.

Challenges

One of the major problems in the synthesis of nanocomposites involving the use of nanofiller particles is the aggregation of the nanoparticles that severely limits the filler loading level and, therefore, the content of the nanophases. The scientific challenges encountered in this thesis can be summarized as follows:

- To realize a dual phase composite material well-defined on a nanoscale.
- Smaller filler particle sizes than presently obtained for state of the art systems ($\varnothing < 50$ nm) and improved dispersion.
- Suitable filler concentration while retaining the good properties of the polymers.
- Study of the potential material properties of the nanocomposites.

Objectives

Synthesis of dual phase nanocomposites for consumer use consisting of:

- A technically interesting structural polymer matrix such as a polar nylon or apolar polypropylene (PP).
- An extremely well dispersed nanoscale inorganic filler phase that consists of isometric particles with nanoscale dimensions (below the common in the state of the art) and a volume fraction < 0.2 .

It is expected that in these nanoscale composites a large synergetic effect will be present between the filler and the matrix phase. This synergy is expected to provide favourable properties in addition to the properties that follow from a proper application of composite mixing rules. This has the consequence that attention was paid to the dispersion of the filler through the matrix. Van der Waals and adhesion forces that are comparatively strong for nanoscale particles naturally counteract such a well-dispersed state.

This study investigated the synthesis and properties of a nanocomposite material through film casting method using in-house prepared and commercial nanoparticles. Unlike most of the work in exploratory fields effort was focused in scaling-up the nanocomposites synthesized in the laboratory by using a twin-screw extruder.

Prospects

As stated above, this thesis has the objective of obtaining polymer/particle nanocomposites with much smaller particles and largely improved particle dispersion. This is expected to lead to completely new materials in which favourable characteristics of organic polymers and inorganic materials are combined. The developed composite materials are expected to have significantly improved nanostructural homogeneity compared to conventional composite materials. When the volume fraction of inorganic particles is low, the distance between the fillers is relatively large, and the stress field around a particle is only slightly affected by the presence of other particles and the polymer will show normal toughness. By making the particle diameter smaller prior to processing, the volume fraction can be increased and a tougher material might further result (when the volume fraction is beyond the critical value for aggregation, however, the composite becomes more brittle again due to many faults in the composite). The volume fraction of an inorganic component plays an important role in the brittle-to-ductile transition in polymer composites. The dimensions of the filler are required to be in the nanosize order to obtain a large interface, such that even a relatively low filler volume (< 5 wt%) has already a significant effect on the mechanical properties of the complete matrix.

1.2 Structure of thesis

In this thesis the synthesis of nanocomposites is described. The influence of the addition of nanosilica particles on the properties of semi-crystalline polyamide-6 (PA6) and polypropylene (PP) are investigated. A general overview of hybrid organic-inorganic nanocomposites is given in *chapter 2*. The properties of a polymer-reinforced composite are mostly influenced by the size, shape,

composition, state of agglomeration, and degree of matrix-filler adhesion [33] as well as processing parameters. Optimum surface curvature at the polymer-filler interface can be realized when large surface areas are created, which is possible when the filler particles are sufficiently small [34].

This thesis is divided into Parts I and II. Part I deals with nanocomposites based on Polyamide-6/Silica. In Part II, propylene was used as starting material to synthesize PP-SiO₂ nanocomposites. The thesis thus consist of the following chapters:

Part I. Synthesis of Polyamide-Silica Nanocomposites

In *chapter 3* the developed route to homogeneously dispersed silica nanoparticles into a Polyamide-6 is given. A facile synthesis method is demonstrated whereby nanosize silica filler particles (< 30 nm) are incorporated into a polyamide matrix at room temperature. The morphology was studied by means of Transmission Electron Microscopy (TEM) and Scanning Electron Microscopy (SEM). Inorganic filler can act as nucleation site, therefore the degree of crystallinity of the nanocomposites was determined by means of Wide-Angle X-ray diffraction (WAXD). The effect of annealed vs. compression moulded processing conditions was studied with respect to phase transitions within the polymer. Furthermore, mechanical properties of the synthesised nanocomposites are given.

In *chapter 4* the friction and wear properties were investigated on a pin-on-disk tribometer by running a flat pin of steel against the composite disc. The addition of 2 wt% SiO₂ resulted in a friction reduction (μ) when compared with pure nylon-6. Low silica loadings led to a reduction of wear rates by a factor of 140 while the influence of higher silica loadings was less pronounced.

The effects of the nanoparticles into the polymer matrix was investigated by means of Dynamic Mechanical Spectroscopy (DMS), therefore *chapter 5* deals with the melt rheology of nanocomposites.

Solution impregnations, pultrusion, film stacking are widely used methods to prepare thermoplastic composite materials. Screw extruders are encountered to melt the polymer and then to incorporate fibers to the polymer to modify physical properties. In *chapter 6*, the compounding of colloidal silica nanoparticles filled polyamide-6 (PA6) is performed with a twin-screw extruder, which has a significant market share due to their low cost and easy maintenance. The samples were characterised by Differential Scanning Calorimetry (DSC) and WAXD experiments.

Because the high surface area and interparticle distance many factors could be potentially responsible for the property changes offered by the nanosilica particles. Conventional theoretical models such as the theories of Mori-Tanaka and Kerner are used in *chapter 7* for the

prediction of nanocomposite properties and to better understand the origin of the reinforcing efficiency in the nanocomposites. Model predictions are compared to experimental mechanical property data previously reported in chapters 3 and 7.

Part II. Synthesis of Polypropylene-Silica Nanocomposites

The ever increasing interest in thermoplastics, such as polypropylene, led to research in *Chapter 8* for the feasibility of making polypropylene (PP) samples containing nanosilica particles ($\varnothing < 20$ nm). The composites were prepared *in-situ* within a one-liter Slurry Phase Polymerisation (SPP) reactor utilizing a Ziegler-Natta 4th generation catalyst. The surface of the silica particles was modified with octadecyltrimethoxysilane to prevent catalyst deactivation and to achieve better polymer/filler interaction. In addition, the kinetics of nanocomposite was studied and compared with a composite with a size diameter of 10 μm .

Following the industrial viability of processing polypropylene, in *Chapter 9* a brief study on the mechanical properties of polypropylene-silica composites is described. Tensile strain-stress and Izod-impact experiments showed that with nanosilica an improvement of the mechanical properties is obtained when compared with the pure polymer.

In *Chapter 10* general conclusions and suggestions for continuation of this research are given.

In this thesis the terms polyamide-6 (PA6) and nylon-6 are used indiscriminately.

1.3 References

- [1] Feynman, R. P. *Eng. Sci.* 23, 22 (1960).
- [2] Volkmer, D. *Chemie in unserer Zeit* 33, 6 (1999).
- [3] Porter, D.B. *Conference Proceedings from Organic-Inorganic hybrids conference* Guildford, U.K. June (2000).
- [4] Coronado, E., Galan-Mascaros, J.R., Gomez-Garcia, C.J. and Laukhin, V., *Nature* 408, 447 (2000).
- [5] Croce, F., Appetecchi, G.B., Persi, L. and Scrosati, B. *Nature* 394, 456 (1998).
- [6] Pinnavaia, T.J. *Science* 220, 365 (1983).
- [7] Wang, Y. and Herron, N. *Science* 273, 632 (1996).
- [8] Winiarz, J.G., Zhang, L.M., Lal, M., Friend, C.S. and Prasad, P.N. *J. Am. Chem. Soc.* 121, 5287 (1999).
- [9] Sidorov, S.N. *et al. J. Am. Chem. Soc.* 123, 10502 (2001).
- [10] Merkel, T.C. Freeman, B.D., Spontak, R.J., He, Z., Pinnau, I., Meakin, P. and Hill, A.J. *Science* 296, 519 (2002).
- [11] Joly, C., Smaïhi, M., Porcar L. and Noble, R.D. *Chem. Mater.* 11, 2331 (1999).
- [12] Hajji, P., David, L., Gerard, J.F., Pascault, J.P. and Vigier, G. *J. Polym. Sci.* 37, 3172 (1999).
- [13] Sanchez, C., Ribot, F. and Lebeau, B. *J. Mater. Chem.* 9, 35 (1999). Sanchez, C., LeBeau, B. and Ribot, F. *J. Sol-Gel Sci. Tech* 19, 31 (2000).
- [14] Pomogailo, A. D. *Russ. Chem. Rev.* 69, 53 (2000).
- [15] Hajji, P., David, L., Gerard, J.F., Kaddami, H., Pascault, J.P. and Vigier, G. *Mater. Res. Symp. Proc.* 576, 357 (1999).
- [16] Novak, B.M. *Adv. Mater.* 5, 422 (1993).
- [17] Lichtenha, J.D., Schwab, J.J. and Reinerth, W.A. *Chem. Innovation* 31, 3 (2001).
- [18] Sanchez, C. and Ribot, F. *New J. Chem.* 18, 1007 (1994).
- [19] Ellsworth, M.W. and Gin, D.L. *Polymer News* 24, 331 (1999).
- [20] Kwiatkowski, K. C. and Lukehart, C. M. in *Handbook of Nanostructured Materials and Nanotechnology, Volume 1: Synthesis and Processing*, Nalwa, H. S. Ed. Academic Press, San Diego, CA (2000).
- [21] Schubert, U., Hüsing, N. and Lorenz, A. *Chem. Mater.* 7, 2010 (1995).
- [22] Morikawa, A., Iyoku, Y., Kakimoto, M. and Imai, Y. *J. Mater. Chem.* 2, 679 (1992).
- [23] Reed, J.S. *Principles of Ceramics Processing* 2nd Ed. (1995).
- [24] Richerson, D.W. *Modern Ceramic Engineering* 2nd Ed. (1992).
- [25] Wypych G. *Handbook of fillers* 2nd Ed. New York (1999).
- [26] Hutchings, I.M. *Tribology. Friction and wear of engineering materials*. Ed. Edward Arnold (1992).
- [27] Schrauwen, B. *Deformation and failure of semi-crystalline polymer systems*. PhD Thesis University of Eindhoven. The Netherlands. (2003).
- [28] Liang, Y., Omachinski, S., Logsdon, J., Cho, J-W. and Lan, T. *Technical paper*, Nanocor, Inc. (2002).
- [29] Sumita, M., Shizuma, T., Misasaka, K. and Ishikawa, K. *J. Macromol. Sci., Phys.* B22(4), 601 (1983).
- [30] Yang, F., Ou, Y. and Yu, Z. *J. Appl. Polym. Sci.* 69, 355 (1998).
- [31] Reynaud, E., Jouen, T., Gauthier, C., Vigier, G. and Varlet, J. *Polymer* 42, 8759 (2001).
- [32] Li, Y., Yu, J. and Guo, Z.X. *J. Appl. Polym. Sci.* 84, 827 (2002).
- [33] Helbert, W., Cavaille, J.Y. and Dufresne, A. *Polym. Comp.* 17, 604 (1996).
- [34] Clegg, D.W. and Collyer, A.A. *Mechanical Properties of Reinforced Thermoplastics*, Elsevier (1986).

2 Hybrid Organic/Inorganic Nanocomposites

Homogeneously dispersed nanoscale inorganic filler particles in a polymer matrix improve the mechanical properties of the resulting nanocomposite. The objective of realising polymer/particle nanocomposites with much smaller particles and largely improved particle dispersion have led to completely new materials in which favourable mechanical characteristics of organic polymers and inorganic materials are combined. Such nanocomposites show a significant improvement in stiffness, toughness, impact resistance and hardness when compared with the pure polymer. Recent developments in inorganic nanoparticle synthesis have created new perspectives for achieving these goals. For future polymer industries, the competitive edge will come from a technology that excels in tailoring polymer properties and in controlling production plants toward maximising product quality.

Part of this chapter was published in:

Proc. 21st Annual European AIChE Colloquium, p 17-21, April (2000)

and it won the prize for the 3rd best poster at the contest 'R&D and its implication for the chemical industries business', Netherlands/Belgium section.

2.1 Polyamides

Products based on polyamides, such as PA6, are used in a broad range of applications in the automotive [1], electrical [2], and other industries [3]. The future success of nylon as thermoplastic (new types or reinforced) rests upon continuous innovation to meet the demands in cost, quality and competition in properties with others plastics. The technical and business aspects of nylon indicate a capacity for change, which will enable the nylon industry to overcome the challenges ahead [4].

Of all the nylons currently known, nylon-6-, -7-, -8-, -9-, -11-, and -12 are, or were manufactured on an industrial scale. Of these, nylon-6 is the best known, the most widely used, and the most studied [5,6]. The tensile strength of the nylons-4, is half that of 6-, 8-, and nylon-12. The Young modulus of nylon-4 filaments is, however, comparable with the Young modulus of nylon-6 fibers [5,6]. While nylon-6 competes mostly on the basis of price, good friction and wear characteristics [7-10], nylon-11 and nylon-12 both contain very small amounts of residual monomer, absorb only small amounts of moisture from the environment, and maintain elasticity and ductility at lower temperatures than nylon-6. The low moisture absorption results in higher strength retention, electric resistance and stability than nylon-6 upon going from the dry to the wet state. Therefore these polyamides can also lead to interesting materials and properties [11-13].

Morphological features of Polyamides.

Aliphatic polyamides (nylons) have been subjected to a variety of studies directed to understanding the crystallization behaviour, which contributes to the exceptional mechanical properties of the nylon family [5]. Morphological features such as degree of crystallinity, spherulite size, lamella thickness and fibre orientation seem to have a pronounced effect on the properties of crystalline thermoplastics and are therefore relevant parameters for prediction of fibre behaviour since (mechanical) properties (e.g. toughness) of such materials depend also on crystallinity [14-23]. Nylon-6 is commercially important and usually regarded as a dual-phase system consisting of crystalline and amorphous regions; the former exhibits two structures, namely the α -phase [24] and the γ -phase [25]. The α - and γ -phases have both monoclinic structures where hydrogen bonds are formed between antiparallel chains in the former and (through twisted chains) between parallel chains in the latter. The α -phase is most commonly observed at room temperature and the crystallization of pure nylon-6 from melt monitored by *in-situ* XRD, has been reported [16].

In nylon-6, for example, clays are used as synergist giving superior mechanical properties when compared with the pure matrix [26].

These phases are sensitive to synthesis, thermal processing conditions and filler percentage, all important aspects in thermoplastic technology. Studies have indicated that trans-crystallization and filler/matrix interfacial bonding strength may be altered during thermal processing of semicrystalline thermoplastic composites [27].

Crystallization and crystallinity

Many semicrystalline materials undergo crystal-phase transitions prior to melting. In nylon-6 crystal-to-crystal phase transition prior to melting has been observed [28-30] as well as for nylon-6/clay nanocomposites [18]. The reasons of the unprecedented improvement in performance of nylon-6 upon the addition of inorganic-nanofillers are still being investigated due to the fact that the origin and some unique behaviours are not well understood. The nature of unexpected hybrid properties synergistically derived from two components is attempted to be related to the crystalline behaviour of the nanocomposite as seen, for example, with the articles dealing with crystallization behaviour and crystal structure of nylon/clay nanocomposites [31-34].

Furthermore, the temperature at which the last vestige of crystallinity disappears plays an important role [35]. This corresponds to the minimum temperatures for melt fabrication and upon the addition of an inorganic filler such temperature could differ. The value is obtained, for example, from the disappearance of the crystalline X-ray diffraction

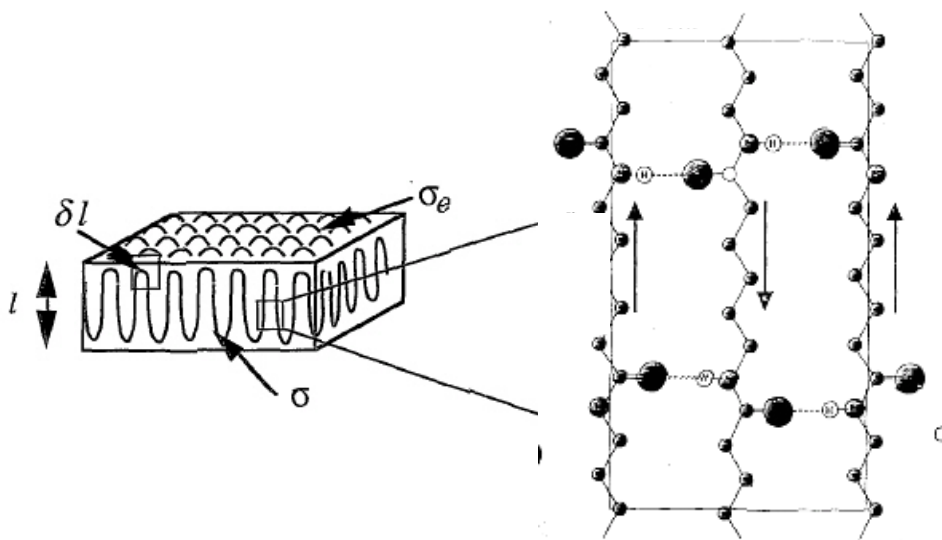


Fig. 1. Folded chains in a crystalline structure with the folded surface free energy, σ_e , and the lateral free energy, σ (left) and a projection of the unit cells of nylon-6 determined by X-ray crystallography. The lattice constants and axis angles are $a = 0.956$ nm, $b = 1.724$ nm (fiber axis) and $c = 0.801$ nm, $\alpha = \gamma = 90^\circ$ and $\beta = 67.5^\circ$ for nylon-6 (α -structure) [36-38].

pattern.

The crystal structure of nylon-6 has explained differences between its physical properties and those of nylon-66 [38]. The molecular chains fold back and forth on themselves [39]. These crystals are regularly shaped, thin platelets (or lamellae) approximately 10 to 20 nm thick, and on the order of 10 μm long. The unit cell for nylon-6 is shown in Fig. 1.

In semi-crystalline polymers, the crystal is an aggregate of a large number of single crystals arranged usually in a radial array (spherulites). It is generally recognized that the growth of a spherulite begins from a single lamellar crystal or a cluster of the lamellae [30]. In the early stages of growth, the crystals have the appearance of a sheaf, named hedrite or axialite and eventually, after equatorial filling a three-dimensional spherulitic appearance develops (Fig 2).

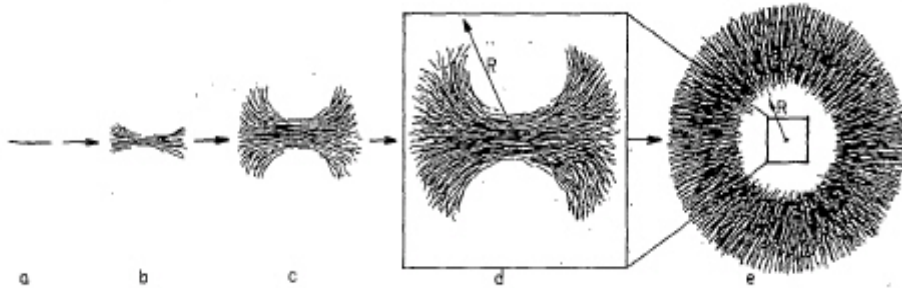


Fig. 2. A schematic representation of the successive stages of lamellar crystallization by growth via hedrites [29,30].

Mechanical Properties of the main Nylons

Nylons absorb water reversibly, which influence its mechanical properties [5]. An important guide to the effect of temperature and moisture on the properties of nylons is the glass transition temperature (T_g). Materials made from the semicrystalline nylons retain some stiffness up to their melting points, but the amorphous resins lose all mechanical integrity above T_g . Tensile strength data depend on the test conditions and temperature (temperature can be below, at or above T_g). Moisture and temperature have similar effects on the tensile properties. From Fig. 3 it can be seen that the tensile stress at the yield point decreases with increasing moisture content.

Nucleation of nylon increases the tensile strength but reduces the elongation and toughness of the resin. The tensile modulus (elastic

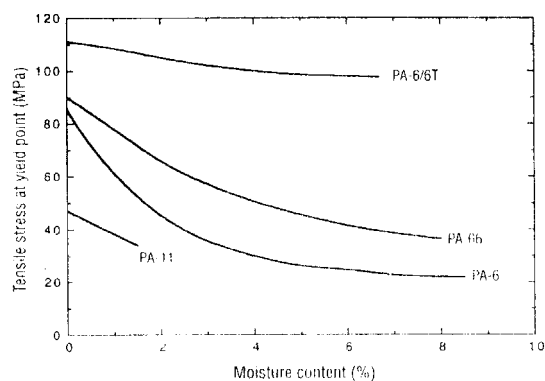


Fig. 3. Tensile stress at yield (23°C) vs moisture content [13]

modulus in tension), are also affected by the absorption of moisture [40]. It reduces the modulus and is associated with the methylene-to-amide ratio for the aliphatic nylons as noted previously.

2.2 Polypropylene

After exposing propylene to both heat and pressure with an active metallic catalyst, the propylene monomers combine to form polypropylene. Among the different commercial processes used for polyolefin production, slurry and bulk processes are the most important at present. Efforts have been concentrated on the development of efficient gas-phase polymerisation processes as well [41]. Developments in processing are combined with developments in the catalyst area. Commercial production of polypropylene is based on the use of Ziegler-Natta [42] type coordination catalysts. Polymerisation is carried out in either the liquid phase with polymer forming as a slurry of particles, or the gas phase with polymer forming dry solid particles. Current process development is strongly orientated toward improving catalyst productivity and stereospecificity to make it unnecessary to remove catalyst residues and atactic polymer from the product. Usually Ziegler-Natta catalysts are divided in four generations. The first generation of catalyst showed a relatively low activity, poor control over powder morphology and because of low activities and low isotacticity indices, the product required removal of remaining catalyst and atactic product from the polymer. An important step during polypropylene production is the pre-polymerisation process. It generally implies the separation of the catalyst activation stage from actual polymerisation stage. Pre-polymerisation is carried out under mild conditions, before the main polymerisation takes place [42].

Nylon (polyamide) and polypropylene (PP) have found widespread applications in diverse areas such as household, automobile and electrical industries. Recently, interest in rigid particle-strengthened thermoplastics has developed. With the growth of nanocomposite materials research, additional unique mechanical and shaping properties can now be realised not previously accessible with traditional composites. Therefore, these polymers derive their usefulness and versatility from their improved toughness, heat and chemical resistance, and good mechanical and electrical properties.

2.3 Inorganic Filler Particles

Inorganic particles are used in different matrices for specific purposes [43]. For metals, fillers improve high temperature creep properties and hardness when compared with the pure metal. For ceramics, fillers are used to improve their toughness [35] and for polymers for the increase of stiffness, strength, electrical properties and occasionally for

toughness. Products such as tennis rackets, golf clubs, or boats abound in our daily lives and can ‘easily’ be manufactured due to the ease with working or shaping polymeric materials because of their low melting points. Compatibility of the matrix and the filler must be considered to prepare a composite and the thermal expansion coefficients must be very close to avoid high thermal stresses that may occur at the filler matrix interface. Fillers that are most commonly added to organic polymers are of an inorganic nature.

Unfortunately, the incorporation of fillers in organic polymers can result in a brittle composite material. In addition, the amount of filler that can be incorporated is limited (sometimes the addition of higher amounts of filler does not improve the mechanical properties of the material) and the filler may not be uniformly dispersed in the organic polymer. The efficiency of the filler to modify the properties of the polymer is primarily determined by the degree of dispersion in the polymer matrix.

Comparing materials in the micro-size domain with nanosize materials could be useful to realise the importance of these nanosizes. For instance, in the 1980’s polypropylene and nylon-6 were filled with ultrafine silica [44]. Yet, in spite of the importance of these nanocomposites, very few studies have been performed so far to compare micro- and nanocomposites [45,46].

Particles typically used

In literature there are quite a lot of materials used as filler [47], but about thirteen are mostly used. Examples are gold [48,49] (gold particles have been dispersed in Nylon 11 [11]), carbon fibers [50], glass fibers [51-53], kaolin clay, mica [54], silica, talc, montmorillonite [55-58] and wollastonite clay [59].

For example, wollastonite, CaSiO_3 (Fig. 4) is a natural, reinforcing filler. The higher the aspect ratio (L/D), the better the reinforcement.

Talcum (Fig. 5) is a plate-like mineral. This kind of morphology gives reinforcing capacity to the mineral, although not all platy minerals are equally suitable for the use as reinforcing filler. A small force can delaminate a talcum particle, which is the reason why talcum would not be used in materials subjected to mechanical

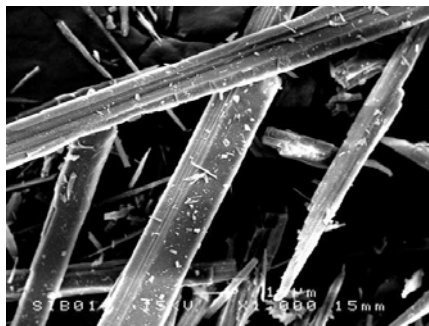


Fig. 4. Wollastonite acicular.
(Reproduced with permission from ref [60])

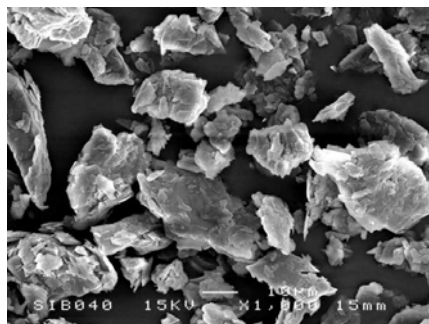


Fig. 5. Talcum (lamellar).
(Reproduced with permission from ref [60])

stresses: e.g. in glue. The affinity with the polymer is an important parameter: Talcum can reinforce PP (polypropylene). The barrier effect of plate-shaped fillers in anti-corrosion coatings is well known.

In protective coatings complex minerals are often used, for example, Plastorite (tabular) is a natural mixture of chlorite, mica and quartz. In Fig. 6 harder cristobalite is shown.

Fillers can cause abrasion (A) in mixing machinery. This abrasion is related to the particle-diameter (D) to the third power [60].

$$A \sim D^3$$

In other words a 40 μm particle is 64 times more abrasive than one of 10 μm . Fillers have also an influence on the rheology, which studies the relation between the deformation of materials and the applied forces. This relation is important during the processing and application of several agricultural and industrial products, such as paints, food, cosmetic products and biological systems [61].

Fillers with low solubility, low electrical conductivity and chemical inertness in acid and alkaline media are attractive for, for example, a paint formulator [61]. From the plastics industry it is known that even additions in small quantities can disturb durability in outdoor exposure conditions. Transition metals accelerate UV degradation of polymer binders. The curing and shelf life of some binder systems can be influenced by organic impurities. The lower the chemical oxygen demand (COD), the better. In this regard, work with 'simple', pure and inert fillers such as silica (SiO_2) or barite (BaSO_4) are desirable. SiO_2 , TiO_2 [62-64] and ZrO_2 [65] have been used as fillers for polyacrylate and polyethylene. On the other hand, polyolefin have used silicate as filler [66]. Rubber particles have reinforced nylon in polyamide-6/rubber blends [67-69].

Silica

Silica has been used in different polymers as a reinforcement material. Examples are in methacrylate [70-73], polyimide [74-75], polyamide [76], rubbery epoxies [77], and acrylic [78].

The specific function of the filler is based on the specific resin system, particle size, surface area, loading and surface modification. Because of the high bond energy in the Si-O bond, SiO_2 has extremely high

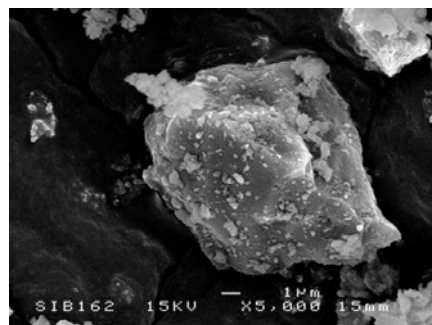


Fig. 6. Cristobalite (nodular).
(Reproduced with permission from ref [60])

thermal stability. SiO₂ also possesses a very low thermal expansion coefficient.

2.4 Stabilising suspensions using polymers

The possible use of polymers for stabilising particles in suspension largely depends on the nature of the side chains. In general, there are three mechanisms by which polymers can stabilise colloidal suspensions [79,80]:

- steric stabilisation
- electrosteric stabilisation
- depletion stabilisation

Using polymers, electrosteric stabilisation is the most common mechanism for stabilising particles in polar liquids, in apolar liquids steric stabilisation is most common. However, the influence of depletion stabilisations mechanisms should not be overlooked. The influence of other parameters (pH, solids loading, temperature, etc.) on stabilisation plays also an important role. An example of this is the influence of the molecular weight of the polymer. It has been proven that steric stabilisation is high enough by itself to fully stabilise a colloidal suspension only if the molecular weight of the polymer macromolecules is higher than 10000. This provides a sufficiently thick steric barrier. Otherwise, coagulation due to the van der Waals forces would take place. In this case the polymer also has to be strongly anchored to the surface [81].

2.5 Hybrid organic/inorganic composites

Polymer-based organic/inorganic nanocomposites have gained increasing attention in the field of materials science [82,83]. Numerous synthesis procedures are available including evaporation of elemental metal with its deposition on a polymeric matrix, plasma-induced polymerisation, etc. Reviews are found in [84,85]. Sol-gel processing, which includes two approaches: hydrolysis of the metal alcoxides and then poly-condensation of the hydrolysed intermediates is a well-known method to prepare nanocomposites [86-89]. The following methods have been lately employed to prepared nanocomposites:

***In-situ* intercalative polymerisation**

In-situ intercalative polymerisation usually implies polymer interaction with clays. The ability of intercalating polymer into silica layers was first obtained by the Toyota group [90]. Using the inherent characteristics of the alumino-silicate layer (e.g. swelling behaviour

and cation exchange), the inorganic phase could be evenly dispersed on a nanometer scale, generating strong interaction between the inorganic and organic phases. The material developed by Toyota's researches was found to have considerably improved properties, as compared to ordinary nylon-6. Through the addition of only 5 wt% clay higher tensile strength (40%), flexural strength (126%) and heat distortion (from 65°C to 152°C) were achieved. More research has been reported to incorporate clays into a polymer using nylon [91]. Nanocomposites of nylons have focused on the intercalation method used to prepare nylon/clay nanocomposites.

How the clay particles achieve these feats is not well understood. The effect seems to be related to the clay's surface area, the extent of dispersion of the clay in the matrix and/or aspect ratio. Many different polymer matrices have been reinforced with clays. Matrices researched include polyamides, epoxy resins, polystyrene, polyurethanes, polypropylene, etc. To date, only few clay nanocomposites have been successfully brought into the realm of commercial application [92-102]. This method, however, is only suitable for clay minerals.

***In-situ* polymerisation**

In-situ polymerisation is a method in which fillers or reinforcements are dispersed in a monomer first and then the mixture is polymerised using a technique similar to bulk polymerisation [103-105]. Ou *et al.* [76,103,104] reported on the preparation of nylon-6/silica nanocomposites by this method, in which silica was pre-treated with aminobutyric acid (modified silica). Scanning Electron Microscopy pictures revealed that silica was quite well dispersed in the polymer matrix and that the addition of silica increased the T_g and crystallization rate of the nylon-6 matrix. The mechanical properties of nylon-6/unmodified silica nanocomposites decreased gradually with the increment of silica content, whereas those of the nylon-6/modified silica system had maximum values at 5 wt% silica content. The feasibility of this method, however, is for polymers able to have an open polymerisation, such as caprolactam, and where the composite can remain stable at high temperatures.

Atom transfer radical polymerisation (ATRP)

The synthesis of hybrid organic/inorganic nanoparticles has been performed using ATRP. A monolayer of a silane was attached to the surface of 55 nm silica nanoparticles [106,107]. The modified nanoparticles were used as macro-initiators for styrene, resulting in a controlled living polymer from the nanoparticle surface. A good review of this method can be found in [108].

The use of microwave radiation has been used to polymerise polyamides in a rapid and efficient way. The polycondensation is

achieved in the presence of a small amount of a polar organic medium that acts as a primary microwave absorber. The reaction gives a high viscosity value for the polyamide in a shorter polymerisation time than the conventional external heating [109-111]. So far, there are several polymers successfully made throughout this method, such as nylon and inorganic materials, but no hybrid compounds have been found in the literature yet.

2.6 Nylon-6-Silica nanocomposites

State-of-the-art nylon-6/silica composites are presently formed through an *in-situ* polymerisation process (*vide supra*). Typically, such reactions require a catalyst and the silica particles require a surface pre-treatment. The solid particles are then dispersed in ϵ -caprolactam (monomer) and the mixture is heated at relatively high temperatures (> 200°C) to form nylon-6 through a ring opening polymerisation (ROP) mechanism. However, due to the thermal energy originating from the heating process, sol particles collide which lead to aggregation and grain growth of the silica particles. The phenomenon becomes particularly problematic when the silica particles are below 50 nm in diameter [45]. Furthermore, such a process is limited to the family of nylons that rely on a ROP mechanism, where the monomer can act as polymer precursor. The method is therefore not amenable to nylons where a condensation mechanism is involved (e.g. nylon-6,6).

More recently, silane treatment has been applied to the preparation of nylon-6/nano-SiO₂ composites, with 4% of silica content, through *In-situ* polymerisation. The results revealed that the reactivity of the silica remained in both treated and not treated silica. In addition, dynamical and mechanical tests showed an improvement of strength and toughness of the composite materials. The activity of silica fillers depends upon the chemical structure of the silica surface. A way to modify the hydrophilic character of the silica is silane coupling, in which agents are used [112,113].

More of the PA6-SiO₂ nanocomposites obtained so far have used powder-state silica. Rusu [114] prepared the nanocomposite through *In-situ* polymerisation by uniaxially rotational moulding. The effects of addition of unmodified and modified silica's on the physical and mechanical properties of PA6 nanocomposites were also investigated. Reynaud *et al.* [45] produced by nanocomposites *in situ* polymerisation using silica sol (Klebosol) (instead of powder silica) and caprolactam.

2.7 Conclusions

In literature, the objective of realising polymer/particle nanocomposites with much smaller particles and largely improved particle dispersion lead to completely new materials. More favourable mechanical characteristics of organic polymers and inorganic materials are combined when compared with conventional (micro) materials.

Presently, nylon-6/silica nanocomposites are primarily prepared by *in-situ* polymerisation of caprolactam and silica powder. A good dispersion of the inorganic filler using colloidal silica with \varnothing 50-80 nm was found only in the recent work of Reynaud *et al.* [45].

The use of colloidal silica is expected to stimulate new concepts for polymer composite and inorganic particle dispersion synthesis. The composite materials to be developed using colloidal silica with $\varnothing \leq 30$ nm are expected to have significantly improved nanostructural homogeneity compared to conventional composite materials. This, in turn, will enable more precise and systematic studies of composite nanostructures.

2.8 References

- [1] Crosbie, P. and Morris, S. *Soc. Plastics Eng.* 3, 2 (2003).
- [2] Comdir.co.uk/products/3056/010/3056_010.pdf
- [3] Lan, T., Cho, J., Liang, Y., Qian, J. and Maul, P. *Nanocor, Technical paper*, June, 25 Chicago USA (2001).
- [4] Novak, B.M. *Adv. Mater.* 5, 422 (1993).
- [5] Aharoni, S.M. *n-Nylons: Their synthesis, structure and properties*. Wiley, Great Britain (1997).
- [6] Kohan, M.I. *Nylon, Plastics Handbook*, Hanser, New York (1995).
- [7] Tanaka, K. *Wear* 75, 183 (1982).
- [8] Watanabe, M.H. and Yamaguchi, Y. *Wear* 110, 379 (1986).
- [9] Theberge, J.E. *Proc. Anniv. SPI (Soc. Plast. Ind.)*, Reinf. Div., 25th, 2-D, 1 (1970).
- [10] Bahadur, S. and Polineni, V.K. *Wear* 200, 95 (1996).
- [11] Sayo, K., Deki, S. and Hayashi, S. *J. Mater. Chem.* 9, 937 (1999).
- [12] Griehl, W. and Ruestem, D. *Ind. Eng. Chem.* 62, 17 (1970).
- [13] Satoto, R., Nakayama, K., Kaito, A. and Kyotani, M. *Asean J. Sci. Technol. Develop.* 11, 99 (1994).
- [14] Mathot, V.B.F. *Thermal states of polymers as related to molecular structure and morphology*. RPK lecture, Utrecht. The Netherlands (2001).
- [15] Muellerleile, J.T. and Freeman, J. *J Appl Polym Sci.* 54, 135 (1994).
- [16] Ramesh, C., Keller, A. and Eltink, S.J. *Polymer* 35, 2483 (1994).
- [17] Klein, N. and Marom, G. *Composites* 25, 706 (1994).
- [18] Fouda, I.M., El-Nicklawy, M.M., Nasr, E.M. and El-Agamy, R.M. *J Appl Polym Sci.* 60, 1247 (1996).
- [19] Liu, X. and Wu, Q. *Polymer* 43, 1933 (2002).
- [20] Zhang, Q., Mo, Z., Liu, S. and Zhang, H. *Macromolecules*, 33, 5999 (2000).
- [21] Joly, C., Smahi, M., Porcar, L. and Noble, R.D. *Chem. Mater.* 11, 2331 (1999).
- [22] Lincoln, D.M., Vaia, R.A., Wang, Z.G. and Hsiao, B.S. *Polymer* 42, 1621 (2001).
- [23] Cho, J.W. and Paul, D.R. *Polymer* 42, 1083 (2001).

- [24] Holmes, D.R., Bunn, C.W. and Smith, D.J. *J Polym Sci.* 17, 159 (1955).
- [25] Arimoto, H., Ishibashi, M., Hirai, M. and Chatani, Y. *J Polym Sci.* 3, 317 (1965).
- [26] Kojima, T., Usuki, A. and Kawasumi, M. *J. Mater. Res.* 8, 5 (1993).
- [27] Saiello, S., Kenny, J. and Nicolais, L. *J Mater Sci.* 25, 3493 (1990).
- [28] Hirschinger, J., Miura, H., Gardner, K.H. and English, A.D. *Macromolecules* 23, 2153 (1990).
- [29] Murthy, N.S., Curran, S.A., Aharoni, S.M. and Minor, H. *Macromolecules* 24, 3215 (1991).
- [30] Vasanthan, N., Murthy, N.S. and Bray, R.G. *Macromolecules* 31, 8433 (1998).
- [31] Kojima, Y., Matsuoka, T., Takahashi, H. and Kurauchi, T. *J. Appl. Polym.* 51, 683 (1994).
- [32] Kojima, Y., Usuki, A., Kawasumi, M., Okada, A., Fukushima, Y., Kurauchi, T. and Kamigaito, O. *J. Mater. Res.* 8, 1185 (1993).
- [33] Mathias, L.J., Davis, R.D. and Jarrett, W.L. *Macromolecules* 32, 7958 (1999).
- [34] Cartledge, H. C.Y. and Baillie, C.A. *J Mater Sci.* 34, 5099 (1999).
- [35] Callister, W.D. *Materials Science and Engineering. An Introduction.* 5th Ed. John Wiley & Sons, Inc. (1999).
- [36] Bulte, A.M.W. *Nylon 4,6 as membrane material.* PhD Thesis. University of Twente. The Netherlands (1994).
- [37] Beekmans, L.G.M. *Morphology Development in Semicrystalline Polymers by in situ Scanning Force Microscopy.* University of Twente. PhD Thesis, Chapter 2 and references therein, The Netherlands (2002).
- [38] Mo, Z. and Zhang H. *J. Macromol Chem Phys*, C35, 555 (1995).
- [39] Magill, J.H. *J. Mater. Sci.* 36, 3143 (2001).
- [40] Gaymans, R.J., Borggreve M. and Spoelstra, A.B. *J. Appl. Polym. Sc.* 37, 479 (1989).
- [41] Mattos Neto, A.G. and Pinto, J.C. *Chem. Eng. Sci.* 56, 4043 (2001).
- [42] Pater, J. *Prepolymerization and morphology.* PhD Thesis. University Twente. The Netherlands (2001).
- [43] Wypych, G. *Handbook of fillers.* 2nd Edition. New York (1999).
- [44] Sumita, M., Shizuma, T., Misasaka, K. and Ishikawa, K. *J. Macromol. Sci., Phys.* B22(4), 601 (1983).
- [45] Reynaud, E., Jouen, T., Gauthier, C., Vigier, G. and Varlet, J. *Polymer* 42, 8759 (2001).
- [46] Petrović, Z.S., Javni, I., Waddon, A. and Bánhegyi, G. *J. Appl. Sci.* 76, 133 (2000).
- [47] Rubin, I. *Handbook of Plastic Materials and technology,* John Wiley & Sons, inc. (1990).
- [48] Deki, S. *et al.*, *J. Mater. Chem.* 9, 937 (1999).
- [49] Kunikate, T., Sutoh, M. and Yonezawa, T. *Chem Lett*, 7, 619 (1997).
- [50] Mucha, M., Marszalek, J. and Fidrych, A. *Polymer* 41, 4137 (2000).
- [51] Javangula, S., Ghorashi, B. and Draucker, C. *J. Mater. Sci.* 34, 5143 (1999).
- [52] O'Donnell, B. and White, J. R. *Plast. Rubber Compos. Process. Appl.* 22, 69 (1994).
- [53] Shaterzadeh, M., Gauthier, C., Gerad, J., Mai, C. and Perez, J. *Polym. Comp.* 19, 6 (1998).
- [54] Watari, T., Yamane, T., Moriyama, S., Torikayi, T., Imaoka, Y. and Suehiro, M. *Mater. Res. Bull.* 32, 719 (1997).
- [55] Aranda, P. and Ruiz, E. *Adv. Mater.* 2, 11 (1990).
- [56] Giannelis, E. and Messersmith, P. *J. Polym. Sci.* 33, 1047 (1995).
- [57] Biswas, M. and SinhaRay, S. *Mat. Res. Bull.* 34, 1187 (1999).
- [58] Okada *et al.* *Polym. Prep.* 28, 447 (1987).
- [59] Hawley, G. and Jaworski, B. *Ann. Tech. Conf. Soc. Plast. Eng.* 56th 3, 2847 (1998).
- [60] van Aken, L. *Strong mineral for better paint performance,* Sibelco, Conference Finland (2000).

- [61] Berlin, A.A., Volfson, S.A. Enikolopian, N.S. and Negmatov, S.S. *Principles of polymer composites*. Springer-Verlag Heidelberg, Chapter 9 (1986).
- [62] Pierre, A., Campet, G., Han, S., Huang, S., Duguet, E. and Portier, J. *Act. Passive Electron. Compon.* 18, 31 (1995).
- [63] Jiang, W. and Tjong, S. *J. Appl. Polym. Sci.* 73, 2985 (1999).
- [64] Colvin, L. *et al. J. Am. Chem. Soc.* 121, 1613 (1999).
- [65] Singh-Nalwa, H. *Handbook of Nanostructures Materials and Nanotechnology*, Acad. press (2000).
- [66] Coates, W. *et al. Chem. Comm.* 73, 2179 (1999).
- [67] Dijkstra, K. *Deformation and fracture of nylon-6 rubbers blends*. PhD Thesis. University of Twente. The Netherlands (1993).
- [68] Borggreve, R.J.M. *Toughening of polyamide-6*. PhD Thesis. University of Twente. The Netherlands (1988).
- [69] Feng, Ch. and Dah, C. *Adv. Chem.* 252, 279 (1996).
- [70] Brinker, J. and Scherer, G. *Sol-Gel Science*, Academic Press (1990). D.H. Everett, *Basic principles of colloid science* Ed. The Royal Society of Chemistry, print. Whitstable, Kent, UK (1988).
- [71] Vigier, G., Pascualt, J., Gerard, J., David, L. and Haiji, *J. Polym. Sci.* 37, 3172 (1999).
- [72] Mallouk, T., Ollivier, J. and Johnson, S. *Science* 283 (1999).
- [73] Landry, Ch. and Coltrain, B. *Polymer* 33, 7 (1992).
- [74] Smaih, M., Joly, C. and Noble, R. *Chem. Mater.* 11, 2331 (1999).
- [75] Yang, Y., Yin, J., Qi, Z. and Zhu, Z. *J. Appl. Polym. Sci.* 73, 2977 (1999).
- [76] Yang, F., Ou, Y. and Yu, Z.-Z. *J. Appl. Polym. Sci.* 69, 355 (1998).
- [77] Kolarik, J., Dukh, O., Matejka, L. *Polymer* 41, 1449 (2000).
- [78] Qiu, k. and Huang, Z. *Polymer* 38, 521 (1997).
- [79] Everett, D.H. *Basic principles of colloid science*. Ed. The Royal Society of Chemistry, print. Whitstable, Kent, UK (1988).
- [80] Horn, R.G. *Particle interactions in suspensions* pp. 58-101 in: Ceramic Processing, edited by R.A. Terpstra, P.P.A.C. Pex and A.H. de Vries, 1st ed. Chapman and Hall, London (1995).
- [81] Israelachvili, J.N. and Adams, G.E. *J. Chem. Soc. Faraday Trans.* 74, 975 (1978).
- [82] Laridjani, M., Lafontaine, E. and Judeinstein, P. *J. Mater. Sci.* 34, 5945 (1999)
- [83] Pinnavaia, T.J. *Polymer-clay nanocomposites*. Ed. Wiley (2001).
- [84] Pomogailo, A.D. *Usp. Khim.* 66, 750 (1997).
- [85] Pomogailo, A.D. *Plat. Met. Rev.* 38, 60 (1994).
- [86] Pierre, A.C. *Am. Ceram. Soc. Bull.* 70, 1281 (1991).
- [87] Scherer, G.W.J. *Non-Cryst. Solids* 87, 199 (1986).
- [88] Wilkes, G.L., Huang, H.A.R. and Glaser H. Eds. J.M. Ziegler and F. G. Feazon *Advances in Chemistry series 224, American Chemical Society, Washington DC*, 207 (1990).
- [89] Brinker, C.J. and Scherer, G.W. San Diego, Academic Press, (1990). Zhu, Z. *et al. J. App. Polym. Sc.* 73, 2977 (1999).
- [90] Kurauchi, T., Okada, A., Nomura, T., Nishio, T., Saegusa, S. and Deguchi, R. *SAE Technical Paper Series*, 910, 584 (1991).
- [91] van Es, M. *Polymer-Clay Nanocomposites. The importance of particle dimensions*. PhD Thesis. University of Delft. The Netherlands (2001).
- [92] Tomlin, A., Fay, A., Lan, T. and Qian, G. US6462122 10.08 (2002).
- [93] Lan, T., Barbee R.B., Gilmer, J.W., Matayabas, J., James Ch. and Psihogios, V. US6391449 05.21 (2002).
- [94] Lan, T., Barbee, R.B., Gilmer, J.W., Matayabas, Jr. and James, Ch. US6387996 05.14 (2002).
- [95] Lan, T., Connell, G., Gilmer, J., Matayabas, Jr, James, Ch., Psihogios, V. and Turner, S. R. US6376591 04.23 (2002).
- [96] Karasawa, K. US6339690 B2 06.04 (2002).
- [97] Lan, T., Liang, Y., Westphal, E. and Psihogios, V. US6262162 07.17 (2001).

- [98] Beall, G., Goldman, A., Sorokin, A. and Tsipursky, S. US5880197 03.09 (1999).
- [99] Goldman, A., Sorokin, A. and Tsipursky, S. US5877248 03.02 (1999).
- [100] Beall, G., Goldman, A., Sorokin, A. and Tsipursky, S. US5698624 12.16 (1997).
- [101] Beall, G., Goldman, A., Sorokin, A., and Tsipursky, S. US5578672 11.26 (1996).
- [102] Tsipursky, S., Beall, G., Goldman, A. and Sorokin A. US5552469 09.03 (1996).
- [103] Ou, Y. *et al. J. Polym. Sci.* 36, 789 (1998).
- [104] Ou, Y. *Appl. Polym. Sci.* 64, 2317 (1997).
- [105] Lantelme, B. *et al. J. Non-Cryst. Solids* 194, 63 (1996).
- [106] von Werne, T. and Patten, T. *Polym. Matter. Sci. Eng.* 80, 465 (1999).
- [107] von Werne, T. and Patten, T. *J. Am. Chem. Soc.* 121, 7409 (1999).
- [108] Kickelbick, G. *Prog. Polym. Sci.* 28, 83 (2003).
- [109] Imai, Y. *Polymer Journal* 28, 256 (1996).
- [110] Imai, Y. *Adv. Polym. Sci.* 140, 1 (1999).
- [111] Rao, K. *et al. Chem. Mater.* 11, 882 (1999).
- [112] Li, Y., Yu, J., and Guo, Z-X. *J. Appl. Polym. Sci.* 84, 827 (2002).
- [113] Jesionowski, T. and Krysztafkiewicz, A. *Appl. Surf. Sci.* 172, 18 (2001).
- [114] Rusu, G. *Materiale Plastice* 39, 3 (2002).

3 Synthesis, Microstructure and Mechanical Testing of Nanocomposites

A hybrid inorganic-polymer composite was formed by incorporating nanosize silica filler particles ($\varnothing < 30$ nm) to a nylon-6 matrix. The composites were microtomed and examined with TEM, which revealed that the silica particles were well dispersed and non-aggregated. Optimisation of the synthesis conditions relied on appropriate choice of organic solvent and pH control. Two types of samples were investigated: annealed thin films (70-200 μm) and compression moulded disks (~ 1 mm) obtained by heat treatment of the aforementioned films. The degree of crystallinity was determined by wide-angle X-ray diffraction (WAXD) and the melting behaviour by differential scanning calorimetry (DSC) measurements. The degree of crystallinity increased with low silica loadings (< 7 wt%) but upon further increasing filler wt%, the degree of crystallinity decreased, more dramatically for the thin films when compared to compression moulded samples. The effect of annealed vs. compression moulded processing conditions was studied with respect to phase transitions within the polymer. Compared to pure nylon-6, mechanical tests on the hybrid composite showed an increase in E-modulus as a function of filler percentage, and a strain-at-break of > 0.5 .

Part of this chapter was presented by the author as an oral presentation during

Materials Research 2001 in Veldhoven, 8-9 May 2001, The Netherlands

2nd poster prize during the First International Silica Conference (2001), in Mulhouse, France.

3.1 Introduction

The chemical industry benefits from the use of inorganic fillers in thermoplastic polymer matrices to save costs and to improve the mechanical properties. Structural composite applications are found in defence, aerospace, and commercial aircraft [1]. The mechanical properties are related to the microstructure, which is influenced by the morphology, surface-structure, size and degree of aggregation of the filler component. Experimental studies have indicated that using conventional micron-sized filler particles, certain physical properties (e.g. increased surface smoothness) cannot be achieved when compared with nanosized particles of similar composition, and the mechanical properties are (generally) also inferior [2]. Intensive research endeavours have therefore been devoted to understand the structure-property relationships in many nanocomposite systems [3].

The final properties of a semi-crystalline polymer are determined by its internal structure, which itself is established during the processing conditions of that product. For example, during injection moulding, a polymer melt is injected into a cold mould and crystallizes subsequently during cooling in the mould. During compression moulding a plastic material is placed in an open mould, which is then closed. Pressure applied to the mould halves that come together forces the plastic to flow and fill the cavity. These flow gradients can act as a source of viscoelastic stresses modifying nucleation and crystallization leading to different types of crystalline structures [4].

3.2 Objectives

The aims of the investigation described in this chapter were to a) seek a general and facile synthesis strategy by which nanoscale inorganic filler particles ($\varnothing < 30$ nm) can be well dispersed into a polyamide matrix, b) compare processing conditions focused on the crystallization behaviour of the nylon-6 in the presence of nanoscale silica particles c) study the way in which silica nanoparticles alters crystallisation behaviour and morphology and d) subject the composites to mechanical tests. The motivation to obtain good dispersion stemmed from the observation that if any properties are to be further improved, then the distribution of the inorganic filler particles in the polymer matrix has to be as homogeneous as possible.

3.3 Experimental

3.3.1 Synthesis

Silica. Silica nanoparticles were provided by Nissan Chemicals (Japan) as a gift under brand name Snowtex[®] as an acidified aqueous sol with particle sizes 10-30 nm with a pH = 2.7. Ethanol based silica particles were prepared in-house. For the preparation of silica nanoparticles, tetraethylorthosilicate (TEOS) was added to ethanol (1:1) in an N₂-glove-box. The mixture was stirred and 11 ml of 0.7 M HNO₃ was added. The sample was heated to 60°C and afterwards placed in an ice-bath. The silica sol was then dispersed in 90 ml ethanol and kept in the refrigerator for one week [5]. The particle size was on average 10 nm as confirmed by Photon Correlation Spectroscopy (PCS). Silica Aerosil[®] (white powder) and Silica Sipernat[®] were used for the melt-extrusion samples.

Polyamide-6. Polyamide (as pellets) and reagent grade formic acid were obtained from Aldrich (PA6-PAL) with molar mass $M_n = 16900$, molecular weight $M_w = 30300$ g/mol, intrinsic viscosity $\eta_{intr} = 1.179$ dl/g and DSM Akulon[®] (PA6-PAK) with $M_n = 17100$, $M_w = 35400$ and $\eta_{intr} = 1.362$ dl/g.

Synthesis. All samples were made by dissolution method or by melt-extrusion. To refer to a sample throughout this thesis, the amount of silica and the dispersed agent in the sample is always mentioned. For example, PASW5 reads PA6 with silica sol dispersed in water 5 wt% and PASE1 reads PA6 with silica sol ethanolic solution 1 wt%.

Polymer Solutions. In a nitrogen atmosphere, nylon-6 (~10 g) was added to formic acid using a volumetric pipette (45 ml) and stirred until a clear solution emerged (~3 hours). The silica sol was added to the nylon solution and stirred gently (rapid stirring enhances aggregate formation) at room temperature for 1-3 hours.

Film formation. Film casting is widely used to produce plastic films. Depending upon the material and the operating conditions, different widths and thickness profiles of the film were obtained. The solution was then cast onto clean glass using a Doctor Blade[™] equipment (35 x 21 x 1 cm) forming a liquid layer, approximately 2 mm in height, covered the whole glass plate. The solvent evaporated under a flow of nitrogen gas. Further vacuum and heat (60-80°C) treatment formed dry, opaque composites consisting of amorphous silica and semi-crystalline nylon-6.

Drying of the samples was done in a vacuum oven at 75°C for 2 days. Annealing was done for 24 hours at 130°C.

Samples were shaped with injection moulding or compression moulding at 250-260°C (see Chapter 4). In the case of compression moulding, plates of 1 mm thick were made and the test samples were machined out of these plates. Elastic modulus (stiffness) has to be

measured in the elastic range of the material and is measured most accurately with the use of an extensometer, with a gauge length of 10 mm. In this case the displacement (strain) was measured up to a strain of 2% with the extensometer. The force was also measured and from the stress-strain curves the elastic modulus was calculated. The testing speed was at 1 mm/min.

To investigate the effect of annealing and water absorption on the nylon, tensile test bars according to ISO 527 type 1BA were injection moulded.

Conditioning in water of the samples was done for 24 hours at 65°C. The weight of the samples was measured before and after this conditioning, and the weight% of water in the wet samples was calculated to be below 10%.

3.3.2 Characterisation of nanocomposites

The amount of silica (as wt%) was verified by means of X-Ray Fluorescence (XRF); X-Ray Diffraction (XRD) was used to determine the crystalline phase of the polyamide [5]. Differential Scanning Calorimetry (DSC) was used to determine the melting point of the samples. Transmission Electron Microscopy (TEM) and Nuclear Magnetic Resonance (NMR) experiments were performed for further characterization of the silica particles and nylon-6. The degree of crystallinity of the nanocomposites was determined by the graphic multiplex resolution method [6].

Quantitative XRF analysis and Solution ¹H-NMR of nanocomposites

Quantitative XRF was used to determine the amount (wt%) silica present in each bulk sample. Analysis was performed on a Philips PW 1480/10 fluorometer (Eindhoven, The Netherlands). The calculation method used the program XRF-COMBI [7]. In the case of flat films masks of Ø 11 mm or 24 mm were used. The used standard consisted of 8.17% SiO₂ in Li₂B₄O₇. The fused beads were made by dissolving the nylon-silica in lithiumtetraborate. The mixture was heated for about one hour at 1100°C until the sample was melted, resulting (after pouring) in a flat bead. The sample was weighed before and after the procedure to allow the calculation by ignition of the sample. Finally for small tablets a certain amount of the sample was pressed and placed in the mask.

¹H and ¹³C NMR spectra were obtained at 300 MHz using a Varian Unity 400 spectrometer.

Transmission Electron Microscopy (TEM)

Transmission Electron Microscopy (TEM) micrographs were obtained using a JEOL 2010F equipped with a field-emission gun operating at 200 kV. TEM samples were prepared by ultramicrotoming thin sections of the polyamide/silica nanocomposite with a diamond knife. These thin sections were then captured on Formvar coated Ni grids. The particles observed in the micrographs were unambiguously identified as silica by using both X-Ray Energy Dispersive Spectrometry (EDAX R-TEM Sapphire detector equipped with a super-ultra thin window) and Energy Filtering (Gatan Imaging Filter 2001) attached to the TEM.

For the particle Measurements, the Soft Imaging System analySIS® program was used.

X-Ray Diffraction

X-ray powder diffraction data were collected on a Philips PW3710 based X'Pert-1 diffractometer in Bragg-Brentano geometry, using a θ compensating divergence slit. Powder diffraction data collection was performed at room temperature, using a "zero"-background spinning specimen holder. Peak positions and peak intensities were extracted using the pattern decomposition program PROFIT available in the PC software package X'PERT LINE supplied by Philips (Eindhoven, The Netherlands). The observed individual lines and clusters of lines were fitted using Pearson VII functions, taking into account the $K_{\alpha 2}$ component. The obtained peak positions and relative intensities are extracted from the analytical $K_{\alpha 1}$ peak profiles. The relative intensities are based on peak heights using a θ compensating divergence slit. From these, relative intensities were calculated for a fixed slit width of 1° . The XRD pattern of amorphous nylon is a broad, diffuse peak with a maximum intensity at *ca.* 22° as shown by Wide Angle X-Ray (WAXD). For XRD measurements loadings of 1, 4, 8, 23, 35, and 57 wt% SiO_2 were used. The degree of crystallinity was determined by graphic multippeak resolution method [5].

Differential Scanning Calorimeter (DSC)

Equilibrium thermodynamic parameters were determined using a Setaran Setsijs 16 Differential Scanning Calorimeter (DSC), the temperature was calibrated with indium. Sample weights were between 10-15 mg. The samples were heated quickly (at $10^\circ\text{C}/\text{min}$) to 20-30°C above the melting temperature, kept constant for 10 min to eliminate residual crystals and then cooled to room temperature. The DSC analyses led to the thermodynamic values of the melting temperature (T_m) and the change in enthalpy (ΔH).

3.4 Results and Discussion

3.4.1 Dispersion

TEM images of PA6

Three different types of silica's with the same filler percentage (5 wt%) were used to make the nanocomposites: Snowtex[®] (SX), Sipernat[®] (ST) and AEROSIL[®] (MOX).

The polyamide matrix contains the smallest spherical silica nanoparticles (SX) with negligible aggregation in the range 10-30 nm reported to date (see Fig. 1 and 2). For the TEM investigation the sample was ultramicrotomed to a thickness where the silica particles showed good visual contrast with the polymer matrix. TEM pictures taken from different sample localities revealed an even distribution of the silica particles throughout the matrix. The TEM micrographs indicated several unique properties of the composite resulting from the new synthesis method, namely a) silica particles were all in the 10-30 nm size range, b) silica particles were non-aggregated and c) silica particles were rather well dispersed (good homogeneity) inside the polyamide matrix. Figs. 1a-1b show the TEM pictures of a sample containing 3 wt% silica. We chose filler additions in the range 1-5 wt% because it is evident from current literature that a maximum of 5 wt% filler loadings already leads to an optimum in mechanical properties [8-11].

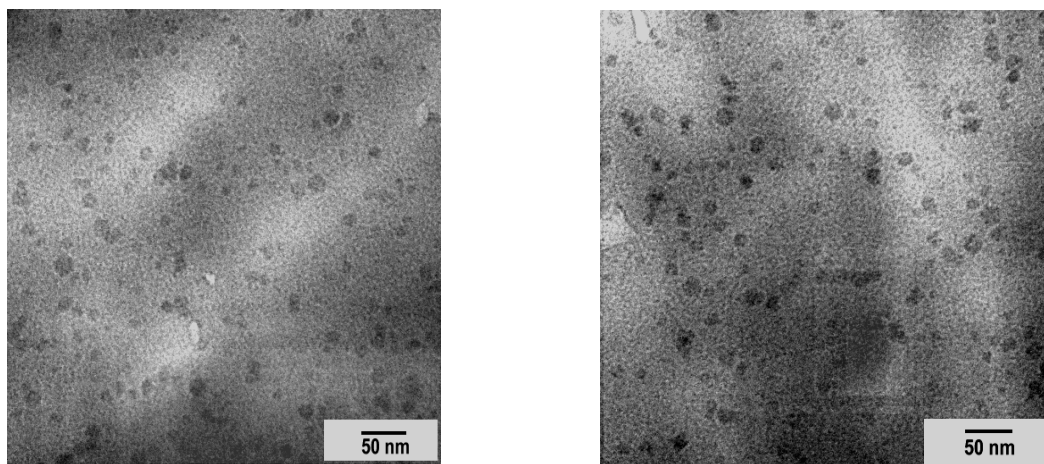


Fig. 1a and 1b. TEM images of a nylon-6/silica-sx (3 wt%) nanocomposite.

TEM images of PA6 with different silica

As can be seen from Fig. 2a and 2b a relatively good dispersion was obtained upon addition of 5 wt% silica sol (SX) with an average particle size of < 30 nm. Upon addition of powder silica in a mini extruder with the same particle size (ST), aggregation was observed (Fig. 3a and 3b) and when higher particles size was used (0.1 μm , MOX) small clusters were encountered as seen in Fig. 4a and 4b.

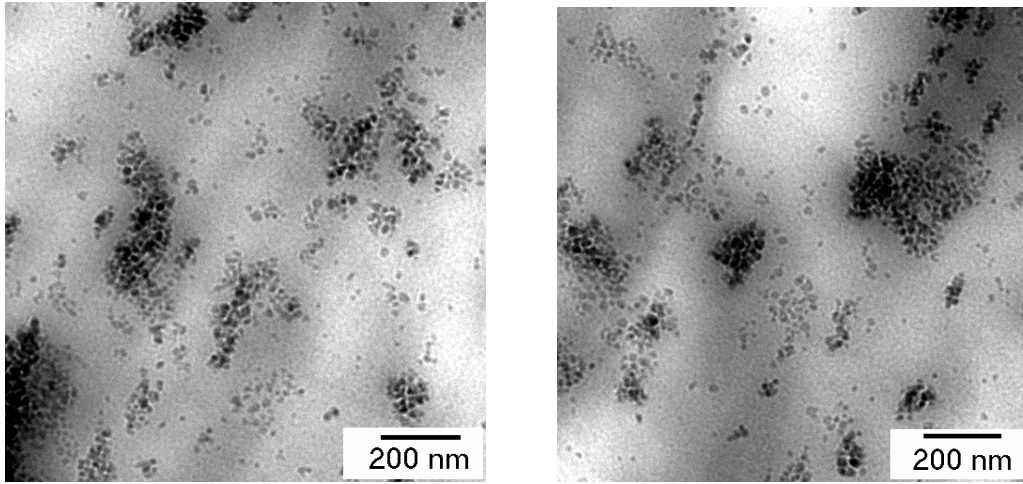


Fig. 2a and 2b. TEM images of a nylon-6/silica SX (5 wt%) nanocomposite.

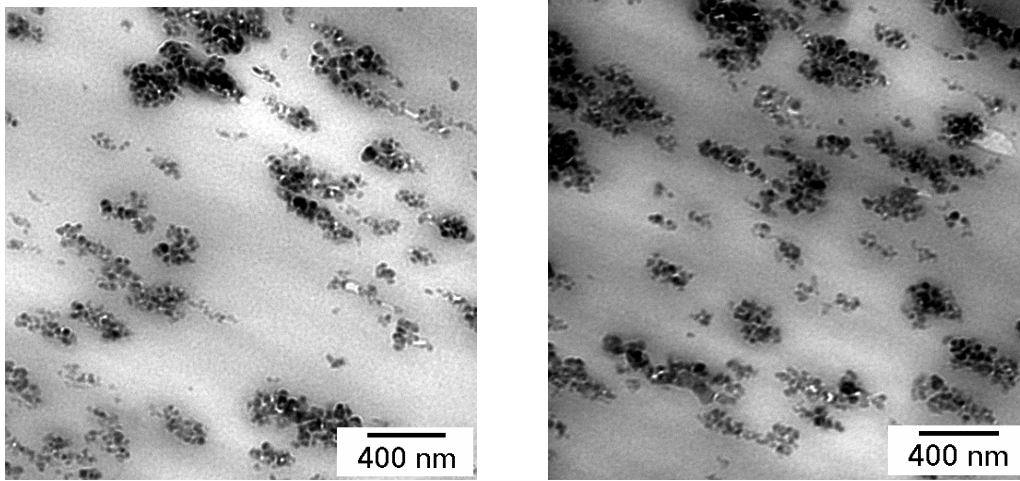


Fig. 3a and 3b. TEM images of a nylon-6/silica ST (5 wt%) nanocomposite.

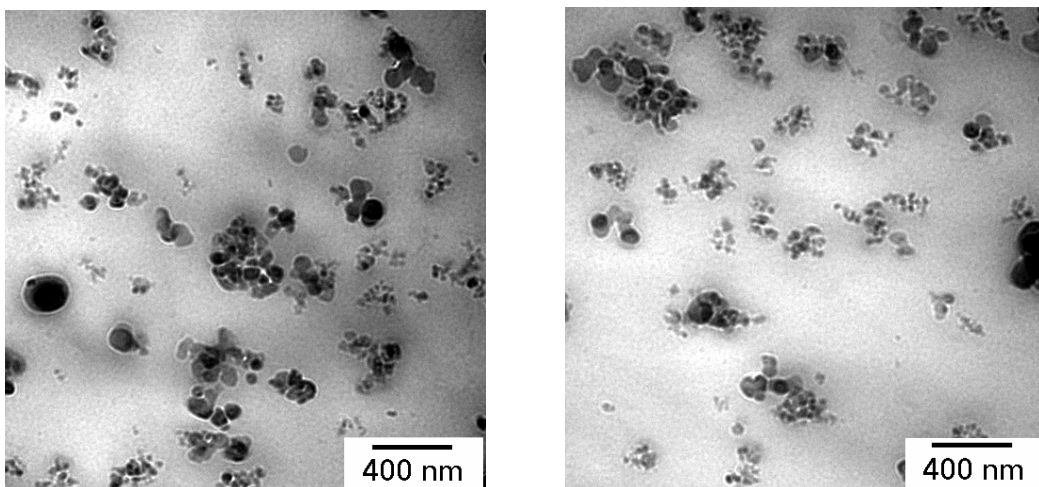


Fig. 4a and 4b. TEM images of a nylon-6/silica MOX (5 wt%) nanocomposite

3.4.2 Solution ^1H and ^{13}C -NMR of nanocomposites

Fig. 5 gives ^1H -NMR spectra of the products. Concentrations of 70 mg polymer per ml solvent were used to perform the experiment. ^1H NMR spectra of pure polymer and composite showed a chemical shift of hydrogen-bonded protons at 12.3 ppm. Chemical shifts of the CH_2 groups adjacent to the NH group and CO group were observed around 3.6 and 2.8 ppm, respectively. Chemical shifts of the remaining aliphatic CH_2 protons were observed around 1.9 ppm (4H) and 1.6 ppm (2H).

^{13}C NMR spectrometry of pure polymer and composite gave a peak at 179 ppm corresponding to the carbon of the amido group (Fig. 6). The peaks at 42 and 33 correspond to the carbon atoms next to the amido groups (*i.e.* $-\text{CONHC}^*\text{H}_2-$ and $-\text{C}^*\text{H}_2\text{CONH}-$, respectively), whereas the signals at 26, 25 and 24.5 ppm belong to the remaining aliphatic carbon atoms. ^1H NMR and ^{13}C NMR spectrum of the composite was completely in accordance to the anticipated chemical structure for nylon-6 [12-14].

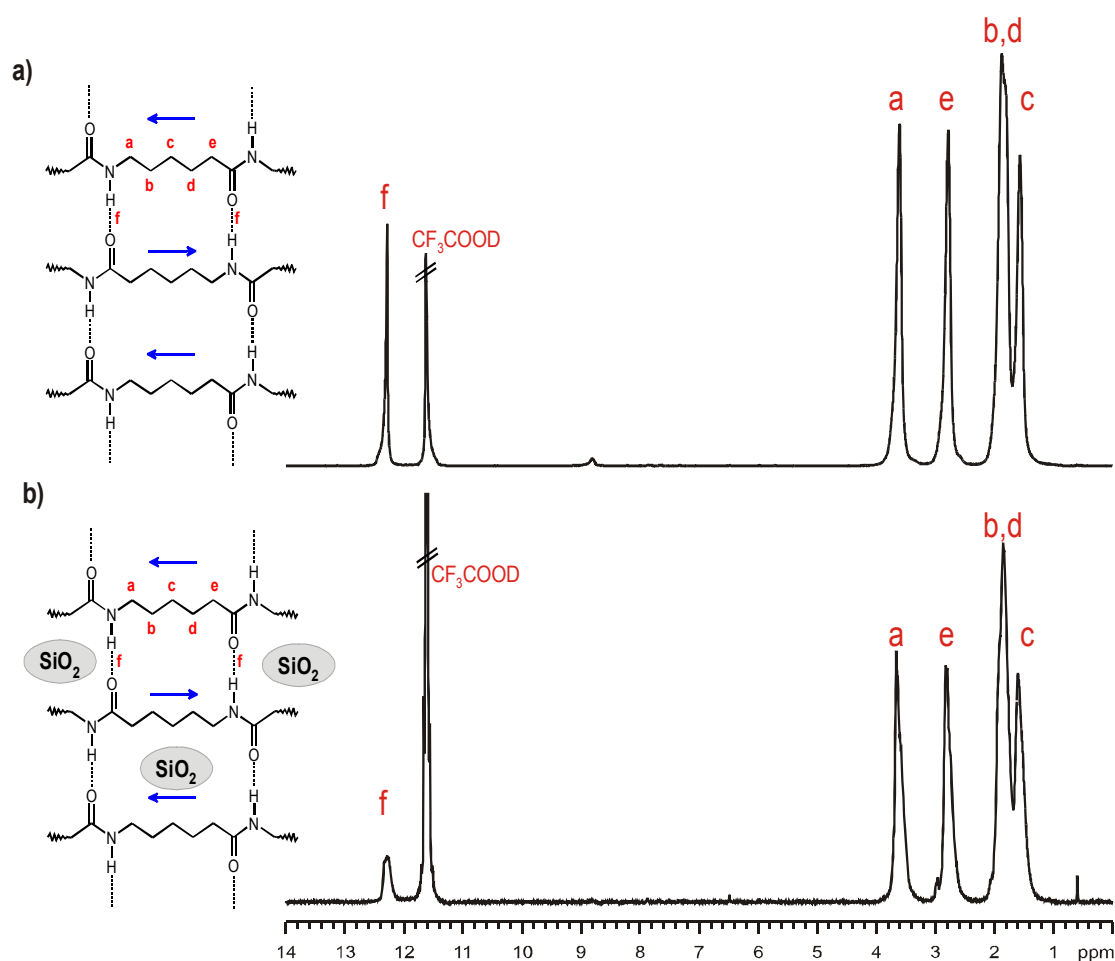


Fig. 5. ^1H NMR spectra of a) Ny-6, b) Ny-6 & SiO_2 in CF_3COOD .

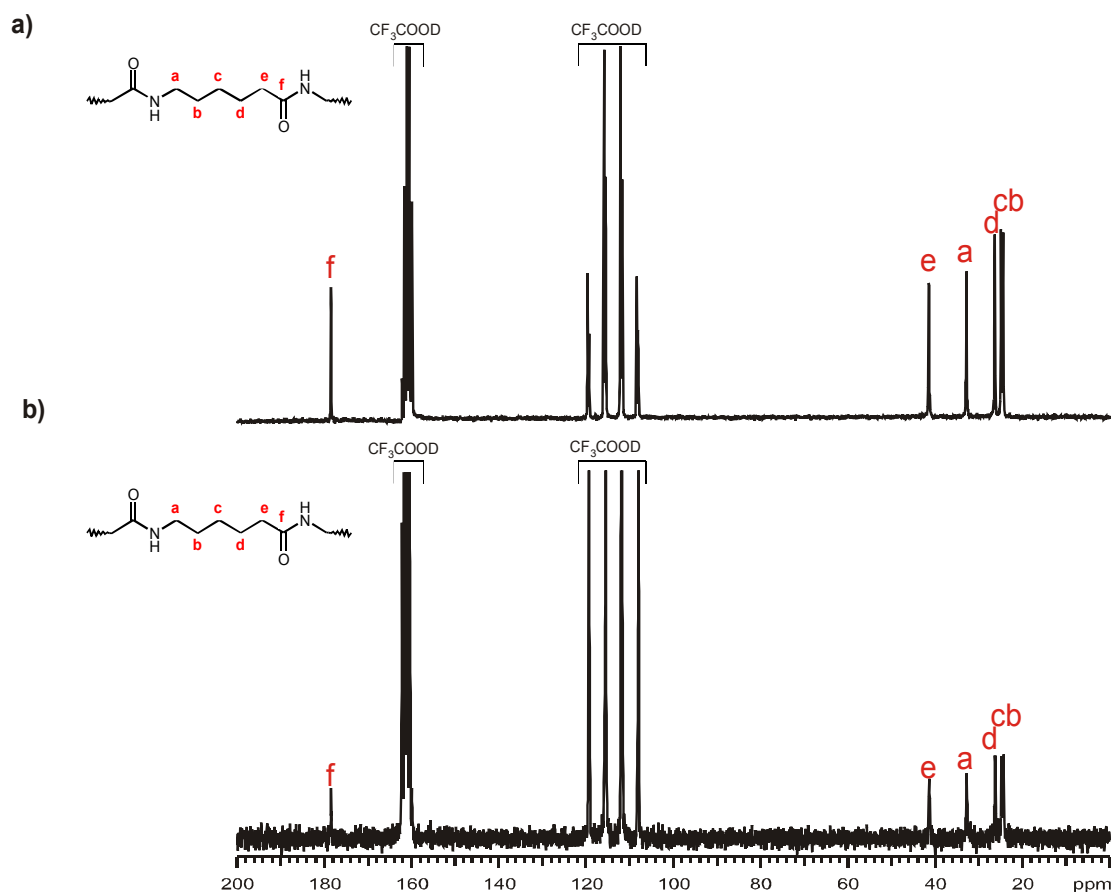


Fig. 6. ^{13}C NMR spectra of a) Ny-6, b) Ny-6 & SiO_2 in CF_3COOD .

3.4.3 Crystallinity and melting of nanocomposites

The presence of the silica/nylon nuclei affects the overall crystallization rate by facilitating the initial nucleation step. For instance, it was demonstrated [15] that silica enhances the crystallization of polyamide-6 (PA6) and leads to changes in mechanical properties. Conversely, Reynaud *et al.* found no influence of the particle on the crystalline phase of PA6 [16].

X-Ray Diffraction

Crystallinity

The glass transition temperature, T_g , is a fundamental parameter describing a glass, materials heated above T_g becomes a viscous liquid. Although glass-forming materials are of technological importance, it is not obvious whether the nature of the glass transition is thermodynamically driven [17] or solely a kinetic feature [18] while attempts have been reported to merge these two concepts through the process of cooperative rearrangement [19]. Nylon is an important member of the polyamide class of semicrystalline polymers, and it has been well established [20] that upon heating its crystalline structure

transforms between T_g and T_m , referred to as the Brill transition [21] in the case of nylon-6,6 while a similar transition has been reported for nylon-6 [22].

The presence of H-bonding in polymer structures has a marked effect on physical properties such relaxation phenomena caused by the onset of increased mobility in the polymer chain segments in the amorphous and crystalline regions, resulting in alteration of both diffusion kinetics and ionic transport mechanisms; such changes are even more prominent in the presence of absorbed water which influences the mechanical modulus as well as the crystallization and dielectric behaviour of the polymer [23].

The XRD data of a composite containing variable amounts (0, 3, 15, 30 wt%) of silica filler percentage is shown in Fig. 7. Two major crystalline peaks are at *ca.* $2\theta = 20.8^\circ$ and 24.3° (indexed as 200 and 002/202 reflections), which, are characteristic of the α -crystalline form of nylon-6 and are labelled α_1 and α_2 respectively [24]. The γ form of nylon-6 centers around $2\theta = 22^\circ$ (001) and 23° (200/201) [25]. It was observed that the nylon-6 component was semi-crystalline while the silica phase was, with no discernable peaks, amorphous.

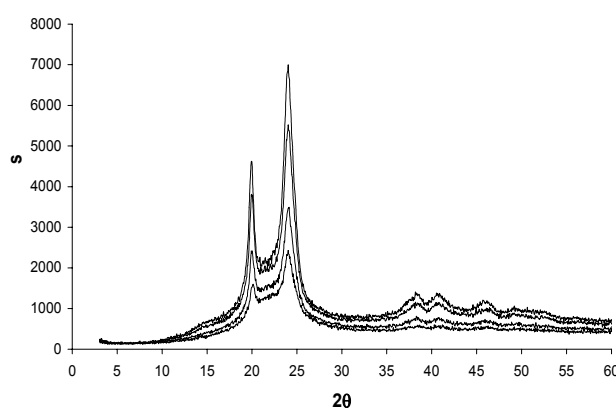


Fig. 7. XRD pattern of nylon-6 with variable quantities of silica added. The spectrum shows a decreasing order of intensity from pure nylon-6 (top) to 3, 15 and 30 wt% (bottom) silica addition. Sample was prepared from 'dissolution' method.

Figures 8-12 show WAXD variable temperature plots of a number of samples analysed in this study to investigate phase transitions. Samples were selected which underwent different processing conditions. Fig. 8 is a plot of pure nylon-6 obtained from a thin film. At 25°C the α_1 and α_2 peaks are discerned and a weak γ peak is observed over temperature range $25 - 240^\circ\text{C}$. With increasing temperature, the sample became more amorphous and the α peaks grow towards each other, starting with 2θ values of 20° and 24° at 25°C to *ca.* 21° and 23° at 220°C . At 240°C the sample is amorphous and a broad peak centered at *ca.* $2\theta = 19^\circ$ is observed. Fig. 9 shows spectra of pure nylon-6 that was previously subjected to heat treatment (up to 240°C) through compression moulding. At lower temperatures weak shoulders of the α -phase is present but the γ -phase predominate throughout the heat treatment and centers around $21-22^\circ$. Fig. 10 shows spectra of a composite sample containing 2 wt% silica colloids and the sample

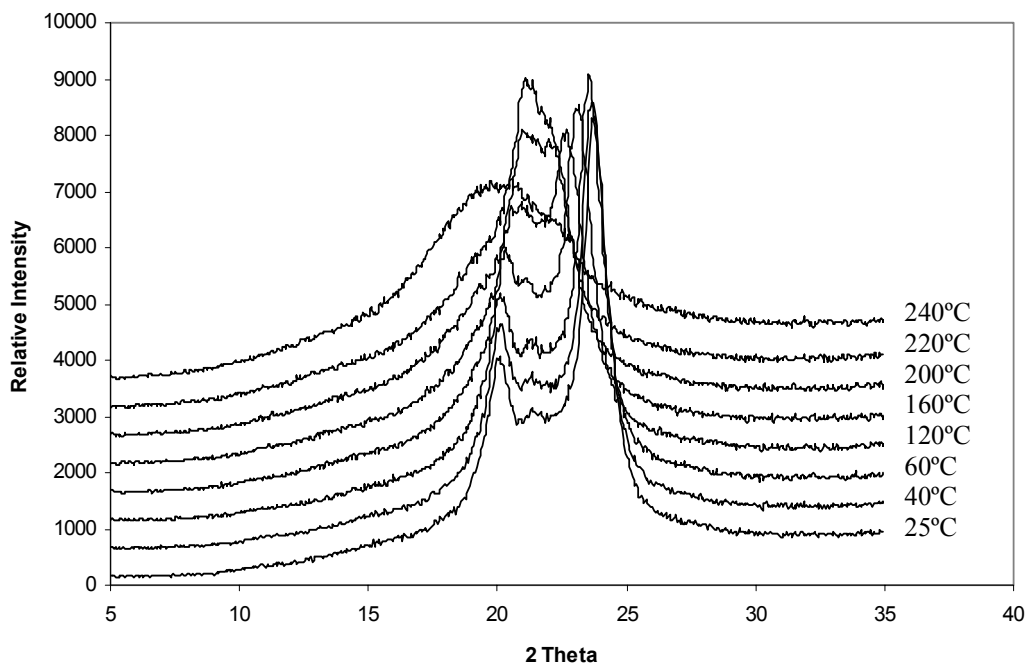


Fig. 8. XRD patterns showing variable temperature of pure nylon film.

processed as a film. The spectra show the α_1 and α_2 peaks predominate with an amorphous peak obtained at 240°C. Fig. 11 shows spectra of a composite with the same composition as Fig. 10 but the silica colloids were obtained from an ethanolic (in-house made) suspension.

A composite with 1 wt% silica addition (obtained from ethanol suspension) in the nylon-6 show a strain-at-break of > 0.5 , whereas a similar composite treated in water prior to compression moulding could not reach the yield stress (*vide infra*) [26]. It was noted that the α_1 value was larger than the corresponding α_2 for Fig. 10, while in Fig. 11 the opposite effect was observed. Fig. 12 shows the spectra of a composite containing 2 wt% silica obtained from compression moulding. When compared with Fig. 9, which contained pure nylon-6 and was also compression moulded, the influence of the silica particles is apparent. The sample show both the α_1 and α_2 phase and the γ phase is also present. With increasing temperature, the γ phase grows stronger (as for pure nylon-6) while the α phase weakens. At 240°C only the amorphous peak centred around 20° is observed.

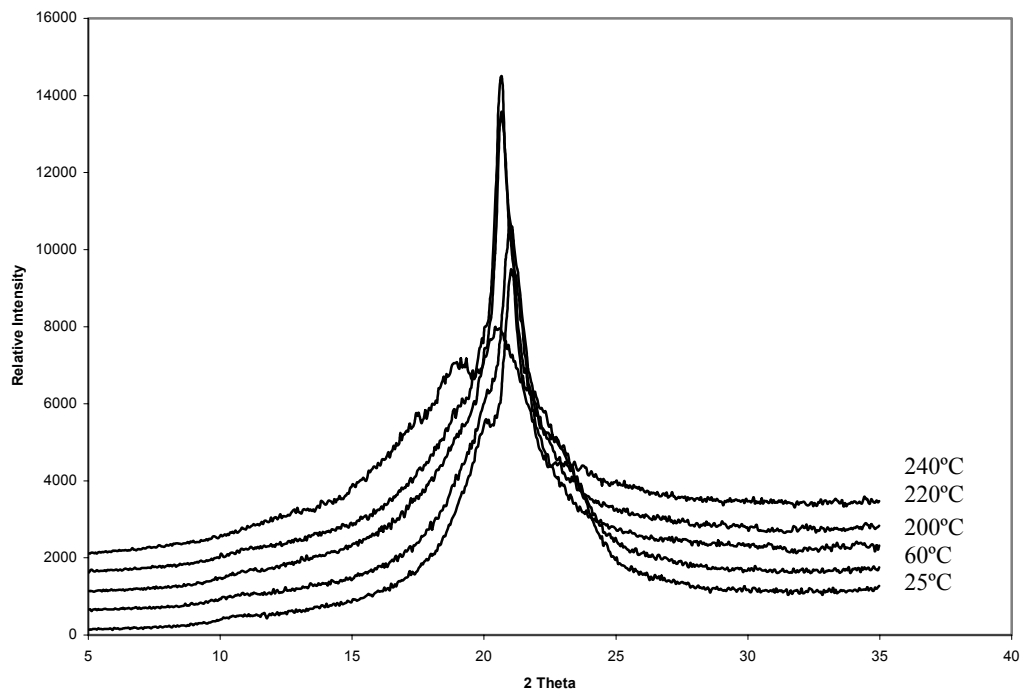


Fig. 9. Pure nylon, compression moulded.

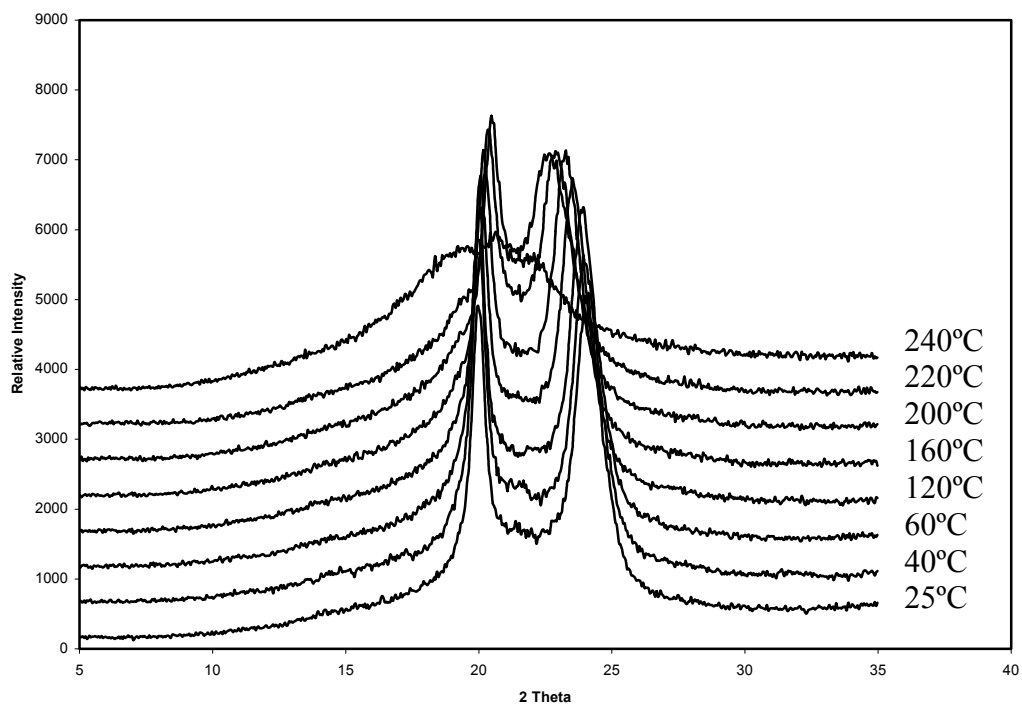


Fig. 10. Nylon with 2 wt% silica (from SX) nanocomposite film.

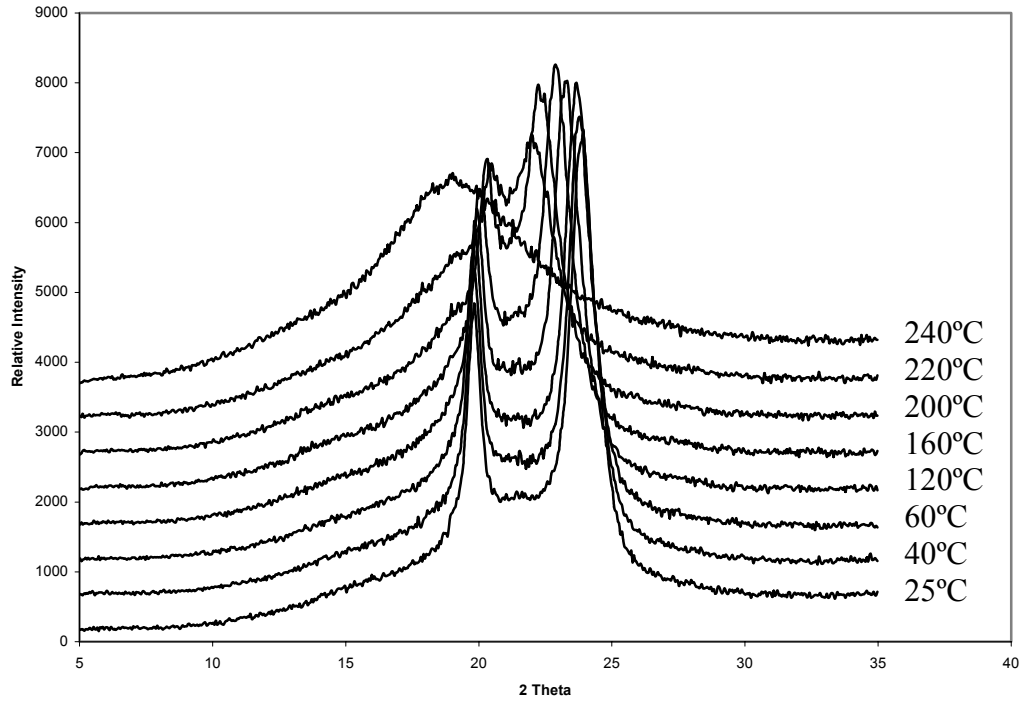


Fig. 11. Nylon with 2 wt% silica (from ethanol) nanocomposite film.

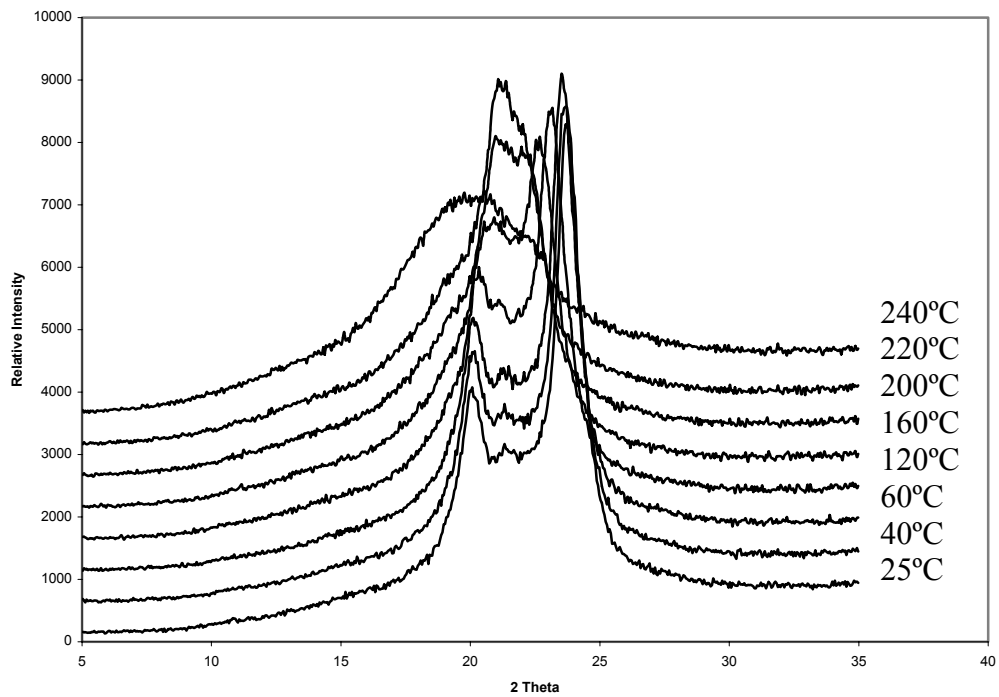


Fig. 12. Nylon with 2 wt% silica nanocomposite, compression moulded.

Fig. 13 shows the crystallinity of samples with variable amounts of silica added and processed in three different ways. The samples were analysed following 3 (A) or 24 (B) hours annealing at 80°C, as well as compression moulded (C). In all three cases there was an initial increase in the degree of crystallinity already after addition of small amounts of silica (< 5 wt%) was added. In the case of the annealed samples there was a subsequent decrease in the degree of crystallinity, with increasing silica (SX) content (> 5 wt%) while the compression moulded sample remained more or less constant with a slight increase. The decrease trend can be attributed firstly due to increase volume occupation by amorphous silica particles substituting possible crystalline lamellae in the polymer and secondly the silica disrupts the growth of lamellae, the primary crystalline source in thermoplastics. It was demonstrated that for the compression moulded samples a significant γ phase was present after processing whereas with the annealed samples the α phase predominate throughout, and we ascribe this to the difference between the annealed vs. compression moulded samples with regard to the respective differences in degree of crystallinity.

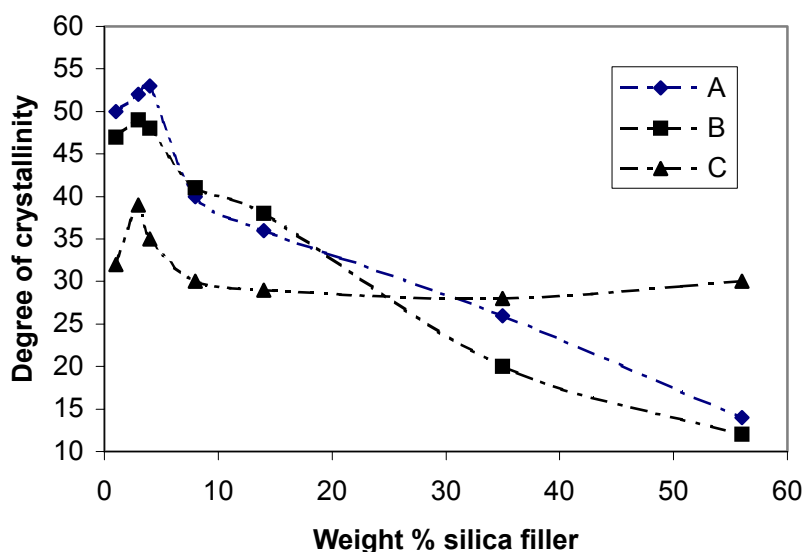


Fig. 13. Plot showing variation in degree of crystallinity with filler wt% for different processing conditions: A = annealed for 3 hours, B = annealed for 24 hours, C = compression moulded sample.

Differential Scanning Calorimetry

To ascertain a precise measure for the degree of crystallinity is a major challenge because of the difficulty in defining both the crystalline and amorphous phases within the polymer precisely [27]. Since intracrystalline defects are either crystalline or amorphous material, and criteria to fix the interphase position is complex, the degree of crystallinity can be understood by simplified models [28,29]. In that regard the two-phase model (crystallinity + amorphous phases) is still the most widely used [30].

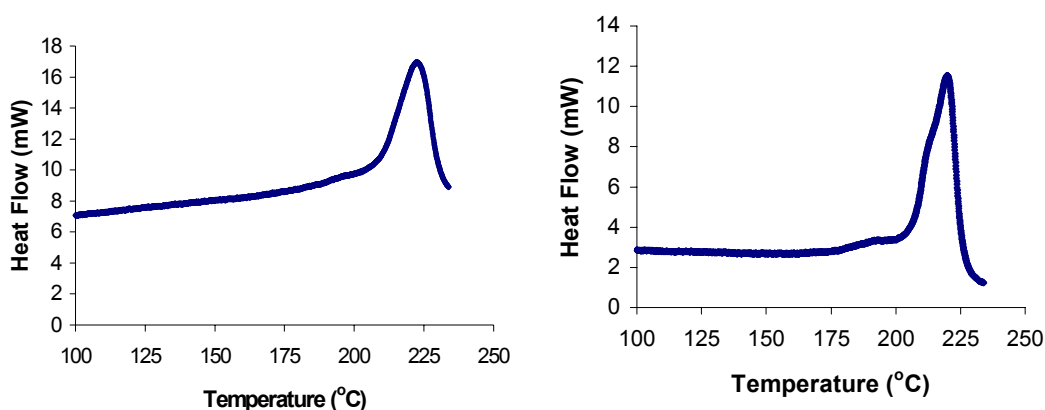


Fig. 14. DSC heating scan of pure nylon (14a left) and DSC heating scan of composite containing nylon with 5 wt% silica (14b right).

The DSC heating scans of pure nylon and 5 wt% silica (SX) composite are shown in Figs. 14a and 14b, respectively. The pure nylon had a 228°C peak melting temperature (T_m) while the melting process begins at *ca.* 190°C (Fig. 14). A glass transition temperature (T_g) of 40°C, a crystallization temperature (T_{cryst}) of 69°C and melting enthalpy (ΔH_m) of 50.42 J/g were measured. The 5 wt% silica composite had a 221°C peak melting temperature (T_m), a glass transition temperature (T_g) of 35°C, a crystallization temperature (T_{cryst}) of 60°C and ΔH_m of 74.9 J/g.

3.4.4 Mechanical tests of nanocomposites

Elastic Modulus

Table 1. E-Modulus of the samples.

Sample	Modulus [MPa]
PA	2422
PASW1	2561
PASW3	2749
PASW5	3050

The elastic modulus for composites with different filler percentages as tested with an extensometer is shown in table 1. Already with 1 wt% silica addition, an increase in E-modulus could be observed; an E-

modulus increase for 3 and 5 wt% loadings was sustained. Data represent the average value after four tests for each sample.

Yield stress (PAL)

To measure the tensile strength (yield stress) the displacement had to be larger and the extensometer has to be removed. If the specimen does not break before the yield point, a neck is often formed in the sample, which causes the engineering stress to drop. Yield stress, strain at yield and strain at break were measured at a tensile speed of 5 mm/min. The results are shown in Fig. 15 and Tables 2-4.

Table 2. Tensile stress of PAL matrix under different processing conditions.

IM = Injection Moulding,
CM = Compression moulding,
AN = Annealed and W = Wet..

Sample	Yield stress (MPa)	Strain at yield	Strain at break
PA IM	68	0.06	0.6
PA CM	68	0.09	0.5
PA AN	72	0.09	0.25
PA W	29	0.17	1.5

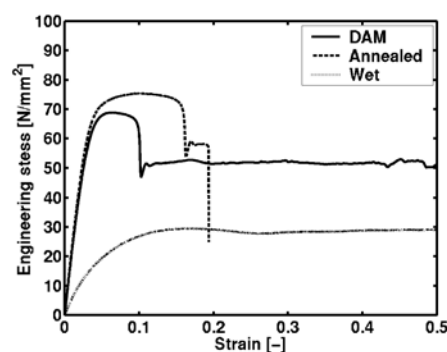


Fig. 15 Tensile test of PA6

Table 3. Tensile stress of PAL-silica nanocomposites (SX).

Sample	Yield stress (MPa)	Strain at yield	Strain at break
PASW1	-	-	0.03
PASW3	-	-	0.02
PASW5	-	-	0.015
PASE < 1	65	0.14	0.5

Table 4. Mechanical properties of PA6 (PAK) and PA6 with silica.

Sample	Modulus (GPa)	Yield stress (MPa)	Strain at yield	Strain at break	Impact (kJ/m²)
PAK IM	2.1-2.3	73-75	0.07-0.11	0.08-0.24	9.74
PAK CM	2.0	67	0.12	0.29	
PAK-Annealed	2.6	72	0.04-0.07	0.04-0.08	9.71
PAK-wet	0.49	33	0.34	0.83	11.23
<i>Silica Aerosil</i>					
PAK SA5	2.8	74	0.08	0.19-0.21	11.05
PAK SA5-Annealed	-	-	0.07	0.079	8.00
PAK SA5-Wet	0.5	31	0.32	0.57	12.21
<i>Silica Sipernat</i>					
PAK SS5	2.8	73	0.05	0.05	5.44
PAK SS5-Annealed	-	70	0.03	0.03	7.23
PAK SS5-Wet	0.7	32	0.18	0.78	6.31

3.4.5 Morphology

Spherulites and crystallite size

The morphology of spherulites of polyamides has been already reported [31]. Physical, mechanical and chemical properties of crystalline polymers have depended on the morphology of spherulites as well as the degree of crystallization. For example, the tensile properties of nylon-6,6 were improved with decreasing the size of spherulites [32] and the frictional properties of polyamides were improved by a high degree of crystallinity and fine homogeneous spherulitic structure [33]. A recent review dealing with spherulites (including those of polyamides) is found in [34]. Spherulite morphology is very dependant upon factors such as crystallization conditions, polymer composition and molecular weight. An illustration of the spherulite morphology of the nylon-6 and nanocomposites is in Figures 16-18. Nylon samples with the same crystallinity have shown different properties depending on the size of the spherulites [11] while in some thermoplastics, the spherulite size did not appear to have a direct influence on yield stress and mechanical properties thus depends on the interrelationship between morphology and crystallinity.

During crystallization numerous voids may occur at the spherulite boundaries, which are source of defects on the materials. These voids are seen in Figs 16 (pure polymer film) and 17. The addition of silica nanoparticles led to fibrillar overgrowths, as can be seen in Fig. 18 a and b.

As mentioned before, upon cooling, the transformation from the molten state to solid indicates some nylon-6 chains are folded and packed orderly forming thin and flat platelets (lamellae crystals) *ca.* 100 Å thick and 100-1000 nm in lateral dimension. The thickness of the lamellae depends on a variety of factors during thermal processing (temperature, pressure, heating- and cooling rates). An attempt was

made to calculate thickness of the lamellar crystals in the three composites using the Scherrer equation:

$$L_{lt} = K\lambda/(\beta_o \cos\theta)$$

where L_{lt} is the lamellar thickness in Å, $K = 0.9$, the wavelength $\lambda = 1.54059$ Å, β_o = the width of the diffraction curve (in radians, FWHM, Full Width at Half Medium) and θ = half of the Bragg angle.

The mean thickness of the lamella crystals was calculated from XRD using the peak broadening technique, see Table 5.

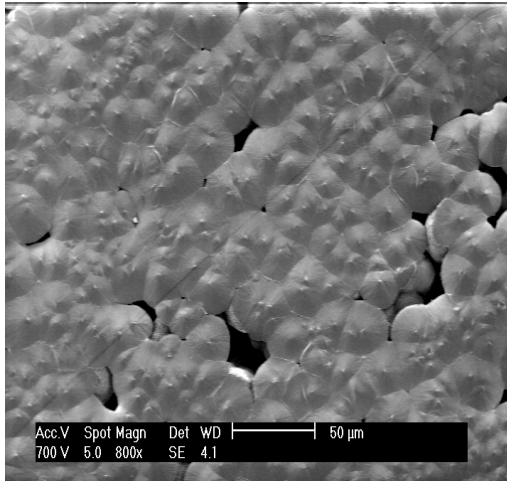


Fig. 16. Solution cast of pure nylon-6, dissolved in formic acid.

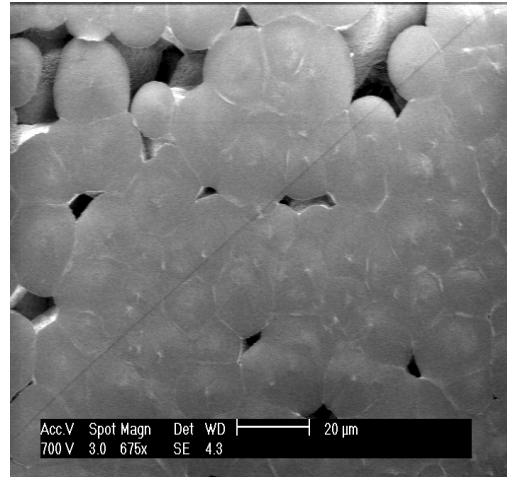


Fig. 17. Solution cast of nylon-6 and silica nanoparticles. The filler was dispersed in alcohol.

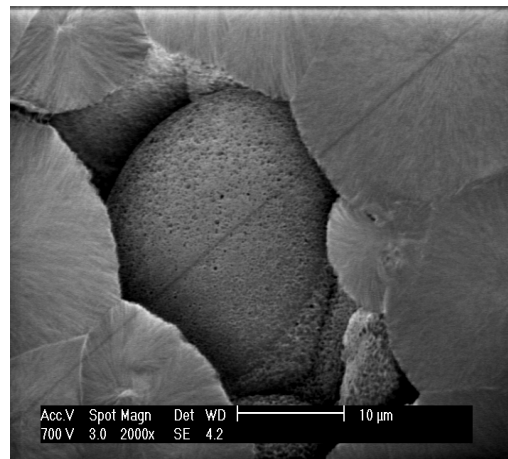
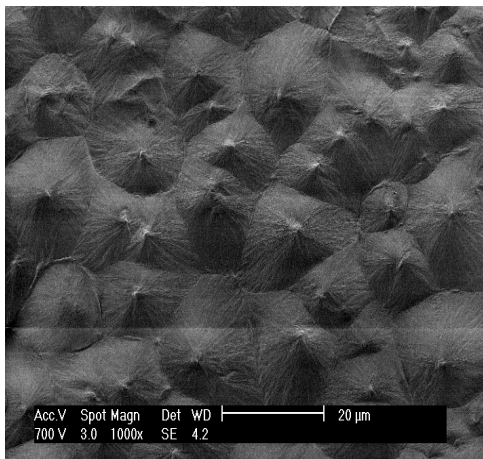


Fig. 18a (left) and 18b (right). The spherulites produced by film casting of PA6/SX.

Table 5. Crystallite size of polyamide-6/ silica. ^a(200), ^b(002/202)

Silica wt%	Broadened Profile Width (°2θ)	Standard Size Profile Width(°2θ)	Broadening Peak Position (°2θ)	Crystalline Size (Å)
0 ^a	1.2	0.15	1.05	197
0 ^b	1.6214	0.15	1.4714	81
1 ^a	0.5837	0.15	0.4337	186
1 ^b	1.1183	0.15	0.9683	84
4 ^a	0.6042	0.15	0.4542	177
4 ^b	1.1334	0.15	0.9834	82
8 ^a	0.5848	0.15	0.4348	185
8 ^b	1.0946	0.15	0.9446	86
20 ^a	0.6549	0.15	0.5049	159
20 ^b	1.0737	0.15	0.9237	88
50 ^a	0.7733	0.15	0.6233	129
50 ^b	1.239	0.15	1.089	74

The crystallite size varies depending on the addition of silica (Table 4). The XRD experiments allow calculation of the lamellar spacing in semicrystalline polymers. The two main crystalline peaks of nylon-6 (200, 002/202) showed lamellar thickness of 197 and 81 Å, respectively. The lamellar thickness decreased while the E-modulus increased with the addition of silica filler up to 4 wt%, at 20 wt% the E modulus still increased while the α_2 component showed an increase as well. With increase filler percentage, the α_1 value decreased and the α_2 value slightly increased in this study. Liu *et al.* [35] analysed the phase transitions of nylon-6/clay composite on annealing and found with constant filler percentage, the α_1 value increased with increasing temperature, while the α_2 value varied slightly.

3.4.6 Impact Toughness

The impact toughness of PA6 silica composites (PAK) is seen in table 5. The impact toughness can be measured by a high speed (1 m/s) tensile test on a notched sample, but from the tensile test results we already have an idea on whether a material has a low or high impact toughness. A sample that is brittle in a tensile test will have lower impact toughness than a sample that is ductile in a tensile test. Also from the tensile curves of a ductile sample an indication can be obtained for the level of impact toughness. Impact toughness is a measure for the amount of energy that is dissipated before the sample breaks. This energy is higher if there is delocalisation of deformation (if the deformation is local, only a small part of the sample is deformed and less energy is dissipated than in case the deformation spreads over a larger part of the sample). The localization effect is observed in a tensile test in the presence of a neck that is formed. If small neck is formed (large drop in stress) than the deformation is localized and if no neck (no yield drop) is formed (the sample is deformed more

homogeneously) than the deformation is not localized, resulting in a higher impact toughness. The results of Table 4 give an indication that the composites (PAK) with aggregated silica ($\varnothing = 10\text{-}30\text{ nm}$) and bigger particle size ($\varnothing = 0.1\text{ }\mu\text{m}$) do not significantly improve the impact toughness of the polyamide.

3.5 General Discussion

In their recent study, Reynaud *et al.* [16] used the *in-situ* polymerisation method and found that small silica particles ($\phi \sim 12\text{ nm}$) 'do not appear as single entities...but tend to form aggregates'. By contrast, larger particles ($\geq 50\text{ nm}$) 'are rather well dispersed'. Our study departs from those results and demonstrates that for particles in the 10-30 nm range, a low degree of aggregation could be obtained. We ascribe this result as a consequence of the new synthesis method we employed (*vide infra*).

Our procedure was based on selecting appropriate reaction conditions, particularly with regard to solvent choice and pH control. The silica dispersion remained stable due to sufficient proton adsorption that maintained a (positively) charged surface in solution. The best result was therefore obtained from addition of silica particles (either from aqueous or ethanolic acidified sol medium) to formic acid as bulk solvent; the least successful result (premature gel-formation and inhomogeneity) was obtained from a basic (pH 8-10) silica sol medium added to cresol. The low pH of the silica sol was necessary since the iso-electric point of silica is in the pH 2-3 range. Solvent use was kept to a minimum to ensure concentrated, viscous solutions could be cast on clean glass surfaces followed by a combination of vacuum and heat (60-80°C) treatments to remove solvent.

The appropriate choice of organic solvent was essential. For example, although cresols, trifluoroethanol and chloro-xylenes all dissolve polyamides over a period of time, such solutions showed immediate and unwanted gel-formation upon addition of the sol. Polyamides react strongly with acids such as H_2SO_4 , HCl and HCO_2H and it has been established that dissolution of this class of polymers is associated with the protonation of the amide group [36-38]. We utilized the *polyamide:formic-acid:water* ternary phase diagram [39] to obtain an estimate of nylon-soluble regions (as mol% fraction). The challenge was therefore to obtain an uniform not aggregated transparent solution after the addition of colloidal silica before casting. An isothermal three-component phase diagram for a polymer, solvent and a non-solvent is schematically given in Fig. 19. At lower polymer and non-solvent concentrations a homogeneous phase is obtained.

The 'dissolution-method' used for this composite system has a number of advantages when compared to other preparative methods currently available, namely a) the formation and isolation of the desired

composite could be performed at ambient temperature, b) no particle surface modification, initiator, or catalyst was required c) a variety of inorganic filler types could be considered, also metallic and non-oxidic phases, and d) the method is suitable for all nylon classes susceptible to formic acid dissolution, including nylon-6,6. Because the synthesis procedure can be conducted under mild conditions, the filler size in the final composite was unchanged compared to the filler size in the initial sol (and can thus be tuned to the appropriate size); the filler sizes are not affected by the reaction conditions employed. Clear, transparent solutions were obtained which resulted in better control of homogeneity at the macromolecular level. This is an important requirement for all ensuing properties/processes to be investigated, for example in the areas of chemical modifications (e.g. addition of soluble organic dyes and fire retardants), mechanical reinforcements (e.g. formation of transparent electrospun fibers) and processing (e.g. spin coating, casting) [40].

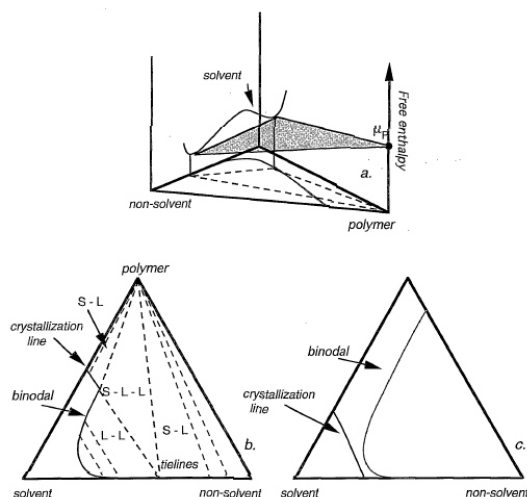


Fig. 19. (a) A three dimensional perspective of the phase diagram with the free enthalpy of the mixture shown on the vertical ordinate. (b) An isothermal phase diagram for a forming system with crystallization of the polymer. (c) A special situation in which the crystallization line does not intersect the binodal curve.

The media (water vs. ethanol) in which the silica sol was initially prepared influenced the mechanical results. Composites derived from polyamide PAL and water-suspended silica particles were brittle and fractured during determination of the elastic modulus at *ca.* 2-3% strain; the yield stress was not reached. This result was somewhat akin to that found by Reynaud *et al.* where they noted for ‘smaller particles, the draw stress was not reached, the rupture occurring rapidly after the yield point’. We obtained much improved results from composites that were formed from ethanol-suspended silica particles. In such cases the composite did not rupture immediately after the yield point. It started to yield at 4% while at 20% a complete neck was formed and a strain-at-break of > 0.5 could be reached. Furthermore, there was a distinct decrease in yield stress from 68 MPa for pure nylon-6 to 65 MPa for a 1 wt% silica composite (Tables 3 and 4), which is a promising result with respect to impact toughness. Impact toughness is a measure of the amount of energy dissipated when the sample breaks and is typically derived from a high-speed (1 m/s)

tensile test on a notched sample. Analysis of the tensile curves (Fig. 20) gives a qualitative measure for the degree of toughness because the dissipated energy is higher if there is delocalisation of deformation. The localization effect is observed in tensile tests in the presence of a neck that is formed. When a small neck is formed (large decrease in stress) then the deformation is localized and if no neck is formed (no decrease in stress) then the sample is deformed more homogeneously, resulting in a higher impact toughness.

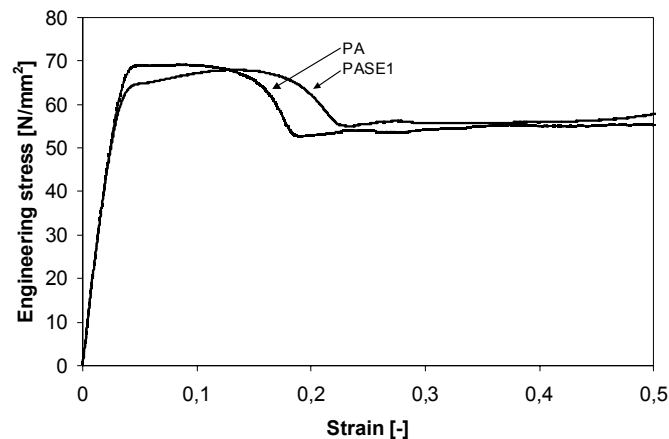


Fig. 20. The tensile stress of a composite with 1 wt% filler (PASE1) compared to pure polyamide (PA). The composite was compression moulded from silica sol dispersed in ethanol.

3.6 Conclusions

The synthesis method described can be generally applied to all classes of polyamide-based composites that are susceptible to solvent dissolution. Inorganic filler material can be readily incorporated into the polymer matrix resulting in a hybrid nanocomposite with unprecedented control in particle size, mono-dispersity and homogeneity. The procedure relied on initiating a positive charge on the silica surface and appropriate solvent choice was important to obtain satisfactory homogeneity. Sample processing conditions (drying, dispersion media) were of particular concern for mechanical testing. An increase in E-modulus as a function of filler percentage added (0-5 wt%), a small decrease in yield strength (improvement in impact toughness) and a strain-at-break of > 0.5 (from ethanol derived silica sol and PAL) were obtained.

The degree of crystallinity was determined for a PA6/silica nanocomposite and results indicated an initial increase of crystallinity with low loadings while a general decrease in crystallinity with increasing silica content was then observed. The crystallize size

decreased and the E-modulus increased with addition of filler. The study showed phase transition behaviour as a result of different heat treatments and processing conditions.

3.7 References

- [1] Buckey, D.T. *Modern Plastics* Mid-November D-39-D41 (1998).
- [2] Sumita, M., Shizuma T., Miyasaka K. and Ishikawa K. *J. Macromol. Sci. Phys.* B22,601 (1983).
- [3] Rong, M.Z., Zhang M.Q., Zheng Y.X., Zeng H.M. and Friedrich, K. *Polymer* 42, 3301 (2001). Petrovicova R., Knight, R., Schadler L.S. and Twakowski, T.E., *J. Appl. Polym. Sci.* 78, 2272 (2000). Fu, X. and Qutubuddin, S. *Polymer* 42, 807 (2001).
- [4] Eder, G., Janeschitz, H. and Liedauer, S. *Prog. Polym. Sci.* 15, 629 (1990).
- [5] Mo, Z. and Zhang, H. *J Macromol Chem Phys* C35, 555 (1995).
- [6] Bernards, T.N.M., Bommel van, M.J. and Boonstra, A.H. *J. Non. Cryst. Solids* 134, 1 (1991).
- [7] Bekkers, M.H.J. and van Sprang, H.A. *X-Ray Spectrom.* 26, 122 (1997).
- [8] Ou, Y., Yang, F. and Yu, Z. *J. Polym. Sci. Polymer Physics* 36, 789 (1998).
- [9] Wu, S. *Polymer* 26, 1855 (1985).
- [10] Borggreve, R.J.M. *Toughening of polyamide-6*. PhD Thesis. University of Twente. The Netherlands (1988).
- [11] Zuiderduin, W.C.J. *Polymer* 44, 275 (2003).
- [12] Li, W. and Yan, D. *J. Appl. Polym. Sci.* 88, 2462 (2003).
- [13] Kohan M.I. *Nylon plastics handbook*, Hanser Publishers, New York. Ch. 5, p. 126 (1995).
- [14] Aharoni, S.M. *n-Nylons: their synthesis, structure and properties*, John Wiley and Sons, Chichester (1997).
- [15] Vasanthan, N., Murthy N.S. and Bray R.G. *Macromolecules* 31, 8433 (1998).
- [16] Reynaud, E., Jouen, T., Gauthier, C., Vigier, G. and Varlet, J. *Polymer* 42, 8759 (2001).
- [17] Gibbs, J.H. and DiMarzio, E.A. *J. Chem. Phys.* 28, 373 (1958).
- [18] Götze, W. and Sjögren, L. *Rep. Prog. Phys.* 55, 241 (1992).
- [19] Adam, G. and Gibbs, J.H. *J. Chem. Phys.* 43, 139 (1965).
- [20] Hirshinger, J., Miura, H., Gardner, K. and English, A.D. *Macromolecules*, 23, 2153 (1990). Starkweather, H.W. *Macromolecules* 22, 2000 (1989).
- [21] Brill, R.J. *Prak Chem* 161, 49 (1942). Ramesh, C., Keller, A. and Eltink S.J. *Polymer* 35, 2483 (1994).
- [22] Murthy, N.S., Curran, S.A., Aharoni, S.M. and Minor, H. *Macromolecules* 24, 3215 (1991).
- [23] Pathmanathan, K. and Johari, G.P. *J Chem Soc, Faraday Trans* 91, 337 (1995).
- [24] Ramesh, C. and Bhoje, E. *Macromolecules* 34, 3308 (2001). Khanna, Y.P. and Kuhn, W.P. *J. Polym. Sci.* 35, 2219 (1997).
- [25] Murthy, N.S., Bray, R.G., Correale, S.T. and Moore, R.A.F. *Polymer* 36, 3863 (1995).
- [26] van Zyl, W.E., Garcia, M., Schrauwen, B.A.G., Kooi, B., De Hosson, J.Th.M. and Verweij, H. *Macromol. Mater. Eng.* 287, 106 (2002).
- [27] Chen, H.L. and Hwang, J.C. *Polymer* 36, 4355 (1995).
- [28] Wu, Q., Liu, X. and Berglund, L.A. *Macromol. Rapid Commun.* 22, 17 (2001).
- [29] Bunn, C.W. and Gardner, G.V. *Proc. Roy. Soc. A*189 39 (1947). Inoue, M. *J. Polym. Sci.* 2013 (1963).
- [30] Starkweather, H.W. and Brooks, R.E. *J. Appl. Polymer Sci.* 1, 236 (1959).

- [31] Müller, A. and Pflüger, R. *Kunststoffe* 50, 203 (1960).
- [32] Fraenkel, G. and Franconi, C. *J. Am. Chem. Soc.* 82, 4478 (1960).
- [33] Schaeffgen, J.R. and Trivisonno, C. *J. Am. Chem. Soc.* 73, 4580 (1951).
- [34] Duffy, J.A. and Leisten, J.A. *J. Am. Chem. Soc.* 82, 853 (1960).
- [35] Liu, X. and Wu, Q. *Polymer* 43, 1933 (2002).
- [36] Fraenkel, G. and Franconi, C. *J. Am. Chem. Soc.* 82, 4478 (1960).
- [37] Schaeffgen, J.R. and Trivisonno, C. *J. Am. Chem. Soc.* 73, 4580 (1951).
- [38] Duffy, J.A. and Leisten, J.A. *J. Am. Chem. Soc.* 82, 853 (1960).
- [39] Cheng, L.P., Dwan, A.H. and Gryte, C. *J. Polym. Sci.* 32, 1183 (1994).
- [40] *Hybrid Organic-Inorganic Composites* Eds. J. E. Mark, C. Y.-C. Lee, P. A. Bianconi. American Chemical Society, Washington D.C. vol. 585 (1995).

4 Friction and Wear Studies on Nylon-6/Silica Nanocomposites

Composites of nanometer sized silica (SiO₂) filler incorporated in a nylon-6 polymer were prepared by compression moulding. Their friction and wear properties were investigated on a pin on disk tribometer by running a flat pin of steel against a composite disc. The morphologies of the composites as well as of the wear track were observed by scanning electron microscopy (SEM). The addition of 2 wt% SiO₂ resulted in a friction reduction (μ) from 0.5 to 0.18 when compared with neat nylon-6. This low silica loading led to a reduction in wear rate by a factor of 140 while the influence of higher silica loadings was less pronounced. The smooth morphology obtained after the wear test indicated the negligible contribution to friction of the pin to the nanocomposite. Furthermore, a deterministic model was applied to calculate the coefficient of friction of the nanocomposites.

Part of this chapter was presented by the author as oral presentation and published in:

Mat. Res. Soc. Symp. Proc. 740 11.9.1-11.9.6 (2003)

during the fall meeting *Material Research Society* (MRS), on Dec. 2-6 2002, in Boston MA, USA.

4.1 Introduction

In recent years there has been a rapid growth in the use of thermoplastic polymers to replace metal components in wear-resistant applications [1]. Dry metal-polymer bearings are used for cost reduction and facile assembly in production. Due to their hardness, toughness, and friction properties, polyamides (PA) are used for gear and bearing materials [2]. For these applications carbon, copper compounds (e.g. CuO) or glass fibres as filler components and polytetrafluoroethylene (PTFE) or MoS₂ as solid lubricants have been added to PA [3-6]. The former improves mainly the mechanical strength and wear resistance of polymers, while the latter improves friction characteristics and contribute to the control of wear [1,7].

Nylons are semicrystalline and its crystallinity can be modified by decreasing cooling rates during the thermal moulding [8] and by the addition of a nucleating agent such as fumed silica or aluminium. However, high amounts of nucleating agents can cause brittleness or unwanted tribological properties in the materials.

The role of the filler component in influencing the tribological behaviour of polymers is not yet completely understood but plausible explanations have been provided [9,10]. The mechanical and/or chemical interaction between composite and counterface are believed to affect the tribological process [11]. Sliding tests of a steel pin on polymer discs have shown that part of the polymer is transferred to the surface of the pin producing shielding of the soft polymer surface from the hard metal asperities. The excellent heat-transfer characteristics of the metallic counterpart contribute to this film formation during frictional processes in almost all polymers with viscoelastic properties [6,12]. The wear of spherulitic nylon is preceded by interfacial frictional heating and subsequent removal of the material and transfer to the counterface as well. Therefore, the wear resistance of nylon is attributed to its ability to form thin films while sliding against a steel counterpart. A self-lubricating polymer-matrix material is used in the aviation and aerospace industry [13] because their coefficient of friction is low (typically between 0.1 and 0.5) compared to metal-to-metal contacts. Corresponding values of the specific wear rate (k_w) are typically in the range 10^{-6} to 10^{-3} mm³ (Nm)⁻¹. A specific wear rate of 10^{-6} mm³/Nm is usually set as limit above which a material is no longer considered wear-resistant. Thermoplastic polymer matrix composites are also used as coating materials for the bore of tubulars used as water injectors in the oil industry. Nylon-6 occupies a prominent position in engineering thermoplastics due to its wide spectrum of properties, such as high crystallinity, high strength and feasibility of fabrication and processing [14]. The tribological behaviour of polyamide and their composites has been reported previously [6,15].

Polyamide has superior wear-resistance sliding against a steel counterface relative to other polymers.

Factors that exert influence on friction and wear characteristics of polymer composites are the particle size, morphology and concentration of the filler. If the particles are large and hard, they are easily pulled-out of the matrix material and contribute to wear of the composites by their abrasive action and cause wear and damage of the counterpart material. For example, when fused silica and dolomite fillers with a particle size of 5 and 10 μm were used in polymeric coatings, the filled nylon showed the worst abrasive wear resistance [16]. Due to the poor bonding between filler and matrix material the fillers were pulled out causing cracks in the material, rather than supporting the load. The incorporation of filler to polymers has modified the coefficient of friction (μ) and/or wear rate (k_w) although the detailed mechanism is still unclear [3,7]. By using nanoparticles, particle pull-out can be avoided because better adhesion between polymer and filler is expected due to the high surface area of the nanoparticle.

Silica nanoparticles [17] are currently used for the enhancement of the mechanical properties in Nylon 6 [18]. In this study, the effect of nano-silica addition in nylon-6 on the tribological performance was investigated. Cooling rates were kept constant for the consolidation of the nanocomposites. The materials microstructure and dispersion of the nanocomposite were studied by Scanning Electron Microscopy.

4.2 Experimental

4.2.1 Synthesis

The preparation of the nanocomposite has been described in chapter 3 [19]. Nylon films were produced by drawing a steel knife over a pre-treated glass containing a solution of the polymer-silica system in formic acid at a rate of 1 mm min⁻¹ using a Doctor Blade™ equipment. The glass surface was treated with ethanol for a better adhesion of the polymer solution to the glass. The composite was left overnight in inert atmosphere and a film-coating of 1 mm was formed on the glass.

Prior to tribological measurements, the film cast nanocomposites were compression moulded into sheets of size 19 x 5.5 x 1 mm at 250-260°C. Compression was performed in 3 steps: 2 min at 5 MPa, 3 min at 10 MPa, and 5 min at 20 MPa at 250°C and subsequently the samples were cooled to room temperature.

4.2.2 Characterisation

Wide Angle X-ray Diffraction (WAXD) patterns at room temperature of the nylon-6 with nanosilica were obtained by using a Philips PW3710

diffractometer. Partially crystalline nylon consisted of a broad amorphous halo on which the peaks from the crystalline regions were superimposed. Thus, the normalized area of the crystalline peaks could be used to obtain the degree of crystallinity [7]. Microstructures and wear tracks were characterised by means of Scanning Electron Microscopy (SEM) using a Hitachi S800 with an in-lens detector. To determine phase distribution and the presence of impurities, Energy-Disperse X-ray Analysis (EDX) with a Kevex detector was used coupled with SEM. Quantitative XRF [20] was used to determine the amount (as wt%) silica present in each sample utilising a Philips PW 1480/10 fluorometer. The composition of the outermost atomic layer of the nanocomposites was measured by Low Energy Ion Scattering (LEIS) [21,22]. The samples were first bombarded with low-energy (noble gas) ions using a 3 keV $^3\text{He}^+$ beam. During the measurements an area of 1.4 mm² was analysed and only about 0.3 atomic layer were removed.

4.2.3 Tribological conditions

The compression-moulded polymers were cut into discs with diameter of *ca.* 40 mm and thickness between 0.9 and 1.07 mm. The disc surface roughness varies from $R_a = 0.5$ to 1.4 μm . The roughness of the pin was $R_a = 0.15$ μm . Dry sliding-wear tests were performed with a pin-on-disc tribometer (CSEM, Neuchatel, Switzerland), placed in a climate chamber (Heraeus, HC4057, Balingen, Germany) at 23°C and 40% relative humidity. A picture of the test set-up is shown in Fig. 1 and consisted of a flat round steel-pin (diameter 1.3 mm) 100MnCrW4 sliding against a rotating polymer sample. The sliding velocity for the nanocomposites was set at 0.1 m/s to avoid the occurrence of a high *PV* value (pressure on surface multiplied by sliding velocity) for nylon and of possible thermally induced fracturing. The load used was 1 N and the mean contact pressure was 0.75 MPa with a pin of 1.3 mm. The resulting *PV* was 70000 N/m·s. The sliding distance of the tests was adapted for each specific measurement to obtain significant wear and to detect possible fatigue and was set at a distance of 10 km. The coefficient of friction was measured on-line by monitoring the ratio between the measured shear force and the applied normal force through measurement of the deflection of the pin-arm (lever) with two inductors. The wear track depth after the test was measured with a Micromap 512 opto-profiler.

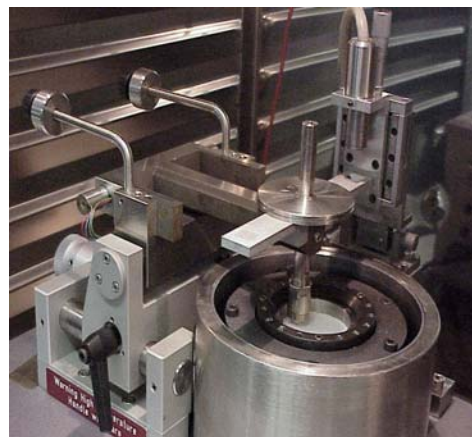


Fig. 1. Test set-up.

4.3 Results

4.3.1 Sample characteristics

WAXD patterns of the nylon-6 with nanosilica at room temperature were obtained. Two strong peaks located at 2θ values of 21° and 23° were characteristic for the α -form of the nylon-6 crystal, which was assigned as the (200), (002) and (202) reflections. The assignments and patterns have been already discussed in Chapter 3. The degree of crystallinity of the α -phase of nylon-6 was obtained from the multipeak resolution method [23]. Table 1 shows the intensities and assignments of the pure PA6, PA6 compression moulded with 2 wt% of nanosilica filler (PA6-2), and PA compression moulded with 14 wt% of silica (PA6-14). The degrees of crystallinity of the samples were 33, 39 and 36%, respectively.

Table 1. Degree of crystallinity ($W_{c,x}$) of the composites.

Sample	2θ	β , measured FWHM	$W_{c,x}$ (%)
PA6	23.54	1.31	33
PA6-2	23.71	1.17	39
PA6-14	23.76	1.22	36

The results for the LEIS measurements of the PA6-14 nanocomposite before the friction experiments are shown in Fig. 2. The Si, O, C and Cl peaks were clearly observed. The value of the Si/O ratio corresponded with the ratio of a pure silica sample, indicating the presence of SiO_2 nanoparticles on the surface.

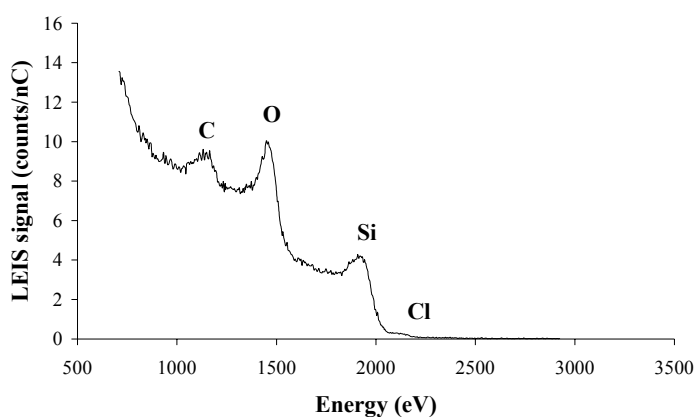


Fig. 2. LEIS results of the PA6-14 nanocomposite before testing.

The silica particles in PA6-2 were well dispersed and had an average particle size of 20-30 nm as observed by SEM (Fig. 3). The picture showed individual non-aggregated white particles characterised by EDX as SiO_2 . This was in agreement with the LEIS study, which showed that silica could be detected in the outermost atomic layer of the composite.

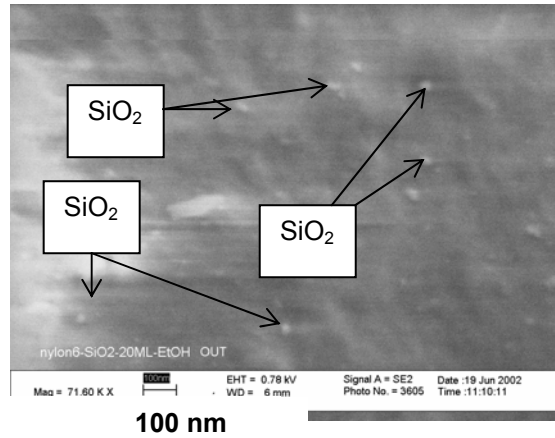


Fig. 3. Silica nanoparticles dispersed in the polymer matrix (PA6-2).

Table 2. Wear rate and coefficients of friction of PA6 (C) nanocomposites. Velocity = 0.1 m/s, Load = 1N, Distance of sliding 10 km.

Wt% silica	Coefficient of friction (μ)	Specific Wear rate (k_w) [mm^3/Nm]
0	0.45	5.29×10^{-5}
2	0.20	2.0×10^{-7}
14	0.40	2.81×10^{-5}

4.3.2 Tribological tests

Table 2 shows the coefficient of friction (μ) and specific wear rate (k_w) of the PA6, PA6-2, PA6-14 nanocomposites and the corresponding μ measurements against sliding distance are shown in Fig 4. Pure nylon showed a μ of 0.18 at the beginning of the friction measurements. During the test, the μ was gradually elevated up to a steady-state of μ

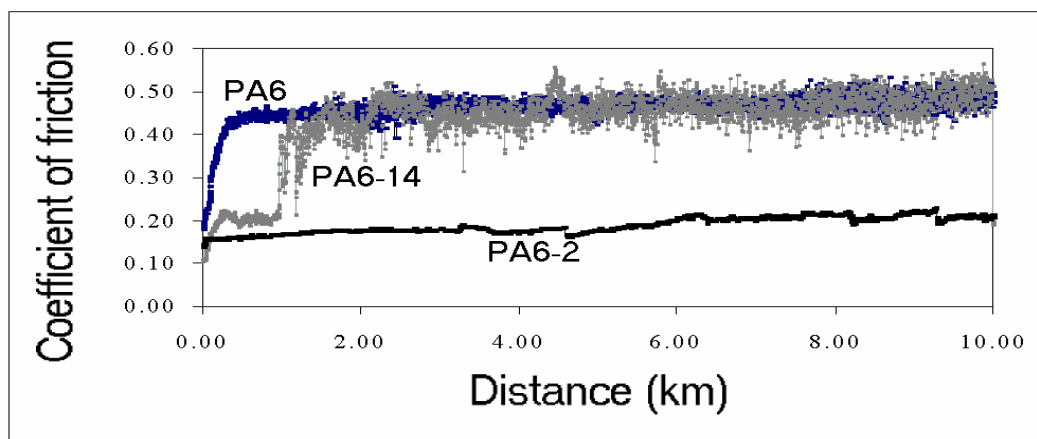


Fig. 4. Plot of coefficients of friction (μ) against sliding distance for PA6 and nanocomposites on steel counterface. Velocity = 0.1 ms^{-1} , Load = 1 N.

= 0.45. At filler loadings of 2 wt% the starting μ was 0.14. This

nanocomposite rapidly reached a steady value of $\mu = 0.18$. The addition of 14 wt% of silica in the PA6 resulted in an initial μ of 0.11. After 0.1 km a transient period resulted in a $\mu \approx 0.2$, while after 1 km an increase of μ was again observed up to almost the same steady state value of the neat polymer ($\mu \approx 0.40$). The opto-profiler of the resulting wear track in the PA6-14 is shown in Fig. 5. As seen from this figure, a higher volume was lost close to the middle of the track.

It was observed that the coefficient of friction for 2 wt% of SiO₂ filled composite was lower than that of unfilled nylon-6. Addition of 14 wt% of SiO₂ resulted in a coefficient of friction value (μ) slightly lower than pure nylon-6 after few kilometres of sliding distance. So, the PA6-2 composite had a lower wear rate and a lower coefficient of friction when compared to PA6 and PA6-14.

Fig. 6 shows the worn disc surface after the test of the PA6-2 nanocomposite. An overview of the PA6-2 nanocomposite wear track is shown in Fig. 6a. A detailed photograph of the edge of the PA6-2 wear track is shown in Fig. 6b. This micrograph showed different surface microstructure when the wear track is compared with the area outside. A higher magnification as given in Fig. 6c showed a patchy layer formed after the test, while in Fig. 6d a smooth character is seen along the wear track.

SEM pictures of the PA6-14 nanocomposite are shown in Fig. 7. The edge of the wear track at these silica loadings is seen in Fig. 7a. Irregular and large patches were formed along the wear track (Fig. 7b). At higher magnifications a rough surface topography was observed and groove formation with particle dislodging during sliding was evident (Fig. 7c). The surface also showed accumulation of worn material in the wear track in the form of lumps (Fig. 7d). These lumps are presumably made out of clustered nanosilica into the polymer matrix.

SEM pictures of the steel pin of the experiments with the PA6-14 sample were taken to verify film formation on the counterface, are shown in Fig. 8a. The surface seemed to be covered with worn material that has probably been back-transferred from the counterface to the pin surface. At higher magnifications compacted long patches were also seen (Fig. 8b). After the wear test, good dispersion of the nanoparticles in the polymer was seen on the pin counterface as indicated in Fig. 8c.

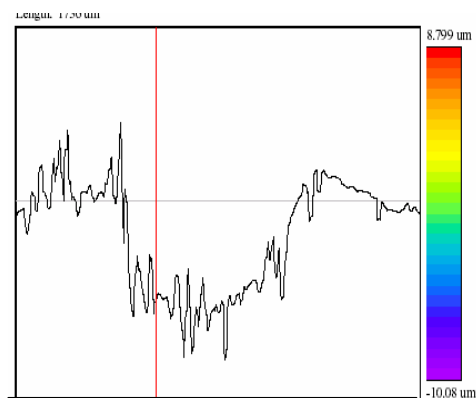


Fig. 5. Opto-profiler of the wear track of the filled nylon (14 wt%)

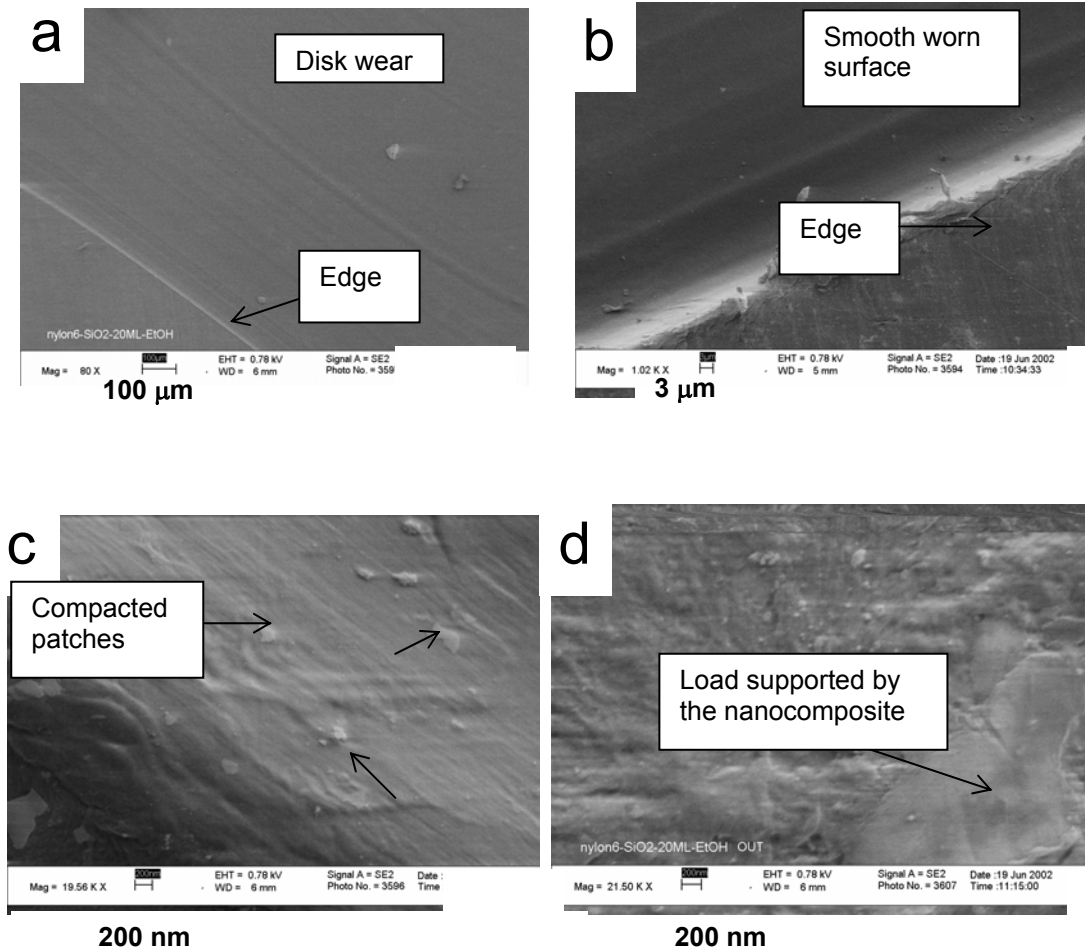


Fig. 6. Wear track of PA6-2 nanocomposite as shown by SEM.

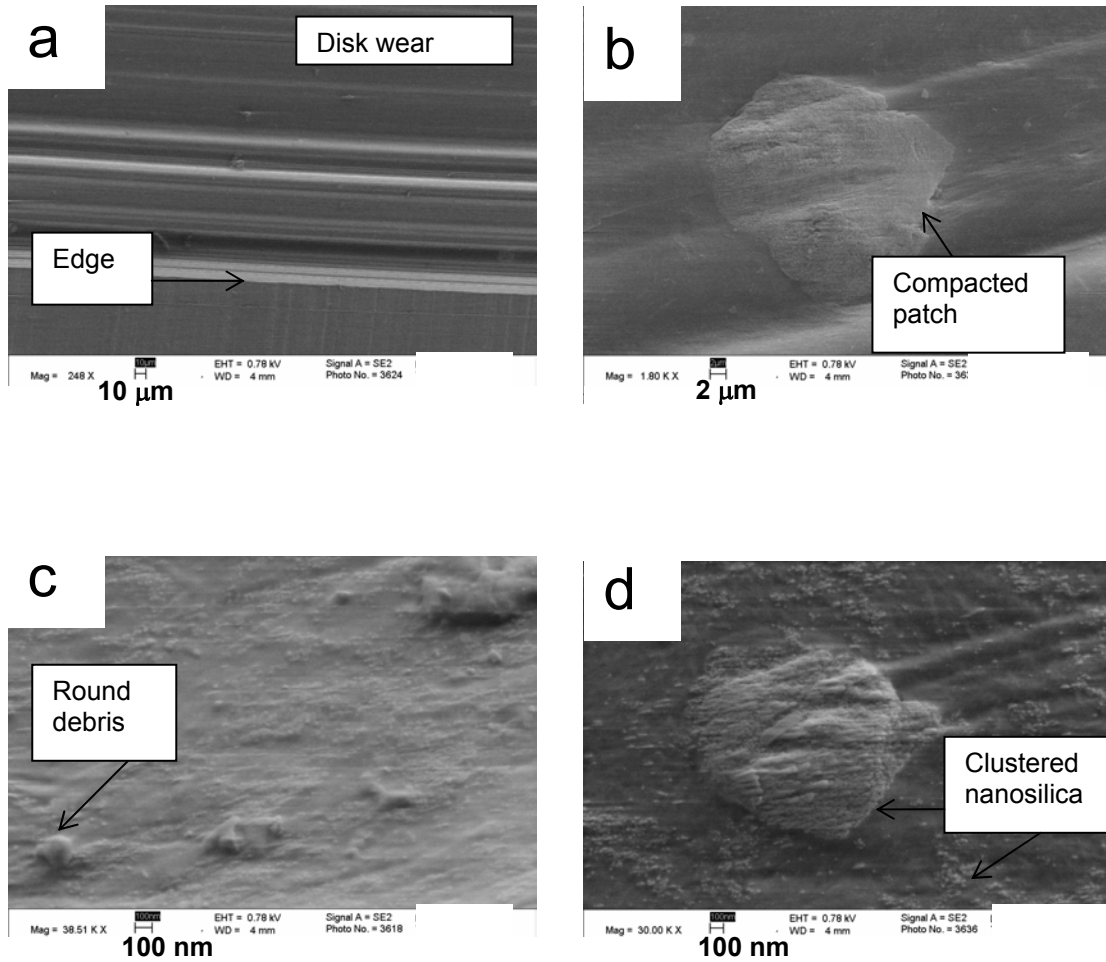


Fig. 7. Wear track of the PA6-14 nanocomposite.

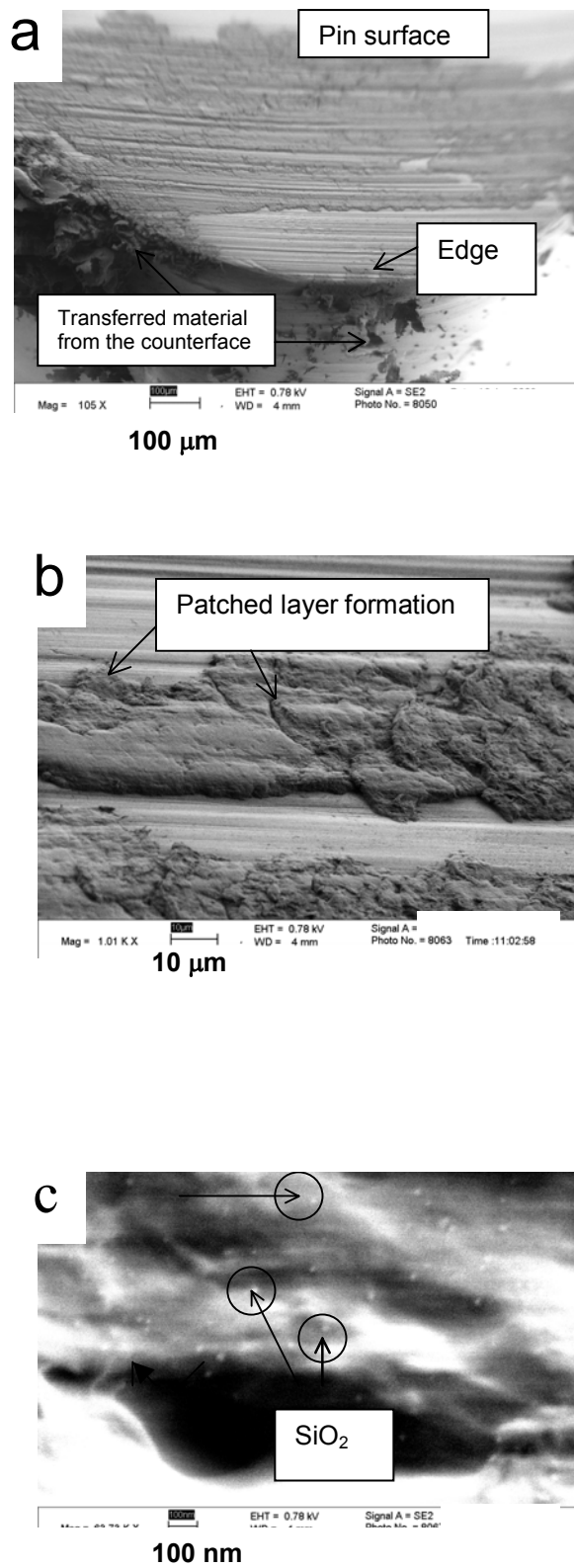


Fig. 8. Pin counterface of PA6-14 nanocomposite.

4.4 Discussion

The XRD results indicated the positive effect of the filler on nucleation. As indicated in Table 1, the degree of crystallinity was slightly higher for the PA6-2 composite when compared with pure nylon-6. As a semicrystalline polymer, nylon-6 is regarded as a two-phase system consisting of crystalline and amorphous regions. The chain segments existed as folded chain lamellae organized into spherulites. Crystalline structures have higher density than amorphous structures due to the highly ordered packing. More energy is required to damage orderly packed crystalline material than for disrupting the loosely packed amorphous materials [24]. Cartledge *et al.* [8] demonstrated that higher crystallinity (varying cooling rates) results in a hard composite with high wear resistance.

Friction and wear

All quantitative discussions of friction depend critically on the experimental conditions under which it was measured. The neat polymer showed an initial coefficient of friction of 0.2, which gradually elevated up to a steady state of 0.45 (Fig. 4). This study showed that the silica nanoparticles were effective in reducing the coefficient of friction (μ) and specific wear rate (k_w) of PA6 when added in an amount of 2 wt% (Table 2). The plate abraded the pin slightly; this process increased the coefficient of friction at the start of the test. After this transient period the plate reduced the surface roughness of the polymer and also provided a cleaner surface. Both factors tended to avoid a further increase in the coefficient of friction. The resulting μ and k_w for the PA6-2 composite was lower than for the PA6-14 composite. The latter showed during the first km a μ of 0.20 while after 1.32 kilometers μ varied until a steady coefficient of friction was achieved comparable to that of unfilled nylon-6 ($\mu \approx 0.4$).

A transfer of polymer to the metal surface initiated by adhesion between the two materials, during sliding contributed to shear in the subsurface region of the contact. Even in static contact this transfer has been reported in a polymer such as polytetrafluoroethylene (PTFE) [9].

In Fig. 9 a schematic illustration of the friction model for PA6-2 and PA6-14 during sliding is shown. In the initial stage of sliding there was an intimate contact between pin and disc (Fig. 9a and 9b). Further sliding involved the transfer of polymer to the harder metallic counterface caused by electrostatic forces (e.g. van der Waals) or tribochemical reactions on the surface (Fig. 9c and 9d). Nanosilica particles in the composite might improve the interaction to the counterface resulting in a decrease in wear rate by a factor of 10^2 in the case of PA6-2. The bonding between polymer and counterface was in this case stronger. The contact of the nano-composite with the pin led to a layer formation by material removal from the disk to the

counterface (*vide infra*). Processes occurring close to the interface were part of an interfacial wear. Adhesive wear was the most important mechanism for this layer formation.

The layered-film formation observed on the pin in the PA6-14 experiment as visible in Fig. 8a was explained as follows: Part of the nanocomposite was transferred to the steel counterface and upon sliding a secondary contact occurred. After consecutive sliding the material was transferred to the counterface filling the uneven surface of the pin (Fig. 9c and 9d). In the case of PA6-14, repeated movement over the pin led to progressive built-up of a transferred layer as seen in Fig. 8b. The detachment of material from the disc to the pin was aided by the clustered nanoparticles as seen at higher magnification in Fig. 8c. This is schematically represented in Fig. 9f.

The smooth and compacted patches observed in Fig. 6c suggested that in the PA6-2 case, the material was re-transferred to the disc in patches, supporting the total load of the pin during sliding. This process led to a deformed material as seen in Fig. 6d. Upon consecutive contact the migration of the nanocomposite took place forming a film on the pin as schematically illustrated in Fig. 9e. The difference in frictional behaviour of PA6-2 and PA6-14 composite was then attributed to the difference in composite-counterface interaction.

SEM photographs from the edge of the PA6-2 material (Fig. 6b) suggested that the smooth surface observed on the wear track, was due to the formation of a protective film. It was observed that for PA6-2 a uniform layer was formed on both faces and that during sliding the surface molecules of the polymer were highly oriented in the direction of sliding. The layer adhered well to the pin, and further sliding occurred between the surface of the bulk polymer, which contained similarly oriented molecules and the transfer film on the counterface (Fig. 9g).

On the contrary, the PA6-14 involved peeling-off of material from the transfer film followed by rolling as seen in Fig. 7c. The difference in coefficient of friction can be related to higher degree of interfacial wear of the disc and the counterface. Higher amounts of silica particles in PA6 filled the rough parts of the counterparts in less time than in PA6-2. Even though a layer in PA6-14 was formed more rapidly than in PA6-2, this layer eventually became detached, forming round debris asperities, as illustrated in Fig. 9f. Under these conditions, the polymer was transferred to the counterface in lumps (Fig. 7c) and patches of 0.1 to 10 μm thick (Fig. 7d). The wear rate appeared to be dictated by the rate of removal of the transfer film from the counterface.

In order to study possible chemical changes during sliding XPS experiments on the pin and transfer material was performed. Fe_2O_3 formation was seen caused by the oxidation of steel. Except for the Fe_2O_3 , no chemical change has occurred in the process of nylon-6/nanosilica sliding against the steel disk.

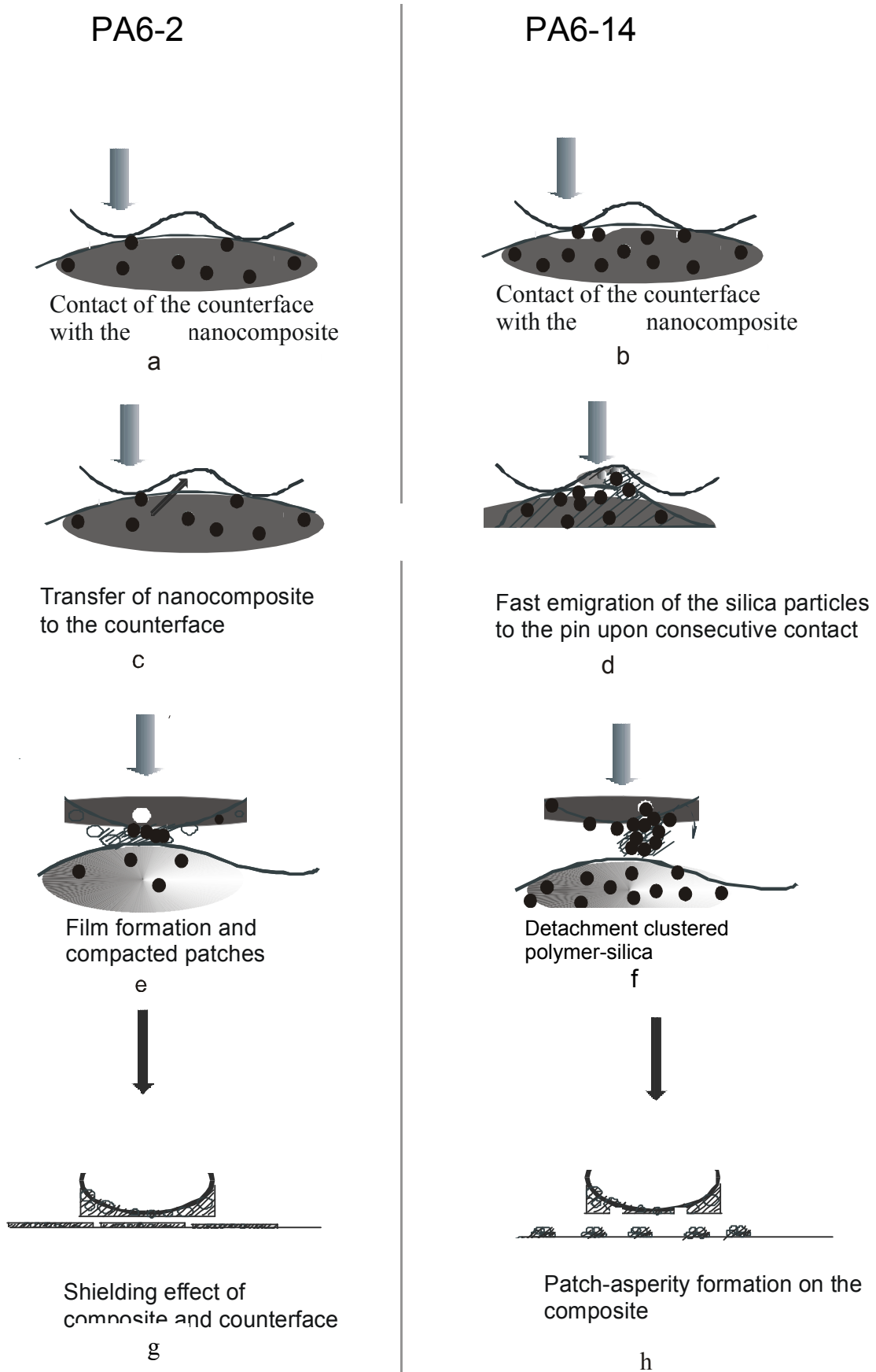


Fig. 9. Scheme and proposed mechanism of the film formation when using nanoparticles.

4.5 Contact Model and Friction Model

Better understanding of the tribological behaviour of the polymer nanocomposite, was achieved by applying a contact model. Nominally flat (layered) surfaces contacts were carried out assuming that the surface was covered by an array of spherically shaped asperities with different radii and heights. The calculation considered the summation of contacts of spheres with a flat layered surface.

This section discusses the contact of a sphere with a flat layered surface. This model is later extended to a multi asperity contact.

4.5.1 Single-asperity contact model

Suppose that a sphere is in contact with a flat-layered surface, both the layer and the substrate will react against the normal load. The combined influence of the layer and the substrate depends on the layer thickness (t), the radius of the sphere (β) and the indentation depth (ω) [25]. It is assumed that the mechanical properties of the layered surface vary as a function of indentation depth and that the layer is perfectly bounded to the substrate. The model is illustrated in Fig. 10, where E is the Young's modulus, H the hardness, F the applied force and ν the Poisson ratio. The subscript 'eff' stands for effective, and refers to the properties of the material as a whole.

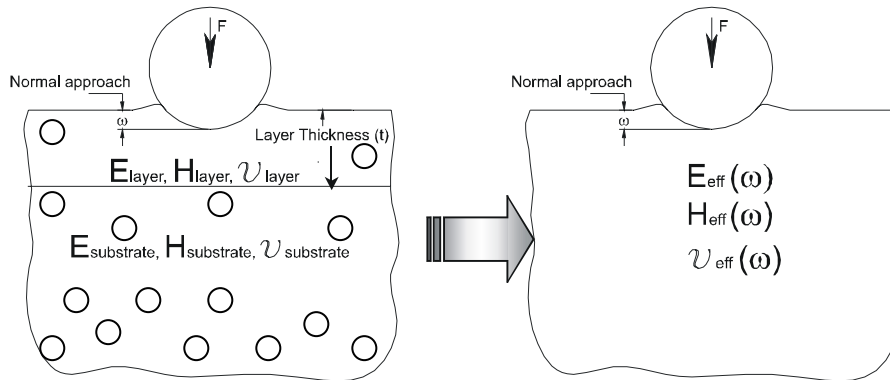


Fig. 10. Representation of the single-asperity contact model

Elastic contact

Swain and Mencik [25] proposed an equation to calculate an effective Young's modulus for a layered surface based on the weight function derived by Gao *et al.* [26].

$$E_{eff}(\omega) = E_s + (E_l - E_s)I_0(\xi(\omega)) \quad (1)$$

Where:

$$I_0(\xi(\omega)) = \frac{2}{\pi} \tan^{-1}(\xi(\omega)) + \frac{1}{2\pi(1-\nu_{eff})} \left[(1-2\nu_{eff})\xi(\omega) \ln \frac{1+\xi(\omega)^2}{\xi(\omega)^2} - \frac{\xi(\omega)}{1+\xi(\omega)^2} \right] \quad (2)$$

$$\text{with} \quad \xi(\omega) = t/a(\omega) \quad (3)$$

$$a(\omega) = \beta^{0.5} \omega^{0.5} \quad (4)$$

$$\text{and} \quad \nu_{eff}(\omega) = \nu_s + (\nu_l - \nu_s) I_1(\xi(\omega)) \quad (5)$$

$$I_1(\xi(\omega)) = \frac{2}{\pi} \tan^{-1}(\xi(\omega)) + \frac{\xi(\omega)}{\pi} \ln \frac{1+\xi(\omega)^2}{\xi(\omega)^2} \quad (6)$$

In which a is the contact radius and the subscripts s and l refer to the substrate and the layer respectively.

The equivalent elasticity modulus of a flat-layered surface against a sphere then can be calculated using equation 7.

$$E_{1eff}^*(\omega) = \frac{E_1 E_{eff}(\omega)}{E_1(1-\nu_{eff}^2) + E_{eff}(\omega)(1-\nu_1^2)} \quad (7)$$

where E_1 is the Young's modulus of the sphere.

The load carried (P_e) by a flat-layered surface elastically deformed by a sphere can be calculated as:

$$P_e(\omega) = \frac{4}{3} E_{1eff}^* \beta^{0.5} \omega^{1.5} \quad (8)$$

A good agreement of experimental data with the load calculated using equation 8 has been reported [27].

Fully Plastic Contact

Bhattacharaya and Nix [28] performed a finite element analysis to simulate an indentation of a pyramid shaped indenter against a flat-

layered surface. Their simulation showed that the hardness of a layered surface increases as the penetration depth increases. By fitting the numerical result, they derived the relation of the hardness with the indentation depth as:

$$H(\omega) = H_s + (H_l - H_s) \exp\left(-\frac{\sigma_{yl} E_s}{\sigma_{ys} E_l} \left(\frac{\omega}{t}\right)^2\right) \quad (9)$$

Where H is the hardness, E is the Young's modulus, σ_y is the yield stress of the material, ω is the indentation depth, t is the layer thickness and subscript s and l refer to substrate and layer.

The contact area (A_p) and the load carried (P_p), at the fully plastic contact condition can be calculated as follows:

$$A_p(\omega) = 2\pi\beta \omega \quad (10)$$

$$P_p(\omega) = H(\omega)A_p(\omega) \quad (11)$$

Elastic-plastic Contact

Tabor [29] observed that in metal, the onset of the first yield occurs when the maximum Hertzian contact pressure reaches 0.6 times the hardness of the deformed material. It is assumed in this model that the layered material is following the Hertzian behaviour, the critical indentation depth (ω_{c1}) to initiate the onset of yielding can be calculated as:

$$\omega_{c1}(\omega) = 0.89\beta \left(\frac{H(\omega)}{E_{1eff}^*(\omega)}\right)^2 \quad (12)$$

Further deformation after the onset of yielding will lead to an elastic-plastic condition. Based on Johnson [30], Zhao *et al.* [31] derived that the fully plastic condition will occur when an asperity is deformed more than 54 times the onset of the first yielding, so adopting this result one can write:

$$\omega_{c2}(\omega) = 54\omega_{c1}(\omega) \quad (13)$$

Following the transition from elastic to fully plastic condition proposed by Zhao *et al.*, the contact area (A_{ep}) and the load carried by the

deformed layered surface (P_{ep}) under elastic-plastic conditions can be calculated as:

$$A_{ep}(\omega) = \pi\beta\omega \left[1 - 2 \left(\frac{\omega - \omega_{c1}(\omega)}{\omega_{c2}(\omega) - \omega_{c1}(\omega)} \right)^3 + 3 \left(\frac{\omega - \omega_{c1}(\omega)}{\omega_{c2}(\omega) - \omega_{c1}(\omega)} \right)^2 \right] \quad (14)$$

$$P_{ep}(\omega) = \left[H(\omega) - 0.6H(\omega) \frac{\ln \omega_{c2}(\omega) - \ln \omega}{\ln \omega_{c2}(\omega) - \ln \omega_{c1}(\omega)} \right] A_{ep}(\omega) \quad (15)$$

The model showed a good agreement when compared with experimental results [32,33]. However, some deviation between the experimental result and the calculated result were observed. One of the reasons is that the method does not consider the effect of the roughness of the ball used for the experiments. Therefore the multi-asperities model was introduced.

4.5.2 Multi-asperities contact model

A nominally flat surface is rough on microscopic scale. It can be seen as a population of spherically shaped asperities with different radii and heights. If two surfaces are in contact, then the contact will occur between the asperities. This causes the real contact area to be small compared to the opposing contact area.

Greenwood and Williamson [34] introduced a method to calculate the real contact area of two nominally flat surfaces. The model assumed that a nominally flat surface consists of an array of asperities with the same radius (β_{ave}). The height of each asperity varies from the asperity mean plane following a Gaussian distribution. It is also assumed that the deformation solely occurs at asperity level.

Nowadays, there are many kinds of commercially available three dimension surface topography measurement apparatus where the radius and the height of every single asperity on the measured surface can be obtained [35]. It allows calculating the number of asperities in contact, the contact area and the load carried by each asperity. The total load carried by asperities is calculated by summarizing all the loads carried by each asperity. This method will diminish the assumption of average asperity radius and enable us to calculate the contact in case of non-Gaussian surfaces more precisely. This method is described further in this report.

4.5.3 The static contact model

Suppose a rough surface is modelled as an array of i numbers of spherically shaped asperities with different radii (β_i) and height (z_i). The

height of each asperity is measured from the asperities mean plane. When the surface approaches a flat-layered surface, some asperities might have contact with the flat-layered surface (if $z_i > d$) and some might not (if $z_i < d$) depends on the separation (d) of the two surfaces (see Fig. 11). Assuming that the deformation solely occurs at asperity level, the indentation depth of each asperity (ω_i) is determined by:

$$\omega_i = z_i - d \quad (16)$$

When the layered surface is pressed, both the layer and the substrate will give contribution to support the load. The more the indentation depth the more the substrate contributes to react against the normal load. Therefore, the layered surface can be modelled as a solid material with effective properties ($E_{\text{eff}}(\omega_i)$; $H_{\text{eff}}(\omega_i)$; $\nu_{\text{eff}}(\omega_i)$) as a function of indentation depth (ω_i). It is assumed in this model that the layer is perfectly bounded to the substrate. This model is simply illustrated in Fig. 11.

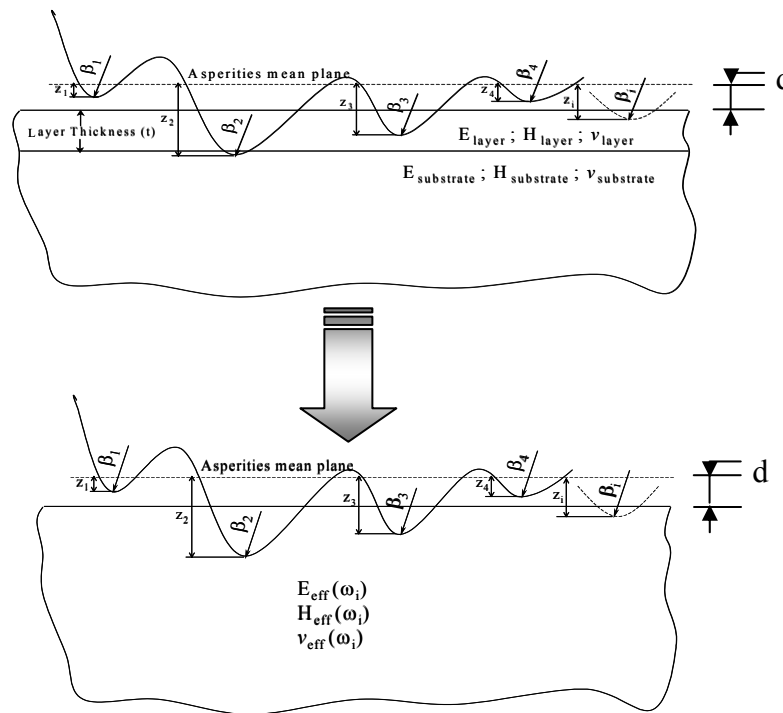


Fig. 11. Representation of the static contact model

Calculation of the separation

At a certain separation (d), the indentation depth of each asperity can be determined. As the asperities are assumed to have spherical shape, the load carried by each asperity was calculated as a contact of a sphere with a flat-layered surface [35].

The calculation of load carried and the contact area of each asperity in contact at elastic (P_{ie} ; A_{ie}), elastic-plastic (P_{iep} ; A_{iep}) or fully plastic condition (P_{ip} ; A_{ip}) can be found in detail in [36]. A summary is given next:

Elastic contact:

$$P_{ie}(\omega_i) = \frac{4}{3} E_{1eff}^* \beta_i^{0.5} \omega_i^{1.5} \quad (17)$$

Plastic contact:

$$P_{ip}(\omega_i) = H_{eff}(\omega_i) A_{ip}(\omega_i) \quad (18)$$

And Elastic-plastic :

$$P_{iep}(\omega_i) = \left[H_{eff}(\omega_i) - 0.6 H_{eff}(\omega_i) \frac{\ln \omega_{c2}(\omega_i) - \ln \omega}{\ln \omega_{c2}(\omega_i) - \ln \omega_{c1}(\omega_i)} \right] A_{iep}(\omega_i) \quad (19)$$

In which E is the Young's modulus, H is the hardness, σ_y is the yield stress involved for the calculation of H_{eff} , t is the layer thickness, a is the contact radius and ν is the Poisson ratio (subscript 1, s and l refer to the rough surface, the substrate and the layer respectively).

The total load carried (P_{tot}) by all asperities in contact then can be calculated by summing up all the loads carried by each asperity as:

$$P_{tot} = \sum_{ie} P_{ie} + \sum_{iep} P_{iep} + \sum_{ip} P_{ip} \quad (20)$$

where i is the number of asperities in contact and subscript e , ep and p corresponds to elastic, elastic-plastic and plastic contact conditions respectively.

Contact area with substrate and layer ($\omega_i > t$)

After the calculation of the separation is done, the model is transformed back into the condition of rough surface in contact with flat-layered surface. The contact area (A_i) and the load carried by each asperity (P_i) are obtained from the calculation of separation.

Friction tests have been performed on balls covered with lead and sliding against steel disc [33]. Evidences that the hard asperity might penetrate through the layer and having contact with the substrate were found. This condition is schematically shown in Fig. 12. Based on this observation [33] it is in this model assumed that when the indentation depth (ω_i) of an asperity is less than the layer thickness,

the asperity has contact only with the layer whereas when the penetration depth is more than the layer thickness some part of the asperity has contact with the layer and some other part has contact with the substrate.

The contact area (A_{iel} , A_{iepl} , A_{ipl}) and the load carried (P_{iel} , P_{iepl} , P_{ipl}) by asperities that has contact only with the layer are equal to the contact area (A_{ie} , A_{iep} , A_{ip}) and the load carried by asperity (P_{ie} , P_{iep} , P_{ip}) obtained from the calculation of the separation.

$$A_{iel} = A_{ie} ; A_{iepl} = A_{iep} ; A_{ipl} = A_{ip} \quad (21)$$

$$P_{iel} = P_{ie} ; P_{iepl} = P_{iep} ; P_{ipl} = P_{ip} \quad (22)$$

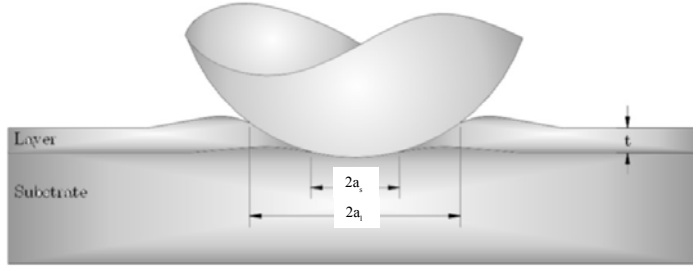


Fig. 12. Schematic representation of asperity contact with substrate

For asperities that penetrate through the layer and having contact with the substrate, some part of the load will be carried by the substrate and the layer will carry the remains part. The amount of load carried by substrate and the amount of load carried by layer depends on the depth of indentation by asperity into the substrate. The indentation depth of an asperity into the substrate is defined as:

$$\omega_{is} = z_i - (d + t) \quad (23)$$

Depending on the value of ω_{is} the contact condition with the substrate can be elastic, elastic-plastic or fully plastic. The load carried by the substrate at elastic (P_{ies}), elastic-plastic (P_{ieps}) or fully plastic condition (P_{ips}) respectively can also be calculated [36]:

$$P_{ies} = \frac{4}{3} E_{12}^* \beta_i^{0.5} \omega_{is}^{1.5} \quad (24)$$

4.6 The friction model

When a plastically deformed asperity starts to move, the contact area that carries the load is only half of the total contact area at static condition. Therefore, the plastically deformed asperity tends to sink more into the surface in order to balance the normal load. At elastic contact condition, the contact area at static condition is in fact slightly changing due to movement that is accompanied by friction. In this model, the moving contact area at elastically deformed asperities is assumed to be equal to the static elastic contact area. For the elastic-plastic contact situation of moving asperities, the contact area can be assumed to be linearly changed as shown in Fig. 13.

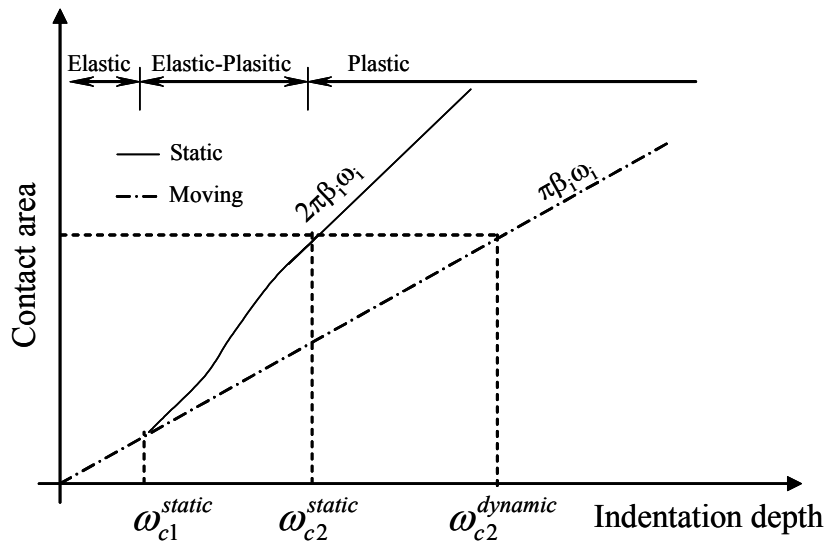


Fig. 13. Contact area of a single moving asperity.

Based on this assumption, the contact area of a moving asperity at elastic (A_{iem}), elastic-plastic (A_{iepm}) or fully plastic (A_{ipm}) condition can be calculated using

$$A_{iem} = A_{iepm}(\omega_i) = A_{ipm} = \pi\beta_i\omega_{im} \quad (25)$$

where ω_{im} is the indentation depth of each moving asperity.

Accordingly the load carried by a moving asperity at elastic (P_{iem}), elastic-plastic (P_{iepm}) or fully plastic (P_{ipm}) can be calculated as:

$$P_{iem}(\omega_i) = \frac{4}{3} E_{1eff}^* \beta_i^{0.5} \omega_i^{1.5} \quad (26)$$

Where the separation (d_m) of the moving surface in contact can also be determined [36].

The contact area (A_{ielm} , A_{ieplm} , A_{iplm}) and the load carried by the asperity (P_{ielm} , P_{ieplm} , P_{iplm}) that has contact only with the layer is equal with the

contact area (A_{iem} , A_{iepm} , A_{ipm}) and load carried by the asperity (P_{iem} , P_{iepm} , P_{ipm}) obtained from the separation calculation.

$$A_{ielm} = A_{iem} ; A_{ieplm} = A_{iepm} ; A_{iplm} = A_{ipm} \quad (27)$$

$$P_{ielm} = P_{iem} ; P_{ieplm} = P_{iepm} ; P_{iplm} = P_{ipm} \quad (28)$$

And the contact area and the load carried by asperities in contact with substrate at moving situation are:

$$A_{iesm} = A_{iepsm} = A_{ipsm} = \pi\beta_i\omega_{ism} \quad (29)$$

4.6.1 Friction force due to adhesion

The moving contact model enables us to calculate the contact area of each asperity (A_i). If the interfacial shear strengths of each asperity in contact with substrate and layer at elastic (τ_e), elasto-plastic (τ_{ep}) and plastic (τ_p) condition can be determined or measured, then the friction force due to adhesion can be calculated using equation 30.

$$F_{ad} = \sum_{iesm} \tau_{ies} A_{iesm} + \sum_{iepsm} \tau_{ieps} A_{iepsm} + \sum_{ipsm} \tau_{ips} A_{ipsm} + \sum_{ielm} \tau_{iel} A_{ielm} + \sum_{ieplm} \tau_{iepl} A_{ieplm} + \sum_{iplm} \tau_{ipl} A_{iplm} + \sum_{ism} \tau_{ipl} A_{ilm}^s \quad (30)$$

4.6.2 Friction force due to ploughing

When an asperity is in contact with the substrate or the layer at a fully plastic condition then the resistance to motion will also given by the ploughing of the softer material. The schematic representation of the ploughing phenomenon is shown in Fig. 14. For a certain value of θ_i the coefficient of friction can be calculated using equation 31.

$$f_{ipl} = \frac{2}{\pi} \frac{\theta_i - \sin\theta_i \cos\theta_i}{\sin^2\theta_i} \quad (31)$$

The corresponding friction force due to the ploughing at the fully plastic condition of substrate (F_{pls}) and layer (F_{pll}) can be calculated as follows:

$$F_{pls} = \sum f_{pl} \times P_{ips} \quad (32)$$

$$F_{pll} = \sum f_{pl} \times P_{ipl} \quad (33)$$

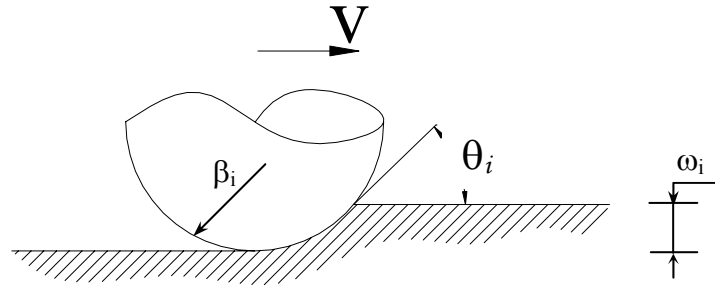


Fig. 14. Schematic representation of the friction force due to ploughing through the layer.

4.6.3 The Total friction force

Assuming that the resistance to motion are due to adhesion (F_{ad}) and ploughing (F_{pl}) only, the total friction is then:

$$F_{tot} = F_{ad} + F_{pl} \quad (34)$$

and the coefficient of friction is:

$$f = \frac{F_{tot}}{P} \quad (35)$$

4.7 Model validation

Pure nylon 6 (PA6), samples with ≈ 2 wt% of silica (PA6-2) and with 14 wt% (PA6-14) were evaluated. Indentation measurements were performed on each specimen. The use of the loading and unloading curve, the elastic modulus and the hardness were obtained and summarized in table 3.

Table 3. Modulus of elasticity and Hardness of PA6 and nanocomposites.

Specimen	Elasticity (MPa)	Hardness (MPa)
PA6	1263	54
PA6-2	2034	83
PA6-2	1760	81
PA6-14	3078	115

As can be seen from the table, as expected, the higher the amount of silica the harder is the material.

In Fig. 15 the surface topography of the steel pin is shown:

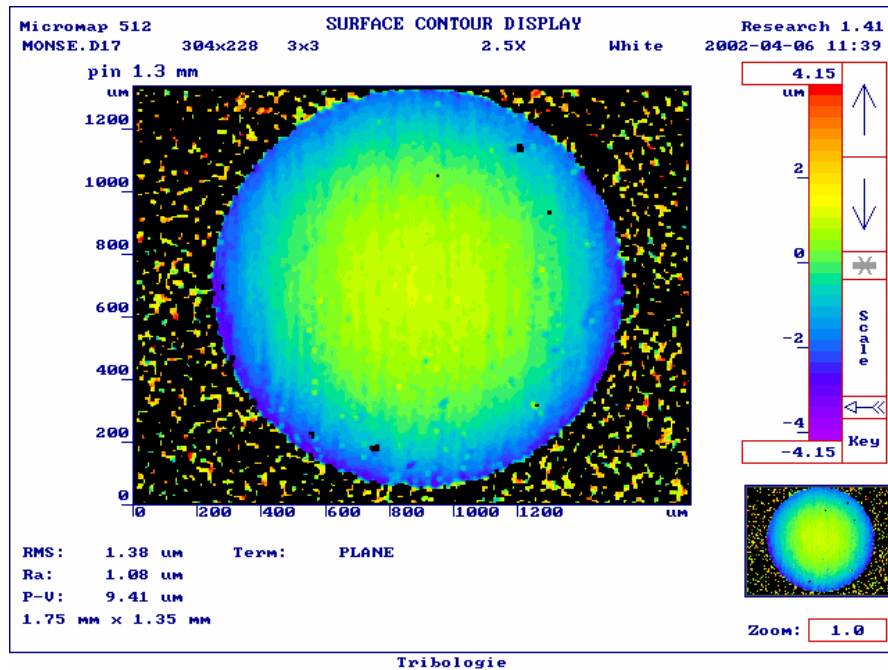


Fig. 15. Surface topography of the steel pin.

Based on the surface topography measurement, the summit contact was determined for the PA6-2 samples. The coefficient of friction (μ) was then calculated using the deterministic model above described. The results are summarized in table 4. As can be seen from the table, a reasonable good agreement is found between the experimental results and the deterministic model. The μ measured was 0.45 and the model indicates 0.38 (≈ 0.4). Experimentally, upon addition of 2 wt% of silica, μ decreased to 0.20 and the model indicated an average value of 0.27.

Table 4. Coefficient of friction calculated by means of the deterministic model developed by Pasaribu *et al.* [36].

Specimen	Load	Separation (m)	Elastic contact area (m ²)	Elastoplastic contact area	Plastic contact area	Coefficient of friction
PA6	1.00E+00	1.05E-06	1.28E-08	2.97E-08	0.00E+00	0.38
PA6-2	1.00E+00	1.19E-06	1.07E-08	1.80E-08	0.00E+00	0.26
PA6-2	1.00E+00	1.17E-06	1.58E-08	1.52E-08	0.00E+00	0.28

4.8 Conclusions

The addition of a second phase was one of the methods used to improve the tribological properties of the thermoplastic PA6 (such coefficient of friction and wear rate). The addition of 2 wt% nanosilica particles improved the coefficient of friction and wear resistance of nylon-6 composites. Smooth surfaces were obtained in the nanocomposites, indicating a well functioning tribological system. A transfer film on the steel pin was developed caused by adhesion and interlocking of fragments of material into metal asperities. Wear depended upon the adhesion of the transfer film to the counterface, and the protection of polymer surface from metal asperities by transfer film. Furthermore, the deterministic model gives good agreement with the experimental results obtained for PA6-2 nanocomposites.

4.9 References

- [1] Hironaka, S. *Jpn. J. Tribol.* 42, 931 (1997).
- [2] Theberge, J.E. Proc. Anniv. SPI (*Soc. Plast. Ind.*), Reinf. Div., 25th, 2-D, 1-12 (1970).
- [3] Bahadur, S., Gong, D. and Andereg, J. W. *Wear* 154, 207 (1992).
- [4] Bahadur S. and Polineni, V.K. *Wear* 200, 95 (1996).
- [5] Bahadur, S., Gong D. and Andereg, J.W. *Wear* 160, 131 (1993).
- [6] Tanaka, K. *Wear* 75, 183 (1982).
- [7] Kohan, M.I. *Nylon Plastics Handbook*. Hanser, New York (1995).
- [8] Cartledge, H.C.Y. *J. Mater. Sci.* 37, 3005 (2002).
- [9] Bahadur, S. *Wear* 245, 92 (2000).
- [10] Martin, J.M., Grossiord C. and Le Mogne, T. *Wear* 245, 107 (2000).
- [11] Jintang, G. *Wear* 245, 100 (2000).
- [12] Tanaka K. and Miyata, T. *Wear* 41, 383 (1977).
- [13] Jintang, G. *Wear* 245, 100 (2000).
- [14] Palabiyik, M. and Bahadur, S. *Wear* 246, 149 (2000).
- [15] Watanabe, M. and Yamaguchi, H. *Wear* 110, 379 (1986).
- [16] Xu, Y.M. and Mellor, B.G., *Wear* 251, 1522 (2001).
- [17] Bernards, T.N.M., van Bommel, M.J. and Boonstra, H.A. *J. Non-Cryst. Solids* 134, 1 (1991).
- [18] Reynaud, E., Jouen, T., Gauthier, C., Vigier G. and Varlet, J. *Polymer*, 42, 8759 (2001).
- [19] van Zyl, W.E., Garcia, M., Schrauwen, B.A.G., Kooi, B., De Hosson, J.Th.M and Verweij, H. *Macromol. Mater. Eng.* 287, 106 (2002).
- [20] Bekkers, M.H.J. and van Sprang, H.A. *X-Ray Spectrom.* 26, 122 (1997).
- [21] Maas, A.J.H., Viitanen, M.M. and Brongersma, H. H. *Surf. Interface Anal.* 30, 3 (2000).
- [22] van Welzenis, R.G. *Ionics*, 5, 13 (1999).
- [23] Mo, Z. and Zhang, H. *J.M.S.-Rev. Macrom. Chem. Phys.* C35 (4), 555 (1995).
- [24] Hutchings, I.M. *Tribology*. Edward Arnold, London (1992).
- [25] Swain M.V. and Mencik, J. *Thin Solid Films* 253, 204 (1994).
- [26] Gao, H., Chui C. and Lee, J. *Int. J. Solids Structure* 29, 2471 (1992).
- [27] Chudoba, T., Schwarzer N. and Richter, F. *Surface coatings technology* 154, 140 (2002).
- [28] Bhattacharaya, A.K. and Nix, W.D. *Int. J. Solids Structures* 24, 1287 (1988).
- [29] Tabor, D. *The hardness of metals*, Oxford University press (1951).
- [30] Johnson, K.L. *Contact mechanics*, Cambridge university press, Cambridge (1985).
- [31] Zhao, Y., Maietta D.M. and Chang, L. *Journal of Tribology* 122, 86 (2000).
- [32] El Shafei, T.E.S., Arnell, R.D. and Halling, J. *ASLE Trans.* 26, 481 (1983).
- [33] Sherbiney, M.A. *Tribological properties of ion-planted soft metallic film*, PhD. Thesis. Univ. of Salford (1975).
- [34] Greenwood J. A. and Williamson, J.B.P. *Proc. R. Soc. London, Series A* 295, 300 (1966).
- [35] de Rooij, M.B. *Tribological aspects of unlubricated deepdrawing processes*, PhD Thesis. University of Twente. The Netherlands (1998).
- [36] Pasaribu, H.R. *Contact of a sphere with a perfectly flat-layered surface. CTW,-OTR-03.2271 and CTW-OTR-03.2271 A multi-asperity contact model and friction model of a rough surface sliding against flat layered surface*. Internal Reports. University of Twente. The Netherlands (2003).

5 Rheology of Nanocomposites

The rheological properties of nanocomposites based on polyamide-6 and colloidal silica were studied under small deformation conditions. The results showed that dynamic viscosity decreased noticeably with higher filler content (18 wt% and 22 wt%) at strains larger than 1%. It can be observed an increase of 3 decades in the viscosity at these filler loadings. This effect may come from the fact that all samples show some post-condensation, as it can also be seen in the increase of dynamic modulus. Addition of silica to PA6 increased the elasticity and the viscosity when compared to unfilled PA6.

5.1 Introduction

The flow behaviour of polymer melts is of great importance in polymer manufacturing. Therefore, the description of flow phenomena by rheological studies is highly desirable to assist in the material (industrial) processability [1,2]. Polymer melt flow behaviour is strongly affected by the presence of filler particles including its morphology, surface chemistry and concentration.

Melt polymers filled with fine particles have shown yield stress [3,4] i.e. a stress below which there is no flow or the appearance of a plateau in the storage modulus at low frequencies in a dynamic deformation experiment. Some materials will not flow until a critical yield stress σ_y is exceeded (Bingham behaviour). Density and strength formed by the interaction between the filler particles is associated with the existence of this behaviour. For shear-thinning materials the general shape of the curve shows a first Newtonian region (low shear rate or stresses with constant viscosity) and a second Newtonian region also referred as zero-shear viscosity (high shear rate or stresses with constant viscosity). It has been reported [5] that non-linear viscoelastic properties of nano-filled polymer melts are similar to those observed in filled rubbers. However, the three dimensional network of rubber particles has been found to be different than that of the silica network. Alternatively, the molecular weight of the matrix, entanglement characteristics of the polymer and trapping of polymer chain loops at the filler surface appear to be the primary factors determining the non-linear viscoelasticity [5]. Adsorption of polymer chains on the silica surface of spherical particles (3 μm) has been an explanation for the rheological behaviour of polybutadiene chains filled with rigid spheres. Tethering of polymer chains to (clay) particles has been used as explanation for its elastic behaviour. If the polymer chains are not tethered, the slopes G' and G'' are similar to that of the neat polymer. In the case of nanoparticles, aggregation in clusters has been observed which led to the formation of a percolation-like filler network [5]. Therefore it is expected to be of high elasticity and viscosity and according to [3,4] high yield stress. Nevertheless, the mechanisms for reinforcement and non-linearity remain controversial.

Constitutive equations often apply over limited parts of the flow curve. For example, the Bingham equation describes the shear stress/shear rate behaviour of many shear-thinning materials at low shear rates, but only over a one-decade range (approximately) of shear rate [6].

Strong interaction between particles, tethering of polymer chains to the filler or network formation on elasticity are responsible mechanisms for the elasticity of a filled polymer. In this chapter, rheological measurements at low shear rates are performed to get additional information of the effect of the silica dispersed in PA6.

Theory

Dynamic experiments are periodic experiments at frequency ω . These kinds of experiments are qualitatively equivalent to a transient experiment at time $t = 1/\omega$. If the viscoelastic behaviour is linear, the strain will be out of phase with stress. This can be shown from the constitutive equation for the shear deformation (γ) with γ° as the maximum amplitude of the strain.

$$\gamma = \gamma^\circ \sin \omega t \quad (1)$$

The shear rate ($\dot{\gamma}$) is:

$$\dot{\gamma} = \omega \gamma^\circ \cos \omega t \quad (2)$$

This expression substituted in the following linear constitutive equation for linear viscoelasticity in simple shear gives the following equation for the shear stress σ_{21} :

$$\sigma_{21}(t) = \int_{-\infty}^t G(t-t') \dot{\gamma}_{21}(t') dt' \quad (3)$$

where $\dot{\gamma} = \partial \gamma_{21} / \partial t$ is the shear rate and $G(t)$ the relaxation modulus. The integration is carried out over all the previous times t' up to current time t . This linear constitutive equation is based on the principle that effects of sequential changes in strain are additive. Denoting now $t-t'$ by s , we have the following equation for the stress σ :

$$\begin{aligned} \sigma(t) &= \int_0^\infty G(s) \omega \gamma^\circ \cos[\omega(t-s)] ds = \\ &= \gamma^\circ \left[\omega \int_0^\infty G(s) \sin s ds \right] \sin \omega t + \gamma^\circ \left[\omega \int_0^\infty G(s) \cos s ds \right] \cos \omega t \end{aligned} \quad (4)$$

The integrals converge only if $G(s) \rightarrow 0$ as $s \rightarrow \infty$; the term in $\sin \omega t$ is in phase with γ to a degree depending on the relative magnitudes of these terms. The quantities in brackets are functions of frequency but not of elapsed time, so the last equation can be conveniently written as:

$$\sigma = \gamma^\circ (G' \sin \omega t + G'' \cos \omega t) \quad (5)$$

Thereby defining two frequency-dependent functions: the shear storage modulus $G'(\omega)$ and the shear loss modulus $G''(\omega)$

It is useful to write the stress in an alternative form displaying the *amplitude* $\sigma^\circ(\omega)$ of the stress and the phase angle $\delta(\omega)$ between stress and strain. From trigonometric relations,

$$\sigma = \sigma^\circ \sin(\omega t + \delta) = \sigma^\circ \cos \delta \sin \omega t + \sigma^\circ \sin \delta \cos \omega t \quad (6)$$

Comparison of equations (4) and (6) shows that

$$\begin{aligned} G' &= (\sigma^\circ / \gamma^\circ) \cos \delta \\ G'' &= (\sigma^\circ / \gamma^\circ) \sin \delta \\ G'' / G' &= \tan \delta \end{aligned} \quad (7)$$

It is evident that each periodic, or dynamic, measurement at given frequency provides simultaneously two independent quantities, either the complex shear modulus (G^*) as defined by $\sigma^* / \gamma^* = G^* = G' + iG''$, and G'' or else $\tan \delta$ and $\sigma^\circ / \gamma^\circ$, the ratio of peaks stress per peak strain. It is usually convenient to express the sinusoidally varying stress as a complex quantity, the modulus is also complex, given by:

$$\sigma^* / \gamma^* = G^* = G' + iG'' \quad (8)$$

$$|G^*| = \sigma^\circ / \gamma^\circ = \sqrt{(G'^2 + G''^2)} \quad (9)$$

This corresponds to a vectorial resolution of the components in the complex plane. It is evident that G' is the ratio of stress in the phase with the strain to the strain, whereas G'' is the ratio of the stress 90° out of phase with the strain. The data from sinusoidal experiments can also be expressed in term of a complex compliance

$$J^* = \gamma^* / \sigma^* = 1 / G^* = J' + iJ'' \quad (10)$$

The storage compliance J' is the ratio of the strain in phase with the stress to the stress, whereas the loss compliance J'' is the ratio of the strain 90° out phase with the stress to the stress. The *storage modulus* G' and *compliance* J' are so named because they are *directly proportional to the average energy storage in a cycle of deformation*. The *loss modulus* G'' and *compliance* J'' are *directly proportional to the average dissipation or loss of energy as heat in a cycle of deformation*. Note that $J'' / J' = G'' / G' = \tan \delta$.

Reference to the complex modulus $J^* = 1 / G^*$, their individual components are not reciprocally related, but are connected by the following equations:

$$J' = \frac{G'}{(G'^2 + G''^2)} = \frac{1 / G'}{1 + \tan^2 \delta} \quad (11)$$

$$J'' = \frac{G''}{(G'^2 + G''^2)} = \frac{1 / G''}{1 + \tan^2 \delta} \quad (12)$$

$$G' = \frac{J'}{(J'^2 + J''^2)} = \frac{1 / J'}{1 + \tan^2 \delta} \quad (13)$$

$$G'' = \frac{J'}{(J'^2 + J''^2)} = \frac{1/J''}{1 + \tan^2 \delta} \quad (14)$$

Periodic measurements can be made, depending on circumstances, at frequencies from 10^{-5} to 10^8 Hz, our experimental method runs from 0.1 to 100 Hz. As an alternative to G^* , the phase relationships can equally be expressed by a complex viscosity $\eta^* = \eta' - i\eta''$, which is frequently used to describe viscoelastic liquids. The ratio of stress in phase with rate of strain to the rate of strain is η' , and η'' is the stress 90° out of phase with the rate of strain divided by the rate of strain. Thus the phase relationships are the opposite of those for G^* , and the individual components are given by:

$$\eta' = G'' / \omega \quad (15)$$

$$\eta'' = G' / \omega \quad (16)$$

The in-phase or real component η' for a viscoelastic liquid approaches the steady-flow η_0 as the frequency ω approaches zero.

5.2 Experimental

Dynamic mechanical spectroscopy (DMS) was performed on the samples described in chapter 3 ((PA6 30,300 g/mol and colloidal silica SNOWTEX[®]) isothermally in a controlled-strain rate instrument ARES Rheometrics Spectrometer at a temperature of 230°C [7]. The angular displacement (or the angular velocity) is the independent variable and the viscous drag-torque the dependent variable. The linear viscoelastic strain limit of the composites was determined using strain sweeps experiments (where the—angular—frequency dependency of the polymer melt is determined). The dynamic viscosity and the shear modulus were both obtained by using a set of 25 mm diameter parallel plates, and frequency sweeps were from 10^{-2} to 10^3 rads⁻¹ (Hz) at a 100% strain level. Measurements were performed from high to low frequencies after residence times of 5, 10 and 15 minutes respectively under nitrogen atmosphere. Once the material was mounted on the rheometer the sample was compressed to a 2 mm plate gap.

5.3 Results and discussion

Table 1. Increase in viscosity from 5 minutes to 15 minutes residence for different samples with different filler content. Filled samples increase their viscosity up to 20% or more.

Sample	Silica content (wt%)	Increase in Viscosity (%)
Reference (PA6)	0.00	15.23
25	0.82	24.09
26	4.15	42.05
G	18.01	21.40
27	22.80	28.62

Experiments of the variation of the complex shear modulus versus frequency for pure PA6 and its nanocomposites were performed. The compositions are shown in table 1.

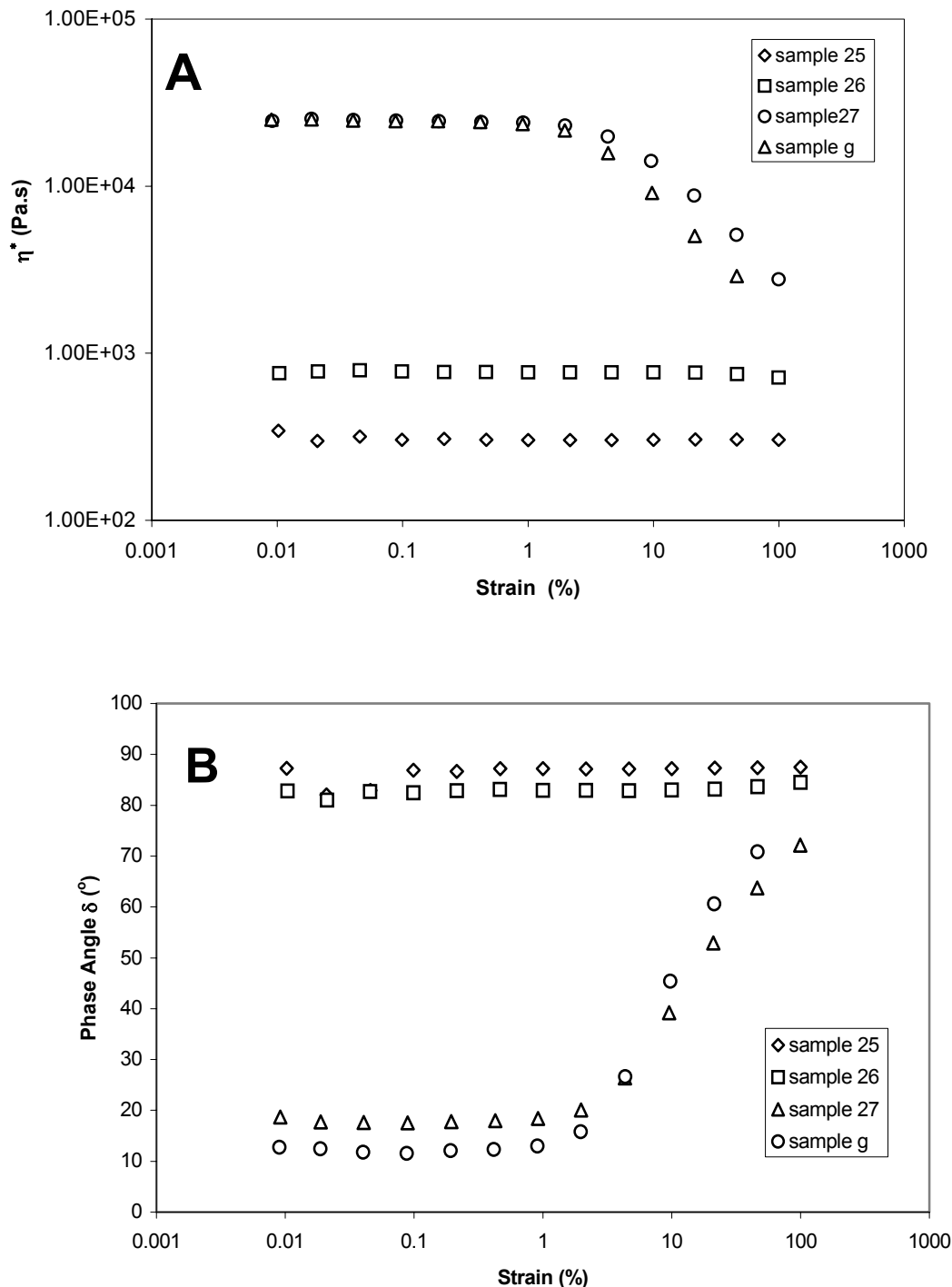


Fig. 1. Strain sweep data, dynamic viscosity (**A**) and phase angle (**B**) as a function of strain. Deviations from the linear viscoelastic behaviour appear at 1% strain for highly filled samples. The frequency used was 10 rad/s.

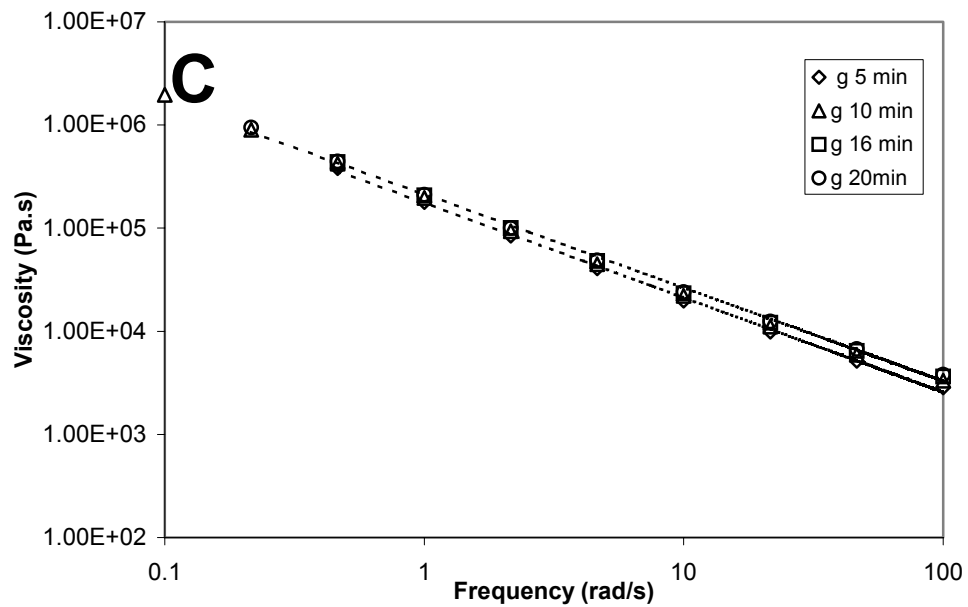
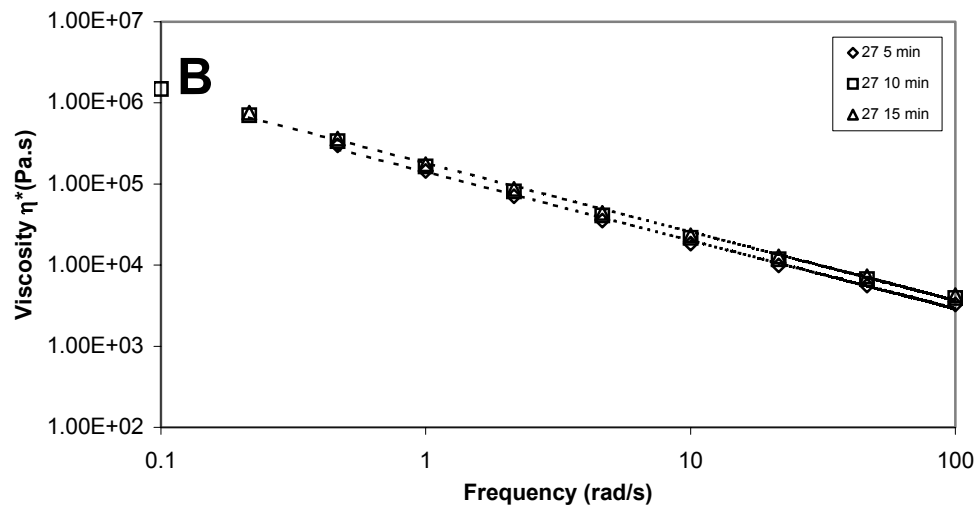
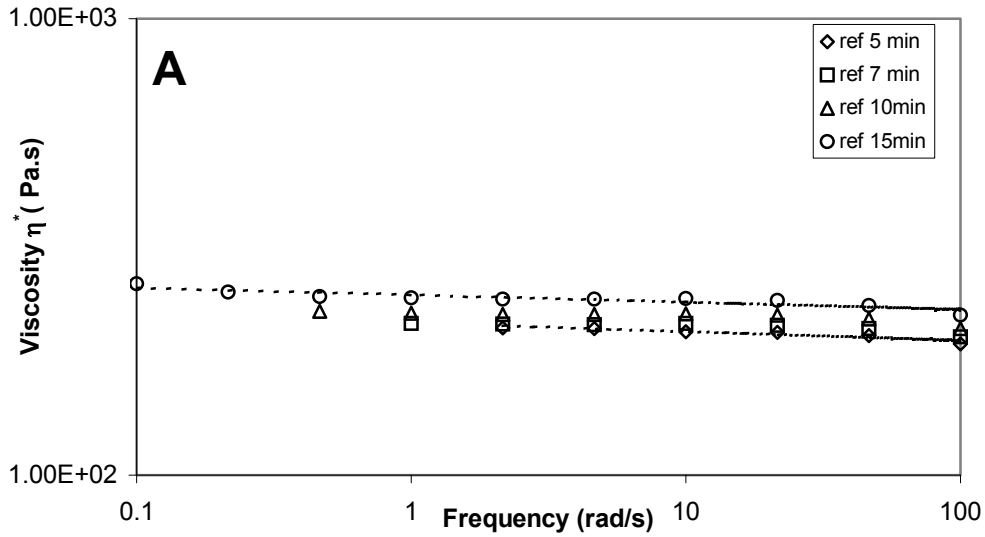
Strain sweeps. Strain sweeps were performed to determine the viscoelastic region of the polymer melts. From these measurements the maximum strain in the frequency sweeps were determined. Dynamic viscosity and the phase angle given as a function of the strain in percentage (%) are shown in Fig. 1. In Fig. 1A it is seen that while in samples with a low filler content (lower than 5 wt%, i.e. samples 25 and 26) there is almost no or a little influence of the strain up to strain values of 100%, in samples with higher filler content (samples *g* and 27) the dynamic viscosity decreased dramatically at strains larger than 1%.

Such effect is also observed in the phase angles, in Fig. 1B. The phase angle between stress and strain increases from strain values of 1% for samples with higher filler content. Therefore frequency sweeps were done with applied strains smaller than 1%, in other words, to stay in the linear viscoelastic range the strain amplitude of the highly filled samples had to be limited to 1%, covering a frequency sweep of 0.01-100 rad/s.

Thermal stability. The thermal stability is the time interval for which the polymer remains stable at a certain temperature. Beyond that time if the polymer is exposed to a given temperature for a longer period, it degrades.

The thermal stability of the samples was checked by performing frequency scans after 5, 10 and 15 minutes. It was found that the viscosity of most (filled) samples was increased by about 20% or more after 15 minutes (See table 1).

These effects were also seen in Fig. 2 where the dynamic viscosity (η^*) is given as a function of the frequency for several residence times (time that the material is held at melt range temperatures in the barrel). Therefore only experiments after 5 minutes are used in this work. The increase in viscosity could be caused by degradation or structural changes in the polymer network. However, the measurements were carried out at 230°C and degradation of the nylon melt occurs at 280°C. An interesting point is that prior heat treatment was performed at 80°C and the solvent used in the samples boils at temperatures > 100°C. Therefore the increase in the viscosity was very likely caused by the solvent removal while performing the measurements.



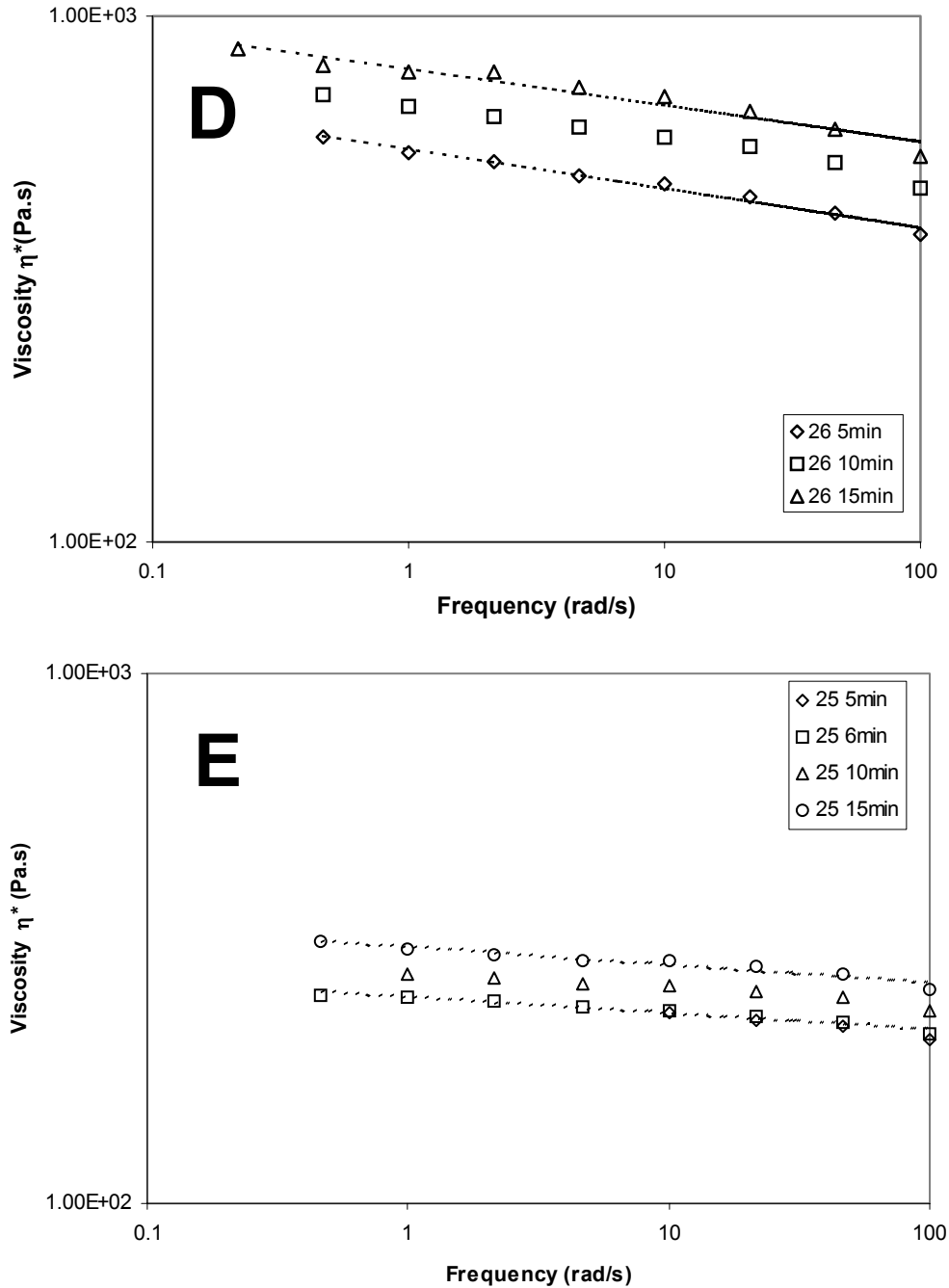


Fig. 2. Increase in dynamic viscosity (η^*) after several residence times. All filled samples show at least a 20% increase in viscosity: 15.23%(A), 24.09%(B), 42.05%(C), 21.40%(D) and 28.62% (E). Lines are given for the shortest and longest residence time.

Small strain shear rheology. In principle the knowledge of one of the functions described above: $J(t)$, $G(t)$, $G'(\omega)$, $G''(\omega)$, $J'(\omega)$, $J''(\omega)$ over the entire range of time or frequency allows calculation of every one. Small strain shear experiments provide us with several of these functions.

The rheological behaviour of PA6 nanocomposites filled with silica nano-particles, is seen with the *storage modulus* $G'(\omega)$ and *loss modulus* $G''(\omega)$ plotted as a function of angular frequency (Fig. 3).

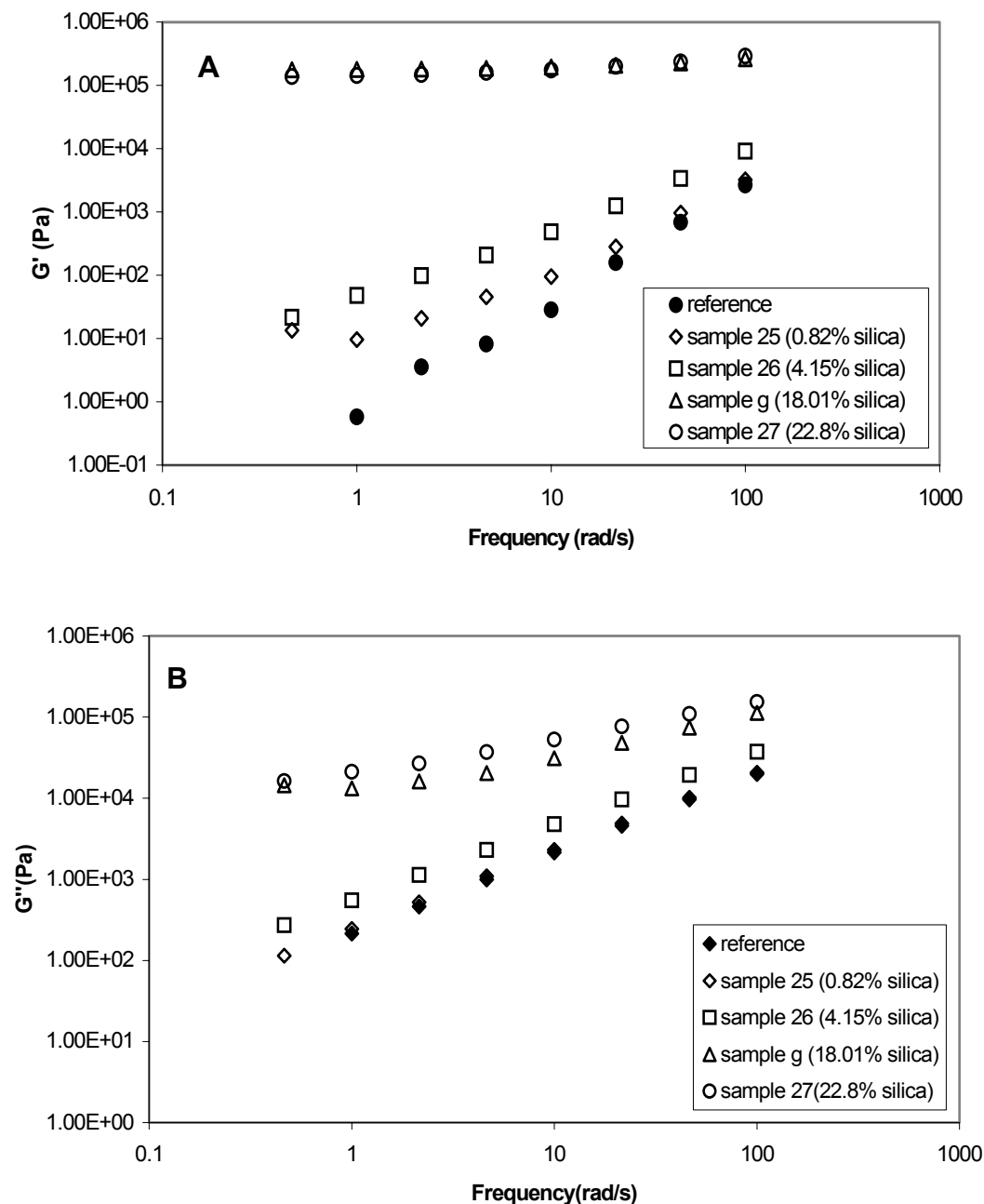


Fig. 3. Storage (A) and Loss (B) Modulus for PA6 nanocomposites. The addition of silica particles changed drastically the viscoelastic properties of the unfilled polymer.

The storage modulus gives information about the *elastic character* of the fluid or the energy storage that takes place during the deformation. In Fig. 3A it can be seen that curves for samples 25 (0.82 wt% silica)

and 26 (4.15 wt% silica) have a shape similar to the one for unfilled PA6 (similar elastic behaviour). The elastic behaviour of samples with 0.82 wt% and 4.15 wt% silica does not differ much from that of the unfilled polymer. However, at low frequency range, an intermediate elastic plateau-like has been given an additional process of relaxation due to an adsorption of the polymer chain on the silica surface [5]. In both samples the storage modulus increases with the frequency. Nevertheless, curves from *samples g* (18.01 wt%) and 27 (22.8 wt%) show a different shape than those ones mentioned before. This substantial change in shape indicates a different elastic behaviour due to the presence of silica. Both curves gave the same shape, therefore the elastic behaviour of samples *g* and 27 might be similar. The behaviour of G' at low frequencies in the case of highly filled samples is likely due to network formation. The polymer chains are attached to the filler particles, and a continuous, physical network was formed. The reference sample (PA6) fell in the terminal region (for the whole frequency range observed). Only the longest relaxation time was observed indicating Maxwell type behaviour.

The *loss modulus* gives information about the *viscous character* of the fluid or the energy dissipation that occurs in flow. In Fig. 3B, the shape of the curves for *samples 25* (0.82 wt% silica) and 26 (4.15 wt% silica) are similar to the shape of the unfilled polymer, therefore similar viscous behaviour is expected. Sample *g* and 27 differed substantially from the rest of the samples. This is also an indication that the viscous character of the samples *g* and 27 is different.

The effects are also observed in the slopes of the curves. The slopes are listed in Table 2. It is expected that at lower frequencies the polymer chains should be fully relaxed and exhibit characteristic homopolymer-like terminal flow behaviour with slopes of 2 and 1 for G' and G'' . The slope of pure PA6 is 1.80. This slope is in the range expected for polydisperse polymers [3]. Silica addition increases both the storage and loss modulus, but the effect in the slopes is greater for G' than for G'' . That is, the slope of the storage modulus decreases more pronouncedly when the amount of silica is higher in the sample than the slope of the loss modulus.

Table 2. Slope of G' and G'' in the terminal region of the master curves (Fig. 3) of nanocomposites compared to PA6.

Sample	Filler content (wt%)	Slope of G'	Slope of G''
Reference PA6	0.00	1.80	0.99
Sample 25	0.82	1.09	0.97
Sample 26	4.15	1.12	0.92
Sample <i>g</i>	18.01	0.07	0.41
Sample 27	22.80	0.13	0.42

If silica addition increases the storage modulus, it means that more energy storage takes place during deformation and decreases the slope of the curve showing almost a plateau-like region. It is thought that the higher the G' and the smaller the slope, as it happens for samples g and 27, the more pronounced the interaction between the filler particles and network forming which implies that for these samples the viscosity is mainly caused by interaction between the particles and not by the viscosity of the polymer.

All these effects can be clearly seen by plotting the dynamic modulus G^* and the phase angle δ as a function of angular frequency, see Fig. 4.

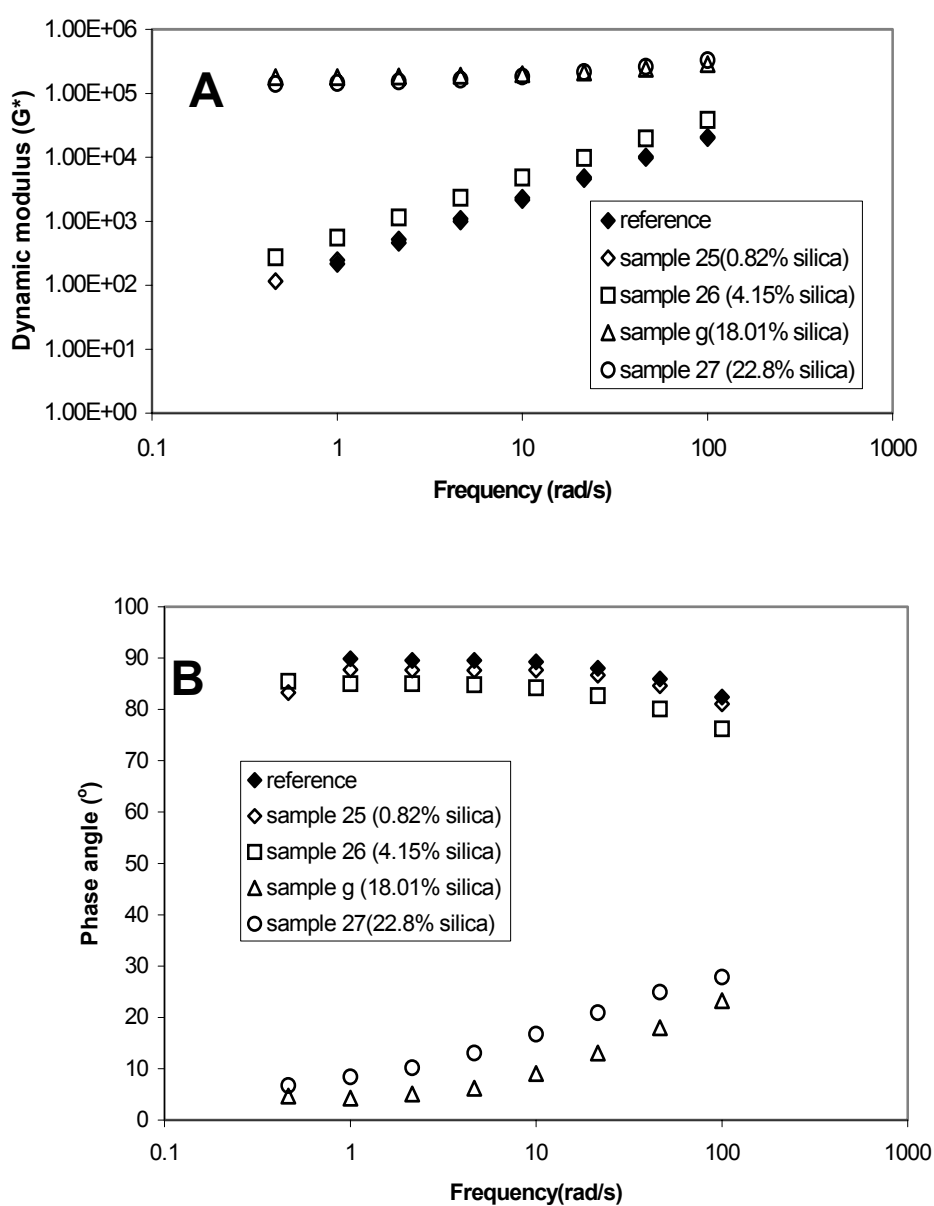


Fig. 4. Dynamic modulus(A) and Phase angle (B) for PA6 nanocomposites

Samples with silica percentage of 18.01 wt% and 22.8 wt% deviated from the results obtained by the other samples. The highly filled polymer produced higher dynamic shear modules. The same effect was already observed with PA6 and silica aerosil with $\varnothing \sim 40\text{-}50$ nm [4]. Plots for dynamic modulus and phase angle showed identical shape at lower filler content and only above 20 wt% filler a clear deviation is observed.

This indicates that only samples with 18.01 wt% silica and 22.8 wt% silica have a viscoelastic behaviour that is significantly different from that of the reference. The phase angle of samples with 0.82 wt% and 4.15 wt% silica is not different from that of the unfilled polymer, indicating a rheological behaviour dominated by the polymer matrix.

The slope of the dynamic modulus curves shows an interesting feature: at lower silica concentrations the slope of the loss modulus is very similar to the dynamic modulus (Fig. 3B and 4A), while at higher silica concentration the slope of the storage modulus is similar to the dynamic modulus (Fig. 3A and 4A). Increasing the silica content increases the amount of elasticity, At 18.01 wt% the rheological behaviour is mainly elastic and G^* shows a plateau at low frequencies.

Small strain shear viscosity. Fig. 5 shows the dynamic viscosity plotted as a function of the frequency. Data are only given for small strain measurements. The shape of the curves for 0.82 wt% and 4.15 wt% silica are the same as the one of the unfilled polymer. Sample with 0.82 wt% showed almost no variation. In the sample with 4.15 wt% the viscosity was slightly higher. As discussed previously, the behaviour of these samples was strongly influenced by the polymer matrix; therefore their viscosity is expected to be quite similar to the

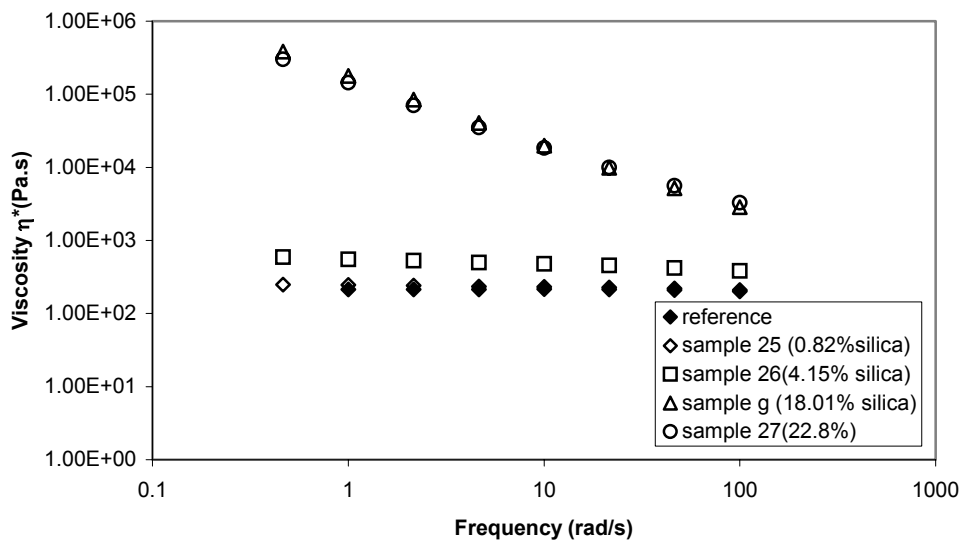


Fig. 5. Dynamic Viscosity (η^*) for PA6 nanocomposites. The addition of silica particles shows a different effect at higher frequencies than that at lower frequencies.

one of the unfilled polymer. For the reference sample as well as for the sample with little silica addition, Newtonian behaviour is observed, and it can be expected that the same would be true in a steady shear rate experiment.

Samples with high filler content showed a similar behaviour between them, which differed substantially with the low filled samples. With the high-loaded samples the viscosity is likely dominated again by the particle-particle interaction. In these samples a slope of -1 is approached at small frequencies (i.e. the shear stress approaches a constant value), which is an indication of the existence of a yield stress in these materials. These samples are Bingham materials: apparently solid systems that only plastically flow if a certain force is exceeded (a finite shear stress is needed to rupture the physical network and to induce flow).

During small strain measurements a possible network formed by the filler particles stays intact at lower frequencies while it may break up at larger strains [8].

Comparison between the relative viscosities at higher and lower frequency

The relative viscosity is give by $\eta_r = \eta_c / \eta_m$, where η_c is the viscosity of the composite at given strain and η_m is the viscosity of the polymer matrix, also at a give strain. The relative viscosities are showed in Table 3.

Table 3. Relative viscosities for PA6 nanocomposites at lower and higher frequency (strain).

Sample	Filler content (wt%)	Relative Viscosity	
		$\omega = 1$ rad/s	$\omega = 100$ rad/s
Sample 25	0.82	0.99	1.08
Sample 26	4.15	1.83	2.43
Sample g	18.01	13.62	791.27
Sample 27	22.8	15.65	640.48

Correlation between the dynamic viscosity data with the amount of silica added to the samples is shown in Fig. 6. The addition of silica increases the viscosity at lower and higher frequencies. Pronounced increase of viscosity was observed at high frequencies. From the frequency sweep, it can be seen that at lower strains the amount of filler changes the viscosity dramatically. An increase can be observed of 3 decades in viscosity. This effect may also come from the fact that all samples show some post-condensation, as it can also be seen in the increase of dynamic modulus.

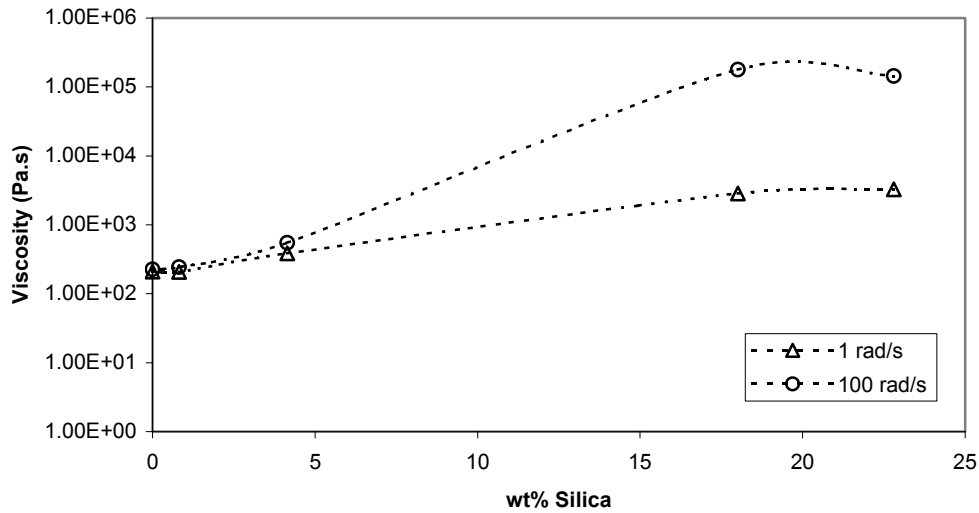


Fig. 6. Dynamic viscosity as a function of silica added to the sample at low and high frequency. The addition of silica increases the viscosity of all samples.

If the dynamic viscosities of these PA6/silica composites are compared, where the silica particles have $\phi < 30$ nm with the results obtained for the same system [4] but using aerosil particles as fillers (40 -50 nm) for small strain measurements some special features are found (see Table 4).

Table 4. Dynamic viscosities for PA6/silica and PA6/aerosil nanocomposites at lower and higher frequency (strain). The smaller the particle the higher the increment of viscosity.

Sample	Filler content (wt%)	Dynamic Viscosity(Pa.s)	
		$\omega = 1\text{rad/s}$	$\omega = 100\text{ rad/s}$
Sample 26	4.15	548.15	384.674
Sample g	18.01	179000	2857.24
Sample Aerosil I	5.00	420	360
Sample Aerosil II	20.00	10200	1030

At lower filler content the viscosities for samples with silica are slightly higher than for samples with aerosil, but for both series of samples the values are in the same or quite comparable order of magnitude. But comparing samples with higher filler content, it is clearly seen that for silica with $\phi < 30$ nm the viscosity is increased more. It can be through decreasing the particle size and increasing the volume fractions, particle-particle interactions become more important giving a considerable viscosity increase.

5.4 General discussion

Addition of silica to PA6 increased the elasticity and also the viscosity. The high elasticity of the nanocomposites is a consequence of a network of touching particles. Other mechanisms [9] that may explain this increase in elasticity involve the formation of an electrical layer, which can increase the interaction between particles and contribute to the elasticity, Brownian motion and spinning of the spherical particles. Flocculated systems might also play a role (Fig. 7).

i) The double layer mechanism relies on electrostatic repulsion and it seems that it prevents particles from touching each other. However, this mechanism could be altered by the presence of adsorbed polymer chains in the surface of the particles.

ii) Brownian motion is a thermodynamical effect: Brownian motion dominates at very low strains, lower than the lower limits used in our experiments. This is true for dilute concentrations where particle-particle interactions can be neglected. In the nanocomposites under study the concentrations is not considered to be diluted and iii) spinning is caused by flow of the polymer. These effects seem not very important since we are working with spherical particles. The relative importance of these mechanisms are expressed in the rotary Peclet number. The Peclet number is the ratio of the time scale for Brownian rotation ($1/D_r$) to that of convective motion $1/\dot{\gamma}$:

$$Pe = \frac{\dot{\gamma}}{D_r} \quad (17)$$

For spheres the rotary Brownian diffusion coefficient D_r is given by Stokes-Einstein equation, with the temperature (T), the Boltzmann-constant (k_B), the viscosity (η) and the radius of the sphere (r).

$$D_r = \frac{k_B T}{6\pi\eta r} \quad (18)$$

As the concentration increases, particles start to enter the neighbourhood of surrounding particles. This disturbs the flow around

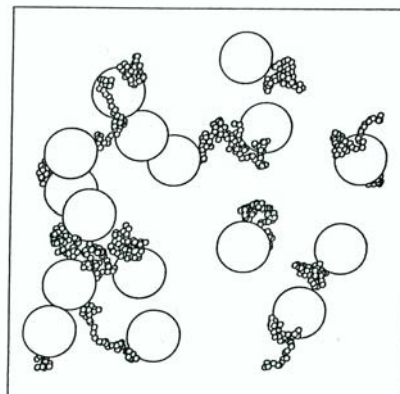


Fig. 7. Snapshot of bridging flocculation of spheres and adsorbing polymer. Reproduced with permission from [10].

the particles and consequently increases viscosity. At low concentrations, bi-particle interactions are most probable, while at high concentration more than two particles can interact simultaneously. If particle interactions occur, the viscosity can increase dramatically. The concentration at which strong viscosity effects become noticeable depends on the morphology of the dispersed phase and on morphological parameters.

5.5 Conclusions

Rheological measurements with two extreme sets of values were performed. The viscosity showed very dependant behaviour at different filler loadings. The viscosity of highly filled samples was mainly caused by interactions between particles and not by the viscosity of the polymer. Within the investigated shear rate domain, the composite behaviour becomes all the more non-Newtonian as the filler loading increased. The deviation from the Newtonian behaviour was attributed to the strong particle-particle interactions due to the extended surface areas, and hence to the tendency of silica particles to form aggregates. This was especially true in the case of the 18 wt% and 22 wt% silica loadings. Due to the fact that small strain viscosity increased upon the addition of the spherical particles, the mechanism most likely relies on the direct contact between particles. Large shear experiments would confirm this since the network formation would break down under large shear strain.

5.6 References

- [1] van Krevelen, D.W. *Properties of Polymers. Their estimation and correlation with chemical structure*. Elsevier, Amsterdam (1976).
- [2] Holland, B.J. and Hay, J.N. *Polym. Int.* 49, 943 (2000).
- [3] Malkin, A.Y. *Adv. Polym. Sci.* 96, 69 (1990).
- [4] Wu, G., Asai S, Sumita M, Hattori T, Higuchi R, Washiyama J. *Colloid Polym Sci* 278, 220 (2000).
- [5] Cassagnau, P. *Polymer* 44, 2455 (2003).
- [6] Barnes, H.A., Hutton, J.F. and Walters, K. *An introduction to Rheology*. Elsevier (1989).
- [7] Barry J. Holland and James N.H. *Polym. Int.* 49, 943 (2000).
- [8] van Es, M. *Polymer-Clay Nanocomposites*. PhD Thesis. University of Delft (2001).
- [9] Mewis J. and Macosko, C.W., *Rheology Principles, Measurements, and applications* in C.W. Macosko, VCH, N.Y. (1994).
- [10] Dickinson, E. and Euston, S. *Adv. Coll. Interf. Sci.* 42, 89 (1992).

6 Production of Nanocomposites: Processing and Characterization

Solution impregnations, pulltrusion and film stacking are widely used methods to prepare thermoplastic composite materials. Extruders are used to melt the polymer and to incorporate fibres into the polymer in order to modify physical properties. In this chapter, the compounding of colloidal silica nanoparticles filled polyamide-6 (PA6) is achieved using a twin-screw extruder, which has a significant market share due to its low cost and easy maintenance. The experiments were performed at 250 rpm and the bulk throughput was 6 kg h⁻¹ with a pump pressure of 30 bars. The composites were characterized with Nuclear Magnetic Resonance (NMR), Wide Angle X-Ray Diffraction (WAXD), Differential Scanning Calorimetry (DSC) and Transmission Electron Microscopy (TEM). As determined by WAXD, the PA6 showed higher amounts of γ -phase when compared to other synthesis methods such as in-situ polymerisation. TEM pictures showed that the silica particles aggregated nevertheless, upon addition of 14 wt% silica the E-modulus increased from 2.7 GPa to 3.9 GPa indicating that an effective mechanical coupling with the polymer was achieved. The behaviour, illustrated with Dynamic Mechanical Analysis (DMA) curves, indicated that in general when a filled system is compared to unfilled material, the values of the moduli (E' and E'') increased and $\tan\delta$ decreased. Determination of molecular mass distribution of the samples by means of Size Exclusion Chromatography (SEC) revealed that the addition of silica did not decrease the average molecular weight of the polymer matrix, which is of importance for composite applications.

Part of this chapter was presented by the author as an oral presentation and published as:
Paper number 86, *Symp. Proc. Int. Symp. Polymer Nanocomposites Sci. and Tech.* (NRC-IMI)
during the conference *Polymer Nanocomposites 2003*, on October 6-8, 2003 in Montréal,
Canada.

6.1 Introduction

Presently, polymer composites with nanosilica are prepared by *in-situ* polymerisation where inorganic particles are dispersed in for example ϵ -caproamide and aminocapric acid, followed by heat treatment of the reaction mixture to induce polymerisation, and post-addition of solid silica (modified or unmodified) and *in-situ* polymerisation of the inorganic fillers, where silica sol is added to caprolactam and mixed into a reactor [1-9]. The most prominent physical effect of fillers is the stiffening or modulus increase in the composites. Colloidal silica has been also added to reinforce polyurethane prepared by mixing polyol with the filler and subsequent curing using di-isocyanate. The investigation showed that at low temperatures (below -40°C) the addition of nanoparticles at 10 vol% increased the storage modulus of the polymer, but at room temperature an opposite effect was observed [10]. Both the moduli and Poisson's ratio, (ν), of the material are influenced since the fillers are generally much more rigid than polymers. Due to the manner in which test specimens are usually moulded, at certain filler percentage aggregation will occur. However, agglomerates or flocculated particles can provide higher modulus [11], since that portion of the matrix which is isolated in the agglomerate is less free to react to stress and strain than the continuous phase at values below the maximum packing fraction P_f . Under conditions where the particles have been treated with coupling agents, the matrix is severely restricted by interfacial bonding, so tensile strengths are improved and elongations are reduced. Agglomerated particles have been assumed to behave as a rigid unit under the action of small stress, but above some critical stress, relative motion of the particles within the agglomerate can occur [11]. As mentioned in chapter 1, Sumita *et al.* [12] have reported the advantages of nano- over micro-sized particles, and investigations for the optimal preparation and processing for the enhancement of mechanical properties are ongoing. For example, in the suspension process where (micro-sized) solid particles pass through a suspension state brought in contact with the granules of the thermoplastic, proved to be an effective way to make composites for large-scale extrusion [13].

In this chapter the preparation of PA6 silica nanocomposites is reported. The nanocomposites present a primary particle size of 30 nm, and were made by the devolatilization method in a twin-screw extruder. The process is particularly trouble-free where colloidal nanosized silica particles and polyamide pellets are used, and it furthermore leads to better modulus values compared to those obtained by common methods. The effect of the nanofiller on the modulus of PA6 is discussed and compared with the theoretical models available in literature.

6.2 Experimental

Materials

Polyamide-6 (PA6) Akulon K122 (relative viscosity = 2.2) was provided by DSM (Geleen, The Netherlands). Polypropylene (PP) Stamyran P19MN10 (Melt Flow Index 230°C = 20 dg/min). Colloidal silica ST-0, with a particle size of 10-20 nm and viscosity < 3 mPa.s. at 25°C was provided by SNOWTEX® Chemical Europe GmbH (Düsseldorf, Germany). Silica additions of 0, 1.85, 3.2, 7 and 14 wt% were used. The samples were labelled as PA6, PA6-1, PA6-3, PA6-7 and PA6-14, respectively.

Processability

In Fig. 1 the rheological behaviour of PA6 and PP is shown at their processing-temperatures. Control and monitor functions such as screw rpm, barrel and die temperatures, vacuum level, melt pressure, melt temperature, and motor amperage are crucial in the process development. The rotating screws impart shear and energy into the process to mix the components, devolatilize, and pump as required.

To better understand the process that was conducted for the elaboration of PA6 and PP nanocomposites, some background knowledge seems appropriate.

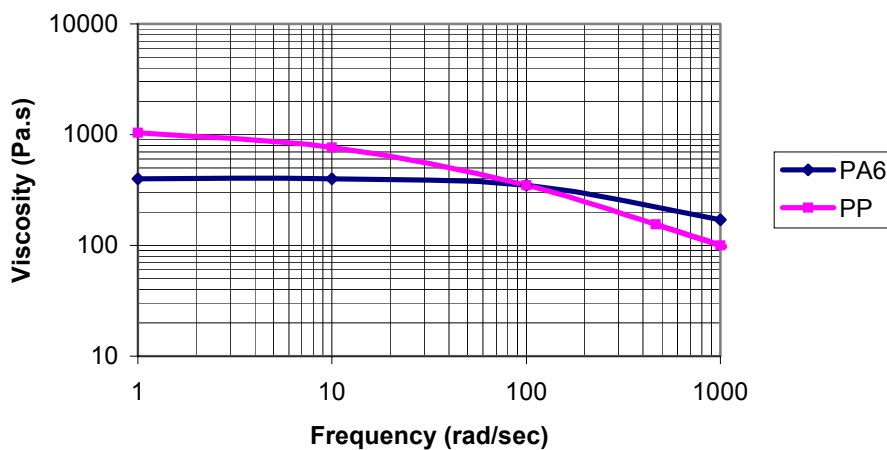


Fig. 1. Dynamic viscosity vs frequency curves for the tested polymers. PA6 Akulon K122 is measured at 230°C, polypropylene is measured at 190°C

Parameters

For direct extrusion, the feeding and materials handling system to the twin screw extruder is critical to maintain formulation accuracy and to maintain front-end pressure stability.

Twin-screw compounding extruders perform these basic functions: feeding, melting, mixing, venting, developing die/localized pressure, and conveying. The segmented nature of the twin-screw extruder in combination with controlled pumping and wiping allows specific screw and barrel geometries to be matched to the required process tasks. This allows the same machine to perform both dispersive and distributive mixing, which is a major benefit for certain products that are fabricated by direct extrusion, such as the mixing of glass microspheres into an extruded part, so that the spheres never experience the high shear stress associated with plastisation in the single screw extruder [14].

The pressure gradient in the twin-screw extruder is determined by the selection of screws. There are a large number of screw design variations possible. There are, however, only three basic types of screw elements: flighted elements, mixing elements, and zoning elements. Since the twin screw extruder is a starve fed device, flighted elements are placed strategically so that the screw channels are not filled and there will be zero pressure underneath downstream vent/feed sections, which facilitates downstream feeding of fillers (i.e. calcium, flame retardants, talc, titanium dioxide, etc.). This feature also facilitates single or multi-stage devolatilization.

During solid resin melting the viscosity is high, so in the early stages of the extrusion process the strain rates can produce high stress rates, which may be critical to attain dispersive mixing, but can also cause degradation of shear sensitive materials. In the latter stages of the extruder the viscosities have fallen so that high strain rates factored against a decreased viscosity produce comparatively low stress rates that enable heat and shear sensitive materials to be mixed with a minimal peak shear. Combining compounding/devolatilizing with direct extrusion in a high speed twin screw extruder presents significant process design challenges, in that the system will require high mass transfer in combination with consistent pumping. The selection of screw elements must take into account the mixing requirements, and also provide stable pumping to the die or front-end device [14].

Extrusion in forming Nanocomposites

For a stable extrusion process in the production of polymer/SiO₂ nanocomposites (using water as the filler dispersant) it is desirable to avoid pressure fluctuations during processability since it gives instabilities in the throughput. The vapour pressure of water varies with temperature; therefore it is an important parameter to be considered. To find the right parameters to make the nanocomposites, the experiments described in the compounding part were performed. Due to the fact that polymer-6/clay nanocomposites have been successfully deployed by direct extrusion and they are widely used in industry [15], effort was put in adjusting the parameters of that method with this method. If the PA6/SiO₂ pellets formation was

obtained in the same way than PA6/clay no further adjustment would be necessary for the implementation and research of PA6/SiO₂ nanocomposites.

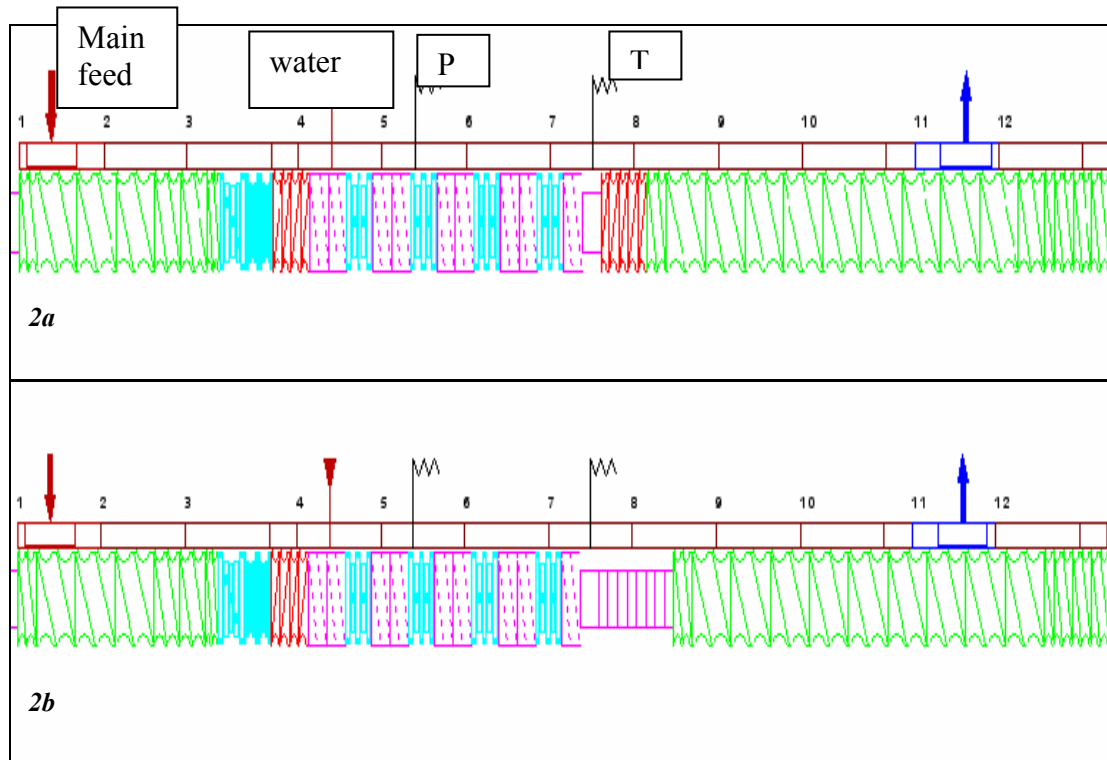


Fig. 2. Screw configuration with high pressure mixing zone for water injection and venting zone. Dynamic seal consist of standard left-handed elements (2a) or blister-discs (2b).

To determine the use either of left-handed or blister elements experiments were performed as described below [16].

Compounding

The compounding of the PA6/nanoSiO₂ composites was performed feeding the colloidal (silica) in the melted nylon in a high-pressure reaction zone. The process was developed on a ZSK-30 twin-screw extruder. An important parameter was the additional mixing of the silica to the molten polymer: the water, in which the silica was dissolved, should not evaporate. Therefore, conditions to be fulfilled were a) the pressure in the mixing zone should be higher than the vapour pressure of the water, and b) the pressure drop (passage of the melt through the left handed elements) should be faster than the destabilizing foam forming process (devolatilization). The pressure drop prevents pressure fluctuations and instabilities to occur in the throughput.

The screws were first designed with a ‘reaction zone’ for mixing polymer/clay with 20-30% water and vented in the degassing zone. In Fig. 2 the two screw configurations are shown with different dynamic seals. In Fig. 2a a standard seal with 5 left handed elements is seen. Fig. 2b displays dynamic seals using 8 blister-discs. A detailed photograph is shown in Fig. 3.



Fig. 3. Blister discs from screw configuration (2b).

As previously stated, the processing route must get a higher pressure than that of the water vapour pressure. In Fig. 4, the vapour pressure curves of water above a PA6 and PP melt are given. As can be seen, the water vapour pressure is lower in PA6. An important parameter is to prevent water to go into the gas phase; therefore, the pressure inside the extruder must stay above the vapour pressure.

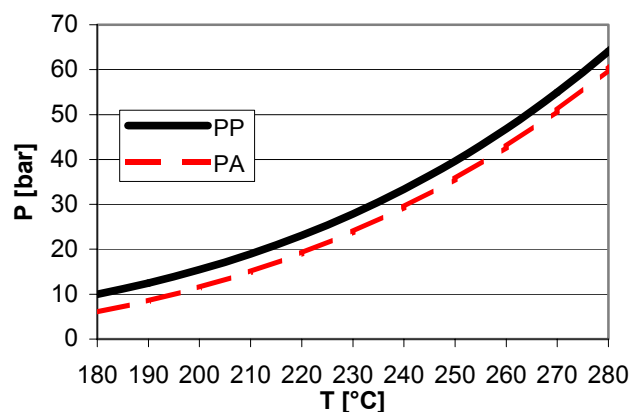


Fig. 4. Vapour pressure of water versus temperature

A real-melt thermocouple (the sensor was placed in the melt between the two screws, which were interrupted by spacers) and a pressure transducer monitored the temperature and the pressure in the “reaction-zone”. The experiments were performed at 250 and 450 rpm.

The throughput was 5, 10 and 15 Kg/h. The temperatures of the polymer/water mixtures and their water vapour pressure are listed in table 1.

Table 1. Vapour pressure of water as a function of temperature.

Polymer	rpm	Temperature (°C)	Water vapour pressure (bar)
PP	250	210	19
PP	450	230	28
PA6	250	215	17
PA6	450	220	19

Pressure inside the reaction zone at different operating conditions is seen in Figures 5 and 6. The evaluation of pressure without injection water with left hand elements (LHE) is seen in Fig. 5a. In Fig. 5b the behaviour of the melt pressure in the blister zone is observed. The injection of 30% water to the LHE and blister zone resulted in Fig. 6a and 6b respectively. From the comparison of Fig. 6a and 6b is seen that from left handed elements the required high pressure in the reaction zone cannot be obtained. In all cases the pressure remains close to 20 bars, which is the vapour pressure of water at the operation temperature. From Fig. 6b is seen that the pressure is higher than the vapour pressure as required.

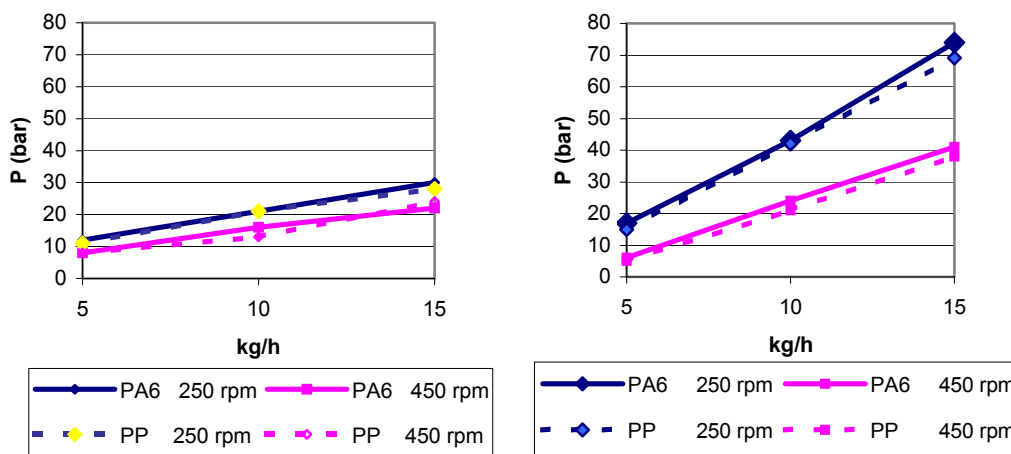


Fig. 5. ZSK 30: melt pressure LHE-zone (a) and melt pressure blister-zone (b).

Therefore, it is concluded from these set of experiments that a dynamic seal of 5 left handed element first resulted in throughput instabilities when processing PA6 and PP with the unmodified clay in the presence of water. This was caused because the pressure in the reaction zone was very close to the water vapour pressure. When a dynamic seal of 8 blister-discs was used, the pressure level in the reaction zone increased resulting in a stable process.

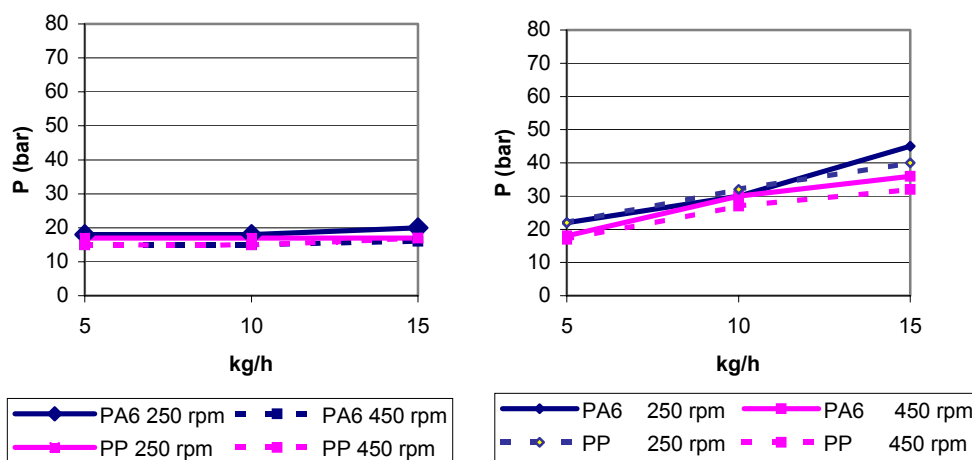


Fig. 6. Addition of water: LHE-zone (a) and melt pressure blister-zone (b).

The experiments for the nanocomposites with colloidal SiO_2 were performed at 250 rpm and the throughput was 6 kg h^{-1} with a pump pressure of 30 bar. The screw of the extruder was designed with a reaction zone for mixing the PA6/silica with different filler loadings.

6.3 Characterization Methods

The DSC measurements were performed according to DIN 51007/53765 and ASTM D3417-97 protocol. The dynamic mechanical spectra were recorded on a Perkin-Elmer DMA 7E Dynamic Mechanical Analyser. Small rectangular bars of the samples, size approximately $1.25 \times 3 \times 20 \text{ mm}$, were subjected to a sinusoidal deformation at constant frequency, using a three point bending platform of 15 mm. Measurements were carried out at a fixed frequency of 1 Hz and a heating rate of 5°C min^{-1} , in the temperature range between -100°C and 200°C . The amplitude of the sinusoidal deformation was $10 \mu\text{m}$ during the run. The static force was always 10% more than the dynamic force, in order to ensure good contact between the probe and the sample. The data was collected using Pyris software for Windows, version 3.81.

Prior to the DMA measurements, the samples were compression moulded into sheets of size $30 \times 5.5 \times 0.1 \text{ cm}$ at $250\text{-}260^\circ\text{C}$. Prior to testing, sample strips of $25 \times 2\text{-}3 \times 0.05\text{-}0.1 \text{ cm}$ were made. For the tensile test, the samples were dried in a vacuum oven at 80°C for 2 days. Plates of 1 mm thickness were moulded and the test samples were machined out of the plates. The elastic modulus was measured at a tensile speed of 1 mm min^{-1} and the displacement was measured with an extensometer with a gauge length of 10 mm.

X-ray powder diffraction (XRD) data were collected using copper radiation on a Philips PW3710 based X'Pert-1 diffractometer in Bragg-Brentano geometry. The k_{β} component was removed by a secondary monochromator. Powder diffraction data were collected at room temperature using a "zero"-background spinning specimen holder. The intensities were measured using a θ compensating divergence slit. The measured data were converted to a fixed divergence slit width of 1° . Peak positions and peak intensities were extracted using the pattern decomposition program PROFIT available in the PC software package X'PERT LINE (Philips, Eindhoven). The observed individual lines and clusters of lines were fitted using Pearson VII functions, taking into account the $k\alpha_2$ component. The obtained peak positions and relative intensities were therefore extracted from the analytical $k\alpha_1$ peak profiles. Quantitative X-Ray Fluorescence (XRF) was used to determine the amount (as wt%) of silica present in each sample. The XRF analysis was performed on a Philips PW 1480/10 fluorometer (Eindhoven, The Netherlands) and the calculation method used the program FPMulti.

For TEM studies, a JEOL 2010F operating at 200 kV, equipped with a EDAX-EDS detector and a Gatan Imaging Filter, was used. TEM specimen were prepared by embedding the PA6/silica composite in Epon, cutting it into thin films with a thickness of 100 nm using ultramicrotomy after which the films could be captured on Cu grids. TEM images were recorded on a Gatan DualVision 300 W CCD camera.

Mechanical properties of injection moulded PA6 nanocomposites

The specimens for the tensile tests were dog-bone shaped samples which were injection moulded in a $\phi = 30$ mm Engel 80A machine set up according to the ISO 527 standard and functioned at 100 rpm. The melt temperature was 270°C and the mould-temperature 85°C . The raw materials were dried overnight at 110°C in vacuum prior to injection moulding. The prismatic part of the tensile samples had dimensions $60 \times 10 \times 4.2$ mm. The tensile modulus was determined between 0.05 and 0.25% strain according to DIN-53457 protocol at 23°C and 5 mm min^{-1} .

6.4 Results and discussion

Molecular Parameters

Besides the morphology of the matrix and characteristics of the filler, the properties of the plastics depend also on the matrix molecular weight (M_w) of the polymer. The effects of PA6 molecular weight stems from both chemical and rheological issues. The molecular weight can potentially affect the toughness in different ways. In general, the inherent ductility, or the ability for the polymer to be toughened, increases with molecular weight (M_w). At high silica loadings (14 wt%)

the viscosity slightly varied from 1.36 to 1.37 dl/g and the M_w was not decreased as seen in Table 2.

Table 2. Molecular structure parameters of PA6 and PA6-14 as obtained from SEC-triple molecular weight in g/mole and $[\eta]$ in dl/g.

Sample name	M_n	M_w	M_z	M_w/M_n	M_z/M_w	intr. visc.	Mark-Houwink slope ' α '
PA6	17100	35400	56500	2.07	1.60	1.362	0.641
PA6-14	19600	42600	71200	2.17	1.67	1.378	0.643

XRD and DSC experiments

To calculate the crystallinity from a XRD scan the method based on the use of amorphous templates was used [3]. The amorphous template was derived by stripping the crystalline peaks from a resolved pattern of a highly crystalline sample of the same polymer. From Fig. 7 three components are observed consisting of α_1 , α_2 and γ -form crystal diffraction peaks centred at $2\theta = 20.3^\circ$, 22.6° and 21.2° respectively. The amorphous component was taken from the areas below the α -form crystal peaks and the γ -form crystal peak. The crystallization and melting behaviour of the composites has been studied by DSC analysis and it has been summarized in table 3.

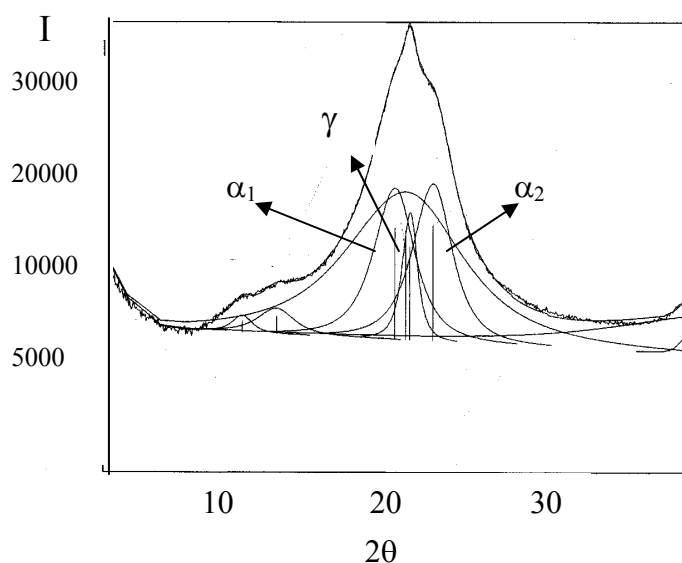


Fig. 7. Profile analysis of the diffraction scan from PA6 indicating α and γ phases.

From the DSC heating curves in Fig. 8, the influence of silica on the melting temperature (T_m) and on the crystallisation temperature was observed. Pure PA6 showed a T_m of 225.3°C as seen in Fig. 8a. This melting temperature is typical for α -polyamides. At higher silica

loadings, the melting temperature was shifted towards lower temperatures while at the same time a second peak at around 213°C emerged at temperatures below the normal melting temperature of PA6 (Fig. 8b). Such temperature is typical for γ -crystalline PA6, which is in agreement with the results obtained from the XRD spectra. Melting and crystallisation peak-temperatures and enthalpies are listed in Table 3. $T_{\text{melt}1}$ is the low melting temperature, $T_{\text{melt}2}$ the high melting temperature.

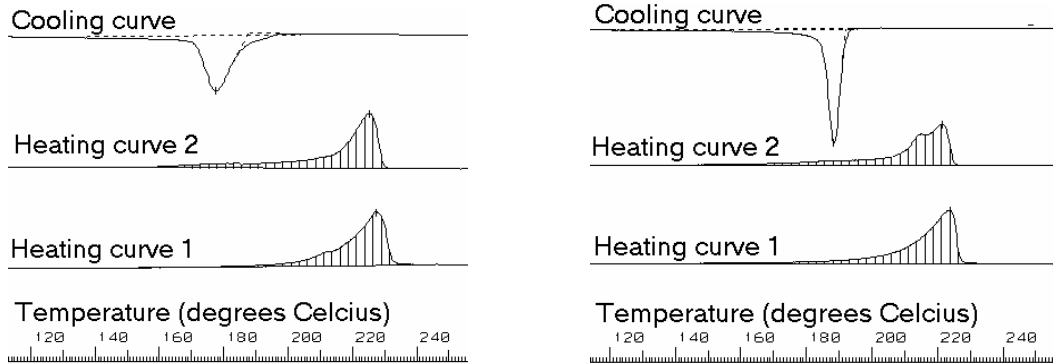


Fig. 8. Crystallization enthalpies and melting temperatures of the nanocomposites. **a)left: PA6 b)right: PA6-14.**

Table 3. DSC data of PA6-nanocomposites.

Code	SiO ₂ wt%	$T_{\text{melt}1}$ °C	ΔH_{melt} J/g	ΔH_{melt} per g PA6 J/g	$T_{\text{melt}2}$ °C	T_{cryst} °C
PA6	0.0	225.3	83.9	83.9	-	177.6
PA6-1	1.8	213.2	73.3	75.1	220.4	189.1
PA6-3	3.2	212.0	69.8	73.0	220.7	188.3
PA6-7	7.0	212.0	66.3	73.3	220.7	188.9
PA6-14	14.0	212.0	67.1	81.1	221.3	188.3

The shifting of T_m to lower temperatures upon addition of silica can probably be attributed to a decrease in lamellar thickness of the polymer crystals. The degree of crystallinity was determined from the enthalpy of melting as:

$$W_{c,x} = \frac{\Delta H_f}{\Delta H_f^0} \quad (1)$$

where ΔH_f is the experimentally measured enthalpy of melting and ΔH_f^0 the bulk enthalpy of melting, respectively. The heat of fusion for PA6 was taken as 188 J/g for the crystalline fraction [3]. Upon addition of silica nanoparticles, the degree of crystallinity did not vary significantly which was in accordance with the XRD experiments. The silica had two effects on the crystallization of PA6 [15]: 1) the silica acts as a nucleation site, accelerating the process of PA 6 crystallization; 2) the

interaction between PA6 and the silica impedes the free motion of the PA 6 molecular chains (this effect is more pronounced when the silica surface is modified) [16]. By using techniques such as the NMR relaxation time or quasi-elastic neutron scattering (QENS) it is possible to characterise the dynamic restrictions of polymer chains in polymer-filler composites [17].

Dynamic Mechanical Analysis (DMA)

Modulus and $\tan \delta$ ($\tan \delta$) for the silica particles in the polyamide matrix are measured as a function of temperature for several values of volume fraction of filler. Fig. 9 shows data for the storage modulus (E'), Fig. 10 for the loss modulus (E'') and Fig. 11 the $\tan \delta$ or damping

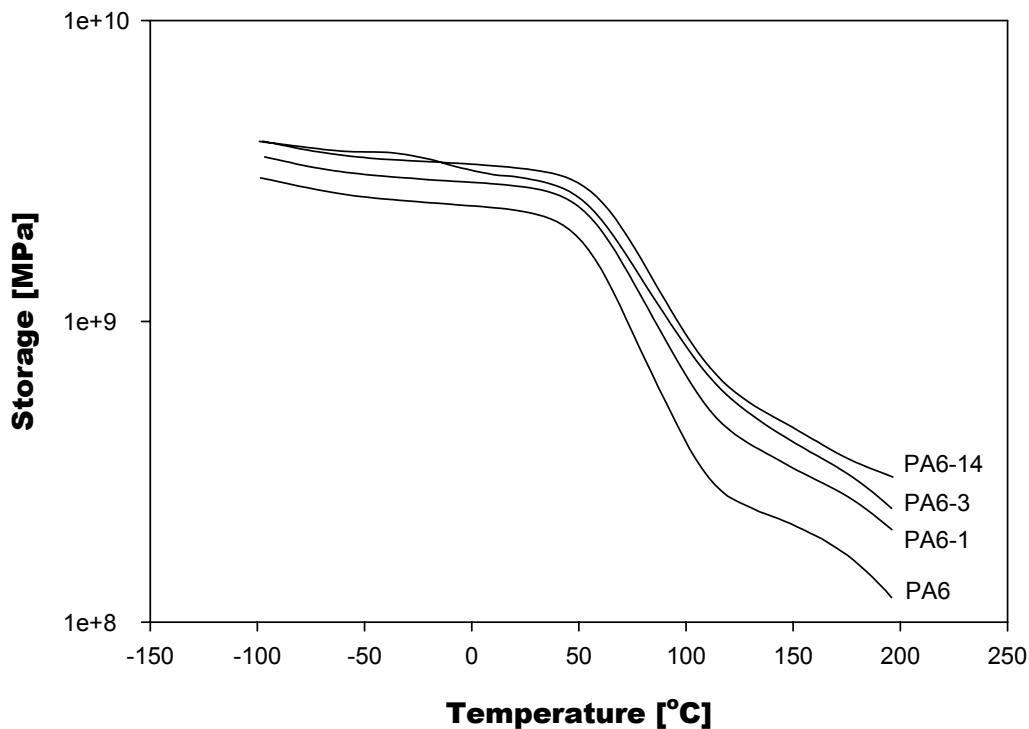


Fig. 9. E' relaxations of PA6, PA6-1, PA6-3 and PA6-14.

values. For the storage modulus below the glass transition (T_g), $\log E'$ decreased linearly with temperature and about 20°C below the T_g decreased with nearly one order of magnitude. As expected, the storage modulus curve shifted to higher modulus upon addition of 1 and 3 wt% of silica. Upon addition of 14 wt% the increment was not significant anymore. The addition of 5 and 7 wt% of silica caused an increase in modulus between the values of 3 wt% and 14 wt%. For clarity only PA6-1, PA6-3 and PA6-14 composites are shown. However, because of the presence of a crystalline matrix, the material does not drastically soften above the glass transition.

Above the T_g the mobility of the amorphous regions caused a reduction in the storage modulus, but the material exhibited useful solid-state properties until the material approached the melting point, about 100°C above the glass transition. As seen from Fig. 10, the T_g does not change significantly with increasing filler content. The rise in the tan delta curve coincided with the decline in the storage modulus as seen in Fig. 11. Above 60°C the $\tan\delta$ curve rose rapidly and reached a peak of 0.6. Once the glass transition temperature is passed; the loss modulus drops back to a level close to the pre-transition values.

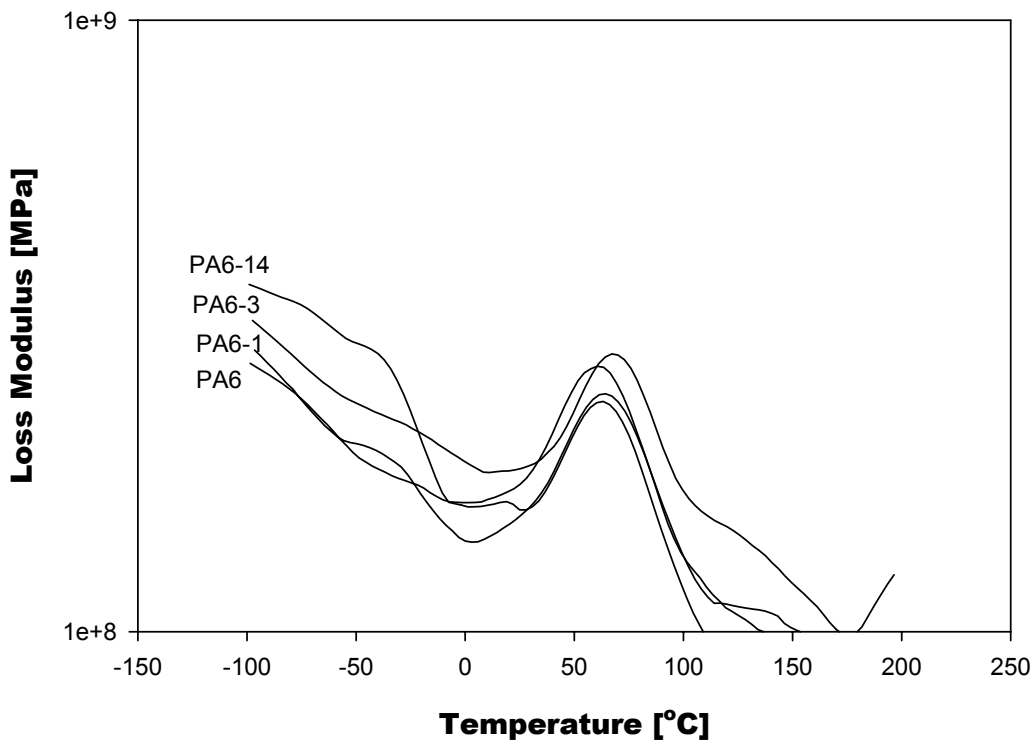


Fig. 10. E'' relaxations of polyamide 6 (PA6) and composites.

However, because of the drastic reduction in elastic properties, the $\tan\delta$ curves do not decline significantly. Once the semi-crystalline material approached the melting point, the $\tan\delta$ value increased as the material changed from an elastic solid into a viscous liquid. The lower $\tan\delta$ values throughout the scan, and in particular the lower peak associated with the glass transition, reflected the improved load bearing properties of the filled system. One transition is observed at about -40°C , which corresponds to the secondary relaxation. In addition, at about $50\text{--}60^\circ\text{C}$ the α -relaxation is visible, corresponding to the T_g of the matrix.

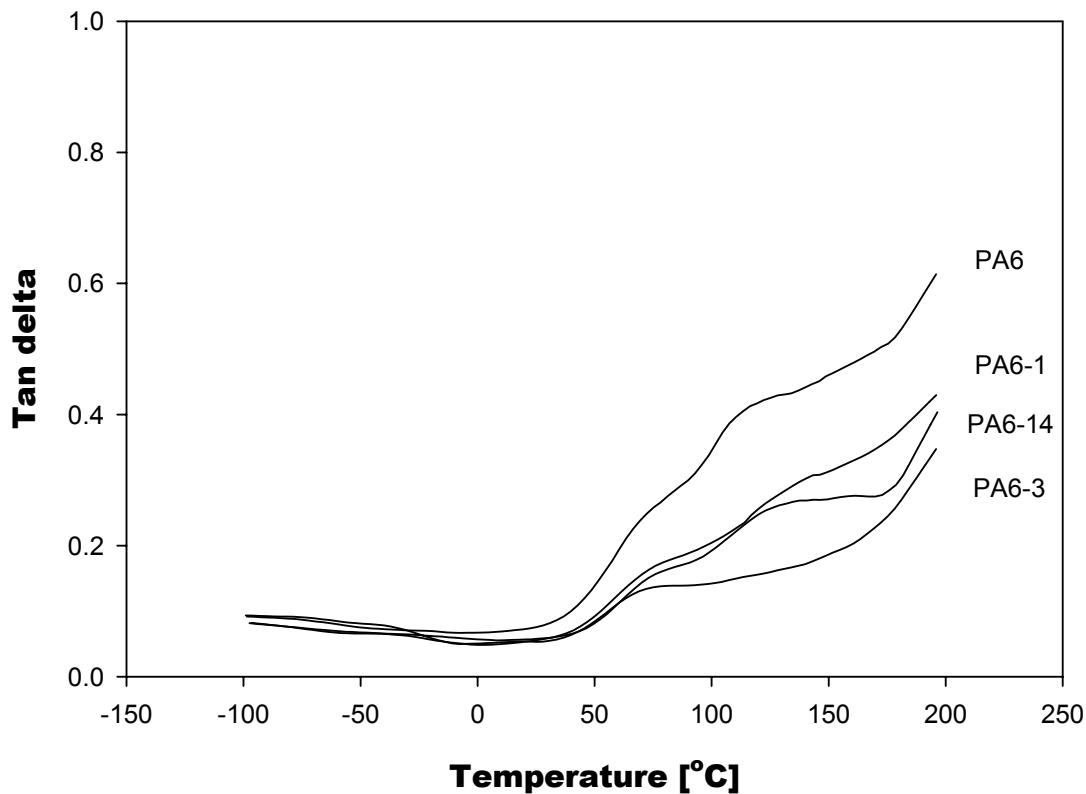


Fig. 11. Tan δ relaxations at different filler percentage.

The damping can be explained as follows: Below the glass transition temperature, part of the decrease in relative damping as the temperature was raised may be due to the frozen-in stresses caused by the mismatch in the coefficients of thermal expansion of the two materials or to a decrease in motion of particles within agglomerates as the polymer softens. The microstructure of the nanocomposite is seen in Figures 12a and 12b. The silica nanoparticles showed a primary particle size of 30 nm as observed by TEM. The presence of silica was confirmed by using EDAX-EDS. As the modulus of the polymer decreased on raising the temperature, the polymer exerted less force on the agglomerate particles, so there was a smaller probability that one primary particle will move with respect to another within agglomerates [18]. In the neighbourhood of T_g , the modulus of the polymer decreased to such a small value that deformation of the material no longer produces forces large enough to deform agglomerate particles, so they appear to be rigid. At this point, the relative damping is small since most of the damping originates from the polymer.

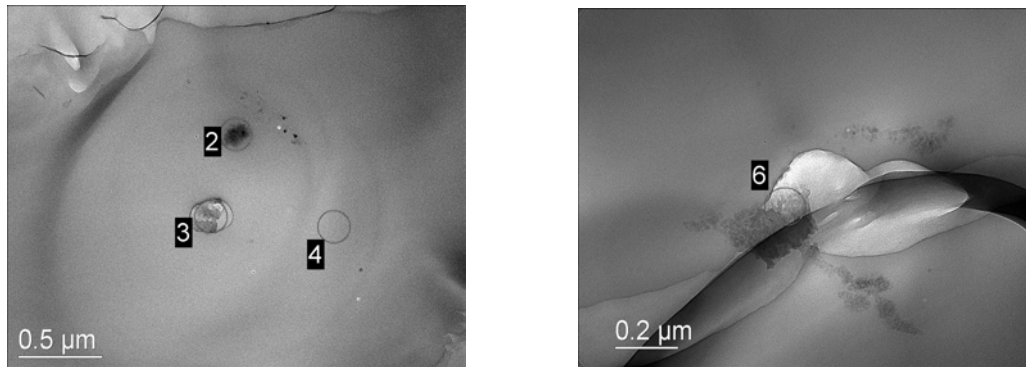


Fig. 12a (left) and 12b (right). TEM pictures of PA6-3 (numbers indicate the presence of silica)

Beyond the T_g , damping increased at higher temperatures because the coefficient of thermal expansion of the polymer is much greater than of the filler and the polymer exerts less force on the agglomerate particles as temperature increases. As the force between the polymer and the filler particles decreased, it became more facile for either polymer-filler or filler-filler motion to occur at the interfaces. This frictional motion at interfaces generates heat that produces an increase in the relative damping as the temperature increases.

As mentioned before, the change in relative modulus with temperature is primarily due to induced tensile stresses by the difference in thermal expansion coefficient of the phases [19].

6.5 Conclusions

Nylon-6/silica nanocomposites were prepared by devolatilization technique for the first time. The filler used was added as sol in a twin-screw extruder apparatus instead of the *in-situ* polymerisation technique, providing bulk amounts of composite material at industrial scale. The screw of the extruder was designed with a reaction zone for mixing the PA6/nanosilica with different filler loadings. The use of a dynamic seal increased the pressure in the reaction zone and resulted in a stable process. After the first heating rate the enthalpy of crystallization increased and the XRD spectra showed a constant degree of crystallinity for all the composites. The behaviour illustrated with the DMA curves indicated that in general when a filled system is compared to an unfilled material, the values of the moduli (E' and E'') increased and damping decreased.

Additionally, the production of (nano)-composites using this method brings new insights to the properties of PA-filled materials.

6.6 References

- [1] Kojima, Y., Usuki, A., Kawasumi, M., Okada, A., Kurauchi, T. and Kamigaito O. *J. Polym Sci. Part A*. 31, 983 (1993).
- [2] Merkel, T.C., Freeman, B.D., Spontak R.J., He Z, Pinnau, I, Meakin, P and Hill, A.J. *Science* 296, 519 (2002).
- [3] Kohan, M.I. *Nylon, Plastics Handbook*. Hanser, New York (1995).
- [4] Ou, Y., Yang, F. and Yu Z.-Z. *J. Polym. Sci.* 5, 789 (1998).
- [5] Wypych, G. *Handbook of Fillers*, 2nd Ed. New York (1985).
- [6] Brook, M.A. *Silicon in Organic, Organometallic, and Polymer Chemistry*, John Wiley & Sons, New York (2000).
- [7] Rothon, R. *Particulate-filled Polymer Composites*, Essex, Longman (1995).
- [8] Li, Y., Yu, J. and Guo, Z. *J. Appl. Polym. Sci.* 84, 827 (2002).
- [9] Reynaud, E., Jouen, T., Gauthier, C., Vigier, G. and Varlet J. *Polymer* 42, 8759 (2001).
- [10] Petrović, Z.S., Javni, I., Waddon, A. and Bánhegyi, G. *J. Appl. Sci.* 76, 133 (2000).
- [11] Nielsen, L.E. *J. Polym. Sci. Polym Phys.* 17, 1897 (1979).
- [12] Sumita, M., Shizuma, T. and Miyasaka, K. *J. Macromol. Sci.Phys.* B22(4), 601 (1983).
- [13] Bussi, P. and Thierry-Mieg, J. US 6,239,196 B1 (2001).
- [14] Leistritz, Ch. M. *Plastics Eng.* 59, 50 (2003).
- [15] Van Es, M. *Polymer-Clay Nanocomposites. The importance of particle dimensions*. PhD Thesis. University of Delft. The Netherlands (2001).
- [16] Van Vliet, G. *Stable extrusion process for the production of a polymer-clay nanocomposites using water as a compatibilizer*. Internal report. DSM.
- [17] Li, W. and Yan, D. *J. Appl. Polym. Sci.* 88, 2462 (2003).
- [18] Yang, F., Ou, Y. and Yu, Z. *J. Appl. Polym. Sci.* 69, 355 (1998).
- [19] Gagliardi, S., Arrighi, V., Ferguson, R. and Telling MTF. *Physica B*. 301, 110 (2001).

7 Mechanical Models

Conventional (mechanical) theoretical models such as the Mori-Tanaka and Kerner models are used in this chapter for the prediction of reinforcing efficiency in nanocomposites. Model predictions are compared to experimental mechanical property data previously reported in chapter 3 and here in chapter 7.

7.1 Introduction

Many factors could be potentially responsible for the property changes offered by the nanosilica particles because their high surface area and interparticle distance. A significant question is whether the observed properties of nanocomposites can be explained by conventional composite theories. Classical mechanical models are normally used to better estimate the effect of fillers presence into the polyamide-6, with reference to the observed modulus increase [1]. The well known Reuss and Voigt models, respectively assume a series and a parallel mechanical coupling between the various composite phases: they define the largest domain for the composite modulus values.

A brief explanation of these classical approaches is given below [1,2].

Boundary Conditions

From the principle of minimum energy of elasticity theory, it is possible to obtain equations for the upper and lower bounds for both the bulk and shear moduli of heterogeneous materials with N different phases.

$$\frac{1}{\sum_{i=1}^N \phi_i / k_i} \leq k \leq \sum_{i=1}^N \phi_i k_i, \quad (1)$$

$$\frac{1}{\sum_{i=1}^N \phi_i / \mu_i} \leq \mu \leq \sum_{i=1}^N \phi_i \mu_i, \quad (2)$$

where ϕ_i is the volume fraction of the i -th phase, k is the bulk modulus and μ is the shear modulus. The index i refers to the properties of the i -th phase (matrix or filler) and the quantities without sub-index refer to the composite.

The lower bounds in Equation 1 are referred to as the Voigt bounds, and the upper bounds are designated as the Reuss bounds.

A set of more strict bounds for a two-phase medium (r denotes the filler and m the matrix) is given by

$$\frac{\phi_r}{1 + \phi_m (k_r - k_m) / (k_m + \frac{4}{3} \mu_m)} \leq \frac{k - k_m}{k_r + k_m} \leq \frac{\phi_r}{1 + \phi_m (k_r - k_m) / (k_m + \frac{4}{3} \mu_r)}, \quad (3)$$

$$\frac{\phi_r}{1 + \phi_m (\mu_r - \mu_m) / (\mu_m + \frac{4}{3} \mu_L)} \leq \frac{\mu - \mu_m}{\mu_r + \mu_m} \leq \frac{\phi_r}{1 + \phi_m (\mu_r - \mu_m) / (\mu_m + \frac{4}{3} \mu_U)}, \quad (4)$$

$$\text{where } \mu_L = \frac{3}{2} \left(\frac{1}{\mu_m} + \frac{10}{9k_m + 8\mu_m} \right)^{-1}, \quad (5)$$

and

$$\mu_U = \frac{3}{2} \left(\frac{1}{\mu_r} + \frac{10}{9k_r + 8\mu_r} \right)^{-1}, \quad (6)$$

A generalisation of these bounds has been provided by Nielsen [2]:

$$C^n = \phi_f C_f^n + (1 - \phi_f) C_m^n \quad (7)$$

where C stands for either the bulk modulus, k , or the shear modulus, μ , the subindex f represents the filler properties, the subindex m the matrix properties, and ϕ_f represents the volume fraction of the filler. Quantities without any subindex refer to the properties of the composite. Different values of the exponent n give rise to different forms of the law of mixtures. With $n = -1$, Eq. 7 is referred to as the series law of mixtures (Reuss upper bound). With $n = 1$, Eq. 7 is referred to as the parallel law of mixtures (Voigt lower bound). Figures 1 and 2 show a comparison of these bounds with the measured moduli for the composites considered in this work: for figure 1 the composites of chapter 3 (PAL-SX) and for figure 2 the composites of chapter 6 (PAK-SX). Although these bounds provide theoretical limits for the values of the moduli, for typical composite materials they are too far apart and are thus of limited practical value.

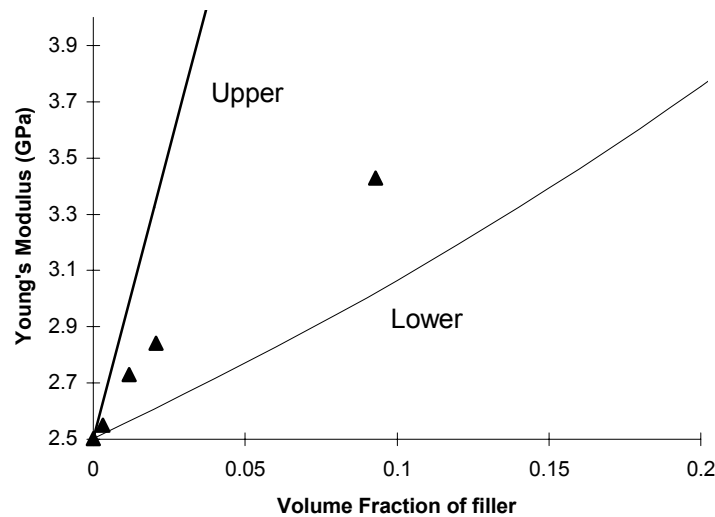


Fig. 1. Experimental Young's modulus (symbols) and theoretical upper and lower bounds (solid lines) for the Aldrich Polymer reinforced with silica particles (PAL-SX).

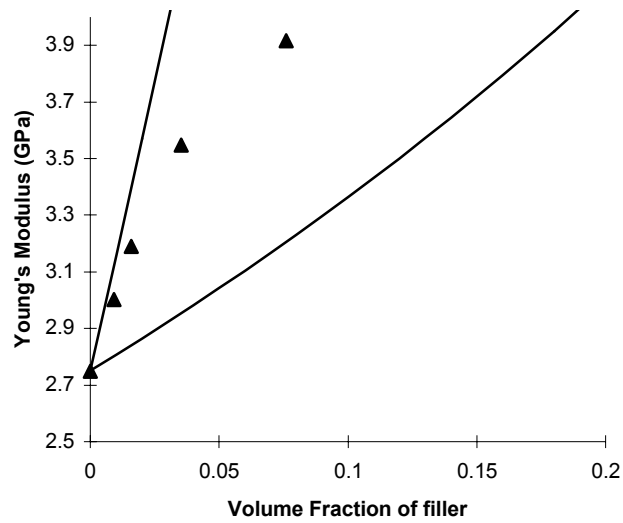


Fig. 2. Experimental Young's modulus (symbols) and theoretical upper and lower bounds (solid lines) for the Akulon polymer reinforced with silica particles (PAK-SX).

7.2 Mechanical Models

Several models are available in the literature to account for the increase of elastic moduli with the presence of filler particles. Notable examples are the models by Kerner [3], Hashin [4] and Christensen's three-phase model [1]. Models that are not limited to spherical particles but that take into account the aspect ratio of the filler particles, such as the Mori-Tanaka model, can also be found in the literature [5]. This model can be applied in our case considering the limit in which the aspect ratio equals the unity. For all the calculations the following values of the properties of the pure materials were used (table 1):

Table 1. Properties of pure materials.

	Young's Modulus, E (GPa)	Poisson's Ratio, ν
Polymer Matrix, Akulon	2.750	0.4
Polymer Matrix, Aldrich	2.503	0.4
Silica	73.1	0.17

The Young's Modulus is related to the bulk and shear modulus by the general equation:

$$E = \frac{9 \mu k}{3 k + \mu}, \quad (8)$$

Kerner's Model

By an averaging procedure, Kerner derived equations for the moduli of a composite with spherical inclusions, perfectly bonded to the suspending medium.

$$k = \frac{\sum \frac{k_i \phi_i}{3k_i + 4\mu_m}}{\sum \frac{\phi_i}{3k_i + 4\mu_m}}, \quad (9)$$

$$\mu = \mu_m \frac{\sum^* \frac{\mu_i \phi_i}{(7-5\nu_m)\mu_m + (8-10\nu_m)\mu_i} + \frac{\phi_m}{15(1-\nu_m)}}{\sum^* \frac{\mu_m \phi_i}{(7-5\nu_m)\mu_m + (8-10\nu_m)\mu_i} + \frac{\phi_m}{15(1-\nu_m)}}, \quad (10)$$

where the symbol \sum^* stands for a summation excluding the index for the matrix and ν denotes the Poisson's ratio.

Mori-Tanaka

This treatment has the advantage of allowing calculation of the effect of different shapes of the inclusions (aspect ratio). The results here are obtained are with aspect ratio = 1.

The lengthy tensor model concerning Mori-Tanaka is well documented in literature [6].

Generally, the Young's Modulus is obtained from the elements of the compliance tensor of the composite, \mathbf{S}_c given by

$$\mathbf{S}_c = (c_m \mathbf{S}_m + c_r \mathbf{S}_r \mathbf{B})(c_m \mathbf{I} + c_r \mathbf{B})^{-1}, \quad (11)$$

where \mathbf{S}_m and \mathbf{S}_r are the compliance tensor of the matrix and filler, respectively, \mathbf{I} is the identity tensor and \mathbf{B} is the so-called "stress concentration tensor", given by

$$\mathbf{B} = \mathbf{C}_r \mathbf{A} (\mathbf{C}_m)^{-1}. \quad (12)$$

\mathbf{C}_r and \mathbf{C}_m are the elastic stiffness tensors of the filler and matrix, respectively, and \mathbf{A} is the so-called "strain concentration tensor", given by

$$\mathbf{A} = [\mathbf{P}_m \mathbf{C}_m^{-1} (\mathbf{C}_r - \mathbf{C}_m) + \mathbf{I}]^{-1}. \quad (13)$$

Finally, \mathbf{P}_m is the Eshelby's tensor.

The tensors \mathbf{C}_m , \mathbf{C}_r , \mathbf{S}_r and \mathbf{S}_m are constructed using the moduli of the filler and composites. The Poisson's ratio is used in the Eshelby's tensor.

7.3 Results

We found that for the relatively low volume fractions of filler used in this study, these two methods yield predictions for the Young's modulus of the composite which are very close to each other, but are consistently and significantly below the values measured experimentally, as is shown in Figures 3 and 4.

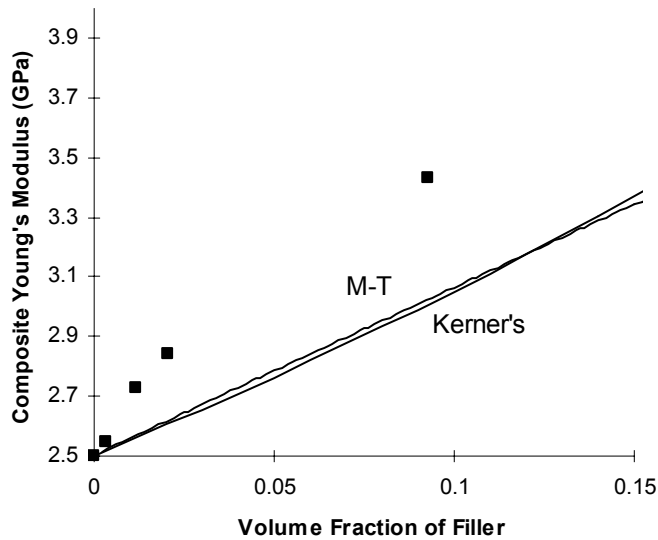


Fig. 3. Experimental Young's Modulus (symbols) and models (lines), M-T: Mori-Tanaka, and Kerner's. Data for the Aldrich polymer reinforced with silica particles.

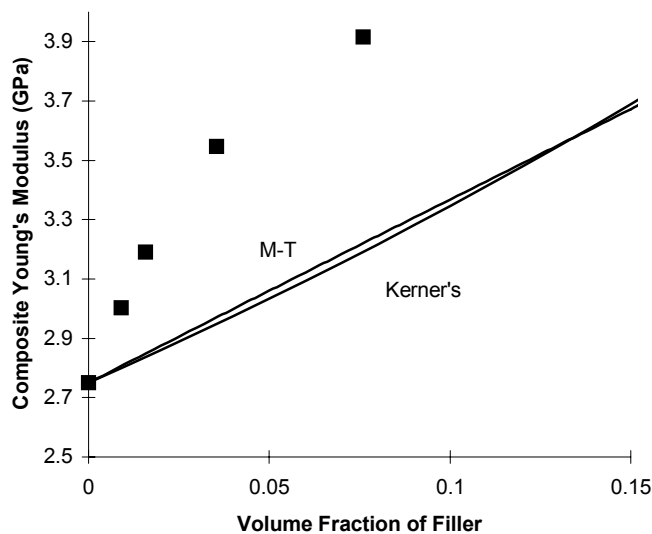
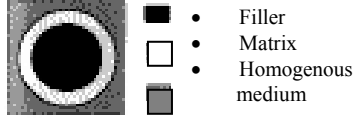


Fig. 4. Experimental Young's Modulus (symbols) and models (lines), M-T: Mori-Tanaka and Kerner's. Data for the Akulon polymer reinforced with silica particles.

7.4 Discussion

It can be seen from Figures 3 and 4 that Mora-Tanaki and Kerner's give very similar predictions. The measured moduli for both the Akulon and Aldrich composites are definitely above the theoretical predictions of these purely mechanical models (although well inside the theoretical bounds).

In general, factors to be considered when comparing results of model calculations with experimental data are [7]:

- **Adhesion.** Most models imply an absolute matrix-to-filler adhesion. This might be true for materials in the range of small deformations. A composite material is defined as, in the simplest case, an inorganic filler surrounded by a shell of polymer matrix, embedded in an infinite homogeneous medium, which undergoes the external deformation. Known as the Christensen and Lo model [1] Fig. 5 provides a scheme that represents a composite material. The existence of a third phase, like an interface, between the filler and the matrix could affect the models calculations. At low filler fraction, this model leads to composite modulus values close to those calculated from the Kerner approach [3]
- 

- Filler
 - Matrix
 - Homogenous medium
- Fig. 5.** Three phase self-coherent approach. After [12]
- **Existence of pores** and voids in the material. These two factors, adhesion disruption and porosity influence the elastic modulus.
 - **Non-uniform filler dispersion:** filler agglomeration. Most models imply a uniform filler distribution in the matrix. At low filler concentrations, if agglomeration is present, it does not practically affect the elastic modulus. At higher filler concentrations, agglomeration results in an apparent rise of the filler bulk fraction, i.e. the modulus is higher than expected from v_{fi} , due to this agglomeration.
 - **Real shape of filler particles.** The shape of disperse filler particles differs usually from an ideal sphere or rectangle. However, the particle shape effect on the properties of a material is generally assumed to be insignificant.
 - **Uncertainties in the polymer matrix properties.** The physico-mechanical properties of polymer matrices depend on the degree of crystallinity, molecular weight, molecular weight distribution, etc. These parameters are a function of the processing conditions and they change after the filler introduction.
 - A combination of all or some of the above

All these circumstances should be borne in mind when calculated results are to be compared with experimental data.

7.5 Conclusions

There are many factors that may be held responsible for the mentioned limitations, some of which have been discussed previously by other authors. One is the formation of an interface between the filler particle and the matrix. However, in the present case, until firm evidence of the nature of such an interface is found, this modification may be regarded only as a means to compensate for the limitations of the models.

7.6 References

- [1] Christensen, R.M. *Mechanics of Composite Materials*, John Wiley & Sons (1979).
- [2] Nielsen, L.E. and Landel, R.F. *Mechanical Properties of Polymers and Composites*, 12th Ed. New York (1994).
- [3] Kerner, E.H. *Proc. Phys. Soc.* B69, 808 (1956).
- [4] Hashin, Z., *J. Mech. Phys. Sol.* 39, 745 (1991).
- [5] Mori, T. and Tanaka K. *Acta Metall.* 21, 571 (1973).
- [6] van Es, M. *Polymer-Clay Nanocomposites. The importance of particle dimensions*. PhD Thesis. University of Delft. The Netherlands. (2001).
- [7] Berlin, A.A., Volfson, S.A., Enikolopian, N.S. and Negmatov, S.S. *Principles of Polymer Composites*. Springer-Verlag. 79, New York (1985).

8 PP/Silica Nanocomposites in a Slurry Phase Polymerisation Reactor

Polypropylene (PP) composites containing nanosized ($\phi \sim 10$ nm) spherical silica particles were prepared in-situ utilizing a one-liter Slurry Phase Polymerisation (SPP) reactor containing a $MgCl_2$ -supported Ziegler-Natta (fourth generation) catalyst. Composites were prepared with two filler sizes ranging from the nano- to micro-size domain. The surface of the silica particles was modified with a silane-coupling agent to prevent catalyst deactivation and to achieve better polymer/filler synergy by increasing the hydrophobicity surrounding the bulk particle surface. The feasibility of the process was tested with low loadings additions (~ 3 wt% for each sample) of (nano)-silica. The effect of the filler on the crystal structure and crystallite size of PP was studied with Differential Scanning Calorimetry (DSC) and Wide-Angle X-ray Diffraction (WAXD). The reaction kinetics of the nano-composite (~ 10 nm) was studied and compared with samples containing larger micro-sized particles. It was demonstrated that the former did not decrease the catalyst activity when compared with the latter, comparisons were also made with pure PP. Particle size influenced the reactivity of the catalyst and the addition of silica influenced the degree of crystallinity of the PP.

8.1 Introduction

During the past few decades polypropylene (PP) has been used as a commodity engineering thermoplastic with numerous fields of application [1]. The incorporation of inorganic particles (SiO_2 , CaCO_3 , etc.) in PP-composites leads to material properties that depend strongly on the filler shape, size, degree of dispersion and its surface characteristics [2]. When high particle loadings ($> 20 \text{ vol}\%$) are used, the processability of the material becomes deteriorated and the weight of the end composite becomes much larger than the neat polymer [3]. A low filler-particle concentration in the polymer matrix is therefore preferred, particularly when improved mechanical properties (i.e. stiffness) are sought. Filler-surface modification is a useful procedure to achieve better processability and thus material properties [4]. Since the surface of bulk silica (SiO_2) can be readily tailored [5,6] through variation in the particle size, pH, morphology, etc., it is a useful filler in thermoplastic polymers and has been applied in automotive applications, electronics, appliances and consumer goods [7-9].

Typical composite processing techniques are extrusion [10] or injection moulding [11]. Both these processes, however, may result in poor particle distribution (aggregation) of the filler even when a coupling agent is used, and improved preparation methods for the PP-filler composites are ongoing [12,13]. The most extensively used synthesis method to obtain PP from propylene (C_3H_6) is through Ziegler-Natta catalysis [1], which accounts for *ca.* 98% of all PP produced worldwide. The catalyst/polymer materials need to be formed in a controlled manner to investigate the mechanistic processes such as catalyst fragmentation behaviour. Pater *et al.* [14] used a one-liter Slurry Phase Polymerisation (SPP) reactor in which very low reaction rates could be obtained, allowing for reaction kinetic measurements also in early stages of polymerisation. The addition of silica particles to PP using a SPP reactor is not facile due to catalyst sensitivity towards oxophilic species [15] as well as the chemical incompatibility of non-polar propylene around hydrophilic silanol functionalities present on the amorphous silica surface [16]. However coupling agents are used to modify the hydrophilicity of silica surface. The modification with hydrophobic chains is therefore a key factor in the *in-situ* polymerisation synthesis of PP/ SiO_2 nanocomposites using a SPP reactor. The modification of the filler surface can also influence the effect of the filler on the crystallization behaviour. The advantages of *nano-* over *micro-*size filler particles in polymer matrices was reported by Sumita *et al.* almost two decades ago [17].

In this chapter, the formation of PP/ SiO_2 nanocomposites prepared *in situ* is reported. The synthesis was performed in a SPP reactor with silica nanoparticles pre-modified with a silane coupling agent resulting

in good dispersion of the filler in the matrix as shown by SEM. The modified nanoparticles were added to the monomer without mechanically (thermal) mixing treatment, (which may cause aggregation) while modification of the silica surface prevented catalyst deactivation. The chemical kinetics of the formed composites were also studied [14].

Pre-polymerisation (polymerisation under mild conditions) is an essential step in the polymerisation processes of PP. The conditions (temperature, monomer and catalyst concentration, etc.) in SPP are milder compared to current industrial pre-polymerisation processes and appropriate scale-up of the SPP process should therefore be feasible not only to produce neat PP but also composites thereof. The yield of the final product for the current reactor design was 5g/g (grams of polymer per gram of catalyst), which allowed the study of catalyst efficiency in the presence of silica where the morphological development takes place in early stage of particle existence.

A 4th generation Ziegler-Natta catalyst used in this study was the first step towards a composite pilot plant production (in a liquid-pool and/or gas phase reactor), which lays the basis for the current industrial production of 30-100 kg pure PP per gram of catalyst.

The morphology of the composite was studied by Scanning Electron Microscopy (SEM) and based on X-ray scattering intensity theory the degree of crystallinity was derived by a graphic multippeak resolution method [18].

8.2 Experimental Section

8.2.1 Materials and Silica Modification

Triethyl aluminum (donated by Witco GmbH) was used as the co-catalyst. The catalyst components were prepared in a glove box and in a nitrogen gas atmosphere. Pro-Analysis grade hexane (Merck) was used to suspend the catalyst. Propylene was obtained from Indugas with a purity > 99.5% and with propane gas as main impurity. The nitrogen gas used was of > 99.999% purity. For the preparation of silica nanoparticles, 21 ml of tetraethyl orthosilicate (TEOS) was slowly added to 21 ml of dry ethanol (1:1 vol/vol). The mixture was stirred and 8 ml of 1 M HNO₃ was added. The sample was heated to 60°C for 3 h together with 3 ml of deionised water and then placed in an ice-bath. Silica sol (5 ml) was dispersed in EtOH (90 ml) and kept in the refrigerator for one week [19]. The particle size was on average 10 nm as confirmed by Photon Correlation Spectroscopy (PCS). To modify the silica surface, an excess of the coupling agent (octadecyltrimethoxysilane) was added to 30 ml of the silica-sol and stirred for 72 h at room temperature. To the resulting product acetone was added and the precipitate was separated by centrifugation in a Hettich Universal centrifuge. The precipitated powder was dispersed in EtOH

and sedimented through centrifugation, the process was repeated three times to remove all excess reagent. Excess EtOH was decanted and the sample dried in vacuum. The solid was then dispersed in hexane. For the composite containing micro-sized silica, 0.05g of solid silica with particle size 10 μm (Alltech) was dispersed in 20 ml of hexane within an argon atmosphere to remove any oxygen traces.

8.2.2 Reactor Set-up and Catalyst

The experimental set-up and reactor design is schematically shown in Fig. 1 [14]. High purity nitrogen gas was used to pre-flush the system. The purified propylene was pressurized in a cylinder and fed to the system via a mass flow meter. An injection system was used for the mixture of catalyst/co-catalyst into the reactor. The reactor system consisted of 1 litre glass reactor with a jacket through which hot or cold water could be circulated. The reactor has four entries at the top; one for the thermocouple, one for injection needles, a third for hexane supply (also connected to a vacuum pump) and the fourth for the dip-pipe and outlet which was connected to a membrane pump and which re-circulated the gas in the reactor and kept the reaction slurry in a homogeneous state. The outlet of the membrane pump was also connected to nitrogen gas and monomer supply, whereas the inlet was connected to the pressure meter and a relieve-valve set at 0.4 bar over-pressure.

A number of parameters such as the reactor temperature, pressure, the jacket inlet and -outlet and water temperature, and the mass flow meter opening readings are recorded at pre-specified intervals by computer. A commercially available 4th generation Ziegler-Natta

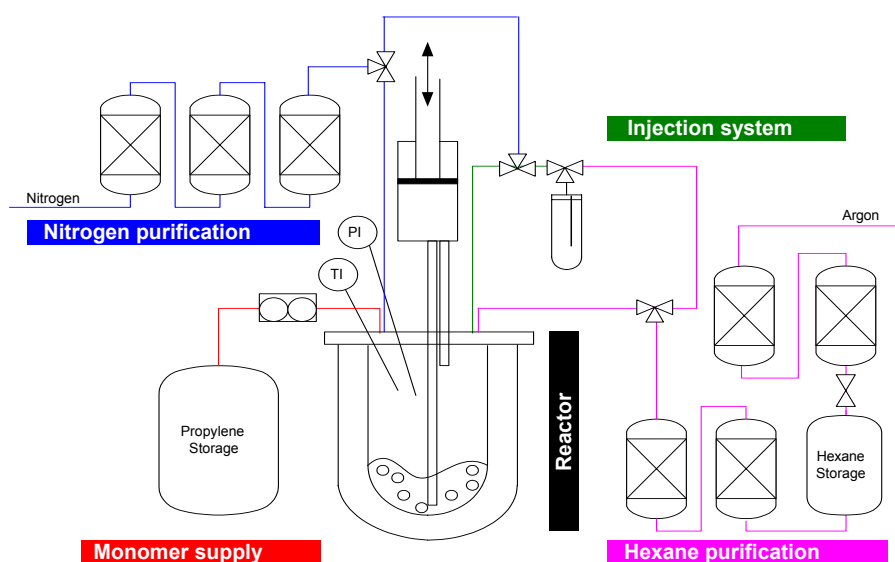


Fig. 1. Schematic diagram of the Slurry Phase Polymerisation reactor design and experimental set-up used in this study.

catalyst on a MgCl_2 support was used in this work [1,14]. The catalyst slurry was prepared in a glove box and the co-catalyst was weighed and then contacted with the required amount of catalyst in presence of hexane. A typical amount of catalyst for the slurry reactor was 100-300 mg.

8.2.3 Pre-Polymerisation Reaction and Filler Addition

The reactor was filled with hexane, and the catalyst subsequently introduced into the system. The modified silica (*ca.* 3 wt%) was slowly added. When the system reached equilibrium with constant temperature and pressure, the monomer pulse was injected into the reactor. There was an increase in pressure, which gradually decreased as the reaction proceeded. When the pressure became constant, the next pulse was either injected or the reaction stopped. The catalyst remained active until the hexane/polymer slurry became slowly exposed to the atmosphere, which slowly deactivated it. When the reaction ceased, the excess hexane was removed and the polymer powder was dried. The samples of neat PP, PP containing nanosilica (10 nm) and PP with micro-silica (10 μm) were labelled as samples PP, PPN10 and PPM10, respectively.

8.2.4 Characterization Methods

Equilibrium thermodynamic parameters (DSC), XRD and XRF conditions were determined using the same conditions described in chapter 3. The colloidal particle size was measured with PCS on a Zetasizer 3000HS under ambient conditions at a count rate of 9.2 Cps, a detector angle of 90° , and at wavelength of 633 nm.

The micro particle size was measured with a Microtrac X-100 (Leeds and Northrup, Pennsylvania) laser diffraction analysis using unified scatter technique. The FT-IR spectrum was recorded on a 410 Jasco spectrophotometer with a resolution of 4 cm^{-1} (1000 scans collected). Surface analysis was performed with X-Ray Photoelectron Spectroscopy (XPS) and spectrum recorded on a Quantum 2000 Scanning Esca Probe (Physical Electronics). The aluminum K_α X-ray beam had a power of 25 Watt and the analysis area was $1000\ \mu\text{m} \times 500\ \mu\text{m}$. For calibration of the spectra the C1s line of aliphatic carbon (284.8 eV) was chosen as internal reference. For the electron micrographs, a LEO 1550 (Germany) high-resolution low-voltage Scanning Electron Microscope (SEM) equipped with an in-lens detector and a Energy Dispersive X-ray Analysis (EDAX) system (Noran Vantage) was used. The samples were uncoated and low voltage was used to avoid charging problems. A magic angle spinning (MAS) solid state ^{29}Si nuclear magnetic resonance (NMR) spectrum was obtained at 79.49 MHz using a Varian Unity 400 spectrometer. MAS at 5 kHz was used to acquire all data in proton-decoupled mode. Samples were

finely ground prior to analysis. The NMR spectrum was deconvoluted using a Gaussian fit in terms of Q^i where $i = 2, 3, 4$, which corresponds to the number of siloxane bridges bound to the silicon atom of interest. Q_2 represents middle groups in chains or cycles, Q_3 chain branching sites and Q_4 fully cross-linked groups [20].

8.2.5 Kinetics: Theory

The rate of polymerisation R_p (mol/l*s) depends on the concentration of active sites C^* (mol/l), the concentration of monomer at these active sites C_m (mol/l), and the lumped propagation constant K_p [1/mol*s] as shown in equation 1,

$$R_p = K_p \cdot (C_m)^q \cdot (C^*)^r \quad (1)$$

The dependence of the reaction rate on the monomer concentration and active site concentration is of first order, i.e. $q = 1, r = 1$.

A first order deactivation of active sites was assumed as shown in equation 2,

$$-\frac{dC^*}{dt} = K_d C^* \quad (2)$$

where K_d is the deactivation constant.

The propylene partial pressure in the gas phase and thus the concentration of the dissolved propylene in hexane decreased gradually as the reaction proceeded as shown in equation 3,

$$-\frac{dC_m}{dt} = R_p \quad (3)$$

The first order dependence of the reaction rate was estimated based on the monomer and active site concentration. Combining equations 1, 2 and 3 followed by integration yields equation 4 ($K_d \rightarrow 0$):

$$-\ln\left(\frac{C_m}{C_{m0}}\right) = \frac{-K_p C_0^*}{K_d} \cdot [1 - e^{(-K_d \cdot t)}] \quad (4)$$

where C_0^* is the initial active site concentration at $t = 0$, and therefore,

$$-\ln\left(\frac{C_m}{C_{m0}}\right) = K' \cdot [1 - e^{(-K_d \cdot t)}] \quad (5)$$

where K' is a function of the derived constants.

Using Henry's law, $C_m = H \cdot P_m$, where H is Henry's constant and P_m the partial pressure of the monomer in the reactor, equation 5 is reduced to equation 6:

$$-\ln\left(\frac{P_m}{P_{m0}}\right) = K' \cdot [1 - e^{(-k_d \cdot t)}] = \frac{K_p C_o^* t}{H} \quad (6)$$

from which the value of K_d could be estimated.

8.3 Results and Discussion

8.3.1 Synthesis

This study focused on the room temperature synthesis of (nano)-composites of PP/SiO₂ formed in a SPP reactor instead of a melt mixing procedure. Silica loadings were kept constant at 3 wt%. The silanol groups present on the bulk silica surface proved detrimental to catalyst activity and therefore the hydrated silica was modified with silane coupling agents. Two different silica filler particle sizes of 10 nm and 10 μm were used and compared. The modified silica was slowly added when the reactor was partially filled with hexane followed by the introduction of the catalyst into the system. The polymerisation started when the monomer pulse was introduced. As observed from several experiments, the reaction did not proceed when an excess of silanol groups were present and therefore an excess of hydrophobic C₁₈ chains were used to modify the silica surface [21]. Low loading additions of filler in PP were used to preserve the inherent properties of the matrix material. The colloidal nanosilica particle size determined by PCS prior to modification showed a unimodal distribution at a fixed angle of 90°. The micro-silica particle size determined by laser diffraction analysis showed a Gaussian distribution and an average particle size of 10 μm. The light rays, which strike particles, were scattered through angles inversely proportional to particle size (see Fig. 2 for nanoparticles).

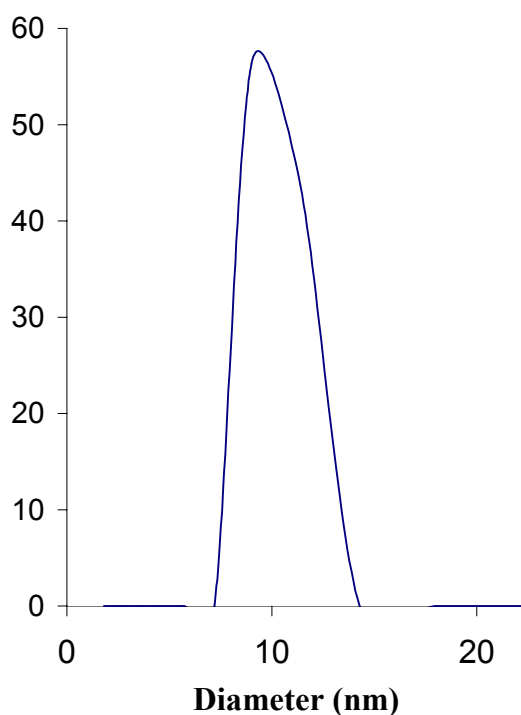


Fig. 2. Particle size distribution for nano-sized silica.

8.3.2 Spectroscopy

To investigate the presence of silica atoms on the surface of the hybrid system, XPS measurements were performed to a maximum depth of 10 nm. The spectrum indicated the presence of silicon atoms on the surface of the polymer implying the spherical particles are located throughout the polymer network, see Fig. 3. The Si 2p spectrum has a maximum centered at *ca.* 101.9 eV representing Si-O-C_nH_m type compounds. This gives an indication of the filler/matrix compatibility due to the modified character of the silica system.

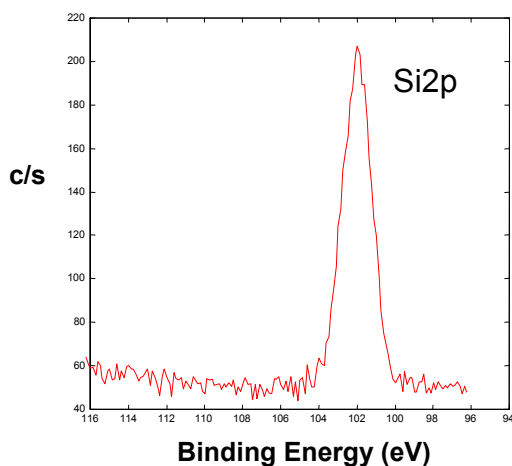


Fig. 3. X-ray Photoelectron Spectrum (XPS) showing the silicon peak in SiO₂ particles in the PPN10 sample.

For a semi-quantitative determination of the compositional disordering of silanol groups in the local environment of silicon atoms inside amorphous networks, MAS solid state ²⁹Si NMR was utilized to characterize the nature of the hydroxy-derivative around the silicon atoms (conventionally denoted by Qⁿ [22-24]; indicated by the relative proportions of Q², Q³, and Q⁴ species, as shown in Fig. 4. Typical ranges of peak positions δ (ppm) for the Si nuclei are -80 to -90 for Q² (n = 2), -90 to -110 for Q³ (n = 3), -110 to -125 for Q⁴ (n = 4) as in formula [Si(O)_{4-n}(OSi)_n] and it was observed that the system displayed a very condensed silicate structure due to the majority of Q⁴ species present.

The FT-IR spectrum of pure PP and the hybrid PP/SiO₂ system was recorded. A broad and large band at ~3424 cm⁻¹ and small sharp band at 960 cm⁻¹ were assigned to ν(O-H) stretches of Si-OH moiety. Absorptions in the range

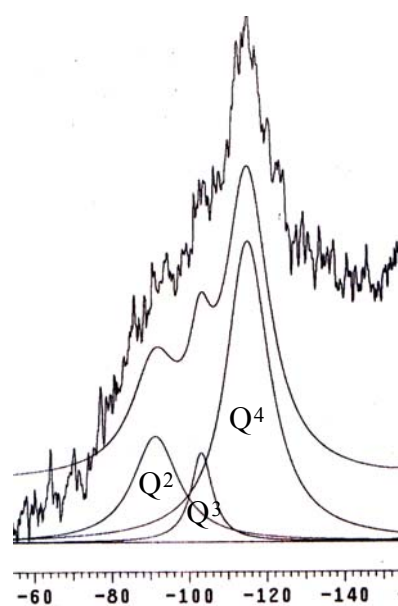


Fig. 4. Solid state ²⁹Si-NMR spectrum with Qⁿ (n = 2, 3, 4) labelling of peaks in ppm.

1080–1120 cm^{-1} were assigned to $\nu(\text{C-H})$ stretches of Si-O-C species while absorption in ranges 1050-1100 and 815-485 cm^{-1} were assigned to the stretching modes of Si-O-Si moieties.

8.3.3 Degree of crystallinity

Differential Scanning Calorimetry (DSC). The crystallinity ($W_{\text{c,x-DSC}}$) of PP and PP/SiO₂ composites by means of DSC were determined from the enthalpy evolved during crystallization using the following equation, where ΔH_m is the melting enthalpy, ΔH_m^0 the melting enthalpy of a 100% crystalline sample and ϕ the weight fraction of the filler:

$$W_{\text{c,x-DSC}}(\%) = \frac{\Delta H_m}{(1-\phi)\Delta H_m^0} \times 100 \quad (7)$$

The $W_{\text{c,x-DSC}}$ of pure PP (37%) decreased to 33 and 34% respectively when nano- or micro-silica was used. In the case of PPN10 the observed melting peak shifted towards lower temperatures when compared with PP. The melting peak of the α form was shifted towards higher values with increasing particle size of silica in PP. We proposed that the T_m of PP increase may result from some hindrance in the melting process of PP caused by the presence of silica particles. It has been reported [25] that carbon black particles subjected to the amorphous phase during crystallization of polypropylene delayed the starting mobility of polymer segments in the regions of lamellae surfaces during the polymer melting process. Thus, the PP sample has a more rigid amorphous phase (containing the micro silica particles) and it melts at high temperature. The melting point temperature T_m of the polymer increases with rising lamellar thickness L_{lt} and depends on the specific fold surface free energy (σ_e), the melting

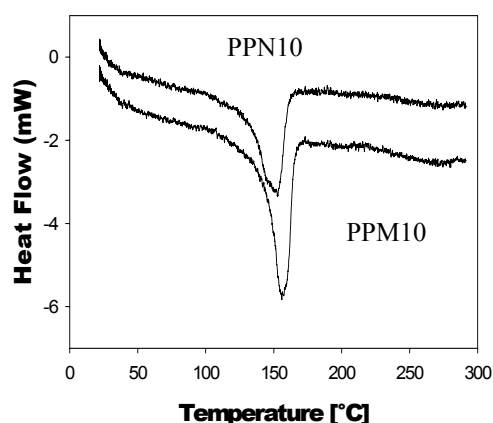


Fig. 5. DSC scans of PPN10 (above) and PPM10 (below).

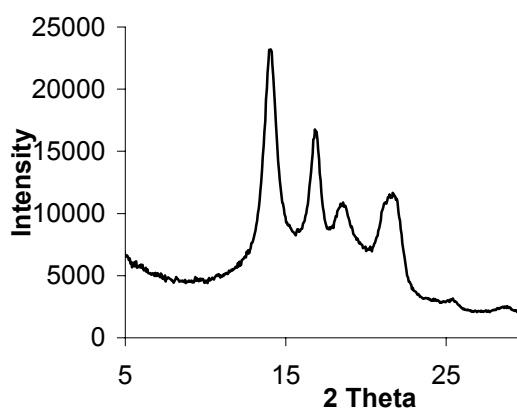


Fig. 6. WAXD scan of the PP-SiO₂ composite prepared *in-situ* by SPP method.

surface free energy (σ_e), the melting

temperature of the pure polymer T_m^0 and the melting enthalpy ΔH_m , according to the following equation [1]:

$$T_m = T_m^0(1 - 2\sigma_e / L \Delta H_m) \quad (8)$$

A modification of σ_e (decreasing) due to the presence of micro-silica may explain the observed change in T_m .

Degree of Crystallinity by Wide Angle X-ray Diffraction (WAXD). The breadth of X-ray diffraction lines are interpreted as a result of a disorder within the lamellae and can therefore be used to measure the degree of crystallinity of the polymeric system [26]. Fig. 6 shows the WAXD spectrum of a PP/SiO₂ composite recorded at room temperature. Three strong peaks located at low 2θ values are characteristic of the α -form of PP crystals (thermodynamically stable), which can be indexed as the (110), (040) and (130) reflections. Consistent with the literature, these three peaks are located at $2\theta = 14.3, 17.0$ and 18.7° [27-29]. The degree of crystallinity of the α -form of PP was obtained from the following equation [18]:

$$W_{c,x} = \frac{I_c}{I_c + 1.25I_a} \quad (9)$$

where $W_{c,x}$ is the degree of crystallinity of PP, I_a the integral of the amorphous peak and $I_c = I_{110} + 1.63I_{040} + 2.14I_{130} + 3.5I_{041}$, where I_{110} , I_{040} , I_{130} , and I_{041} are the integral intensities of the corresponding crystalline peak. The degree of crystallinity of PP in the samples PP, PPN10 and PPM10 showed the same tendency as in DSC, namely lower crystallinity upon addition of silica particles to PP. Characteristic lines of the filler used were observed in the XRD spectrum. Taking into account the WAXD measurements were performed at room temperature and that the used silica was amorphous as confirmed by XRD, it can be concluded that the spherical SiO₂ particles decreased the crystallinity of the α -form of PP with a more pronounced effect than when larger particle size was used.

Additionally, the crystallite size (L) of the α -PP may be calculated from the Scherrer equation [30]

$$L_{hkl} = \frac{k\lambda}{\beta_o \cos \theta} \quad (10)$$

where L_{hkl} (nm) is the crystallite size perpendicular to the direction of the (hkl) crystal plane, λ (nm) the wavelength of the incident X-ray, θ (degree) half of the Bragg angle, β_o (in radians) the FWHM of the peak, and k the constant factor of the crystal shape (which is 0.9). An estimation of L was made. The crystallite sizes of the main crystal planes of α -PP in sample PPN10 were slightly smaller than those of

pure PP, while those of the sample PPM10 were slightly larger in L_{110} and L_{040} , as shown in Table 1.

Table 1. Estimated crystallite sizes (nm) of α -PP and nanocomposites.

Sample	L_{110}	L_{040}	L_{130}	L_{041}
PP	10.37	14.08	4.20	5.82
PPN10	9.34	13.92	14.61	6.72
PPM10	10.55	20.77	11.75	6.47

In many instances, the crystallite size is a useful parameter for estimation of mechanical properties since a specimen with a large L is usually brittle [26]. Even though the nanosilica decreased the crystallinity compared to pure PP, the crystallite sizes were increased slightly. These results indicated that the positive effect of the silica as a nucleation site in the PP was diminished and was in accordance with findings by Janigová *et al.*, [4] that the silica surface covered by a layer of low-density polyethylene led to a deactivation of the filler's positive effect on PP crystallization rate parameters. Considering the nucleation effect, the silica surface was therefore affected by the presence of the C_{18} chains while an influence on the crystallinity could result from the degree of silica dispersion inside the PP matrix.

8.3.4 Composite morphology

The silica particle distribution and its influence on the PP morphology were investigated by SEM. Micrographs showed the developed shape of the PP particles and the filler distribution in the PP. A homogeneous dispersion of the silica (as verified by EDAX) in the PP matrix was observed. In Figures 7a-c, the surface morphology of the nanocomposite is shown. The polymerisation was carried out under non-isobaric conditions forming a wax-like polymer with low molecular weight when the monomer concentration was low. The micrographs showed that the morphology of the PP particles was not influenced when nanosilica was added as seen at lower magnifications of the composite in Fig. 7a. This observed morphology was comparable to that of a standard polypropylene sample as reported in literature [14]. The homogeneous dispersion of the

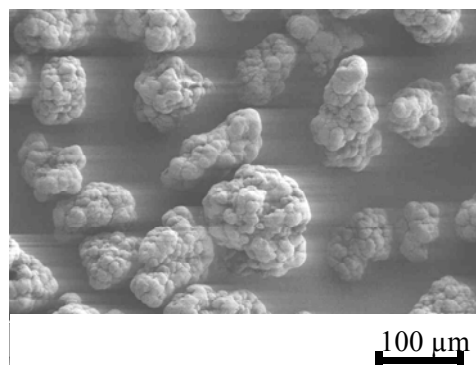


Fig. 7a. SEM micrographs of (nano)composite showing surface morphology.

silica was seen at higher magnifications, as observed in Fig. 7b and 7c. The interaction of the nano-filler with the catalyst occurred by mixing the diluted catalyst in hexane with the modified silica (facilitated by their nanosize). In Fig. 8a and b SEM micrographs of the micro-sized composite are shown and it appeared that the particles had interaction only with the surface of the PP.

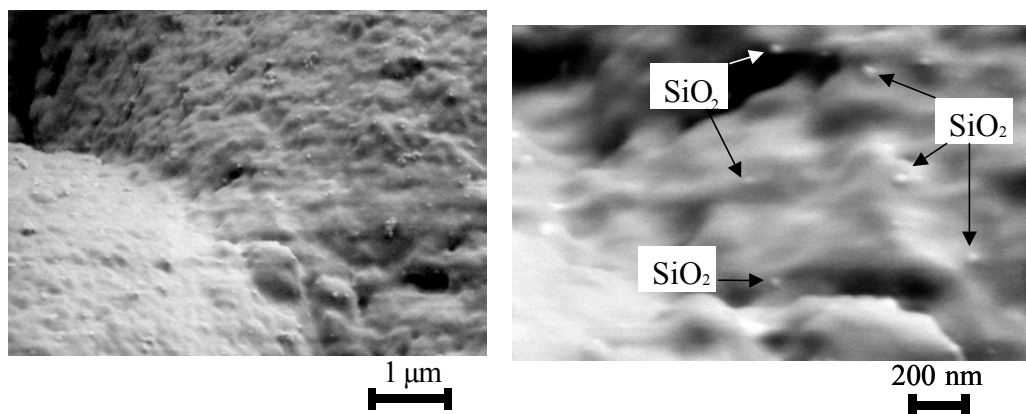


Fig. 7b and c. SEM micrographs of (nano)composite showing surface morphology under different magnifications (b left, c right).

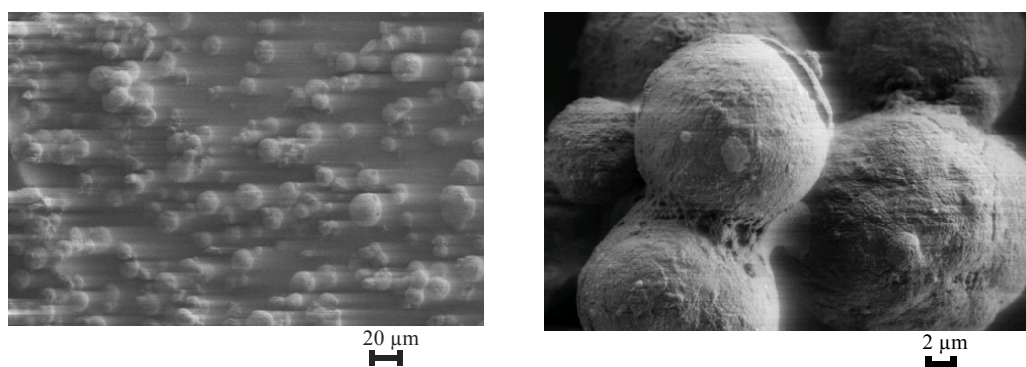


Fig. 8a and b. Morphology of the composite containing micro-sized (~10 μm) silica particles at different magnifications.

It is plausible that the nanosilica interacted with the catalyst at the initial stage of the polymerisation, while the micro-silica particles (in an agglomerate slurry state rather than colloidal dispersion), were more embedded in the initially formed polymer.

8.3.5 Catalyst

Three experiments are plotted in relation to the reaction rate and normalized reaction rate vs. time as shown in Fig. 9 and Fig.10, respectively. PP and PPN10 showed a similar deactivation behaviour suggesting that the nanosilica did not influence the activity of the catalyst. The slight difference at low reaction times between PP and PPN10 is in the acceptable range of reproducibility. As the reaction

proceeded the deactivation behaviour of PPN10 became similar to pure PP. The use of micro-silica caused a large drop in catalyst activity as seen in the same rate vs. time curve of Fig. 9. It is known that the catalyst is sensitive to external agents that can affect the dormant state of the active sites. As the initial propagation frequency in these experiments is on the order of 0.1 to 25 monomer molecules per second, the decay of catalyst activity with increasing yield in the early stages of the polymerisation reaction could be the result of an increasing number of active sites being deactivated by the micro-silica. The deactivation caused by the microsilica on the catalyst may occur by masking or pore blockage, caused by the physical deposition of micro-particles on the outer surface of the catalyst and thus obscuring the active sites. That would explain the dropping of the catalyst activity in the PPM10 but not the measured initial reaction rate (higher than pure PP) of the microcomposite. The filler effects were better observed when the reaction rate were normalized with respect to initial reaction rate at $t = 0$. As seen in Fig. 10 the normalized reaction rate originated at the same point. The reaction rate of PP and PPN10 overlapped showing no effect of the nanoparticles on the catalyst activity. The PPM10 curve showed a rapid decay with the time, confirming the fast deactivation of the catalyst when microparticles were used.

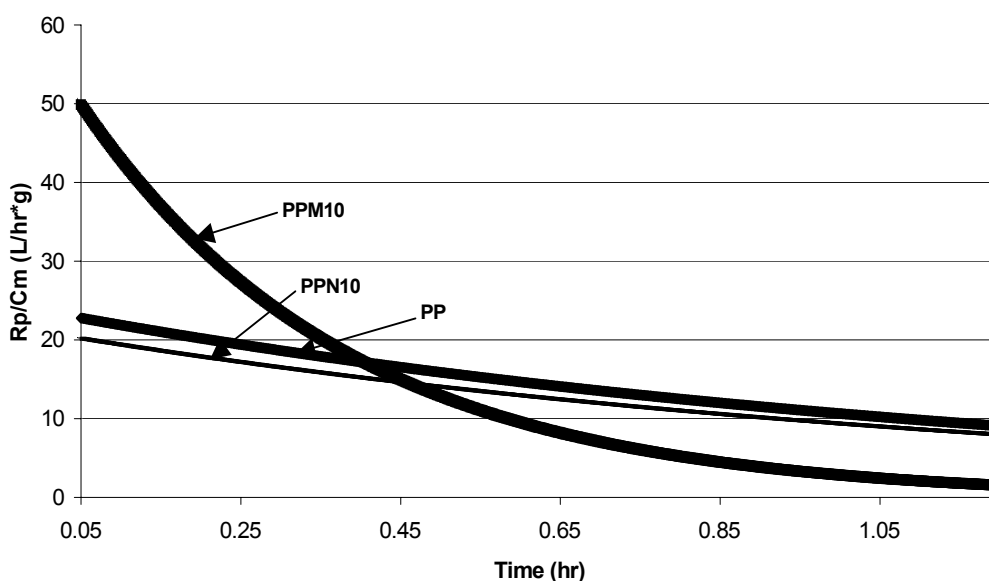


Fig. 9. Kinetic measurements showing reaction rate vs. time curve.

Likewise, the filler surface may not be covered completely and basic groups could be exposed and affect the nature and strength of the acid sites, resulting in catalyst deactivation. This seemed in agreement with the O-H traces observed in FT-IR and MAS ^{29}Si NMR (see above).

Analysis of catalyst/silica interaction was complicated since micro-silica could be detrimental with loadings as low as 3 wt%. The yield of the PP synthesis (on the order 5 g per g catalyst) was not affected when the silica was incorporated. Furthermore, the catalyst remained active upon the addition of the silica sol. Accurate reaction kinetic measurements in the earliest stage of polymerisation were performed after filler addition.

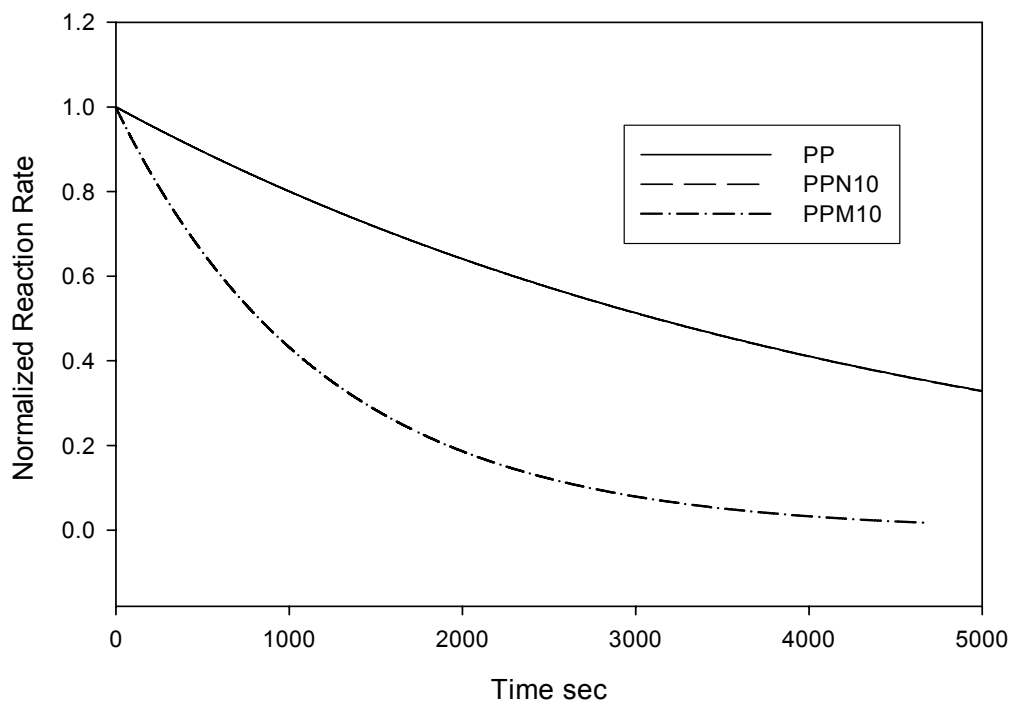


Fig. 10. Normalized reaction rate vs. time curve. The PP and PPN10 lines overlap.

8.4 Conclusions

The *in-situ* synthesis of a PP/SiO₂ nanocomposite using a Ziegler-Natta catalyst was satisfactorily prepared in a SPP reactor. Homogeneous dispersion of filler particles was obtained at loadings of 3 wt% as verified by SEM. It was found that the silica particles did not increase the degree of crystallinity of the PP, and this effect was less pronounced when nano-silica was used. The use of nanosilica in the PP reduced the catalyst decay when compared with micro-silica. The synthesis of (nano)-composites by means of this method brings new insights to the study of PP-filled materials.

8.5 References

- [1] Moore, E. *Polypropylene Handbook: Polymerization, Characterization, Properties, Processing, Applications*, Hanser-Gardner Publications, Cincinnati (1996).
- [2] Karger-Kocsis, J. *Polypropylene: Structure, Blends and Composites*, Chapman & Hall: London, vol. 3 (1995).
- [3] Pukansky B. *Particulate Filled Polypropylene Composites*, Kluwer Academic Publishers, Dordrecht (1999).
- [4] Janigová, I. and Chodák, I. *J. Therm. Anal. Calorim.* 60, 401 (2000)
- [5] Arkles, B. *Silanes, Silicones and Metal-Organics*, Gelest, Inc. Catalog, Tullytown, USA (2000).
- [6] Brook, M. A. *Silicon in Organic, Organometallic, and Polymer Chemistry*, John Wiley & Sons, New York (2000).
- [7] Hideyo, M., Yutaka, S., Sumio, T. and Yasubumi, T. JP 9165478 A.
- [8] Rothon, R. *Particulate-Filled Polymer Composites*, Longman, Essex (1995).
- [9] Mizutani, Y. and Nagō, S. *J. Appl. Polym. Sci.* 72, 1489 (1999).
- [10] Wang, Y. and Huang J.S. *J. Appl. Polym. Sci.* 60, 1779 (1996).
- [11] Nobuhiro, S., Hiroteru, G. and Shigemi, Y. JP 226478 A.
- [12] Van Krevelen, D.W. *Properties of Polymers*, Elsevier, The Netherlands, (1976).
- [13] Rong, M., Zhang, M.Q., Zheng, Y.X., Zeng, H.M., Walter, R. and Friedrich, K. *Polymer* 42, 167 (2001).
- [14] Pater, J.T.M., Weickert, G., Loos, J., Swaaij, W.P.M. *Chem. Eng. Sci.* 56, 4107 (2001).
- [15] Forzatti, P., Lietti, L. *Catal. Today* 52, 165 (1999).
- [16] Zhuravlev, L.T. *Coll. Surf.* 173, 1 (2000).
- [17] Sumita, M., Shizuma, T., Misasaka, K., Ishikawa, K. *J. Macromol. Sci. Phys.* B22(4), 601 (1983).
- [18] Mo, Z., Huang, X., Zhang, H., Yang, B., Zhu, Ch. and Mu, Z. *Chin. J. Polym. Sci.* 12, 278 (1994).
- [19] Bernardis, T.N.M., van Bommel M.J. and Boonstra, A. *J. Non-Cryst. Solids*, 134, 1 (1991).
- [20] Brunet, F., Lux, P. and Virlet, J. *New J. Chem.*, 18, 1059 (1994).
- [21] Krysztafkiwicz, A., Rager, B. and Jesionowski, T. *J. Mater. Sci.* 32, 1333 (1997).
- [22] Laridjani, M., Lafontaine, E., Bayle, J.P. and Judeinstein, P. *J. Mater. Sci.* 34, 5945 (1999).
- [23] Hajji, P., David, L., Gerard, J.F., Pascault, J.P. and Vigier, G. *J. Polym. Sci., Part B, Polym. Phys.* 37, 3172 (1999).
- [24] Brinkmann, D., Engelhardt, G., Jäger, C. Koller, H., Mali, M., Pfeifer, H. and Sebald, M. Springer-Verlag, New York (1994).
- [25] Mucha, M., Marszałek, J. and Fidrych, A. *Polymer*, 41, 4137 (2000).
- [26] Kohan, M.I. *Nylon Plastics Handbook*. Hanser, New York (1995).
- [27] Cho, K., Saheb, D.N., Choi, J., Yang, H. *Polymer* 43, 1407 (2002).
- [28] Ran, S., Zong, X., Fang, D., Hsiao, B.S. and Chu, B. *Macromolecules* 34, 2569 (2001).
- [29] Bond, E.B., Spruiell, J.E., Lin, J.S. *Part B: Polym. Phys.* 37, 3050 (1999).
- [30] Drits, V., Šrodon, J., Eberl, D.D. *Clays and Clay Minerals* 45, 461 (1997).

9 Polypropylene/SiO₂ Nanocomposites: Mechanical and Thermal Properties

Polypropylene-SiO₂ nanocomposites were synthesized using twin-screw extruders. The reinforcing and toughening effects of the nanoparticles on the polymer matrix were found effective at a loading of 4.5 wt%, which is lower than conventional particulate filled composites. The use of silica nanoparticles led to different material morphology when compared with that of the pure polymer. Addition of colloidal silica to the polymer matrix exhibited good filler dispersion while the use of powder silica resulted in aggregated silica particles distributed in the polymer. The properties of the nanocomposites were studied using two different inorganic fillers: colloidal and powder silica nanoparticles. The use of colloidal silica led to better mechanical performance compared with powder silica composites (both filler were in the nano-dimensions range). The presence of colloidal particles in the polymer matrix led to an increase of Young modulus (from 1.2 GPa to 1.6 GPa) and impact strength (from 3.4 KJ/m² to 5.7 KJ/m²) keeping the tensile strength constant but there was no noticeable improvement of the mechanical properties when powder silica was added to the pure polymer.

9.1 Introduction

The problem of rendering composite polymer materials with more impact-resistance without decreasing the material's modulus of elasticity has been attracting the attention of many polymer and material scientists. Some advantages of using polymers are found in their easy processing and its light-weight. During processing, high particle loadings result in end products with much higher weight than that of the pure polymers. Therefore a composite with improved properties at low particle concentration is desired. Reduction of the size of the inorganic filler added to the polymer matrix has produced an enhancement of the mechanical properties when compared with the pure polymer. Nanostructured materials often exhibit combinations of physical and mechanical properties that are not superseded by conventional materials. For example, by decreasing the particle size of silica from the micrometer to the nanometer domain, a change in strength, elongation at break, modulus and yield stress was observed in polyurethane or nylon [1,2]. Polypropylene (PP) is one of the fastest growing turnover polymers to date [3]. One of the difficulties regarding the use of inorganic nanoparticles in PP is their dispersion quality. This is due to the hydrophobic nature of PP, which gives rise to a significant problem in enhancing the adhesion between the 'hydrophilic' filler and the matrix [4] creating poor bond strength between the polymer matrix and filler. This problem has been overcome by tailoring the affinity between the inorganic material and the organic polymer by for example *in-situ* polymerisation, employment of silane coupling agents [5, 6] and other strategies [7,8]. The studies have shown an improvement in properties of thermoplastics when silica has been chemically modified when compared with unmodified silica [9,10]. For PP, low silica concentrations (< 5 vol%) led to an improvement of the mechanical properties [11-13]. Comparisons are however, based on an inhomogeneous dispersion of the unmodified silica upon a homogeneous dispersion of the modified silica. It was thought that at a very small diameter scale (below 20 nm) the damage evolution evolved from a single debonding process to a multiple debonding one with decreasing filler size and with a relatively poor dispersion state [14]. Poorly dispersed inorganic fillers in the polymer matrix generally do not lead to an improvement of the material properties. The presence of inorganic fillers affects the crystallization behaviour of the polymer when the particles act as nucleation sites. It has been reported that the modification of the filler surface can influence the effect of the filler on the crystallization behaviour [15]. It is not evident if the improvement of the properties is due to the change of the stress around the fillers, a significant nucleation effect or both. In order to minimise external effects, introduced by the chemical bond formed between filler and polymer, we have chosen for filler material

that does not have a direct chemical interaction with the polymer matrix.

In this chapter, the preparation of new PP-silica composites that show enhanced mechanical properties are described. The effort was focused on obtaining well-dispersed nanoparticles without using modifiers. The motivation to obtain good dispersion stemmed from the observation that if any properties are to be further improved then the distribution of the inorganic filler particles in the polymer matrix has to be as homogeneous as possible by using a filler size of diameter ≤ 30 nm. Two different inorganic nanoparticles were used: colloidal (abbreviated: Col) and powder silica (abbreviated: MOX). The particle content was kept constant at 4.5 wt% as it has been demonstrated that already at low filling ratios an improvement in the elastic modulus and impact resistance is achieved [12, 13]. The nanocomposites contained primary filler particles with a diameter less than 30 nm. The composites were prepared using a twin screw extruder where colloidal nanosized silica particles are directly used. The system led to better modulus values compared to those obtained by common methods (without chemical modification). Of each composition four samples were tested, the average values obtained for the different parameters are presented. Furthermore the effect of the inorganic filler on the thermal behaviour of the PP was studied by means of Differential Scanning Calorimetry (DSC).

9.2 Experimental

Materials

The polypropylene used was Stanyl PP 17M10 ($M_w = 280,000$ g/mol) provided by DSM. Silica nanoparticles were generously provided by Nissan Chemicals (Japan) under the brand name Snowtex™ as an acidified aqueous sol with particle sizes 10-20 nm. Silica Aerosil MOX-80 (Degussa chemicals) was obtained with an average primary particle size of 30 nm. Pure PP samples were labelled PP, composites with powdered silica aerosil PP-MOX and composites with colloidal silica Snowtex PP-Col respectively. Size Exclusion Chromatography (SEC) was used to determine M_w of nanocomposites using 1,2,4-trichlorobenzene as eluent.

Processing

Mixing of MOX silica with PP was performed with a 25 mm co-rotating ZSK 25 twin-screw extruder. The temperature of the extruder was 185-200°C, the rotation speed of the screws was 150 rpm and the length of the extruder was 1050 mm. The silica powder was fed to the polymer melt by a side feeder situated directly behind the melting zone. The material flux was optimised to get the highest torque of the extruder in order to achieve a proper particle dispersion. The extruded material

was cooled directly at the exit of the extruder in water and subsequently the material strings were palletised. The compounding of the Col nanocomposite was performed as described in chapter 6.

Sample preparation

The materials were compression moulded between brass plates and aluminium foil into a mould of 50 x 75 x 5 mm³. The temperature was kept at 220°C during moulding. The polymer pellets were melted under atmospheric pressure and subsequently the pressure was increased stepwise to a maximum pressure of approx. 500 kPa. Tensile tests were performed on dumb-bell shaped specimens using Zwick Z1020 tensile testing machine, at a constant strain rate of 10⁻² s⁻¹. Notched Izod-impact tests were performed according to ASTM-D 256.

Characterization

The heat of fusion was measured for all samples on a DSC in a standard mode in a Perkin Elmer Pyris series 1 DSC and TA-instrument Q-series in modulated mode were used for studying the thermal behaviour of modified PP and nanocomposites synthesized. Heating and cooling scans at 10°C/min over the temperature range of -60°C to 250°C were performed in the standard mode, while 2°C/min was used during measurement in the modulated mode (to distinguish the effect of recrystallization during melting). Size exclusion Chromatography (SEC) was used to determine the M_w and intrinsic viscosity (η). Scanning Electron Microscopy (Philips XL 30 SEM) was used to determine the dispersion of the silica on the polymer. Fracture surfaces after the Izod-impact test were used for morphology characterization to study the dispersion and fracture behaviour.

9.3 Results

Figures 1a through 1f show the morphology of fractured samples of PP (a,b) PP-MOX (c,d) and PP-Col (e,f). The morphology was studied after the processing experiment post-mortem. Figure 1a and b shows the SEM micrograph of a fracture surface of the pure polymer. In Fig. 1c and d small (micro) aggregates of silica can be observed. No visible particle agglomerates were observed at this magnification in the composites containing colloidal silica (Figs 1e and 1f). This was taken as an indication that the silica remained in the nano domain < 30 nm. A picture of a non-fractured sample was taken at higher magnification (Fig. 2). Well-dispersed particles appear distinguishable from the matrix for the colloidal silica composite. This is in accordance with Figs 1e and 1f where the particle size is below the resolution limit.

The degree of crystallinity of the composites was calculated from the DSC thermographs, using for the heat of fusion 209 J/g for 100%

crystalline PP [16], and is mentioned in table 1, together with the mechanical properties.

Table 1. Mechanical properties and DSC data of the samples.

Sample	E-modulus GPa	Max. Tensile Strength	Izod Impact Test KJ/m²
Pure PP (Pellets)	1.2	33.1	3.44
PP MOX silica powder	1.5	34.4	4.17
PP with silica colloid	1.6	31.4	5.77

Sample	Heat flow J/g	W_{c,x} %
Pure PP (Pellets)	100.5	48
PP MOX silica powder	100.9	50
PP with silica colloid	90.5	45

Fig. 3 shows the thermographs measured during heating of the original sample and the nanocomposites. It was observed that the melting point of the samples was clearly affected by the presence of silica nanoparticles. The heating thermogram of the pure polymer exhibited its first endothermic melting peak at about 145°C, followed by a second endothermic peak at 165°C, which is likely due to the melting of the α -form that is the most common crystal phase of iPP. The γ -phase is not usually observed as a different phase, but (co) crystallizes with and within the α phase spherulites [17]. The small peak below 150°C is due to the presence of the β -phase.

It is interesting to note that the onset of the first endothermic peak is the lowest (in comparison with the other two samples), indicating the beginning of the melting of the metastable β -form. In general, the β -form, which is thermodynamically less stable, melts at lower temperatures and recrystallize as the stable α -form [18]. The PP-Col nanocomposite showed a narrow and sharper peak than those of PP-MOX composite indicating possibly better crystal formation.

The crystallization point of the samples is shown in Fig. 4. PP displays an exotherm (crystallization point) with a main peak at 117°C. A crystallinity value of 48% was calculated from the measurements of the melting enthalpy. PP-MOX showed a peak at 119°C, from which a crystallinity of 50% was calculated. Addition of colloidal silica increased the crystallization point to 121°C, and resulted in a degree of crystallinity of 45%. The significantly narrower peak confirms a more uniform crystal formation than when using MOX.

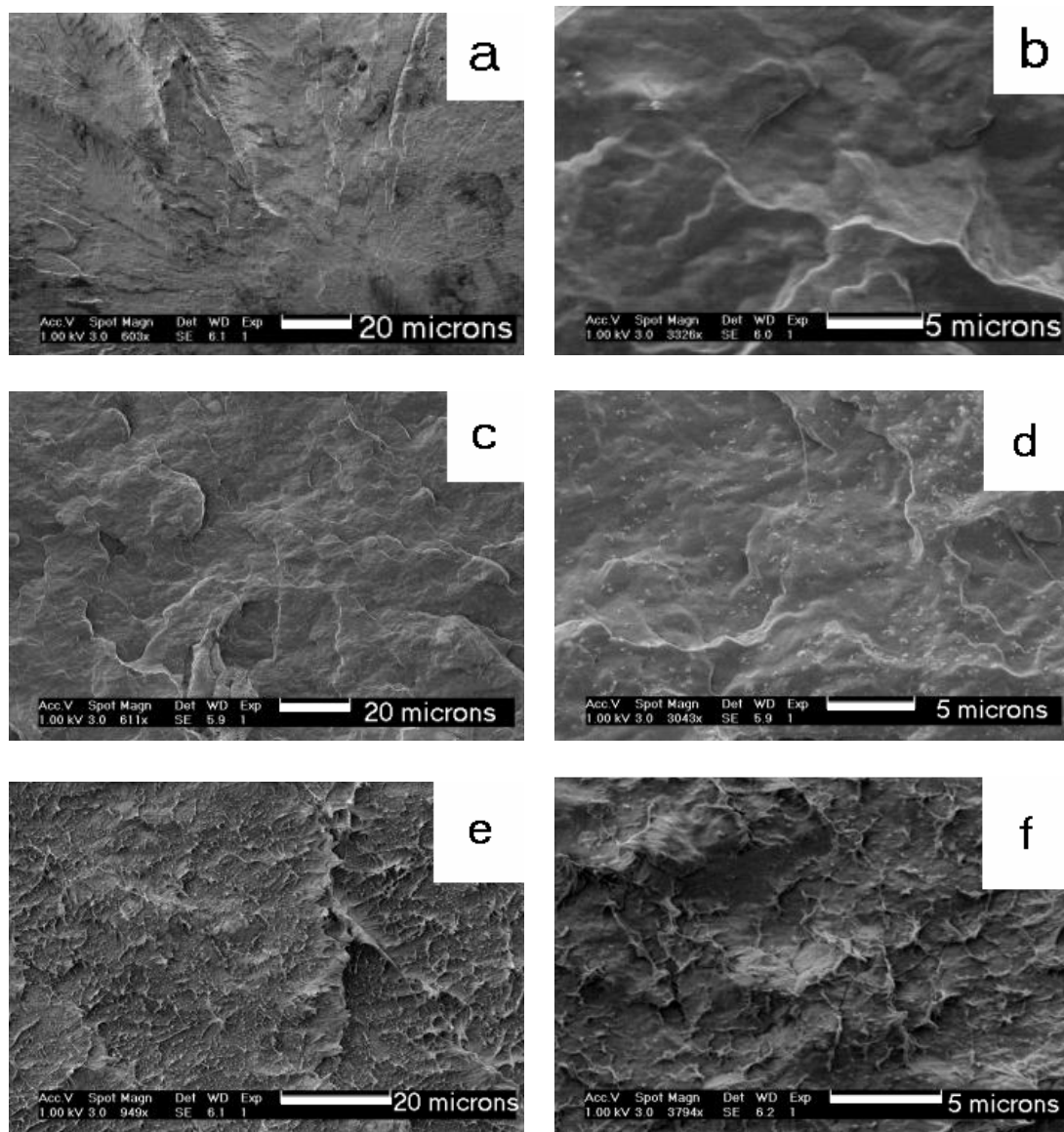


Fig. 1. SEM images of fractured samples. (a, b) PP, (c, d) PP-MOX and (e, f) PP-Col.

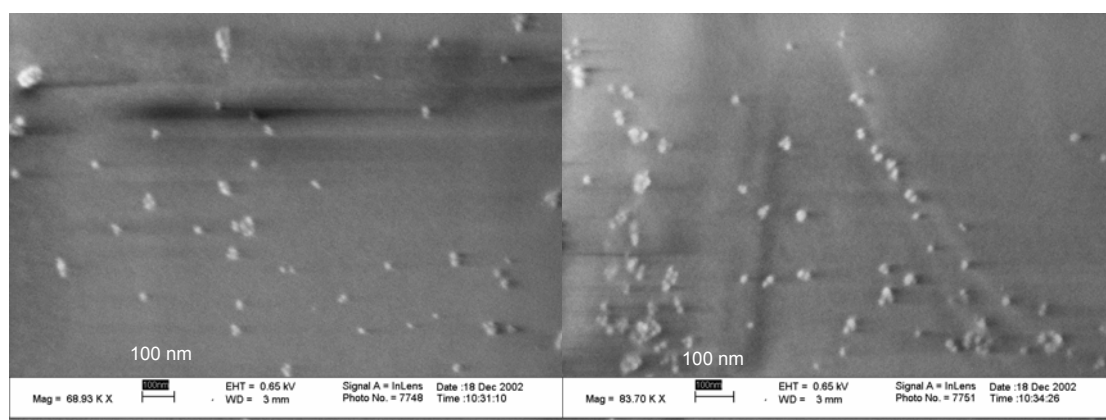


Fig. 2. SEM images of PP-Col samples.

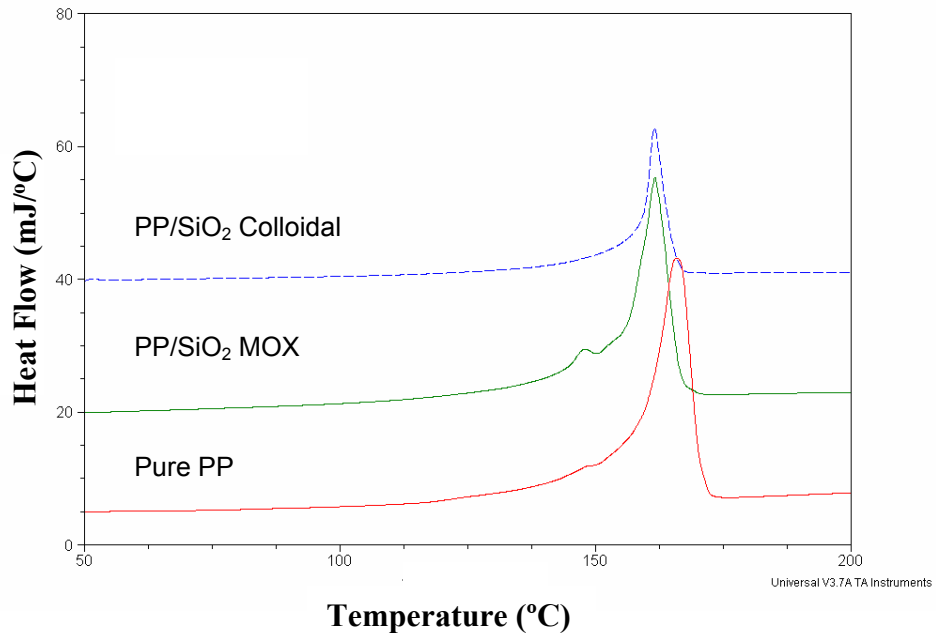


Fig. 3. DSC thermogram of samples. From top to bottom: PP-MOX, PP-Col and PP. (Graphs are displayed vertically).

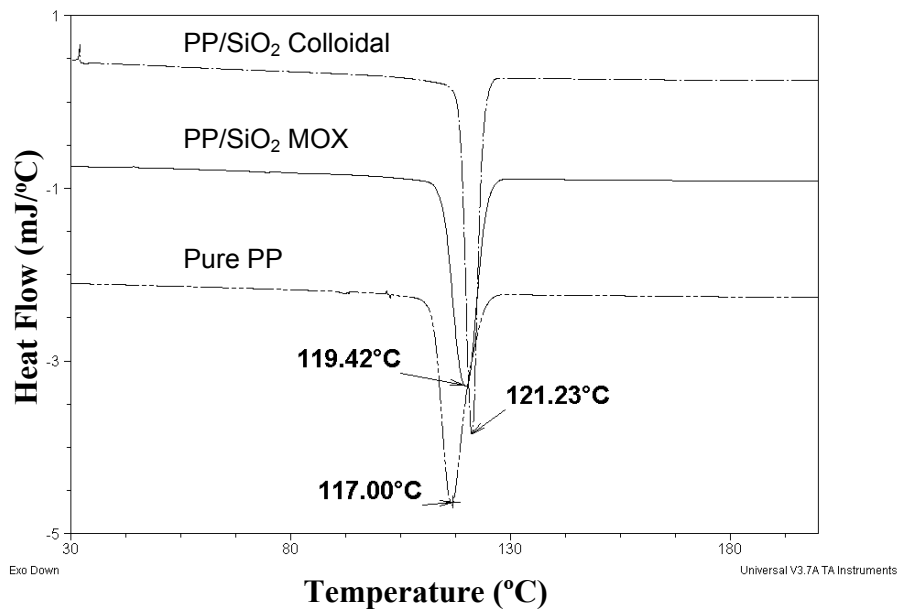


Fig. 4. Crystallization point of the samples. From top to bottom: 117 (PP), 119 (PP-MOX) and 121 (PP-Col).

The number average molecular weight (M_n) and weight average molecular weight, (M_w) of PP, PP-MOX and PP-Col samples are shown in Table 2. Upon addition of colloidal silica the polymer intrinsic viscosity $[\eta]$ and molecular weight (M_w), obtained from SEC experiments, decreased. This is most likely related to the degree of crystallinity, which also slightly decreased from 48% to 45%. Upon addition of MOX silica the molecular weight of the polymer decreased, but to a lesser extent than for the colloidal composite. In contrast, the degree of crystallinity slightly increased to 50%. Within experimental error however, it can be concluded that regardless the type of nanosilica, both M_w and η decreased whereas the crystallinity remained constant. It has been reported [19] for isotactic polypropylene (iPP) that the degree of PP crystallinity was inversely related to the weight average molecular weight of the polymer. This is not the case for PP-MOX and PP-Col nanocomposites.

Table 2. Molecular structure parameters of PP and PP/SiO₂ Nanocomposites as obtained from SEC-triple molecular weight measurements in kg/mole and $[\eta]$ in dl/g.

Sample	M_n	M_w	$[\eta]$
Pure PP (Pellets)	67	280	1.49
PP with silica colloid	59	245	1.38
PP MOX silica powder	61	260	1.43

Regarding the mechanical measurements, tensile stress experiments were performed at a strain rate of 10^{-2} s^{-1} . Samples of the pure polymer showed neck formation at the yield stress. The composite samples, in contrast, fractured before neck formation could start. For the weight percentage of filler used, the yield stress did not change significantly when compared to the pure polymer. A considerable increase in the yield stress has been reported for non-uniformly dispersed composites with 6 and 12 wt% of filler having particles diameters in the 12 and 25 nm range [2,14]. This has been attributed to the complex geometry of the aggregates that leads to a better stress transfer between polymer and filler than for a spherical filler shape [20]. But for our system, a more significant difference is expected for higher filled nanocomposites. Debonding of the filler particles plays also a role during the applied tensile stress, but for small particles debonding is more difficult to occur.

While the influence of the filler particles on the tensile stress test is rather limited, the influence on the Izod impact strength is significant. The addition of colloidal particles led to 68% higher impact strength than the pure polymer matrix (see Table 1). This suggests that for a nanocomposite subject to impact loading, the interfacial regions are

able to resist crack propagation more effectively than the polymer matrix. This can be explained as follows [21]: The use of rigid inorganic filler particles in a polymer matrix under tension, will cause stress concentrations followed by debonding and shear yielding. Due to the formation during crazing of an interconnected network of voids, which are traversed by small fibrils, yielding and crazing are found to be deformation mechanisms in polypropylene [22,23]. Obviously the higher the resistance to separation between matrix and filler, the higher the stresses that can be applied to the specimen before the separation takes place. For large particles (100 μm) matrix de-wetting will create voids that immediately begin to grow destroying the integrity of the composite. The void size however, is determined by the filler particle size. The smaller the particles the smaller will be the resulting voids. If the adhesion strength is higher than cohesion forces of the matrix (i.e. good adhesion), then the stress (σ) to break the specimen will be controlled by the stress concentration in the vicinity of the filler particles. If the resistance to separation is low (poor adhesion), voids will be formed already under low stresses, but this situation might not be damaging the structural integrity of the specimen. Such voids will be responsible for a pseudo-plastic behaviour of the polymer [21]. In case of good adhesion between phases, stress concentration near the particle is independent of their size. In case of poor adhesion between phases, the moment at which the matrix actually separates from the particles depend on the particle size due to subsequent debonding sequence (void forming) that would lead to the specimen failure. Hence, large-sized particles are undesirable when the adhesion between matrix and filler is poor.

9.4 Conclusions

The influence of silica nanoparticles in PP was studied using two different inorganic fillers with particle size ≤ 30 nm. As a basis for comparison, not chemically modified silica that could influence the bound strength between filler and polymer matrix was used. Bearing in mind the differences in preparation route, the filler dispersion state within the matrix varied from round particles to aggregates of different shape (even though the silica particles were in the same diameter range). Colloidal silica nanoparticles added to PP showed good dispersion of the inorganic filler into the polymer matrix whereas the addition of powder nanosilica particles showed a good dispersion of aggregates into the PP as seen from the fracture surfaces. Upon addition of silica an improvement of the elastic modulus of *ca.* 30% was obtained. The yield stress at this filler percentage was found not to be too sensitive to the dispersion state. Nevertheless, it seemed that the dispersed particles slightly decreased the yield stress. However a real change could only be observed at different filler percentage [14]. A significant improvement was found in the Izod-impact tests. Regardless of the kind of inorganic filler, an increase in the fracture

toughness of the material was obtained. An enhancement of 68% was measured with the colloidal silica particles. Furthermore, addition of colloidal particles decreased the melting point of the PP and the heat of fusion whereas the differences with the pure polymer were much less pronounced for the MOX composite.

9.5 References

- [1] Petrović, Z.S., Javni, I., Waddon, A. and Bánhegyi, G. *J. Appl. Polym. Sci.* 76, 133 (2000).
- [2] Sumita, M., Shizuma, T., Misasaka, K., and Ishikawa, K. *J. Macromol. Sci. Phys.* B22(4), 601 (1983).
- [3] Meifang, Z., Qiang, X., Yanmo, Ch., Yu, Z. and Adler, H. *J. China-EU Forum on Nanosized Technology* 46 (2002).
- [4] Gahleitner, M., Bernreitner, K. and Neißl, M. *J. Appl. Polym. Sci.* 53, 283 (1994).
- [5] Khan, M.A., Hinrichsen, G. and Drzal, L.T. *J. Mater. Sci. Lett.* 20, 1711 (2001).
- [6] Garcia, D., Picazo, O., Merino, J.C. and Pastor J.M. *European Polym. Journal* 39, 945 (2003).
- [7] Khunová, V., Hurst, J., Janigová, I. and Smatko, V. *Polym. Test.* 18, 501 (1999).
- [8] Lee, S.Y., Lee, J.D. and Yang, S.M. *J. Mater. Sci.* 34, 1233 (1999).
- [9] Li, Y., Yu, J. and Guo Z.X. *J. Appl. Polym. Sci.*, Vol. 84, 827 (2002).
- [10] Ou, Y., Yang, F. and Yu, Z.Z. *J. Polym. Sci.: Part B* 36, 789 (1998).
- [11] Shang, S.W., Williams, J.W. and Söderholm, K.J.M. *J. Mater. Sci.* 29, 2406 (1994).
- [12] Rong, M.Z., Zhang, M.Q., Zheng, Y.X., Zeng, H.M., Walter, R. and Friedrich, K. *Polymer* 42, 167 (2001).
- [13] Rong, M.Z., Zhang, M.Q., Zheng, Y.X., Zeng, H.M., Zeng, H.M. and Friedrich, K. *Polymer Com.* 42, 3301 (2001).
- [14] Reynaud, E., Jouen, T., Gauthier, C., Vigier, G., Varlet, J. *Polymer* 42, 8759 (2001).
- [15] Janigová, I. and Chodák, I. *J. Therm. Anal. Calorim.* 60, 401 (2000).
- [16] Marinelli, A.L. and Bretas, R.E. *J. Appl. Polym. Sci.* 87, 916 (2003).
- [17] Lotz, B., Wittmann, C. and Lovinger, A.J. *Polymer* 37, 4979 (1996).
- [18] Cho, K., Saheb, D.N., Choi, J. and Yang, H. *Polymer* 43, 1407 (2002).
- [19] Balcerowiak, W. and Maciejewska, H. *Polimery – Tworzywa Wielkocząsteczkowe* 39, 626 (1994).
- [20] Shen Y.L., Finot, M., Needleman, A. and Suresh, S. *Acta Metall* 42, 77 (1994).
- [21] Berlin, A.A., Volfson, S.A., Enikolopian, N.S. and Negmatov, S.S. *Principles of polymer composites*. Springer-Verlag Heilderberg (1986).
- [22] Dijkstra, P.T.S., van Dijk, D.J. and Huétink, P. *Polym. Eng. Sci.* 42, 152 (2002).
- [23] Donal, A.M. and Kramer, E.J. *Philos. Mag. A, Phys. Condens. Matter Struct. Defects Mech. Prop.* 43, 857 (1981).

10 Conclusions and Recommendations

In this chapter the general conclusions and recommendations for future research are presented. The problem of rendering composite polymer materials with, for example, more impact-resistance without decreasing the material's modulus of elasticity has been attracting the attention of many material scientists. Some advantages of using polymers are found in their ease of processing and its light weight. During processability, high particle loadings results in end products with much higher weight than that of the pure polymers. Therefore a composite with improved properties at low particle concentration is desired. In this thesis, the reduction of the size of the inorganic filler added to the polymer matrix has shown an enhancement of the material properties when compared with the pure polymer, while using low particle loadings.

Conclusions

The main goal of this research was to study the influence of the addition of colloidal silica on the properties of nylon-6 and polypropylene to study properties of the newly formed materials.

A silica/nylon-6 nanocomposite was obtained with a very homogeneous dispersion in the polymer matrix of silica nanoparticles (3 wt%) of size 10-30 nm. Such a homogeneous dispersion of nanosilica in a nylon matrix has not been obtained before. This was achieved by dissolving the polymer in formic acid, subsequently mixing a silica sol through the solution, and then casting a film. Two types of silica sols were used for this study: silica dispersed in water and silica dispersed in ethanol. The silica introduced into the polymer matrix through the addition of both an aqueous and ethanolic sol showed a good dispersion, moreover the composite made by the use of an ethanolic sol showed a decrease in yield stress which is a promising result with respect to impact toughness,

The homogeneous dispersion of the silica particles in the nylon matrix, which was obtained with the films, was not obtained when using extrusion. Nevertheless, the mechanical test for extruded materials showed a high E-modulus for the silica/nylon-6 bulk composites, higher than theoretically could be expected for a polymer matrix filled with spherical particles, using the models of Mori-Tanaka and Kerner.

The silica/nylon-6 nanocomposites had a much lower friction than the neat nylon-6, and showed a reduction in wear by a factor 140. The reduced wear probably was caused by a 'self-lubrication' system of the material.

Strain viscosity increased upon addition of the nanoparticles to the pure nylon-6. Direct contact between particles is likely to be the cause for this increase.

The inadequacy of the Mori-Tanaka and Kerner models to predict the correct values of the E-modulus for the nanosilica/nylon-6 composites might be due to the fact that, in these models, the particle size is not taken into account. The exact dependency of the E-modulus on the particle size should be investigated in order to be able to develop a model that is more accurate.

Polypropylene prepared by a catalysed *in-situ* polymerisation reaction could be filled with nanosilica particles without reducing the polymerisation rate due to surface modification of the silica particles with a silane-coupling agent. The mechanical properties of polypropylene were improved by adding nanosilica particles into the material by way of extrusion. Even the Young modulus and the impact strength increased in this system.

Recommendations

The successful synthesis method for obtaining a homogeneous dispersion of silica nanoparticles in a nylon-6 matrix (as a result of the good mixability of the nylon solution in formic acid and the silica ethanolic sol) is not limited to polymers made through a ring opening polymerisation (ROP) mechanism such as nylon-6 and silica. It can be expected that other polymers that are soluble in formic acid can be used just as well, or example nylon-6,6. The same accounts for the filler. Any filler that can be well dispersed in an alcohol could be mixed with the formic acid solution of the polymer. Thus, many different homogeneous filler-polymer composites should be obtainable by this method. By adding (hard) nanoparticles such as alumina, titania or zirconia [1,2,3] the mechanical properties of the polymer could be improved while wear and friction might be lowered as well. The addition of inorganic fillers with (di electric properties might lead to a material with interesting functional properties [4]

The synergistic incorporation of an inorganic component within a polymer matrix is known to influence segmental mobility of the polymer chains [5]. In contrast to results obtained in conventional filled polymer systems [6] the addition of nanosilica particles to glassy polymers has enhanced permeability coefficients for several gases and vapours. Permeation occurs through the amorphous regions of the polymer. The presence of the nano-filler causes a different packing of the polymer chains, which leads to a higher percentage of amorphous phase. A higher rate of gas and vapour permeation through the composite materials is therefore expected. [7,8]. Due to the fact that

the filled polyamide nanocomposites in this study were prepared via film casting, their transport properties can be studied. Water vapour permeation measurements (interesting for food packing applications) as well as gas permeation measurements can be performed at room temperature in order to probe the membrane permeability. From additional studies such as positron annihilation lifetime spectroscopy (PALS) the size of the local free volume (holes) can be estimated [9].

Regarding the reinforcement of polypropylene with nanoparticles, other fillers such as Polyhedral Oligomeric Silsesquioxanes (POSS) can be used to study the possibilities of *in-situ/ex-situ* incorporation with a homogeneous catalyst or heterogeneous catalyst/polymer particle. POSS molecules range from 1-3 nm. Incorporation of POSS *in-situ* seems to be highly beneficial as POSS based co-polymers and blends are already used in aerospace applications. The Industrial Polymerisation Processes research group (IPP) at the University of Twente is currently exploring the addition of POSS to polypropylene in a liquid pool reactor (DPI Project # 428).

10.1 References

- [1] Wondenberg, F.C.M. *Nanostructured oxide coatings via emulsion precipitation*. PhD Thesis. University of Twente. The Netherlands (2001).
- [2] Raming, T.P. *The synthesis of nano-nano dual phase ceramic composites*. PhD Thesis. University of Twente. The Netherlands (2000).
- [3] Wang, Q., Xue, Q., Shen, W. and Zhang, J. *Appl. Polym. Sci.* 69, 135 (1998).
- [4] Williams, M.A., Hall, D.A. and Wood, A.K. in *Electroceramics: production, properties and microstructure* 217, IOM (1994).
- [5] Merkel, T. C., Freeman, B. D., Spontak, R. J., He, Z. Pinnau, I., Meakin, P. and Hill, A.J. *Chem. Mater.* 15, 109 (2003).
- [6] Barrer, R.M., *Diffusion in Polymers*. Eds. Academic Press, New York 165 (1968).
- [7] Goosey, M.T. *Polymer Permeability*. Ed. Elsevier Applied Science: New York, 309 (1985).
- [8] Merkel, T.C., Freeman, B.D., Spontak, R.J. He, Pinnau, Z.I., Meakin, P. and Hill, A.J. *Science* 296, 519 (2002).
- [9] Triftshäuser, W., Kögel, G., Sperr, P. in Positron Annihilation ICPA-12. *Proc. of the 12th Intl. Conf. on Positron Annihilation*. Munchen Trans Tech Publications (2000).

Appendix A

Controlling interparticle forces to create stable suspensions

Stabilising a colloidal suspension means that the interparticle potential is made repulsive, and there is a high-energy barrier to reach the primary minimum (Fig. 1).

The methods of stabilisation are [1]:

1. electrostatically
2. electrosterically
3. sterically
4. depletion
5. masking van der Waals forces

The energy diagrams for these methods of stabilisation can be drawn by adding the different components that influence the stability.

For electrostatic stabilisation small ions in simple salts are used and therefore do not have a steric effect. The stabilisation arises purely from the repulsion between the double-layers that are formed by non-adsorbing counter-ions. The more ions adsorb at the surface, the less the amount of electrostatic repulsion. The energy diagram is shown in Fig. 1. At low salt concentration there is no secondary minimum but a barrier that prevents coagulation into a primary minimum. This barrier height decreases as the pH approaches the iso-electric point (pH_{iep}).

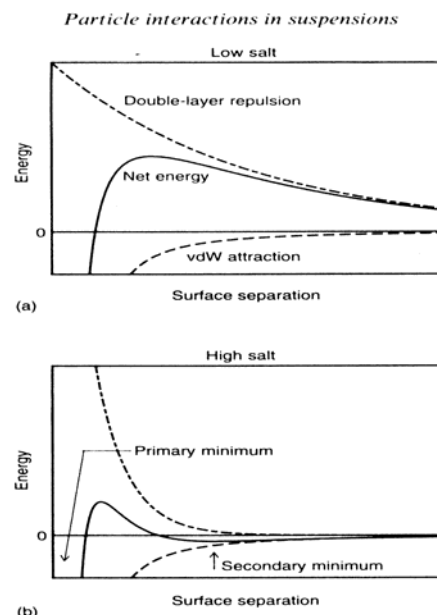


Fig. 1. Interaction energy between colloidal particles in suspension depending on the salt concentration [1]

If large molecules with charge carrying groups adsorb at the surface the stabilisation becomes electrosteric. The electrostatic repulsion arises from the dissociated groups of the molecule that are not bound to the surface. The thicker the layer that is formed by the adsorbed ions, the larger the steric part of the stabilisation. Polyelectrolytes containing many $-\text{COO}^-$ -groups are mostly used for this type of stabilisation. The $-\text{COO}^-$ -groups that bind to the surface do not contribute to the electrostatic stabilisation by the polyelectrolyte. The energy diagram for electrosteric stabilisation does not contain a primary minimum, as the particles in suspension cannot reach each other due to the presence of molecules at the surface. Only if the molecules are removed from the surface, a primary minimum will result. A secondary minimum can be present if the amount of steric or electrostatic stabilisation is not high.

If all the charge carrying groups of a large molecule are bound to the surface no electrostatic stabilisation is present, and the repulsion becomes purely steric. Thus purely steric stabilisation arises from adsorbing large molecules whose charge carrying groups are all bound to the surface or from large non-dissociating molecules that are adsorbed at the surface. Also here the thicker the layer of adsorbed molecules, the larger the steric stabilisation. The steric stabilisation energy will be less compared to the electrosteric stabilisation energy with equally thick layers, due to the lack of electrostatic stabilisation. The energy diagram will not contain a primary minimum. As with electrosteric stabilisation, the particles cannot touch each other. A primary minimum can only be reached if there is no or little adsorption present. The width of the steric barrier normally cannot be varied for a given system. This steric barrier can only be varied by varying the used adsorbent. Depending on the used adsorbent there will or will not be a secondary minimum.

Depletion stabilisation arises when relatively high amounts of large molecules that do not adsorb at the surfaces of the colloidal particles are dissolved in the suspension. Mostly large polymers like polyvinylalcohol (PVA) are used for this. In most cases the depletion

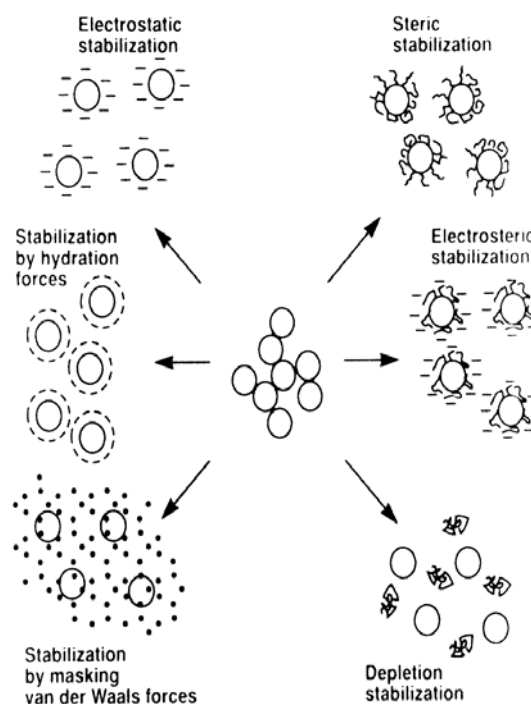


Fig. 2. Methods of stabilising colloidal ceramic particles in liquids [2]

stabilisation mechanism is not the only stabilisation mechanism present, but here the energy diagram purely due to the stabilisation mechanism will be considered. A primary minimum is present, and a certain barrier height to reach this minimum. This barrier height depends on the concentration of the free molecule that causes the depletion stabilisation. With decreasing concentration the barrier height will decrease, eventually leading to depletion flocculation into the primary minimum [2].

The masking of van der Waals forces by using additives is not a real stabilisation mechanism, as it leads to coagulation of the particles into a secondary minimum. However, when present, this mechanism will not be the only stabilisation. Masking of van der Waals forces can arise when molecules are adsorbed at the surface of suspended particles. If the adsorbed molecules have dielectric properties intermediate between those of the particle and the liquid, then the van der Waals forces between the suspended particles will be diminished. However, the adsorbance of the molecules will most often also lead to steric or electrosteric stabilisation, leading to a stable suspension whose stability is partly due to the masking of the van der Waals forces. This last stabilisation mechanism will always be less important than the other present stabilisation mechanisms (Fig. 2).

References

- [1] Everett, D.H. *Basic principles of colloid science*, Ed. The Royal Society of Chemistry, print. Whitstable, Kent, UK (1988).
- [2] Horn, R.G. *Ceramic Processing*, edited by R.A. Terpstra, P.P.A.C. Pex and A.H. de Vries, 1st ed., Chapman and Hall, London (1995).

Appendix B

Quantitative data from TEM analysis

Wu developed a model [1] to explain the rubber toughening mechanism in polymers. Although its physical meaning has been questioned it has shown to be applicable [2]. The current general idea in composites is the use of rigid particles to mimic the rubber toughening mechanism on a sub-micron size level [3]. Possible toughening of silica is out of the scope of this thesis, however Wu's model still is interesting as a background for the silica/polymer systems. In this appendix only a brief introduction is given.

Particle size and particle adhesion play an important role in determining the toughness of polymer blends. Regarding particle adhesion, Wu *et al.* [1] highlighted that strong adhesion alone does not ensure toughening but a combination of adhesion and an interparticle distance that should be smaller than a critical value (*vide infra*). In the case of rubber particles chemically bonded to the matrix, the polymer blend will still be brittle if the interparticle distance is greater than the critical value. As an example, an adhesion of 140 Jm^{-2} (weak) gave a brittle material. However the used particle size was larger than the critical size for toughening ($\sim 25 \text{ }\mu\text{m}$). Furthermore particles shouldn't be detached from the matrix during fracture. It is concluded that van der Waals adhesion could be the minimum adhesion necessary to toughen the material with these rubber particles, which is in the limits of tear energy of the rubber (1000 Jm^{-2}). As can be seen from Fig. 1 a very good dispersion with a 3 wt% filler was achieved, therefore more studies were performed on this nanocomposites.

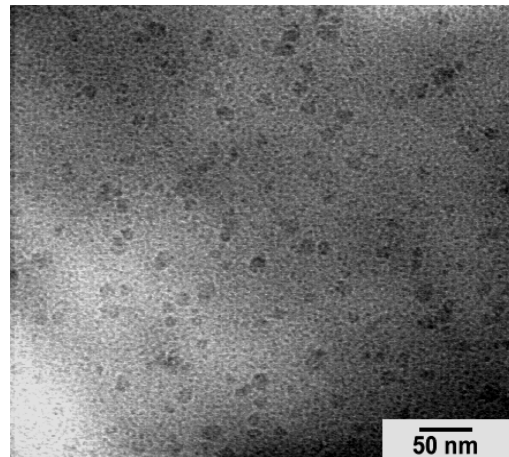


Fig. 1. PA6/SiO₂ nanocomposite. The micrograph was obtained from ultramicrotoming different regions of the composite (see Chapter 3).

In the following section critical parameters are calculated for this nylon-silica system (Fig. 1).

Interparticle distance

A known criterion for (rubber) particle toughening is the interparticle distance τ introduced by Wu. Critical parameters, such as critical particle diameter d_c and critical interparticle distance τ_c are applied. The critical interparticle distance (τ_c) is a material property of the matrix independent of the particle volume fraction (ϕ) and particle size. The critical particle diameter (d_c) is given by:

$$d_c = T_c \left\{ (\pi / 6\phi_r)^{1/3} - 1 \right\}^{-1} \quad (1)$$

Where τ_c is the critical interparticle distance between the surfaces of two nearest neighbouring particles, defined in Fig. 2.

In this model, τ_c is independent of d_c and ϕ . From Fig. 3, the experimental and the theoretical ($\tau_c = 42.11$) d_c values as a function of ϕ can be obtained. The prediction of d_c is given in Table 1. W_s refers to the filler weight fraction.

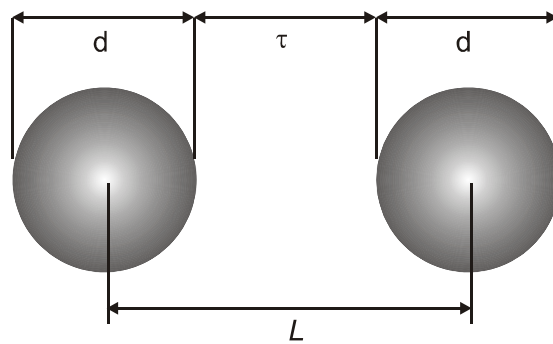


Fig. 2. Model for (surface-to-surface) interparticle distance τ , (centre-to-centre) particle separation L , and particle diameter d .

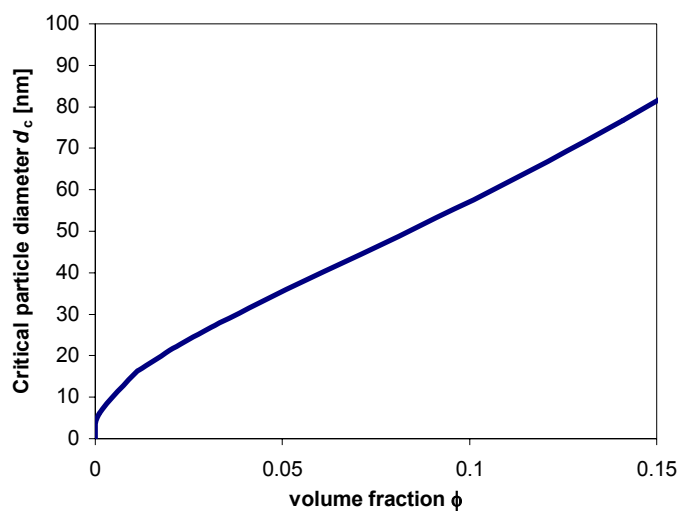


Fig. 3. Theoretical curve for the critical particle diameter. $\tau_c = 42$ nm.

Table 1. $\tau_c = 42.11$ nm, calculated by equation (1) using the experimental d_c value at $W_s = 0.024$.

W_r	ϕ	d_c (nm) calc ^a	d_c (nm) exp
0.024	0.012	16.49	16.49
0.05	0.025	23.98	164.00

Excluding secondary effects and assuming the critical interparticle distance (τ_c) as main parameter to determine the onset of tough-brittle transition (DTB) in blends, the model proposed by Wu assumes that the material will be tough if the τ_c is smaller than the critical value and the material will be brittle if the τ_c is greater than the critical value. In the case of nylon-6/silica nanocomposite $\tau_c > 42$ nm on average.

Equation (1) can rearrange to calculate the critical volume fraction, at which a tough-brittle transition will occur for blends having the same particle size but varying filler content, i.e.,

$$\phi_{rc} = (\pi/6)^{1/3} \{1 + (\tau_c/d)\}^{-3} \quad (2)$$

where ϕ_c is the critical volume fraction for the onset of DTB transition, and d the particle diameter. For a series of composites having a $d = 16.49$ nm, the ϕ_c is calculated to be 0.020 at $T_c = 32$ nm (Fig. 4).

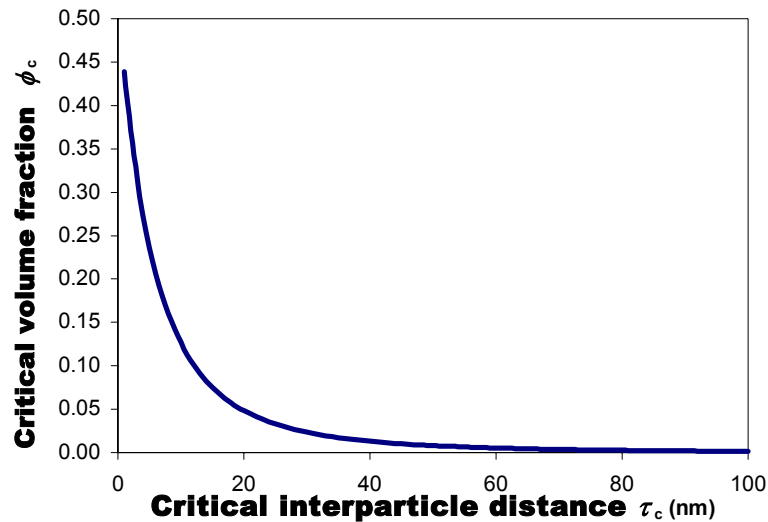


Fig. 4. Critical volume fraction for a DTB transition.

Stress around the particle

When particles are far away from each other, the stress field around one particle is slightly affected by the presence of the other. However, when the particles are sufficiently close together, the field around neighbour

particles will interact considerably resulting in enhance matrix yielding a transition to tough behaviour. This interaction between particles in rubber blends was the origin of the interparticle distance model. The sharp tough-brittle transition seems to occur at a specific τ_c regardless the volume fraction. However in the tough region it has been demonstrated that increasing the volume fraction and decreasing interparticle distance (or decreasing particle size) the impact toughness increased.

Separation to Aggregation Model

As described by Ou *et al.* [4], unlike rubber-polymer blends, the toughening behaviour of inorganic particle-filled composites is much more distinctive due to the diameter of the particles that should remain constant during processing. It has been proposed that when the volume fraction (ϕ) is less than the volume fraction for aggregation (ϕ_a) Wu's theory can be applied. Nevertheless when the ϕ exceeds the critical volume fraction (ϕ_c) for aggregation, the toughness of the polymers decreased with increasing inorganic component (Fig. 5).

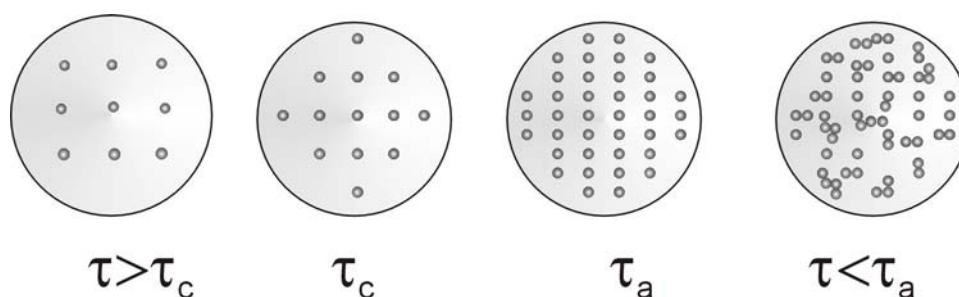


Fig. 5. Separation-to-aggregation process of inorganic particles with increasing of the silica volume fraction.

Unlike the assumption that τ_c as the main parameter for the BDT of a matrix, in the separation-to-aggregation model ϕ plays an important role as well as good adhesion between the filler. Studies of nylon-6/Silica nanocomposites showed that toughness of composite slightly varied with the increase of silica content, while the ϕ of the silica particle was relatively low. When the ϕ of the silica reaches the τ_c or ϕ_c , the BTD transition occurred. Nonetheless, when the ϕ of silica increases beyond another critical value for aggregation (ϕ_a), there is a DTB transition. The main conclusion is that the toughening range of inorganic particles filled composites is $\phi_c < \phi < \phi_a$ or $\tau_c > \tau > \tau_a$.

References

- [1] Wu, S. *Polymer* 26, 1855 (1985).
- [2] Borggreve, R.J.M. *Toughening of polyamide-6*. PhD Thesis. University of Twente. The Netherlands (1988).
- [3] Zuiderduin, W.C.J. *Polymer* 44, 275 (2003).
- [4] Ou, Y. *Appl. Polym. Sci.* 64, 2317 (1997).

Appendix C

Composite models

Halpin-Tsai

A general approach to estimating the properties of composites involves the use of semi-empirical equations, which are adjusted to match experimental results, by the use of curve fitting parameters. These equations are referred to as “semi-empirical” because, although they have terms containing curve-fitting parameters, they also have some fundamental background. Halpin and Tsai [1,2] developed their equations for fibers, so one has to be cautious when applied to other shapes and geometries. It was later generalized by Nielsen [3].

$$E = E_m \frac{1 + \xi \eta \phi_f}{1 - \eta \phi_f} \quad (1)$$

where

$$\eta = \frac{(E_f / E_m) - 1}{(E_f / E_m) + \xi} \quad (2)$$

E is the Young's modulus, the indices c , m and f refer to the composite, matrix and filler, respectively and ξ is the fitting parameter.

It has been shown that with $\xi = 0$, the Halpin-Tsai equation reduces to the lower bound (Voigt) and that with $\xi = \infty$, it reduces to the upper bound (Reuss). Thus, the interpretation of this fitting parameter as a measure of the degree of reinforcement has certain theoretical basis.

Shen-Li

The very recent model developed by Shen and Li account for the presence of an inhomogeneous interface [4]. In this theory, the mechanical properties of medium at the microscopic scale do not change abruptly at the interface between the spherical particle and the polymeric matrix, but a transition region (or interface) exists, in which the properties continuously relax until reaching the properties of the pure matrix at sufficiently long distances from the center of the filler particle. A particle together with its surrounding interface is called a composite sphere. Let r_0 and r_1 denote the radii of the particle and the

composite sphere, respectively, and $C_{eff}/(r)$ be the effective properties of the composite sphere with radius $r \in [r_0, r_1]$. The effective modulus of the particle-reinforced medium with an inhomogeneous interface can be evaluated as

$$\frac{C}{C_m} = 1 + \frac{\phi}{C_m / [C_{eff}(r_1) - C_m] + (1 - \phi)\alpha_m^C} \quad (3)$$

where $\phi = \phi_f (r_1 / r_0)^3$ and α_m^C depends on the particular modulus to be evaluated and is given by

$$\alpha_m^k = \frac{1 + \nu^m}{3(1 - \nu^m)} \quad (4)$$

in the case of the bulk modulus and by

$$\alpha_m^\mu = \frac{8 - 10\nu^m}{15(1 - \nu^m)} \quad (5)$$

in the case of the shear modulus.

The function $C_{eff}(r)$ satisfies the following differential equation:

$$\frac{dC_{eff}(r)}{dr} = -\frac{3}{r} \left[[C_{eff}(r) - C_i(r)] + \frac{\alpha_m^C}{C_i} [C_{eff}(r) - C_i(r)]^2 \right], \quad (6)$$

subject to the initial condition $C_{eff}(r_0) = C_f$

Following Shen and Li we used the following formula for the radial dependence of the Young Modulus at the interface:

$$\frac{E_i(r)}{E_m} = 1 - D \left(\frac{r}{r_0} \right)^{-\beta} \quad (7)$$

with the so-called “damage parameter” $D = -0.5$ and the parameter β was chosen to best represent the experimental data. Equation (5) is integrated numerically from $r = r_0$ to $r = r_1$ sufficiently large to ensure convergence of $C_{eff}(r)$. This value is then substituted in equation (3).

At points sufficiently far away from the particle surface the properties are equal to those of the matrix. The exponent β is a measure of the width of the region in which the properties are substantially different to those of the pure matrix. We found that reasonable agreement with experimental data can be obtained $\beta = 2.9$ and $\beta = 3.0$ for the Akulon and Aldrich polymer composites, respectively. This values of the parameter β correspond to a transition which ends approximately at $r_1/r_0 = 1.74$ and $r_1/r_0 = 1.68$ for the Akulon and Aldrich polymer composites, respectively.

The ξ is treated as a curve fitting parameter, which is a measure of the degree of reinforcement of the matrix by the filler.

Best agreement with measured values of the Young's modulus and those calculated with the Shen-Li model was obtained with $\xi=7.3$ and $\xi=4.5$ for the Akulon and Aldrich polymer composites, respectively.

References

- [1] Ashton, J.E., Halpin, J.C. and Petit, P.H. *Primer on composite materials*. Technomic Publishing Co., Chapter 5 (1969).
- [2] Halpin, J.C., Tsai, S.W. AFML-TR-67-423 (1969).
- [3] Nielsen, L.E., *J. Polym. Sci. Polym. Phys.* 17, 1897 (1979).
- [4] Shen, L., Li J., *Int. J. Solids Struct.* 40, 1393 (2003).

Samenvatting

Anorganische-polymeer composieten werden gevormd door silica-nanodeeltjes (doorsnee < 30 nm) in een nylon-6 matrix te incorporeren. Dunne films werden gemaakt door nylon-6 in mierenzuur op te lossen en deze oplossing te mengen met een silica-sol, waarna de vloeistof uitgegoten werd. Een aantal films werden samengesmolten en vervolgens persgegoten. Het TEM-onderzoek aan de composieten toonde aan dat de silica-deeltjes homogeen verdeeld waren en niet geaggregeerd waren. De kristallisatiegraad nam toe bij lage hoeveelheden silica-vulmiddel (< 7 gew%), maar bij verdere verhoging van het gew% vulmiddel nam de kristallisatiegraad weer af. Dit effect was bij de dunne films sterker dan bij de persgegoten monsters. De nanocomposieten vertoonden een toename van de E-modulus bij toenemend silica-percentages en een verhoogde breukspanning van > 0,5.

De weerstand en slijtvastheid van de persgegoten silica bevattende nylon-6 materialen werden onderzocht met een pin-op-schijf tribometer, door een platte staalpin tegen een silica-nylon composiet-schijf te laten lopen. De toevoeging van 2 gew% silica resulteerde in een reductie van de weerstand (μ) van 0,45 tot 0,18, in vergelijking met silica vrije nylon-6. Dit lage silica-gehalte veroorzaakte ook een afname van de slijtsnelheid met een factor 140. Dit effect was geringer bij hogere silica-belading. Het gladde oppervlak van de schijf dat verkregen werd na de slijttest wees op het geringe aandeel van de pin aan de slijtage van het composiet.

De rheologische eigenschappen van gesmolten polyamide-6 met colloidaal silica werden onderzocht bij kleine deformaties. De resultaten toonden aan dat de dynamische viscositeit afneemt bij een hoog vulmiddel-gehalte van 18-22 gew%, merkbaar bij spanningen groter dan 1%. Een 1000-voudige toename in de viscositeit werd waargenomen. Deze toename in de viscositeit werd mogelijk veroorzaakt door agglomeratie van de silica-deeltjes, wat ook afgeleid kan worden uit de toename van de dynamische modulus. Toevoeging van silica aan PA6 verhoogde dus de elasticiteit en viscositeit in vergelijking met silica-vrij nylon-6.

Silica-polyamide-6 composieten zijn ook gemaakt met behulp van een dubbelschroefs extruder. Een silica-sol werd gemengd met gesmolten polymeer in de spuitmachine. Door middel van WAXD kon worden vastgesteld dat de PA6 met nanosilica meer gamma-fase bevat dan de, in de literatuur beschreven, nanosilica bevattende PA6 welke met

andere synthesesmethoden zoals *in-situ* polymerisatie is gemaakt. TEM-foto's toonden aan dat de silica in het gëextrudeerde composiet geaggregeerd waren. Desalniettemin nam bij aanwezigheid van 14 gew% silica de E-modulus toe van 2.7 GPa tot 3.9 GPa. Deze toename is groter dan de toenames vermeld in de literatuur voor vergelijkbare nanosilica bevattende PA6-composieten. Dit geeft aan dat er een effectieve mechanische koppeling is tussen de silica en het polymeer. De toevoeging van silica verlaagde het gemiddelde moleculairgewicht van de polymeermatrix niet. Conventionele (mechanische) theoretische modellen zoals het Mori-Tanaka en het Kerner model zijn gebruikt om de efficiëntie van de versterking van polymeer-composieten met ronde deeltjes te voorspellen. De gemeten moduli van de verschillende nanosilica bevattende composieten waren hoger dan de moduli die door deze modellen werden voorspeld voor sferische deeltjes bevattende composieten.

De invloed van de aanwezigheid van silica op de *in-situ* polymerisatie van polypropyleen (PP) is bestudeerd, gebruikmakende van een 1-liter-slurrie-fase-polymerisatie-reactor met een magnesium chloride ondersteunde Ziegler-Natta katalysator (vierde generatie). De grootte van de silica-deeltjes varieerde van het nano- tot micronbereik. Het oppervlak van de silica-deeltjes was gemodificeerd door middel van een silaan-koppelaar om katalysator-deactivering te voorkomen en om een betere polymeer-vulmiddel-synergie te verkrijgen, dit als gevolg van de verhoogde hydrofobiciteit van het oppervlak van de silica-deeltjes. Het effect van de silica-deeltjes op het smeltpunt en op de kristal grootte van de PP werd bestudeerd met respectievelijk Differential Scanning Calorimetry (DSC) en Wide Angle X-Ray (WAXD). De toevoeging van versterkende nanosilica-deeltjes leidde niet tot een afname van de activiteit van de katalysator, dit in tegenstelling tot micro-silica, waarbij wel een afname van de activiteit van de katalysator geconstateerd werd. Polypropyleen-silica-nanocomposieten zijn ook met behulp van een dubbelschroefs extruder gesynthetiseerd. Toevoeging van colloidaal-silica aan de polymeermatrix leidde tot een goede dispersie van de deeltjes terwijl de toevoeging van poedervormig silica resulteerde in geaggregeerde deeltjes in de polymeermatrix (alle deeltjes waren in het nano-bereik). Bij een belading van 4,5 gew% colloidaal-silica werd zowel een versterkend als verhardend effect bij het polymeer waargenomen. Deze hoeveelheid van 4,5 gew% is laag in vergelijking met composieten, gevuld met conventionele deeltjes. De aanwezigheid van de deeltjes in de matrix leidde tot een toename van de Young modulus van 1,2 GPa tot 1,6 GPa en een slagvastheid van 3,4 kJ/m² tot 5,7 kJ/m², terwijl de trekvastheid constant bleef. Het gebruik van colloidaal-silica leidde tot betere mechanische eigenschappen, dit in tegenstelling tot composieten die poedervormig silica bevatten, waar met de toevoeging van silica-poeder aan polypropyleen geen verbetering in de mechanische eigenschappen kon worden geconstateerd.

Resumen

Un nano-compuesto de polímero inorgánico fue desarrollado mediante la incorporación de pequeñas partículas de sílica ($\varnothing < 30$ nm) en una matriz de nylon-6 (PA6). El polímero fue disuelto en ácido fórmico y posteriormente se le agregó el coloide de sílica disperso en agua. Varias capas fueron moldeadas mediante compresión. El compuesto fue examinado con TEM, el cual mostró que las partículas de sílica estuvieron uniformemente distribuidas sin zonas de aglomeración. El grado de cristalinidad se incrementó con bajos porcentajes de sílica (< 7% en peso), pero cuando éste fue incrementado el grado de cristalinidad volvió a disminuir. Comparado con nylon-6 puro, el nano-compuesto desarrollado mostró un aumento en el módulo de elasticidad (E) como una función del porcentaje de sílica agregado, así también, se presentó un incremento en la resistencia a la ruptura mayor al 0.5.

Las propiedades de desgaste y fricción del nano-compuesto mencionado fueron investigadas mediante el uso de un tribómetro el cual consiste de una pequeña espiga de acero deslizando sobre un disco compuesto de sílica-nylon. La adición de 2% en peso (p/p) de SiO_2 resultó en una reducción del coeficiente de fricción (μ) de 0.45 a 0.18, en comparación con nylon-6 puro. Así también, el bajo porcentaje de sílica agregado al nano-compuesto mostró una reducción en la rapidez de desgaste en un factor de 140. Por otro lado, cuando un mayor porcentaje de sílica fue agregado al compuesto, se mostró una menor influencia en las propiedades mencionadas. La superficie lisa del disco después de haber realizado la prueba de desgaste fue un indicativo de la casi nula contribución del desgaste de la esfera de acero al nano-compuesto.

Las propiedades reológicas de las capas adicionadas al nano-compuesto basadas en polyamide-6 y sílica coloidal fueron estudiadas bajo pequeñas condiciones de deformación. Los resultados mostraron que la viscosidad dinámica decrece cuando los contenidos de aditivo son del 18 y 22% en peso, observando una resistencia mayor al 1%. Un aumento de 3 décadas en la viscosidad pudo ser observado también. Este incremento en la viscosidad pudo haber sido causado por una pos-condensación (aglomeración) de partículas de sílica, lo cuál es también un indicativo en el incremento del módulo dinámico. Un incremento de la elasticidad y la viscosidad fue obtenido cuando se adicionó sílica al nylon en comparación con el puro nylon-6.

El compuesto de silica-polyamide-6 (PA6) fue también hecho usando un doble extractor. Silica sol fue mezclado con un polímero fundido dentro del extractor. Como fue determinado por Rayos-X (WAXD), el nanosilica conteniendo PA6 mostró una gran cantidad de fase- γ cuando ésta fue comparada con muestras de nanosilica conteniendo PA6 descritas en la literatura, las cuales fueron obtenidas mediante otro método de síntesis, tal como polimerización *in-situ*. Fotos de Microscopía de Trasmisión Electrónica (TEM) mostraron que las partículas de silica del compuesto extruído fueron agregadas. Sin embargo, para cantidades mayores al 14% (p/p) de silica, el módulo de elasticidad se incrementó de 2.7 GPa a 3.9 GPa. Este incremento es mayor comparado con el reportado en la literatura para compuestos de PA6 conteniendo nanosilica, indicando así que un efectivo acoplamiento mecánico con el polímero fue alcanzado. El aumento de silica no decrece el peso molecular promedio de la matriz de polímero.

Modelos teóricos (mecánicos) convencionales como los de Mori-Tanaka y Kerner fueron utilizados para predecir la eficiencia de reforzamiento de las partículas esféricas contenidas en el compuesto. Las mediciones del módulo de los diferentes compuestos de nanosilica fueron mayores que el módulo que predicho por estos modelos para compuestos con partículas esféricas.

El efecto de la presencia de silica en la polimerización *in situ* del polipropileno (PP) fue estudiada utilizando un litro de reactante de Slurry Phase Polymerization (SPP) conteniendo un catalítico $MgCl_2$ -supported Ziegler-Natta (cuarta generación). El tamaño de las partículas de aditivo de silica agregado fue nano y micro. La superficie de las partículas de silica fue modificada con un agente de base silano-acoplado para prevenir la desactivación catalítica y alcanzar mejor sinergismo entre el aditivo y el polímero, incrementando la hidrofobicidad de la superficie de las partículas de silica. El aumento del refuerzo de la nanosilica no causa un decremento en la actividad del catalizador, contrario de la adición de micro-silica, la cual condujo a reducir la actividad del catalizador.

Nano-compuestos de polipropileno- SiO_2 fueron sintetizados también mediante el uso de doble extractor. La adición de silica coloidal a la matriz de polímero produjo una buena dispersión del aditivo, mientras que el uso de silica en polvo resultó en una aglomeración de partículas de silica en la matriz del polímero (ambos aditivos estuvieron en el rango nano-dimensional). Con un 4.5% en peso de silica coloidal, se observó un efecto de reforzamiento y endurecimiento de las nanopartículas en la matriz de polímero. La cantidad de 4.5% en peso es mucho menor comparada a compuestos con aditivos de partículas convencionales. La presencia de partículas coloidales en la matriz de polímero produjo un incremento en el módulo de Young de 1.2 GPa a 1.6 GPa y una resistencia al impacto de 3.4 KJ/m² a 5.7 KJ/m², mientras que la resistencia a la fluencia permanece constante.

Curriculum vitae

María Monserrat de la Luz García Curiel was born in México City. After graduating with distinction from high school, she studied chemistry at the National Autonomous University of México (UNAM). During her studies, she worked at the Materials Research Institute (IIM) at the Polymers department on the project pathways for the polymerization of enines. She obtained the medal 'Guztavo Baz' (1st place) for her work.

She graduated in the phytochemistry group at the Chemistry Research Institute (IQ) in 1994, analysing the roots of the plant *Hesperozygis marifolia*.

After her graduation in chemistry she studied a master in business administration (MBA) at the UNAM, which she completed in 1996. In the two following years she studied for master in organic chemistry at the Faculty of Chemistry of the UNAM.

In 1998 she joined the Inorganic Materials Science (IMS) group of Prof. Henk Verweij, as a research fellow, at the University of Twente on the project "Ceramic composites with friction reducing additives". In 1999 she started her PhD on polymer-inorganic nanocomposites.

She graduated in 2003, during her PhD, as polymer scientist (RPK) at the National Dutch Graduate School of Polymer Science and Technology (PTN), The Netherlands.

She finished her PhD under the supervision of Prof. Dave Blank within the IMS group. The results of her work are described in this thesis.

Publications

– Book Contributions

García, M., Norder, B., Chávez, F., Kooi, B., García-Turiel, J., van Zyl, W.E., Verweij, H. and Blank, D.H.A., 'Polyamide-6/Silica Nanocomposites' *Edited by J. Wuerschum, Wiley-VCH 2004. Submitted (Chapter 5)*

– Articles

García, M., van Vliet, G., ten Cate, M.G.J., Chávez, F., Norder, B., Kooi, B., van Zyl, W. E., Verweij H. and Blank, D.H.A., 'New Processing Technique for Hybrid Nylon-6/SiO₂ (Nano)-composites'. Accepted in *Polym. Adv. Technol. (Chapters 6 and 7)*

García M., van Zyl, W.E., ten Cate, M.G.J., Stouwdam, J.W., Verweij, H., Pimplapure, M.S. and Weickert G., 'Novel method of preparing polypropylene-silica (nano)-composites' *Industrial & Engineering Chemistry Research* 42, 3750-3757 (2003). (Chapter 8)

Van Zyl, W.E., García, M., Schrauwen, B.A.G., Kooi, B., De Hosson, J.Th.M. and Verweij, H., 'Hybrid Polyamide/silica nanocomposites: Synthesis and mechanical testing'. *Macromol. Mater. Eng.* 287, 106-110 (2002). (Chapter 3)

García, M., Rooij, M., Winnubst, L., van Zyl, W.E. and Verweij, H., 'Friction and Wear of nanometer SiO₂-filled polyamide-6'. Accepted in *J. Appl. Polym. Sc. (Chapter 4)*

García, M., Barsema, J., Chávez, F., van Zyl, W.E., Verweij, H. and Blank, D.H.A., 'Hybrid organic-inorganic nylon-6/SiO₂ nanocomposites: Transport and mechanical properties'. *Submitted. (Chapters 7 and 10)*

García, M., van Vliet, G., Jahin, S., Schrauwen, B.A.G., Sarkissov, A., van Zyl, W.E. and Boukamp B., 'Polypropylene/SiO₂ Nanocomposites with improved mechanical properties'. *To be submitted (Chapter 9)*

García, M., Galindo, R.E., Cangialosi, D., Norder, B., Chávez, F., Verweij, H. van Zyl, W.E. and Blank, D.H.A., 'Polyamide-6/Silica Nanocomposites: A Positron Annihilation and Dynamic Mechanical Analysis (DMA) Study'. *In preparation.*

García, M., van Zyl, W.E., Kooi, B., Verweij, H. and Blank, D.H.A. 'Studies on the crystallization behaviour of Nylon-6/silica nanocomposites'. *In preparation*.

– **Other publications**

Kerkwijk, B., García, M., Mulder, E., Schipper, D.J. and Verweij, H., 'Device comprising a member of ceramic material and a method for manufacturing a ceramic material having low friction coefficient'. *Patent, Int. Appl.* WO0117926 A 20010315. Mar (2001).

Salcedo, R., Ogawa, T., Pineda, A., Rubio-Arroyo, M., García M., and Guadarrama, P., 'Chemical pathways for the polymerisation of enines'. *Polymer*, 33, 24 (1992).

Kerkwijk, B., García, M., van Zyl, W.E., Mulder, J., Winnubst, L.E., Schipper, D.J. and Verweij, H. 'Friction and wear behaviour of solid oxide lubricants as second phase in α -Al₂O₃ and stabilized ZrO₂ composites'. In press in *WEAR* (2003).

Salcedo, R., Sandores, L., Martinez, A., Alexandrova, L. and García, M., 'Manganese (I) complexes of p-xylene and [2n] cyclophanes from a theoretical sight'. *J. Organometall. Chem.* 603, 225-234 (2000).

Acknowledgements

Flexibility was perhaps the thing I liked the most about my PhD: The fact that some days I was in the office, while on other occasions I had to travel to Eindhoven (Mechanical and Chemical Engineer Department), Delft (IRI-Reactor Institute), Geleen (DSM), Utrecht (RPK-courses) and Amsterdam helped me to know different ways of working and different people.

The flexibility must be within a framework in which clear goals are set and there is clarity about what you want to do. These clear goals were given by my supervisor: Werner. If I had a good idea I could discuss it with Werner, and if he liked it, he would say: go right ahead and do it. Thank you Werner for sharing experience and good talks with me.

I would like to thank my promotor, Dave Blank, for his support and interest throughout the phase of writing my thesis (and checking my final lay-out!). Thank you for being a 'solver-problems' Dave! My debt to Henk Verweij goes further back, he gave me a place in his group and good advice.

I acknowledge Prof. M. Wessling, Prof. Han Meijer, Prof. Lefferts for being part of my committee. Prof. Schipper, Prof. Weickert, and Dr. Martin van Es, for their very assertive help and comments. Dr. Francisco Chávez for the deep discussions, collaboration regarding chapter 7 and sharp remarks. I owe a particular debt of gratitude to Dr. Louis Winnubst who made penetrating remarks on almost every word or so it seemed. Bedankt Louis!

Prof Dr. Manfred Wagner (Berlin), I very much appreciate your critique of my chapter 5. Thank you once again. Dr. Octavio and Dr. Antonio, thanks for the good discussions at NRC-IMI in Montréal.

It's almost every PhD's dream to be able to scale up the material made in the lab. That dream was realised by Gerhard van-Vliet from DSM and described in chapter 6. Thank you Ger.

My thanks also goes out to the many people that collaborated with me: in Eindhoven, especially Bernard Schrauwen for his contribution to chapter 3 (we made long working days), and Sachin and Alex as well (our effort is seen in Chapter 9). I would like to thank Ramon Galindo and Daniel Cangialosi (gracias por su tiempo y entusiasmo!), from Interfaculty Reactor Institute (IRI) Delft for the PALS measurements, and Ben Norder for the DMA measurements. Bart Kooi from Groningen for the TEM pictures. In Twente, Herman Koster for the X-Ray Diffraction and the SEM pictures of the membrane. Mark Smithers and Rico Keim are thanked for the SEM and TEM pictures of the nano-composite and Albert van der Berg for the XPS measurements. The IR-FT made by Louise Vrielinck is also greatly appreciated as well as the LEIS experiments performed by M. Viitanen from Eindhoven.

Henk Kruidhof whose effort was always focussed in providing me with enough financial support for my research.

Bernard (Boukamp), thank you for your continuous and supportive interest in my research (and the brownies?). José, you always solved any (computer) technical problem. Thanks a lot for your efficiency! Jurgen for the solving of (even more) technical questions.

The collaboration with Makarand P. (IPP), Mattijs Ten Cate and J. Wiljan S. (SMCT) was very, very fruitful. Jonathan (membrane group), thank you for your helpfulness. Audrey and Ana Paula for my first DSC experiments. Parasu and Michiel (good suggestions).

To the 'gezellig' Tribology group of Twente: First Erik for his 'everything is possible' philosophy. Matthijn de Rooij (good discussions), Bernd and Rihard (good model!). The joined adventure is seen in chapter 4. I also appreciate the assistance of the STEP group at UTwente.

Wim Vis and Tom, you were so motivated and enthusiastic students. Thanks! Ir. C.W. Struijk and Alejandro Dasburg-Salazar from Netherlands Organisation for Scientific Research (NWO). Gracias!

As suggested I waited to the very, very, very end to do the lay-out. A couple of days before going to the printer I sat next to the *master in calligraphy and style* László. If the reader sees a mistake in the lay-out, it is because I have failed to treat it adequately. Thank you László (2:00 a.m.!).

Cis who is everything anyone could wish for in a secretary and more! You are very tender. To Marion and Lianne that were always very helpful in any kind of subject. Agnes (thanks) and Odette (many things we can talk about...).

Bas (my first supervisor) and Manon helped me a lot during my first year! Special thanks to Natascha who worked with me during the practicum and Cindy for the DSC measurements. Bovendien wil ik Cindy, Natascha, Mieke, Gerrit en Herman bedanken voor de mogelijkheid om mijn Nederlands te oefenen. Attila, jij was een grote hulp op het lab!! Ik zal jou missen. Joop van de workshop, jij was altijd zeer behulpzaam en een goede probleemoplosser. Natty the librarian, thanks for all the articles and books you supplied to me.

During my first year I could share my office with my lieve Kamergenoot Wim and Ben. Lieve Wim, Thanks for my very first mini-Dutch dictionary en het bakje tijd!! Govert, I still keep my first blue cup, you were always so cheerful and so eager to talk about Holland, thank you guys for such a nice time, also outside of working hours. Mercedes tu también contribuiste a esos buenos momentos.

To the former KPM-crew in Twente, Bertha and Laurent (ojalá que siempre mantengamos tan buen contacto), Sergio (sonrisa Argentina), Marco and Monica, Gerhard, J.P., Victor and Sheila (muchas gracias por todas las muestras de afecto por parte de tu familia también!), Cristina, Gautam, László L., Olivier, Bert, Karen.

Lalo, Paty G., Bernardo, Paty P., Paty Arrieta, Jorge Arturo, Fausto, Mila, Claudette. You couldn't believe that I was really taking that plane to The Netherlands! Mayra (gracias por la bonita portada), Morayma, Mary, Liliana and Adys, mis siempre amigas. Gaby Carreón, Lupita y Mónica for our University times. Fernando and Johana. Rogelio e Isaías thanks God I was not the only Mexican at the UT! I always enjoyed our dinners and long talks! Maru que bueno que compartimos buenos momentos. Robert and Mayela nice to meeting you. Lupita y Jorge Ordoño, Adrian (Olda) Roberto G. and Nachito, fam. Trejo y Bonifaz: siempre los tuve presentes.

My flat-mates had the joy (and pain) of sharing their life with me. Thank you for the good moments! Dmitry, Я помню наши интересные беседы и то, что ты научил меня готовить спагетти. Мы провели чудеснейшее время вместе. Draga Nela, Iti multumesc mult pentru timpul petrecut impreuna si pentru discutiile avute in timpul pauzei de cafea, dar mai presus de toate doresc sa iti multumesc pentru bunatatea inimii tale, Margaret, Go raibh mile maith agat do na ndinnear agus an cupan tae Eireannach!

My international RPK study club: Javier (Spain), Maya (Algerian), Menchu (Spain), Marco (Bulgary), Francesca (Italy), Vipin (India) and Wilma (Germany). Thanks for the nice (hard) time! Julius (you too). Javier tú añadiste sal y pimienta a mi vida increíblemente. Gracias por escucharme, por cuidarme y consentirme. ¡Te has ganado mi corazón!

Janusz (Poland), thank you for your details! Marijn (Oomen) for “gezellige tijd” during the summer school. I followed your advice regarding chapter 2! Magda & Alejandro for the dinners and piñatas. Gloria and Hessel for the time in Lausanne, Karen nice time in Eindhoven and again in Heidelberg.

Fred, bedankt voor de lessen en de gezellige tijd met jou en Ruth. Ik heb veel over Nederland geleerd dankzij jou.

Members of AMK showed good camaraderie all around. The people that were there at the beginning: Elise (nice orchestra!), Mark (en Kim), Marco, Arian en Richard (leuke vakantie in Mexico), Henny, Sven, Marjan, George, Sjoerd, Marnix, Jurian and Ronald, Peter Bouwman, Peter Schrap. Ning, Matthijs (den Otter) nice to be your paranimf!, Maarten (‘murciélagó’), Alex, Neva, Christina, Gerald then and Gerald now...nice time as office-mates! (with Wolfi).

Mai and André, I really enjoyed our time and conversations in Boston, NY and Newport!

Shanko thanks for those ‘top-ten’ conversations. Still read more about the zero. Samuel, ik zal altijd de gezellige tijd met jou herinneren. Bedankt voor jouw hulp bij alles! Riaan (baie dankie dat jy soms na my geluister het), Boris, Frank (nice wadlopen!), Tijana, Matthijn Dekkers (goede rekenmachine), Alisia (good scan), Arjen, Thang, Richard, Wika, Samuel Sánchez and of course Ashima (good loyalty during that football match).

Finally Fredo whose patience seemed endless (in the office with three ladies!). If I would have had the possibility to choose my (female) officemates I will never end up thinking about the combination Mexican-Vietnamese -Serbian. Mai and Jelena, I am very glad that you were in my office! Sometimes it was so terribly funny (“without that...”).

Turid for the movie sessions and for introducing me to the Muffin’s culture (nice time in The Hague). Vittorio (tasty pasta) Lianne (nice dinner), Victor (coffee!), Guus (Korte naam, maar toch moeilijk) and especially Arjen (Mr. Janssens) voor de prettige gesprekken!

Wolfgang my office-mate first and later my friend. Wolfi (dear finger), nice tea times at 8:00 a.m. in room 1731. Later great times in Holland, Germany and México.

Manja it seemed to me that one of your goals in Enschede was not leaving me alone. You dragged me out of my place to go to try Glühwein, later I missed you a lot. Vielen dank liebe Manja!

I have to mention some other nice people that I met at the UTwente: Valer, Dejan, Daryl, Gena and Toshi. Also members from other groups such as Menno and Priscila and all nice people from the Rubber group, Kitty, Sybran from membrane and from the supramolecular group Martha, Olga (nice Sauna!), Lourdes, Jessica, Becky (thank you for teaching me the Americans words), Miguel, Fernando, Mercedes, Bart Jan, Peter Timmerman, Roberto (Fiammengó) you are optimist! B. Jeanette and above all Mattijs, thank you for your many, many, advices and help. You indeed have a ‘beautiful mind’ and made my PhD very special!

My Paranimfen: dear Irna, you know the feeling, you meet someone for the first time, and it's as if you've known each other all your lives! That happened to us in the Vrijhof! Thanks to you and EJ for the nice times here in Enschede and in Mexico (don't give up trying to convince me to go on winter holidays!).

Fiona, I liked to surprise you and just showing up to enjoy a cup of cappuccino together or just to go to our step-aerobics (by now you are used to though), I enjoyed our friendship-days ;) as well as our walks in those 'old' times to the mensa. Fionita bedankt voor jouw goede vriendschap!

My family, Mamá siempre recorde nuestra canción, tu además iluminas mi vida Papá, quise seguir tu buen ejemplo y estudiar lo mas que pude, Soco y Marco, gracias por darme la alegría de ser madrina! Mi hermana Chelo (Brodita) y Victor, y mi Crucita y Francisco. Familia, sus correos y el escuchar sus voces siempre me ha sido reconfortante.

En ik heb dit alles niet kunnen doen zonder de hartelijkheid van de familie Raming. José, jij bent een groot voorbeeld voor mij! Clemens, bedankt voor jouw genegenheid en het lekkere eten, Laurens, ik zal minder gaan snoepen!

Everlasting gratitude to Tomas, who understands me better than I understand myself, encouraged and stimulated me a lot! Gracias por tu amor que me ha enseñado tanto.

**"In those whom I like, I can find no common denominator;
in those whom I love I can: they all make me laugh"**

Wyatan Hugh Auden



Monse

Enschede, 2004

List of Abbreviations

ASTM	American Society for Testing and Materials
BTD	Brittle to ductile transition
CCD	Charge Coupled Device
COD	Chemical Oxygen Demand
DIN	Deutsches Institut for Normung
DMA	Dynamic Mechanical Analysis
DSC	Differential Scanning Calorimetry
DTB	Tough-brittle transition
E', E''	Elasticity moduli
EDAX	Energy Dispersive X-Ray Analysis
EDX	Energy Dispersive X-ray
FT-IR	Fourier Transform Infrared
FWHM	Full width at half maximum
GPa	Giga-Pascal
ISO	International Standards Organization
KJ	Kilo Joules
LHE	Left hand elements
LEIS	Low Energy Ion Scattering
LS	Light scattering
MAS	Magic Angle Spinning
MOX	Silica AEROSIL® [Degussa]
nm	nanometers
RI	Refractive index
SEC	Size Exclusion Chromatography
SPP	Slurry Phase Polymerization
TEM	Transmission Electron Microscopy
pH	Potential Hydrogen
wt%	Weight percentage
H-T	Halpin-Tsai model
PA6	Polyamide 6
PAL	Polyamide Aldrich
PAK	Polyamide Akulon

PCS	Photon Correlation Spectroscopy
POSS	Polyhedral Oligomeric Silsesquioxanes
PV	Product of the unit load P and the surface velocity V
PP	Polypropylene
PTFE	Polytetrafluoroethylene
rpm	revolutions per minute
SEM	Scanning Electronic Microscopy
ST	Silica Sipernat® [Degussa]
SX	Colloidal silica SNOWTEX® [NISSAN Chemical Industries]
XRD	X-Ray diffraction
XRF	X-Ray Fluorescence
WAXD	Wide-angle x-ray diffraction

List of Symbols

Symbols	Description	SI-Unit
a	Contact radius	[m]
a	Mark-Houwink constant	[-]
\mathbf{A}	Strain concentration tensor	[-]
A	Contact area	[m ²]
A_{ep}	Contact area (elastic-plastic conditions)	[m ²]
\mathbf{B}	Stress concentration tensor	[-]
C	Bulk (κ) or shear (μ) modulus	[N/m ²]
C^*	Concentration of active sites. Ch. 8	[mol/L]
$\mathbf{C}_c \mathbf{C}_m \mathbf{C}_r$	Stiffness tensor of composite (c), polymer (m) or filler (r)	[N/m ²]
$C_{eff}/(r)$	Effective properties of the composite sphere with radius $r \in [r_o, r_i]$	[-]
C_m	Matrix modulus E_m or G_m	[N/m ²]
C_m	Concentration of monomer at the active sites	[mol/L]
d	Separation of the two surfaces	[m]
d_c	Critical particle diameter	[nm]
D	Damage parameter	[-]
e, ep and p	Subscript e , ep and p corresponds to elastic, elastic-plastic and plastic contact conditions respectively	
E	Young's modulus	[MPa]
E'	Storage modulus	[Mpa]
E''	Loss modulus	[Mpa]
E_c, E_m, E_f	Young's modulus of composite(c), polymer (m) or filler (f)	[N/m ²]
E_{eff}	Effective Young modulus	[N/m ²]
E_1	Young's modulus of the sphere	[N/m ²]
F_{ad}, F_{pl}	Resistance to motion due to adhesion (F_{ad}) and ploughing (F_{pl})	
F_{pls}, F_{pll}	Friction force due to the ploughing at the fully plastic condition of substrate (F_{pls}) and layer (F_{pll})	
G	Shear modulus	[MPa]
$G(t), E(t)$	Relaxation modulus. Time dependent elastic modulus	[MPa]

$G'(\omega)$	Shear storage or elastic modulus (dynamic rigidity)	[Pa]
$G''(\omega)$	Shear loss modulus	[Pa]
G^*	Complex shear modulus (in oscillatory shear)	[Pa]
H	Hardness	[MPa]
H	Henry's constant. Ch. 5	[-]
$\Delta H_{\text{melt}1}$	Melt enthalphy	[KJ/Kg]
i	Imaginary number $i = \sqrt{-1}$	[-]
i	Number of asperities in contact	[-]
I	Identity tensor	[-]
\mathcal{J}	Storage compliance	[Pa ⁻¹]
\mathcal{J}''	Ratio of the strain 90 out of phase	[-]
K_p	Lumped propagation constant	[L/(mol sites)s]
K_d	Deactivation constant	[-]
K'	It is a function of the derived constants	[-]
L_{lt}	Crystallite size	[nm]
L/D	Aspect ratio	[-]
$M_w/M_n, M_z/M_w$	Polydispersity indices	[-]
M_n, M_w, M_z	Number averaged, weight averaged and z-averaged molecular masses	Kg/mole
P	Load	[MPa]
P_e	Load carried	[MPa]
P_e	Péclet number	[-]
P_{ep}	Load carried by the deformed layered surface under	[MPa]
P_f	Maximun packing fraction	[-]
$P_{ie}; A_{ie}$	Load carried and the contact area of each asperity in contact at elastic ($P_{ie}; A_{ie}$) condition	[Pa]
$P_{iep}; A_{iep}$	Load carried and the contact area of each asperity in elastic-plastic ($P_{iep}; A_{iep}$) condition	[Pa]
$P_{ip}; A_{ip}$	Load carried and the contact area of each asperity in contact at fully plastic condition ($P_{ip}; A_{ip}$)	[Pa]
P_{ies}	Load carried by the substrate at elastic condition	[Pa]
P_{ips}	Load carried by the substrate at fully plastic condition	[Pa]
P_m	Partial pressure of the monomer in reactor	[Pa]
P_{tot}	Total load carried by all asperities in contact	[MPa]
r	Radious	[nm]
r_0, r_1	Radii of the particle and the composite sphere, respectively	[nm]
Q_i	Number of siloxane bridges bound to the silicon	[-]

	atom	
R_p	Rate of polymerisation	[mol/Ls]
s	$t-t'$	
s, l	Subscript s and l refers to the substrate and the layer respectively. Ch. 4	
$S_c S_m S_r$	Compliance tensor of composite (c), polymer (m) or filler (r)	[m ² /N]
t	Layer thickness Ch. 4	[nm]
t	Time	[s]
t'	Previous time	[s]
T	Temperature	[°C]
T_g	Glass transition temperature	[°C]
T_{melt1}	Low melting transition	[°C]
T_{melt2}	High melting transition	[°C]
T_{cryst}	Crystallisation temperature	[°C]
T	Interparticle distance	[nm]
T_c	Critical interparticle distance	[nm]
$W_{c,x}$	Degree of crystallinity	[%]
W_s	Filler weight fraction	
z_i	Asperities with different height. (if $z_i > d$) asperities might have contact with the flat-layered surface	

Greek Letters

α	Shen-Li Parameter	[-]
β	Radius of the sphere Ch. 4	[nm]
β	Region width in which properties are different from matrix Ch. 5	[-]
β_0	Width of the crystalline peak at 2θ (increases as the thickness of the crystal decreases)	
β_i	Asperities with different radii	
γ	Shear strain	[-]
$\dot{\gamma}$	Rate of shear $\frac{d\upsilon}{dx}$	[s ⁻¹]
γ^o	Strain amplitude	[-]
η	Shear viscosity	[Ns/m ²]
η_{intr}	Intrinsic viscosity	dl/g
η'	Dynamic viscosity	[Pa·s]
η''	No special name. Related to the dynamic rigidity through $G' = \eta'' \omega$	

η^*	Complex viscosity $\dot{\gamma} = \partial\gamma_{21} / \partial t$	[Pas]
	Ratio of shear stress σ o the rate of shear $\dot{\gamma}$	
η_0	Steady flow viscosity	[Pa·s]
κ	Bulk modulus	[N/m ²]
κ	Thermal diffusivity	[cm ² /s]
λ	Wave length	[Å]
μ	Shear modulus	[N/m ²]
μ, f	Coefficient of friction. Ch. 4	[-]
ν	Poisson ratio	[-]
ξ	Fitting parameter for H-T model: shape factor	[-]
σ	Stress	[N/m ²]
$\sigma^0(\omega)$	Amplitude of the stress	[Pa]
σ_y	Yield stress	[MPa]
σ_{21}	Shear stress (If shear is in X ₁ -direction)	[N/m ²]
τ_e, τ_e, τ_p	Interfacial shear strengths of each asperity in contact with substrate and layer at elastic (τ_e), elasto-plastic (τ_e), and plastic (τ_p) condition	
τ	Matrix ligament thickness	
ϕ	Particle volume fraction	[-]
ϕ_a	Volume fraction for aggregation	[-]
ϕ_c	Critical volume fraction	[-]
ϕ_f	Filler volume fraction	[-]
ω	Frequency	[Hz]
ω	Indentation depth	[μm]
ω_{c1}	Critical indentation depth	[μm]
ω_i	Indentation depth of each asperity	[μm]

Index

A

Active site, 120, 127
 Concentration of active sites, 120
 Concentration of monomer at the active site, 120
Amorphous phase, 36, 37, 123, 142

B

Barrier performance, 2

C

Catalyst, 6, 13, 18, 43, 115-119, 125-128, 143
Coefficient of friction, 47-50, 57, 69-71
 Tables, 52, 70
Composite models, 153
Contact radius, 6, 65
Contact area, 62, 63, 65, 68
Crystallite size, 39, 41, 124
Crystallinity, 3, 10, 11, 31, 36-37, 48, 50, 100
 Degree of, 26, 39, 57, 101, 105, 117, 123-125, 133-137
Critical particle diameter, 148

D

Damage parameter, 154
Deactivation constant, 120
DSC, 26, 36, 133
Dynamic Mechanical Analysis, 98, 102, 105, 163

E

Elastic modulus, 12, 25, 38, 43, 69, 98, 113, 132, 138
 See also modulus of elasticity, 69

F

Free volume, 143
Frequency, 75-87, 98, 127
 Sweep, 77
Friction, 47-71

G

Glass transition temperature, 12, 31, 37, 69, 103, 104
 See also Temperature

H

Halpin-Tsai, 153
Hardness, 2, 13, 48, 60, 62, 65, 69
 Tables, 69

I

Identity tensor, 111
Indentation depth, 60, 62, 64, 67, 151
Inorganic filler particles, 13, 24, 132, 137
Interface, 4, 5, 14, 67, 114, 151, 152
Inter-particle distance, 5, 108, 147-150

K

Kerner's model, 111, 142, 158
Kinetics, 120

L

Lamellar thickness, 40, 41, 101
Loss modulus, 75, 82, 83, 85, 102, 103

M

Mechanical models, 107, 110
Mechanical properties, 113, 116, 125, 131, 134, 142, 151
Modulus,
 Bulk, 108, 109, 152
 Complex shear modulus, 76
 Shear, 76
Molecular weight, 100, 113, 138
Montmorillonite, 14
Mori-Tanaka, 110, 11, 141, 142, 156, 158
Morphology, 39, 125

N

Nanocomposites, 16-18, 20, 21, 26, 27, 30, 31, 38, 39, 47, 49, 50, 52, 69, 71, 73, 78, 82-88, 91-95, 98, 99, 101, 105-108, 114-116, 125, 130, 132-134, 137, 142, 147, 150, 159, 160, 161
Network, 74, 79, 83, 86, 88, 89, 122, 138
Nylon-6, 49, 69
 Silica nanocomposites, 2, 6, 17, 18, 92, 105, 115, 150
 See also Polyamide 6,
NMR, 26, 30, 102, 119, 122, 127,
Nucleation, 5, 12, 124, 31, 57, 102, 125, 131

P

PTFE, 48, 57
Polymerization,
 In-situ intercalative polymerisation, 16
 In-situ polymerisation, 17
Atom transfer radical polymerisation (ATRP), 17
Polypropylene, 17, 94, 116, 117, 125, 132-134, 139, 140, 1433-145
Prepolymerization, 118, 120
Propagation constant, 133, 172
PV value, 50

R

Rate of polymerisation, 120
Rheology, 74-90

Reaction, 17, 18, 42, 43, 57, 92, 95, 97, 98, 105, 116, 119-121, 126-128, 142
Reactor-setup, 118
Residence time, 79, 81, 167

S

Scherrer equation, 40, 124
Semicrystalline, 48
Shear modulus, 154
Shear storage, 76
Shen-Li, 153, 155
Slurry phase, 115, 117, 119, 160
Small strain,
 Rheology, 81
Viscosity, 85
Spherulites, 39
Storage compliance, 76
Storage modulus, 74, 82-85, 92, 102, 103
Strain concentration tensor, 111
Stress concentration tensor, 176
Size Exclusion Chromatography, 133-134

T

Temperature,
 Glass transition temperature, 12, 31, 37, 69, 103, 104
 Crystallisation temperature, 101

T delta relaxation, 102, 103
Toyota, 16
Transmission Electron Microscopy, 26, 92
Topography measurements, 63, 70

U

UV degradation, 15

V

Viscosity,
 Shear viscosity, 75, 86
 Intrinsic viscosity, 25, 35, 139,
 Dynamic viscosity, 78-80, 82, 86-88, 94

W

Wear rate, 5, 47, 49, 52, 53, 57, 58, 71
WAXD, 5, 23, 27, 32, 49, 51, 91, 115, 123, 124, 155, 156, 158
Wollastonite, 14
Wu's model, 149

X

X-Ray Diffraction, 11, 26, 27, 31
XPS, 58, 119, 122
XRF, 26, 50, 99, 119

Y

Yield stress, 33, 38, 39, 43, 62, 65, 74, 138, 139, 141
Yielding, 62, 139, 151
Young's modulus, 60-62, 65, 110-113, 153, 155
 Effective Young modulus, 60
 Young's modulus of the sphere, 61

Z

Ziegler-Natta, 116-118, 128, 156, 158